Refining the neutral competition model to understand stem-cell mediated homeostasis in the *Drosophila* midgut

A thesis submitted in candidature for the degree of

Doctor of Philosophy (PhD)

By

Cristina Fernández García

December 2023

Funding

This work was partly funded by the Biotechnology and Biological Sciences Research Council-funded South West Biosciences Doctoral Training Partnership.

Acknowledgements

My most sincere gratitude to Helen White-Cooper, whose support was unanticipated yet invaluable. I extend this gratitude to Joaquin de Navascués for giving me an opportunity that has significantly shaped my professional career.

I must also thank all the current and former members of the White-Cooper Lab who have helped me during my time at Cardiff – Katia Jindrich, Rob Mitchell, Shrinivas Dighe, Dána Jackson, Sabrina Williams, and Saurabh Chaudhary. My appreciation also extends to the PIs and researchers of the Cardiff *Drosophila* Group, especially Terrence Trinca, with whom I shared all the ups and especially the downs of the journey.

I am very grateful to my family: my mother for teaching me that our beginnings do not define our future, and my father for instilling in me the value of learning from failure. Moreover, to my extended family—Fabio, Olga, Mauro, Pepe, Cuel, Natalia, Pauli, Mario, Ana, Leo, Gael, Yoli, Pati, Sara and Trasky—for always being proud of me.

Big thanks to my friends back home - Adri, Pau, Belen, Andre, Alba, and Javi. Your patience and friendship have been invaluable to me. Also, heartfelt thanks to my friends who made a home away from home: Patricia, Brais, Beckie, and Ben.

A special thanks to Jacin (and Husky and Bengala), whose faith in me and encouragement to push boundaries has helped me grow. And to my sister, my rock. Sharing more than just a room, you've always been there, never complaining about my late-night worries. Your constant support and admiration for me have boosted my confidence.

Finally, a special thanks to myself for embarking on this journey and facing fears, overcoming obstacles, and stepping out of my comfort zone. Whether it’s been moving countries, making tough decisions, or starting anew, I've learned to embrace these challenges.

Covid impact:

The COVID-19 pandemic significantly disrupted my academic journey, particularly following the transition of my primary supervisor to another university. The closure of university buildings and laboratories forced me to adjust my research focus. Unable to conduct in vivo experiments on intestinal stem cells, I redirected my efforts towards molecular cloning, aiming to develop a drug-inducible system based on degron architecture activated by trimethoprim (TMP). Additionally, I engaged in extensive bioinformatics analysis, which allowed me to maintain productive research activities remotely.

Despite these adaptations, the inability to access the lab hindered my progress in certain experimental aspects. Concurrently, I completed a policy placement that profoundly influenced my career aspirations. After returning from this mandatory three-month internship in 2020, another lockdown ensued, further delaying my research. Consequently, I decided to temporarily pause my studies to gain additional job experience.

Eventually, I resumed my academic pursuits part-time and successfully integrated my new professional experiences into my research, enhancing both my practical skills and theoretical understanding.

Summary

Intestinal Stem Cells (ISCs) maintain intestinal tissue homeostasis in mammals and *Drosophila* by dividing and differentiating into various types to replenish cells in a tissue constantly facing challenges like mechanical abrasion or pH shifts.

In *Drosophila*, tissue turnover involves the neutral competition of symmetrically dividing stem cells. ISCs compete for niche occupancy without inherent advantages, leading to stochastic expansion or loss of specific lineages. However, this model of neutral competition assumes that ISCs have uniform division rate, which is challenged by experimental observations.

To address this, we proposed the quiescence-division switch model: two states for ISCs under homeostatic conditions, a static state with no division and a dynamic state where all ISCs in the same compartment divide at the same rate, so areas of fast and slow turnover can coexist. We proposed heat shock (HS) could trigger the switch from these states.

Immunofluorescence analysis on cell cycle markers showed increased mitotic activity after HS, supporting this switch, with no increase in cell loss associated. We employed Weighted Gene Co-expression Network Analysis (WGCNA) to identify gene clusters correlating with this response. Enterocytes demonstrated upregulated genes for DNA repair and downregulated genes for metabolism and growth. An unannotated cluster, likely related to progenitor cells, showed upregulation of cell cycle-related genes.

Homeostasis also includes ISC differentiation. Next, we focused on basic helix-loop-helix (bHLH) transcription factors, specifically Daughterless (Da) and Scute (Sc), which are essential for enteroendocrine (EE) cell differentiation. Our results support a 'Sc Threshold Scenario,' where a critical concentration of Da:Sc heterodimers initiates pre-EE cell differentiation.

Finally, we proposed a novel gene expression system for studying the quiescence-division model, independent of temperature and compatible with Gal4-UAS, which makes use of trimethoprim (TMP) to induce gene expression. We studied TMP's safety and efficacy in the *Drosophila* midgut, which showed no harmful effects.

Table of contents

Figure index

Table index

Abbreviations:

bHLH - Basic Helix-Loop-Helix

BMP - Bone Morphogenetic Protein

BP - Biological Process

CDKIs - Cyclin-Dependent Kinase Inhibitors

CDKs - Cyclin-Dependent Kinases

Da - Daughterless

DDs - Destabilising Domains

Dl - Delta

EBs - Enteroblasts

ecDHFR - E. coli Dihydrofolate Reductase

ECs - Enterocytes

EEs - Enteroendocrine Cells

EGFR - Epidermal Growth Factor Receptor

Gal80ts - Temperature-Sensitive Gal80

GO - Gene Ontology

GS - Gene Significance

HS - Heat Shock

IIS - Insulin/Insulin-like Growth Factor Signalling

Imd - Immune Deficiency Pathway

ISCs - Intestinal Stem Cells

JAK-Stat - Janus Kinase-Signal Transducer and Activator of Transcription Pathway

KEGG - Kyoto Encyclopedia of Genes and Genomes

ME - Module Eigengenes

MF - Molecular Function

MM - Module Membership

MS - Module Significance

PCNA - Proliferating Cell Nuclear Antigen

pre-EE cells - Precursor Enteroendocrine Cells

Sc - Scute

scRNA-seq - Single-Cell RNA Sequencing

TMP - Trimethoprim

Wg - Wingless

WGCNA - Weighted Gene Co-expression Network Analysis

CHAPTER 1: INTRODUCTION TO STEM CELL-MEDIATED HOMEOSTASIS DYNAMICS

1. Background

1.1. Tissue homeostasis

Tissue homeostasis is a crucial process that maintains the proper functioning of various body tissues and involves regulating and maintaining a delicate balance of cell proliferation, differentiation, and cell death (Venkei & Yamashita, 2018).

This equilibrium is achieved through various mechanisms (Morrow et al., 2019). For instance, in tissues like the epidermis, tissue-specific stem cells play a vital role in maintaining this balance by providing new cells to replace those lost during tissue turnover or due to injuries (Das et al., 2020; & Blau, 2020; Mannino et al., 2022).

Conversely, in tissues like the liver, regeneration primarily occurs through hepatocyte-driven liver regeneration, where preexisting hepatocytes proliferate (Michalopoulos, 2017). Likewise, the pancreas relies on the dedifferentiation and proliferation of differentiated cells to replace lost cells (Dong & Wu, 2018). However, alternative mechanisms like neuroplasticity come into play in tissues with limited regenerative capacity, such as the brain (Zamproni et al., 2021).

Despite the diversity of mechanisms involved in tissue homeostasis, there is a growing interest in stem cell-mediated tissue homeostasis. Understanding the biology and behaviour of stem cells and their niches is crucial due to their unique ability to maintain tissue homeostasis in many adult tissues under normal conditions. Tissue-specific stem cells ensure a continuous supply of differentiated cells throughout an organism's life (Mannino et al., 2022).

Imbalances between cell proliferation and loss, leading to the disruption of homeostasis, have been linked to numerous diseases, including obesity, type 2 diabetes, atherosclerosis, autoimmunity, allergies, and certain psychiatric disorders (Kotas & Medzhitov, 2015).

1.2. Stem cell-mediated homeostasis

Tissue homeostasis in postnatal life primarily relies on the presence of tissue-specific adult stem cells. These cells may remain dormant or quiescent within their cellular niches indefinitely, but under the right circumstances, they can differentiate into specialised cell types to replace worn-out or dead cells (Fuchs & Blau, 2020; Montagnani et al., 2016).

The cellular niche is a specific microenvironment encompassing both cellular and non-cellular components. The niche provides crucial structural, biochemical, and biophysical cues that influence stem cell behaviour, including self-renewal and differentiation (Donnelly et al., 2018; Gattazzo et al., 2014; Khlusov et al., 2022; McCarthy et al., 2020). This niche is key in orchestrating cell behaviours in response to internal and external signals and is essential for maintaining stem cell pools (Sagaradze et al., 2019).

Adult stem cells promote tissue renewal or turnover due to their multipotency—their capacity to supply all tissue-specific types of cells—and self-renewal—the ability to maintain themselves as a dividing population over extended periods of time (Drummond-Barbosa, 2008; W. Zhang et al., 2022). This fine balance is regulated at multiple levels: (i) steady-state stem cell proliferation and self-renewal, as well as differentiation, to ensure the long-term maintenance of a pluripotent stem cell pool; (ii) acute induction of stem cell proliferation in response to tissue damage; and (iii) re-entry into a quiescent or non-proliferative state once the tissue has been repaired or regenerated (Biteau et al., 2011; Blank et al., 2008; Ito & Suda, 2014).

Adult stem cells have been found and characterised in many adult tissues in mammals. These tissue-specific stem cells primarily maintain the turnover process, which comprises three key steps. Initially, there is the continual or periodic elimination of specific differentiated cells from the tissue. Subsequently, these eliminated cells are simultaneously replaced through cell division. Lastly, the newly generated cells differentiate and become functionally integrated with the preexisting tissue (Avila et al., 2021; Pellettieri & Sánchez Alvarado, 2007; Zhang et al., 2022)

Tissue-specific stem cells are instrumental in preserving the state of homeostasis through turnover but can also assist in restoring this state once lost through the regeneration process. Regeneration occurs when adult stem cells respond to a previous and disruptive loss of specific cell types by initiating cell division and differentiation programs (Picerno et al., 2021; Zakrzewski et al., 2019).

The critical difference between turnover and regeneration lies in the outcomes: in homeostatic turnover, the tissue maintains a stable composition and size over time, although cells are lost and replaced. However, in regeneration, significant damage or loss of cells, not just everyday wear and tear, alters the tissue's composition or size noticeably (Barker et al., 2010).

1.3. Kinetics of stem cell-mediated homeostasis

The diversity of adult stem cells imposes difficulties in offering a single comprehensive definition that applies to all of them (Kalderon, 2022). For the purpose of this thesis, stem cells will be categorised according to how fast cells are replaced (kinetics) and how they achieve their fate (dynamics).

Based on how quickly they respond to the body's needs, tissue-specific stem cells can be classified into three main groups (**Figure 1**): tissues that, even in normal conditions, have a high turnover of cells to replace quickly worn-out cells (such as the hematopoietic system, inter-follicular skin epidermis, or intestinal epithelia); tissues that typically have little to no turnover and no regenerative response to injury (like the brain and the heart) and tissues that generally only need a basal cell turnover, but can respond well to increased needs, injury, or disease through regeneration (such as skeletal muscle) (Das et al., 2020; Fuchs & Blau, 2020; Mannino et al., 2022; Zakrzewski et al., 2019).

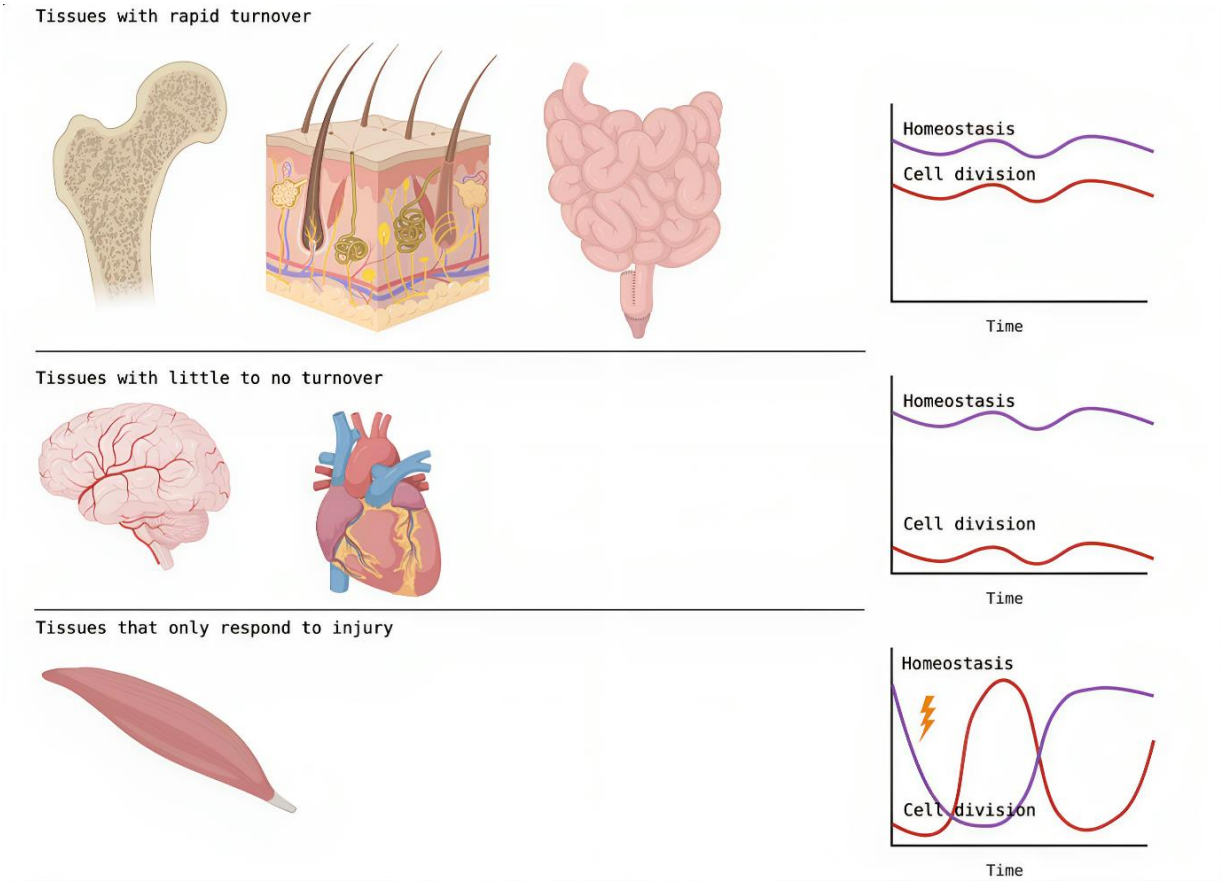

Figure 1. Classification of tissue-specific stem cells based on their kinetics. High-turnover tissues like the hematopoietic system and skin constantly renew cells. Low-turnover tissues, including the brain and heart, show minimal regeneration. Tissues that only respond to injury tissues, like skeletal muscle, have basal turnover with the potential for robust regeneration after injury. Illustration *created with BioRender.com.*

1.3.1. Tissues with rapid turnover

Bone marrow (BM)

Hematopoietic stem cells (HSCs) ensure the continuous production of red blood cells, white blood cells, and platelets (Demirci et al., 2020; Dzierzak & Bigas, 2018).

HSCs can be categorised into two distinct populations: long-term HSCs (LTHSCs) and short-term HSCs (STHSCs) (Lee & Hong, 2019; Sawai et al., 2016).

LTHSCs are predominantly slow-cycling or in a quiescent G0 phase, while STHSCs exhibit rapid cell cycle entry upon mitogenic stimulation, ensuring a continuous supply of HSCs. Upon activation, LTHSCs undergo asymmetric cell division to generate new LTHSCs and STHSCs (Hsu & Qu, 2013).

STHSCs, in turn, give rise to multipotent progenitors capable of supporting normal hematopoiesis for approximately 3-4 months (Eaves, 2015; Kosan & Godmann, 2016). STHSCs and multipotent progenitor cells can differentiate into all hematopoietic lineages, but they lose their self-renewal capacity. Both types can return to dormancy when homeostasis is restored, thus indicating that they can reversibly switch from dormancy to self-renewal according to hematopoietic needs (Wilson et al., 2008).

Skin epidermal tissue

Stem cells in the skin undergo rapid division due to the constant exposure of the outermost layer, the epidermis, along with its appendages, including hair follicles (HFs), sebaceous glands, sweat glands, and nails, to environmental factors (Lu et al., 2012; Yang et al., 2019). This continuous exposure places the skin under ongoing stress, leading to the regular shedding of outer cells, which are replaced by new ones (Fuchs, 2016; Hsu et al., 2014).

These stem cells are primarily located in the skin's basal layer, consisting of three additional layers beyond the epithelium. Within this basal layer, stem cells possess a remarkable capacity for proliferation (Uy Gonzales &, 2017). They continuously replenish the lower layers while ceasing their multiplication as they ascend into the other layers, gradually differentiating into various skin cell types (Klimczak & Kozlowska, 2015; Uy Gonzales &, 2017).

Intestinal epithelial tissue

Intestinal Stem Cells (ISCs) are essential for rapidly maintaining the homeostasis of the intestinal epithelium. Despite the continuous mechanical, chemical, and biological

challenges faced by the intestinal epithelium (Fink & Wrana, 2023), ISCs enable the intestine to perform its essential functions – maintaining the physical barrier, nutrient absorption hormone secretion, defence against pathogens, and immune response (Vancamelbeke & Vermeire, 2017) - while enduring mechanical wear and tear, extreme pH changes, and shifts in the microbiome (Joly & Rousset, 2020; Mannino et al., 2022).

ISC niches are located at the base of the intestinal crypts in mammals, making them some of the most active sites for tissue renewal and maintenance in the body (De Mey & Freund, 2013; Ramadan et al., 2022; Vermeulen & Snippert, 2014).

1.3.2. Tissues that only respond to injury

Skeletal muscle tissue

Satellite stem cells perform a critical function in skeletal muscle tissue regeneration. Their primary purpose is to respond to injury or damage by dividing and differentiating into new myofibers, the long, cylindrical cells that comprise skeletal muscle and contract to generate force and movement (Dumont et al., 2015; Mannino et al., 2022; Pichavant & Pavlath, 2014).

Satellite cells strategically reside adjacent to myofibers to allow them to respond promptly to any damage or insult that may occur, facilitating the rapid regeneration required for muscle tissue recovery and maintenance (Gattazzo et al., 2014b; Pannérec et al., 2012; Yin et al., 2013).

1.3.3. Tissues with little to no turnover

Cardiac tissue

Heart stem, or progenitor cells in adult mammalian hearts, possess self-renewal abilities and can generate coronary vessels and specialised heart muscle cells called cardiomyocytes (Nadal-Ginard et al., 2014; Zhao & Moore, 2018). Recent research challenges the traditional belief that the heart has limited regenerative capacity, as resident populations of cardiac progenitor cells (CPCs) have been identified in the perivascular compartment of adult hearts (Herrero et al., 2022; van Berlo & Molkentin, 2014).

In cases of human heart failure, the abundance of CPCs tends to increase, and some studies and in vitro experiments suggest that they have the potential to give rise to cardiomyocytes, smooth muscle cells, and endothelial cells (Eschenhagen et al., 2017; Mannino et al., 2022).

It is important not to confuse CPCs with cardiomyocytes' ability to respond to conditions like hypertension, vascular disease, and post-infarction overload. In humans, most cardiomyocyte nuclei become polyploid during puberty, and when required, they often restart DNA synthesis without nuclear division (Derks et al., 2020; Leri et al., 2015).

Central nervous system

In the adult central nervous system (CNS), neural stem cells (NSCs) are a population of self-renewing, multipotent progenitors primarily located within the subventricular zone (SVZ) of the lateral ventricle and the subgranular zone (SGZ) of the hippocampal dentate gyrus (Jurkowski et al., 2020; Kempermann, 2015; Mannino et al., 2022).

Despite their stem-cell-like capabilities, the adult vertebrate nervous system has limited regenerative potential when faced with insults or diseases resulting in extensive neuronal or glial loss (Ford et al., 2020). The frequency of division varies according to specific location and developmental stage, with notable differences observed across various neurogenic zones. For example, the SVZ surrounding the ventricles, which has the highest neurogenic rate in the adult brain, shows increased NSC proliferation following brain injury. In contrast, other areas, such as the SGZ of the hippocampus, the olfactory bulb, the subcallosal zone under the corpus callosum, and even the adult cerebellum, exhibit differing rates of NSC proliferation that are influenced by their unique microenvironments and the specific needs of the tissue at various stages of development and in response to injury (De Filippis & Binda, 2012).

1.4. Dynamics of stem cell-mediated homeostasis

Stem cells use distinct mechanisms to maintain tissue homeostasis, in addition to their varying rates of cell turnover.

1.4.1. Asymmetric division

An important property in many stem cell systems is asymmetric division, in which a single stem cell divides into two daughter cells with distinct fates (**Figure 2A**) (Inaba & Yamashita, 2012; Murke et al., 2015; Venkei & Yamashita, 2018). Asymmetric division enables stem cells to self-renew and contribute to multiple lineages while keeping a constant number of stem cells, hence preventing the depletion or overgrowth of the stem cell population (**Figure 2A**) (Knoblich, 2008; Lele et al., 2011; Murke et al., 2015; Neumüller & Knoblich, 2009).

In the context of asymmetric division, "division" refers to the physical separation of the stem cell into two distinct cells (Inaba & Yamashita, 2012; Joly & Rousset, 2020; Venkei & Yamashita, 2018). Several mechanisms ensure that daughter cells adopt distinct fates. These can be the asymmetric distribution of a determining factor, the influence of external cues, or a combination of these (Joly & Rousset, 2020; Pillitteri et al., 2016; Venkei & Yamashita, 2018).

Intrinsic processes include cell polarity, subcellular localisation mechanisms, asymmetric centrosomes and spindles, and cell-cycle regulators (Gómez-López et al., 2014; Loyer & Januschke, 2020; Sunchu & Cabernard, 2020). Extrinsic pathways include physical stimuli, cell-cell connections, and extracellular matrix components from the stem cell niche (Gattazzo et al., 2014; Loreti & Sacco, 2022).

The *Drosophila* germline stem cell is a classic example of an asymmetric division controlled by an extrinsic mechanism. It divides with a reproducible orientation to produce one daughter that remains in the stem-cell niche and retains stem-cell identity and one that is placed away from the niche and begins to differentiate (Knoblich, 2008; Venkei & Yamashita, 2018).

Both intrinsic and extrinsic signals induce asymmetric cell division in *Drosophila* neuroblasts, an additional well-known example (Homem & Knoblich, 2012). Each neuroblast divides into two daughter cells with distinct sizes and fates. The smaller daughter, the ganglion mother cell (GMC), is committed to the differentiation pathway and divides terminally to produce two neurons or glial cells, whereas the larger daughter retains neuroblast identity and can continue to divide asymmetrically and self-renew (Chia et al., 2008; Li et al., 2014; Loyer & Januschke, 2020). As the neuroblast stem cell initiates mitosis in *Drosophila*, two cell-fate determinants, Numb and Prospero, become localised to the basal cortex of the cell. After the neuroblast divides along the apical-basal axis, these determinants are predominantly inherited by the basal daughter, the GMC, ensuring its differentiation pathway (Chia et al., 2008; Li et al., 2014; Loyer & Januschke, 2020).

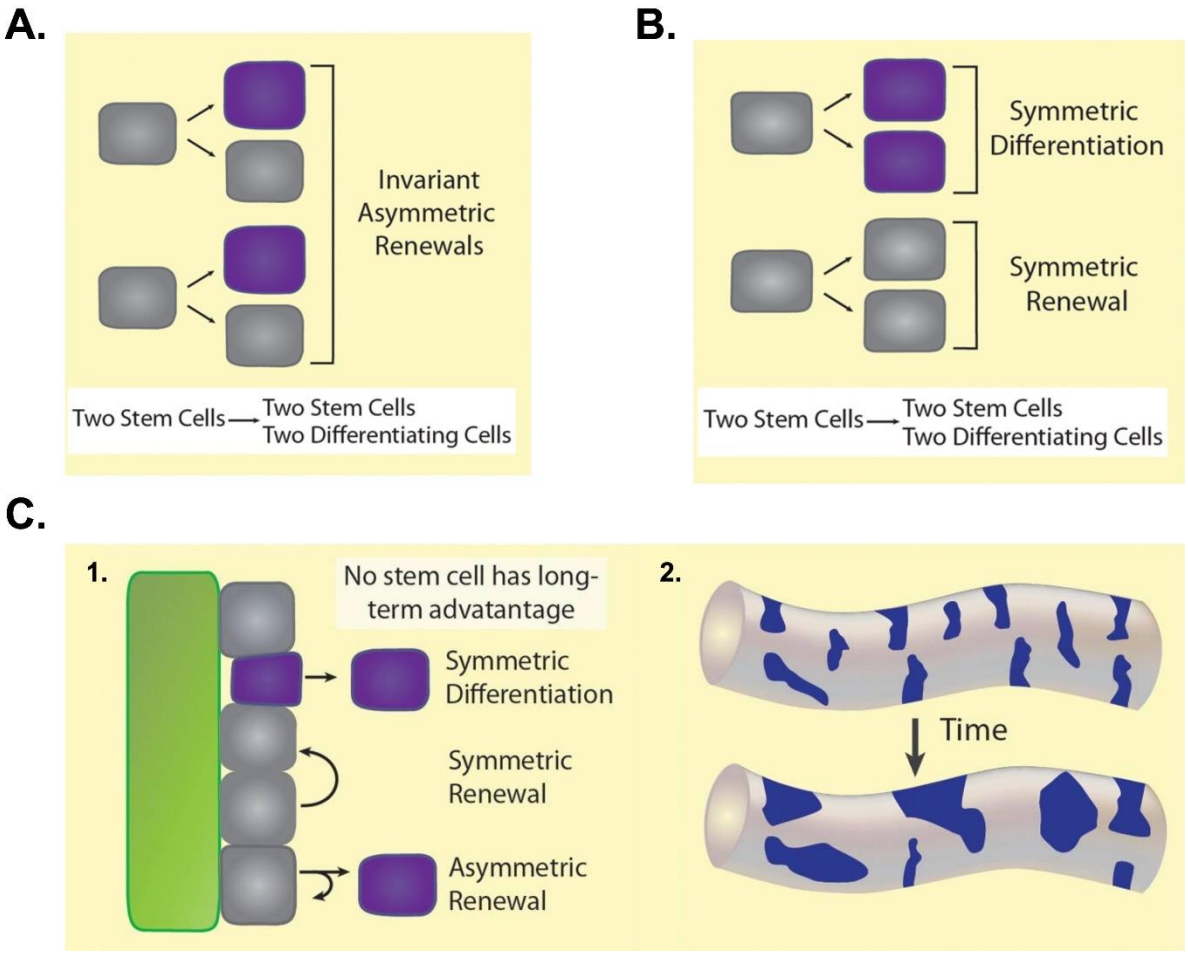

Figure 2. Stem cell population maintenance through asymmetric division or population asymmetry. A. Division asymmetry: Stem cells (grey) consistently divide to produce one daughter stem cell and one daughter cell that differentiates (purple). The stem cell count is the same before and after. **B. Population asymmetry:** Stem cells either undergo symmetric renewal, yielding two stem cell daughters (grey), or symmetric differentiation, yielding two differentiating daughters (purple), with equal frequency. Consequently, the number of stem cells remains constant as the population divides. **C. Neutral competition in stem cell niches:** 1. Neutral competition describes the stochastic loss of stem cells (grey) from the niche (green), subsequently being replaced. 2. In an open environment (e.g., intestinal tube), marked stem cell clones (dark blue) decrease over time while the average size increases, exhibiting a defined scaling behaviour. In an open environment, stem cell clones exhibit scaling behaviour over an extended duration. *Adapted from* (Stine & Matunis, 2013).

1.4.2. Symmetric division and population asymmetry

Symmetric division, in contrast, results in the production of two identical daughter cells. These cells can either remain stem cells, thereby expanding the stem cell pool or become differentiated cells, contributing to tissue formation and repair (**Figure 2B**) (Nakamuta et al., 2022; Reilein, 2017). This mechanism can lead to the ageing and eventual death of some stem cell lineages while simultaneously enhancing the effective growth rate of the population (**Figure 2B-C**) (Shahriyari & Komarova, 2013).

The symmetric division dynamic introduces competition for niche occupancy and survival among stem cells without any inherent advantage or disadvantage, resulting in stochastic expansion of specific stem cell lineages while others are lost, a phenomenon known as neutral drift (Nakamuta et al., 2022; Reilein et al., 2018). In this mode of neutral competition, stem cells have equal chances of occupying the niche and contributing to tissue maintenance, and their fate is determined by stochastic events and environmental cues (**Figure 2C**) (Guisoni et al., 2017; Colozza et al., 2022; Ramadan et al., 2022)

Stochastic behaviours of multiple individual cells collectively result in a balance between stem cell division and differentiation, a process known as population asymmetry.

Adult stem cells can maintain tissue homeostasis through symmetric and asymmetric divisions (Fuchs & Chen, 2013). They are both useful: symmetric stem cell divisions can increase the stem cell population but also risk excessive stem cell numbers, potentially leading to tumorigenesis (López-Lázaro, 2018). Conversely, asymmetric stem cell divisions allow for self-renewal and cellular diversity while maintaining a constant stem cell count (W. Chang et al., 2020; Chhabra & Booth, 2021).

The dynamics of both symmetric and asymmetric divisions have been characterised by various stem cell types, including hematopoietic stem cells (HSCs), mammary stem cells (MaSCs), and intestinal stem cells (ISCs), offering insight into tissue maintenance and repair processes (Chen et al., 2016; Chhabra & Booth, 2021; Snippert et al., 2010).

The intestinal epithelium, known for its rapid self-renewal rate—second only to the skin epidermis in humans—serves as an excellent system for investigating stem cell-mediated mechanisms (Beumer & Clevers, 2016). Symmetric division is crucial as it amplifies the number of stem cells. Without it, the growth of the ISC population would be compromised, potentially impairing tissue maintenance and repair. This process was first characterised in 2010 when it was shown that Lgr5+ stem cells, located at the base of

the intestinal crypts and identified by their expression of Lgr5 (leucine-rich repeat-containing G protein-coupled receptor 5), exhibit a pattern of neutral drift (Lopez-Garcia et al., 2010; Snippert et al., 2010).

Equally important is asymmetric division, which produces not only stem cells but also specialised cells necessary for tissue repair and maintenance. During normal tissue regeneration and after injury, there is a notable increase in asymmetric ISC divisions, underscoring its importance in this process (Lopez-Garcia et al., 2010; Vermeulen & Snippert, 2014; Vertii et al., 2018).

2 Dynamic regulation of stem cell divisions in intestinal homeostasis: insights from *Drosophila* as a model organism

While significant discoveries regarding gut renewal dynamics have been made in vertebrates (Radtke & Clevers, 2005), these organisms are not always the ideal choice for investigating gut replenishment in response to various experimental or environmental challenges due to their cost and time-consuming nature. However, with the discovery of adult *Drosophila* intestinal stem cells in 2006, flies have emerged as a promising model for studying intestinal homeostasis (Micchelli & Perrimon, 2006; Ohlstein & Spradling, 2006).

The cost-effectiveness and time efficiency of studying gut replenishment in *Drosophila* make it an attractive model for investigating the molecular processes governing the balance between symmetric and asymmetric stem cell division during tissue development and homeostasis. Indeed, recent research has shown that *Drosophila* ISCs can do both symmetric and asymmetric divisions (De Navascués et al. 2012; Hu & Jasper, 2019; Ramadan et al., 2022).

2.1. The structure of the midgut of the adult *Drosophila melanogaster*

The gut of *Drosophila* is an ideal system since it shares many structural, functional, and regulatory characteristics with that of mammals. Specifically, the *Drosophila* midgut is analogous to the mammalian small intestine (**Figure 3A**); both systems have a high turnover rate and are replaced by stem cells (Tian et al., 2016). They also share physical characteristics, such as the presence of enterocytes and enteroendocrine cells (Guo et al., 2016; Ohlstein & Spradling, 2006).

In the case of the fly, ISCs are found basally just above the basement membrane, which divides the epithelium from the underlying visceral muscle cells (**Figure 3B**) (Jiang & Edgar, 2011). A chitinous membrane called the peritrophic membrane or matrix separates the epithelium from the ingested food and acts as a barrier to gut bacteria inside the *Drosophila* midgut lumen. ISCs proliferate and differentiate into the main cells of the intestinal epithelium: enteroblasts (EBs), enteroendocrine cells (EEs) and enterocytes (ECs) (**Figure 3C**) (Bond & Foley, 2012; Christofi & Apidianakis, 2013; Jiang & Edgar, 2011).

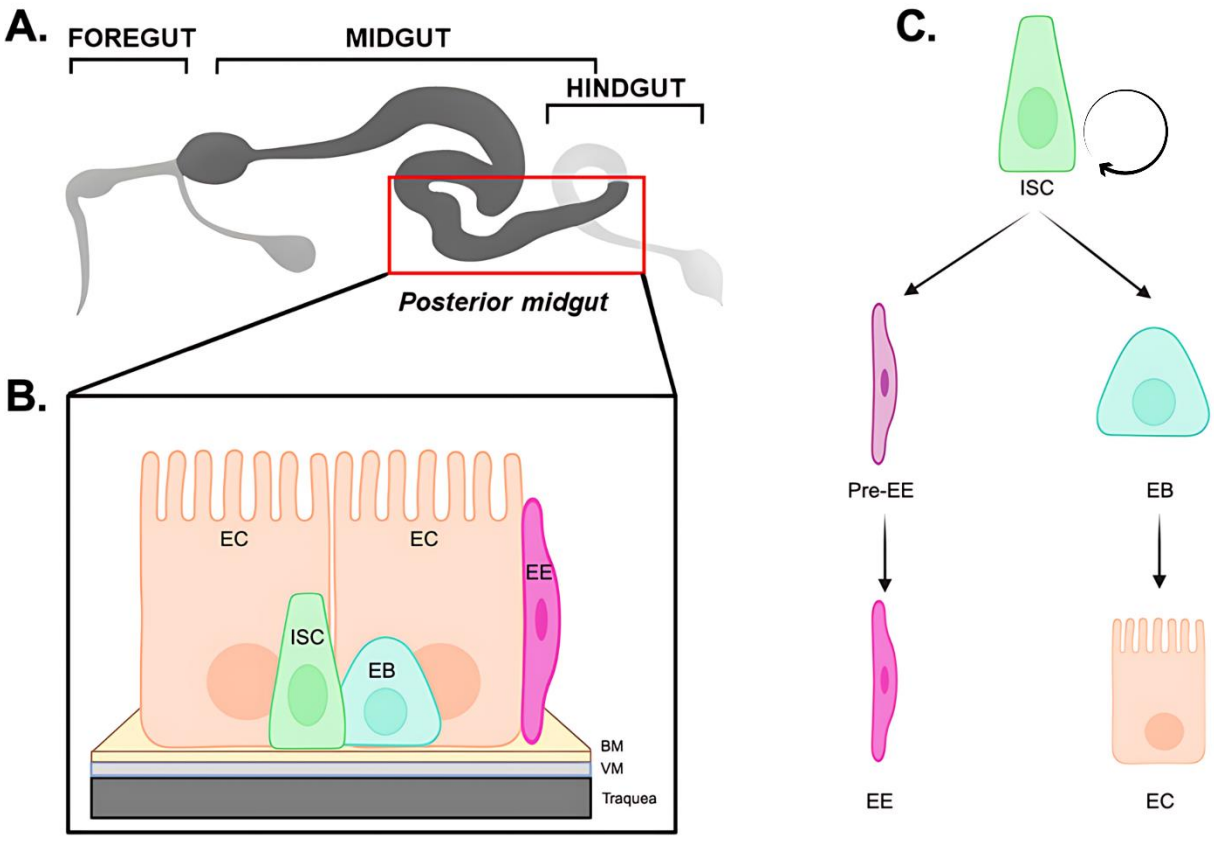

Figure 3. Anatomy and cell differentiation in the adult *Drosophila* midgut. A. Main anatomical features of the adult digestive tract: It shows the foregut, midgut and hindgut. The focus is on the posterior midgut. **B. Cellular composition of the fly adult midgut:** Intestinal stem cell (ISC), enteroblast (EB), enteroendocrine cell (EE) and enterocyte (EC). The basement membrane (BM) and visceral muscle (VM) layers are also indicated. **C. Differentiation pathway of ISC in the midgut epithelium:** ISCs divide and give rise to two distinct pathways. One path leads to pre-enteroendocrine cells (pre-EE), further differentiating into mature EEs. The other path leads to EBs, which eventually become fully differentiated ECs. *Illustration created with BioRender.com.*

2.2. Cell composition in the midgut of the adult *Drosophila melanogaster*

Like the vertebrate small intestine, the *Drosophila* midgut is largely composed of absorptive enterocytes (ECs) with interspersed hormone-producing enteroendocrine (EEs) cells. ISCs can differentiate into pre-endocrine (pre-EE), which further gives rise to EE cells and enteroblast (EB), which further differentiates into ECs (**Figure 3C**) (Guo et al., 2016; Jiang & Edgar, 2011; Ohlstein & Spradling, 2006; Ren et al., 2010).

Enterocytes are the main absorptive cells in the midgut and are responsible for nutrient uptake (Christofi & Apidianakis, 2013). As part of their differentiation program, ECs grow very large and endoreplicate their genomes several times, reaching ploidy levels of 16–32 C. Therefore, these cells make up the bulk of the midgut epithelium (Marianes & Spradling, 2013; Ren et al., 2010; Staley & Irvine, 2010). Enteroendocrine cells produce and secrete regulatory peptides that play a role in digestion and nutrient sensing (Jin et al., 2017).

Approximately 90% of ISC progeny differentiate into ECs, while the remaining 10% become EEs (Biteau & Jasper, 2014).

2.3. Signalling in the midgut of the adult *Drosophila melanogaster*

The adult *Drosophila melanogaster* midgut is a dynamic system where ISCs are regulated by a complex network of signalling pathways. Under homeostatic conditions, these pathways ensure the proper balance of ISC proliferation and differentiation needed to maintain gut integrity (**Figure 4A**). In contrast, disruption of homeostasis, such as during stress, triggers a different set of pathway responses to facilitate tissue repair and adaptation (**Figure 4B**) (Doupé et al., 2018).

2.3.1. Wnt/Wg pathway

During homeostasis, the Wnt/Wg pathway plays a crucial role in regulating intestinal stem cell self-renewal, proliferation, and differentiation in the midgut of *Drosophila (***Figure 4A***)* (Cordero et al., 2012; Jiang & Edgar, 2011). Activation of the Wnt/Wg pathway is essential for maintaining the stem cell population and promoting ISC proliferation during homeostasis and regeneration of the midgut. The Wnt/Wg pathway is primarily activated in enterocytes (Tian et al., 2016). Additionally, the Wnt/Wg pathway is involved in regulating the behaviour of intestinal stem cells and enteroblasts. The activation of the Wnt/Wg pathway in enterocytes has been shown to support ISC proliferation and maintain intestinal homeostasis.

The Wnt/Wg is induced in response to acute stress or damage to the midgut epithelium. This induction is associated with a robust regenerative response characterised by increased ISC proliferation (**Figure 4B**) (Cordero et al., 2012; Liu & Jin, 2017).

The Wnt pathway interacts with other signalling pathways, such as the EGFR/Ras/ERK pathway and the JAK/Stat pathway, to cooperatively maintain ISC function and regulate intestinal homeostasis (Panayidou & Apidianakis, 2013; Tian et al., 2018; N. Xu et al., 2011).

2.3.2. Notch

Notch and its ligand Delta (Dl) signalling plays a crucial role in regulating intestinal stem cell homeostasis in the midgut of *Drosophila* (**Figure 4A**). The level of Notch signalling is bidirectional and context-dependent. Notch signalling is involved in maintaining the balance between stem cell self-renewal and differentiation, as well as regulating the fate determination of progenitor cells (Guo et al., 2016; Kux & Pitsouli, 2014; Takashima et al., 2016).

High Delta expression in ISCs leads to Notch pathway activation in progeny, driving their differentiation into enterocytes. Low Delta levels favour differentiation into enteroendocrine cells, demonstrating the pathway's bidirectional nature (Adlesic et al., 2016; Jiang & Edgar, 2011; Petrovsky & Großhans, 2018; Shi et al., 2021). Additionally, enteroendocrine cells modulate ISC identity and function via Notch signalling feedback (Doupé et al., 2018).

2.3.3. JAK-Stat pathway

The JAK-Stat signalling pathway is pivotal in regulating homeostasis within the adult *Drosophila* midgut. This pathway modulates ISC proliferation and is essential for epithelial regeneration, responding to various stimuli, from tissue damage to stress and ageing (**Figure 4A**).

Under normal homeostatic conditions, JAK/Stat is activated by cytokines, such as Upd2 and Upd3, secreted by various intestinal cell types, including ISCs, EBs, and ECs (**Figure 4A**). (Jiang et al., 2009; Osman et al., 2012; Zhou et al., 2013).

Upd2 and Upd3 serve as ligands that activate the JAK-Stat pathway in *Drosophila*, initiating the JAK-Stat signalling cascade (Osman et al., 2012; Wright et al., 2011; Herrera & Bach, 2019; Zhou et al., 2020).

Under typical conditions, several intestinal cell types produce these ligands at varying levels. It is well-established that upd2 expression occurs in ISCs/EBs/ECs, while upd3 is primarily expressed by ECs (Herrera & Bach, 2019).

When homeostasis is disrupted, for instance, by bacterial infection or physical injury, Upd3 production increases, particularly in stressed EBs and ECs, triggering a more intense JAK/Stat response (**Figure 4B**). This upregulation, in turn, stimulates the secretion of EGF-type ligands such as Spitz and Vein, activating the Epidermal Growth Factor Receptor (EGFR) signalling pathway and leading to a surge in ISC proliferation necessary for rapid tissue repair (**Figure 4B**) (Houtz et al., 2017; Zhou & Boutros, 2023).

The interaction between JAK/Stat and EGFR pathways is crucial for managing the balance between ISC growth and differentiation during this response to stress, which contributes to tissue repair and the restoration of homeostasis (Buchon et al., 2010).

2.3.4. EGFR signalling

The EGFR signalling pathway is also integral in managing intestinal stem cell (ISC) proliferation and tissue regeneration within the adult *Drosophila* midgut (Biteau & Jasper, 2011; Buchon et al., 2010).

Under homeostatic conditions, EGFR ligands, including Vein (Vn), Keren (Krn), and Spitz (Spi), are expressed in the intestine, playing essential roles in ISC maintenance, proliferation, and differentiation (**Figure 4A**) (Jin et al., 2015; Lucchetta & Ohlstein, 2012; Xu et al., 2011).

In addition to its primary role, EGFR signalling also collaborates with other pathways, such as Notch, to coordinate ISC proliferation and differentiation (**Figure 4A**) (Aguirre et al., 2010).

In response to stress or damage to the intestinal epithelium, a different aspect of EGFR signalling comes into play. During these events, cytokines and JAK/Stat signalling ligands, notably Upd2 and Upd3, are secreted by enterocytes. These ligands activate JAK/Stat signalling in stem/progenitor cells, leading to the release of EGF-type ligands from multiple sources. This release, in turn, activates the EGFR/Ras/MAPK pathway in ISCs, driving their proliferation and facilitating tissue regeneration (Jiang et al., 2011; Jin et al., 2015). This reciprocal crosstalk between the JAK/Stat and EGFR pathways is essential for effectively managing the balance of ISC proliferation and differentiation under stress conditions (**Figure 4B**) (Bonfini et al., 2016; Kux & Pitsouli, 2014; Ren et al., 2010).

2.3.5. JNK signalling

The JNK (Jun N-terminal Kinase) signalling pathway is another crucial regulator in the adult *Drosophila melanogaster* midgut, essential for maintaining intestinal stem cell (ISC) homeostasis (Herrera & Bach, 2021).

Under normal homeostatic conditions, JNK signalling contributes to the regulation of ISC self-renewal and differentiation. JNK signalling plays a role in the differentiation of ISCs into enteroblasts and absorptive enterocytes (**Figure 4A**) (Gan et al., 2021; Herrera & Bach, 2021).

In response to stress or damage, such as bacterial infection or DNA damage, the JNK pathway exhibits increased activity in different cell types within the midgut, including ISCs, EBs, and ECs (**Figure 4B**) (Lucchetta & Ohlstein, 2012). In ECs, activated JNK induces the expression of Ets21c, an ETS-domain transcription factor, which triggers caspase-dependent apoptosis of damaged cells (Gan et al., 2021). Furthermore, activated JNK in ECs also stimulates the secretion of growth factors and inflammatory cytokines.

In ECs, activated JNK also leads to the nuclear translocation of Yorkie (Yki) and the expression of Hippo (Hpo) pathway target genes. This, in turn, leads to the secretion of Upd (Unpaired) cytokines, which stimulate ISC proliferation through the JAK/STAT signalling pathway (**Figure 4B**) (Ma, 2014; Jiang et al., 2009).

2.3.6. Other pathways

Several other signalling pathways have been identified as regulators capable of maintaining stemness in addition to the traditional signalling pathways responsible for ISC maintenance discussed above (**Figure 4A**).

First, **integrin** activity is crucial in maintaining ISC status (Lin et al., 2013). For instance, ISC maintenance is carried out by the ß-integrin subunit mys and the two α-integrin subunits PS1 and PS3 (Liu & Jin, 2017).

Signal transduction begins with the interaction of integrins, transmembrane receptors, with specific extracellular matrix components (ECM) components. Upon binding to the ECM, integrins undergo conformational changes that activate downstream signalling pathways, essential for regulating various cellular processes, including proliferation and differentiation in ISCs (Lin et al., 2013).

Additionally, integrin signalling intersects with various proliferative signalling pathways, including Wnt/Wg, JAK/Stat, and EGFR, playing a vital role in ISC proliferation. This

signalling also influences cell cycle regulation, particularly during the S phase, which is essential for ISC division and proliferation (Lin et al., 2013).

In *Drosophila,* nutrient availability also modulates ISC division (Loudhaief, 2016). A family of eight insulin-like peptides, designated Dilp1–8, plays a critical role in mediating the **insulin/insulin-like growth factor signalling (IIS) pathway**. This pathway acts as a sensor linking the fate choice of enteroblasts (EBs) and the growth of enterocytes (ECs) to the availability of nutrients in the gut lumen (Miguel-Aliaga et al., 2018; Strilbytska et al., 2020).

There are also negative feedback mechanisms that act to limit excessive ISC proliferation. Certain cells within the *Drosophila* midgut, such as enterocytes and enteroendocrine cells, secrete **Bone Morphogenetic Protein (BMP**), a member of the Transforming Growth Factor Beta (TGF-β) family, as a response mechanism to regulate the proliferation of intestinal stem cells. BMP, through its specific ligands, decapentaplegic (dpp), glass bottom boat (gbb), and screw (scw), activates a negative feedback loop. BMP then binds to receptors on the ISCs, signalling them to reduce their division rate or enter a quiescent state.(Guo et al., 2013; Tian & Jen, 2014, 2017).

The Hippo signalling pathway is also highly conserved and crucial for controlling organ size, tissue regeneration, and tumorigenesis (Zhao et al., 2011; Zheng & Pan, 2019).

Core components include the kinase Hpo, the kinase Warts, and the transcriptional coactivator Yorkie. When active, Hpo phosphorylates Warts, inhibiting Yorkie, leading to its cytoplasmic retention and degradation. This inactivation prevents Yorkie from entering the nucleus and activating genes related to cell proliferation and survival (Meng et al., 2016; Pan, 2010). In contrast, inactivation of the pathway allows unphosphorylated Yorkie to enter the nucleus and partner with transcription factors like Scalloped, activating genes promoting cell proliferation and tissue growth (Meng et al., 2016).

Moreover, the Hippo pathway influences cell proliferation via non-cell-autonomous mechanisms. For example, alterations in Hpo signalling or Yorkie overexpression in enterocytes stimulate ISC proliferation indirectly. Additionally, the pathway interacts with others, such as JAK-Stat and EGFR, to regulate ISC proliferation (Antonello, 2017; Ren et al., 2010).

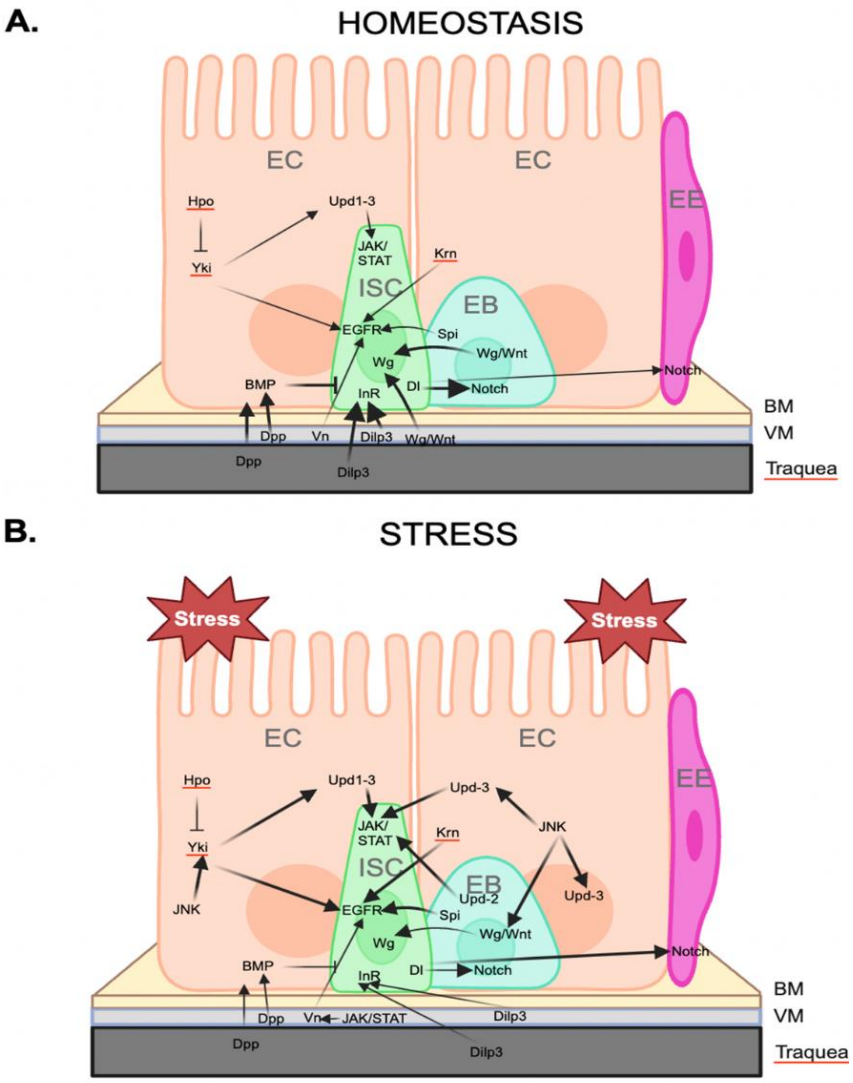

Figure 4. Homeostasis in the *Drosophila* Midgut. A. Under homeostatic conditions: Key signalling pathways — BMP, Wg/Wnt, EGFR, JAK/Stat, and Notch — and their roles in ISC regulation. The BMP pathway, through Dpp, modulates ISC proliferation. The Wg/Wnt pathway contributes to ISC maintenance via Wg signalling. EGFR pathway activation, through Spi, influences ISC proliferation. The JAK/Stat pathway, triggered by Upd1-3, is also involved in ISC maintenance. Notch signalling maintains equilibrium between ISC self-renewal and differentiation through interactions with EBs. **B. During stress response:** Upregulation of pathways that promote tissue regeneration and ISC proliferation. The JAK/Stat pathway, particularly through Upd3, shows increased activity under stress. The EGFR pathway, with ligands like Krn and Spi, responds to stress by facilitating rapid ISC proliferation. JNK signalling becomes more active under stress, thereby adapting ISC behaviour to stress. Thicker arrows denote a stronger influence or increased activity of the respective pathways. *Illustration created with BioRender.com.*

2.4. Neutral competition model in the midgut of the adult *Drosophila* melanogaster

Homeostasis in flies, as in mammals, is maintained by both asymmetric divisions and population asymmetry. Research by de Navascués et al. (2012) in the adult *Drosophila* midgut showed that ISC division could result in three potential outcomes: asymmetric fate division (producing one ISC and one EB), symmetric duplication (two ISCs), or symmetric differentiation (two EBs), with the latter two outcomes occurring with equal frequency to ensure balanced maintenance of stem cell numbers (**Figure 5A**). This process is governed by neutral competition (de Navascués et al., 2012; Guisoni et al., 2017; Joly & Rousset, 2020).

The authors elaborated further to suggest a molecular mechanism for the neutral competition model based on Dl-N signalling involved in lateral inhibition (**Figure 5A**). This mechanism would play a crucial role in regulating ISC self-renewal and differentiation to govern the stochastic fate decisions of ISCs and EBs, contributing to the overall balance and maintenance of the ISC population.

The following sections outline the approach used by de Navascués et al. (2012) to demonstrate the neutral competition model in *Drosophila*.

2.4.1. Methodological approach to demonstrate the neutral competition model

To demonstrate neutral drift dynamics in the *Drosophila* midgut, de Navascués et al. (2012) utilised a heat shock-inducible genetic labelling system (tub-FRT-lacZ clones) to trace lineages of individual cells, which specifically follows only actively dividing clones. This system was complemented with Delta (Dl) staining to visualise ISCs.

Subsequent analysis of the fate of individual clones after division revealed three possible outcomes: the presence of persistent clones consisting of two or more cells expressing Dl, indicating symmetric duplication, i.e. two ISCs (**Figure 5Bi-ii**); multicellular clones lacking Dl expression, suggesting two differentiated cells (**Figure 5B iii-iv**); and single-cell clones with only one Dl+ cell, signifying asymmetric division resulting in one ISC and one differentiated cell (**Figure 5B v-vi**) (de Navascués et al., 2012).

The study also observed clonal size and density over 16 days, noting a gradual decrease in the number of clones accompanied by an expansion of the surviving clones. This pattern supports the concept of neutral drift, where stem cells compete neutrally for niche access and survival, leading to random expansion and contraction of stem cell

clones until one either takes over the niche or is lost (Lopez-Garcia et al., 2010) (**Figure 5 C-E**).

To fit their observations, the researchers developed a theoretical framework to model the turnover of intestinal stem cells. This mathematical model simulated the short-term clonal evolution of ISCs seen by the researchers in the midgut epithelium, integrating key parameters such as the ISC division rate (λ) and the frequency of symmetric divisions (r). The model effectively predicted clonal expansion and turnover dynamics, corroborating experimental data and observations of clonal fate in the *Drosophila* midgut. (de Navascués et al., 2012) (**Figure 5F**).

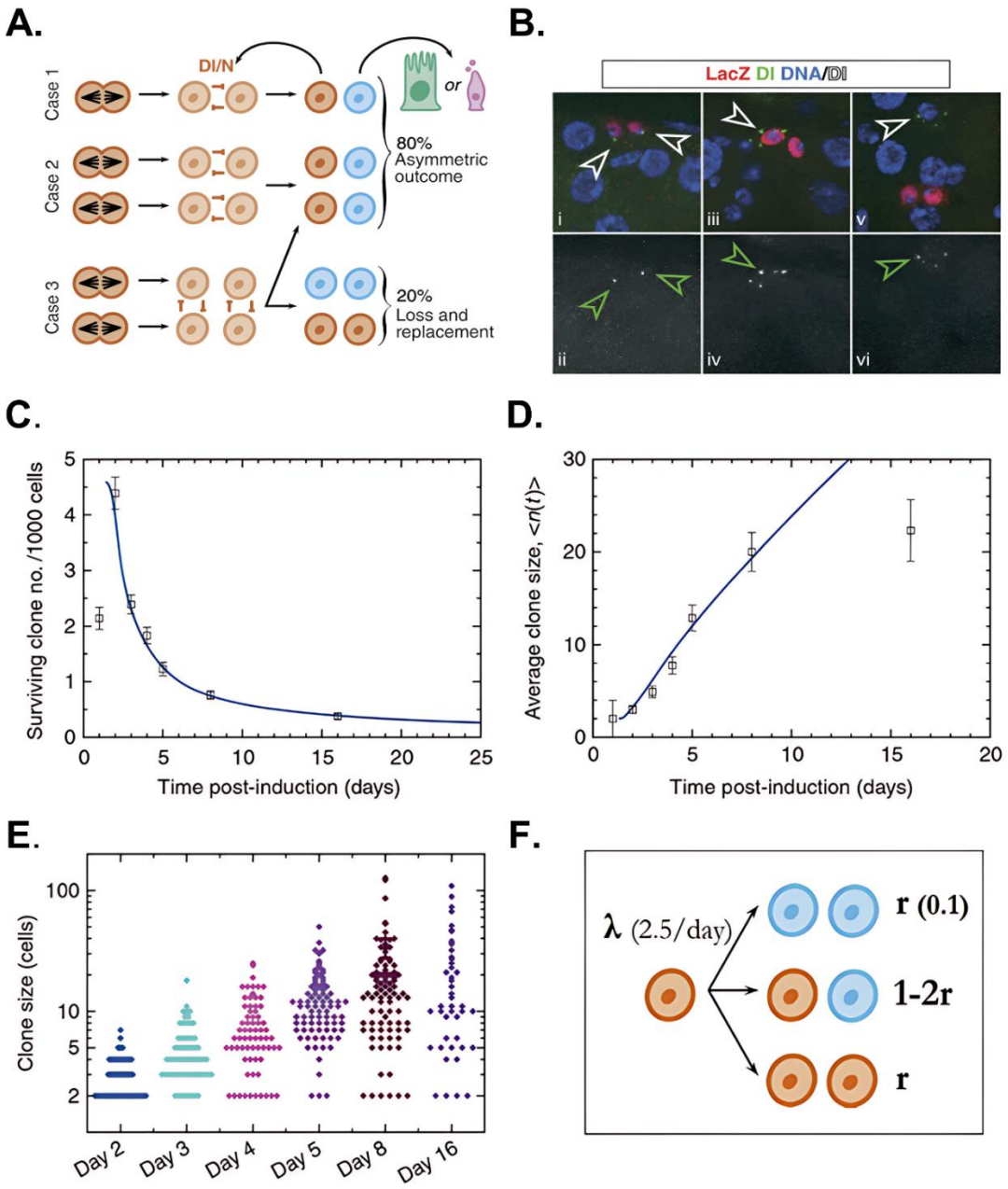

Figure 5. Tissue homeostasis through neutral competition in the *Drosophila* adult midgut. A. ISC division outcomes: 1) One division leads to sibling cell competition, yielding asymmetric outcomes. 2) Divisions among adjacent ISCs promote lateral inhibition, creating exclusive cell fates. 3) Non-sibling cell competition influences symmetrical or asymmetrical divisions, impacting ISC replacement. About 20% of divisions result in turnover. **B. Lineage tracing** confirms neutral competition with outcomes of symmetric duplication, asymmetric fates, or symmetric differentiation**. C. Clone density** decline over 16 days**. D. Increasing average clonal** size over time. **E. Variability in clone sizes. F. Quantitative mode**l explains clonal behaviour and ISC turnover in midgut epithelium. *Adapted from (de Navascués et al., 2012).*

2.5. Contradictions in the neutral competition model

2.5.1. Discrepancies in turnover rate

Although the mathematical modelling effectively accounted for the experimental observations, it also yielded estimates for the division rate that conflicted with previous findings.

The lambda parameter, representing the rate of ISC turnover, was estimated to be 2.5 days (**Figure 6D**) in the neutral competition model, suggesting a rapid turnover of approximately 5 days. This contrasts with Jiang et al. (2009) estimation of an ISC turnover time of 12 days.

The discrepancy could arise from differences in experimental design: de Navascués et al. (2012) utilised a proliferation-based method for clonal labelling that specifically targets actively dividing ISCs, which may primarily capture faster-turnover regions. Conversely, Jiang et al. (2009) employed a method tracing both already dividing and non-dividing cells, likely offering a more comprehensive view of the entire tissue, including regions with slower turnover and faster turnover.

This suggests that de Navascués et al.'s method may selectively capture areas with rapid turnover, while Jiang et al.'s method encompasses both rapid and slow turnover regions.

However, it remained unclear whether regions of rapid and slow turnover can coexist. If slow and fast turnover areas could coexist, it would pose a challenge to a fundamental assumption of the neutral competition model: that ISCs within the same stem cell compartment share the same division rate or λ.

2.5.2. Spatial heterogeneity and turnover dynamics

Further studies indicated heterogeneity in turnover rates across different gut regions, suggesting that rapid and slow turnover areas can indeed coexist within the intestinal tissue (Antonello et al., 2015; Antonello, 2017). This observation further challenged the notion of uniform division rates across the ISC compartment, as assumed by the neutral competition model.

2.6. Existing tools to study the neutral competition model in *Drosophila*

The technical differences in lineage tracing methods used by de Navascués et al. and Jiang et al., particularly the variation in induction temperatures (37°C for single ISC tracing and 29°C for compartment tracing, respectively), are key factors that could

explain the source of the discrepancies in turnover rate estimates. Given the impact of temperature on Drosophila fitness, discrepancies in turnover rates observed between studies may partly stem from these temperature-induced differences in experimental setups.

Despite the importance of validating the hypothesis using methods independent of temperature and other possible confounding factors, the currently available tools for gene expression analysis present several limitations..

2.6.1. Gene expression systems in *Drosophila*

The Gal4-UAS system is a widely utilised binary transgene expression platform that facilitates targeted gene expression in various organisms, including *Drosophila melanogaster* (Meissner et al., 2023). This system comprises two essential components: the Gal4 driver and the UAS responder. The Gal4 driver is a transgenic line that expresses the yeast-derived transcriptional activator Gal4 under specific regulatory regions. Conversely, the UAS responder contains the gene of interest under the control of Gal4 binding sites, known as upstream activation sequences (UAS) (**Figure 6A**) (Brand & Perrimon, 1993; Duffy, 2002; McGuire, Roman, et al., 2004; Yamaguchi & Yoshida, 2018).

The Gal4-UAS system offers several advantages that contribute to its popularity in genetic research. This system is highly versatile and modular, permitting the combination of various genetic tools and techniques (Qian et al., 2023). Furthermore, it is compatible with other genetic tools, allowing the integration of multiple approaches to studying gene function (Elliott & Brand, 2008; Qian et al., 2023).

One of the key advantages of the Gal4-UAS system is the extensive catalogue of available lines, which offers remarkable diversity and specificity for research purposes. This collection is invaluable for studying gene expression and function in precise cell types, tissues, and developmental stages. The Bloomington *Drosophila* Stock Centre (BDSC) maintains an extensive collection of over 22,000 Gal4 or UAS lines. This repository, contributed to by researchers globally, encompasses a broad range of biological contexts and is readily available to the scientific community (*Bloomington Drosophila Stock Centre*, n.d.).

However, the Gal4-UAS system has limitations, prompting efforts within the scientific community to enhance its precision. A key challenge is the lack of cell-type specificity, as Gal4 can be expressed in various cell types. The Split Gal4 system addresses this by

enabling more precise control over where and when genes are expressed. It does this by combining the DNA-binding domain of GAL4 with a transcriptional activator, each part encoded by separate transgenes regulated by different sequences. This approach significantly refines spatial and temporal control of gene expression.

Additionally, the Gal-4 UAS system is not reversible, meaning that once gene expression is induced, it cannot be turned off, making it challenging to study the effects of gene expression changes over time. (Potter et al., 2010).

2.6.2. The Gal4 Gal80ts System:

The Gal80ts system is a variation of the Gal4 system that offers precise temporal and tissue-specific control over gene expression (Caygill & Brand, 2016). It comprises two key components: the Gal4 driver, which expresses Gal4 under tissue-specific promoters, and Gal80ts, a temperature-sensitive repressor protein that inhibits Gal4 at permissive temperatures (McGuire, Mao, et al., 2004). Shifting the temperature to the restrictive range inactivates Gal80ts, enabling gene expression. However, this system has limitations, including incomplete repression in specific contexts and design considerations (**Figure 6B**).

Moreover, temperature fluctuations can impact *Drosophila* behavior and metabolism, adding further complexity to experimental design considerations (Ito & Awasaki, 2022).

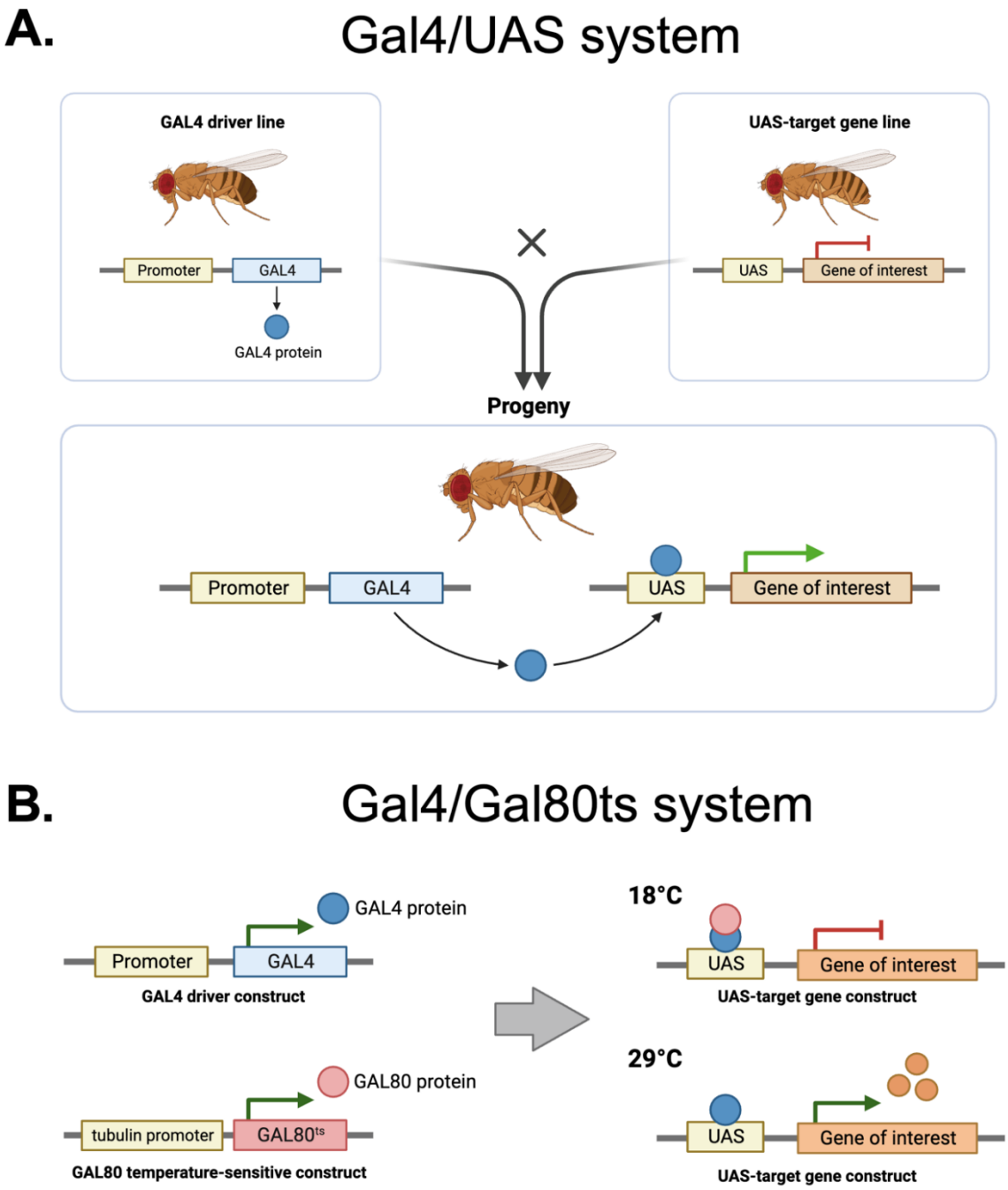

Figure 6.Gal4-UAS system and Gal80ts system. **A. Gal4-UAS system:** This system utilises a Gal4 driver line, which contains the Gal4 gene controlled by a specific promoter, crossed with a UAS-target gene line. In the offspring, the Gal4 protein, expressed from the driver line, binds to the UAS sites on the target gene line. This binding activates the gene of interest's expression in designated tissues. **B. Gal80ts system**: A Gal4 driver construct, designed to produce Gal4 protein under a specific promoter, is paired with a Gal80ts construct, which encodes a temperature sensitive Gal80 protein that inhibits Gal4 activity. At 18°C, Gal80 effectively inhibits Gal4, thereby preventing the target gene's activation. Conversely, at 29°C, Gal80ts is inactivated by the higher temperature, lifting the inhibition on Gal4, and allowing for the activation of the target gene. *Illustration created with BioRender.com.*

2.6.3. The GeneSwitch System

The GeneSwitch system is a versatile tool used for spatial and inducible control of gene expression in *Drosophila* (McGuire, Mao, et al., 2004; Nicholson et al., 2008; Roman et al., 2001). This system comprises a tripartite fusion protein referred to as GeneSwitch. It combines the Gal4 DNA-binding domain, the progesterone receptor ligand-binding domain, and the p65 transcriptional activation domain (Li & Stavropoulos, 2016; Scialo et al., 2016). Activation of this system occurs with the presence of RU486, a progesterone receptor agonist, which induces gene expression downstream of Gal4-bound UAS elements (**Figure 7A**) (Mak et al., 2022).

Upon adding RU486, the GeneSwitch molecule undergoes a conformational change to an active state. In this state, it binds to the UAS sequences (**Figure 7A**). This enables precise temporal control of gene expression (Morant et al., 2023)

GeneSwitch system, while useful, has significant drawbacks. RU486, the critical component of the system, can negatively affect crucial aspects of *Drosophila* biology. These include lifespan, fertility, and female metabolism, as found in recent studies (Landis et al., 2015; Li & Stavropoulos, 2016; Yamada et al., 2017; Zappia et al., 2023).

2.6.4. The AID System

The Auxin-Inducible Degradation (AID) system is engineered to precisely control the degradation of proteins within *Drosophila* cells. This auxin-dependent mechanism allows for the rapid and reversible depletion of proteins, providing a powerful tool for dissecting complex protein functions in a living organism.

This system is particularly useful to conditionally induce the degradation of any protein by the proteasome, simply by the addition of the plant hormone auxin (Shetty et al., 2019, Trost et al., 2016) .

Within this system, degradation proteins are engineered to include an AID degron sequence. In the absence of auxin, the plant hormone required for this system's activation, an AID-tagged protein such as Gal80 remains functional. Gal80 binds to the Gal4 transcription factor, repressing gene expression (**Figure 7B**) (Nishimura et al., 2009; Shetty et al., 2019).

Upon the introduction of auxin, the AID degron-tagged Gal80 binds to the SCF complex, which includes the TIR1 F-box protein of plant origin. Auxin acts as a signalling molecule that allows TIR1 to recognise and attach to the AID-degron, leading to the proteasome's polyubiquitination and subsequent degradation of Gal80. With the degradation of Gal80,

the repression is lifted off the Gal4, which can then activate the transcription of the target gene (**Figure 7B**). This auxin-dependent regulation allows for the conditional control of gene expression in *Drosophila* research (Calderon-Villalobos et al., 2010; W. Chen et al., 2018; Lambrus et al., 2018; Trost et al., 2016).

While beneficial, the AID system is not without its limitations, including potential off-target effects due to auxin interacting with non-target proteins and the requirement for genetic modification to insert the AID tag (Bence et al., 2017; Tanaka et al., 2015).

2.6.5. the Q system

The Q-system is a binary expression platform used for targeted gene expression in *Drosophila*, similar to the widely known Gal4-UAS system (Potter & Luo, 2011). The Q-system includes two primary components: a "driver," which is a transgene containing cell-specific enhancer and promoter sequences linked to the QF transcription factor, and a "reporter," which consists of transgenes with the QF binding sequence QUAS, positioned before genes coding for various output molecules like fluorescent proteins or ion channels (**Figure 7C**) (Li & Stavropoulos, 2016; Riabinina & Potter, 2016).

Additionally, this system incorporates a "repressor" component that carries the QS gene, usually positioned downstream of UAS or other enhancer elements, to inhibit the action of the QF protein. A pharmacological agent, usually quinic acid, can inactivate the QS repressor, allowing QF to activate gene expression through QUAS (Potter et al., 2010; Potter & Luo, 2011) (**Figure 7C**) .

"Driver and "reporter" transgenes are maintained in separate fly stocks and combined through genetic crosses for experimental use, enabling researchers to activate gene expression in specific cell types and at particular developmental stages as required (Potter et al., 2010; Potter & Luo, 2011).

However, the QF/QUAS system does present some challenges. It is generally less efficient than the Gal4-UAS system, with QF/QUAS-induced transgene expression in *Drosophila* being approximately 30-fold less effective. This lower level of efflimit the maximum strength and reach of gene expression that can be achieved using the QF/QUAS system (Potter et al., 2010).

Additionally, the QF/QUAS system may have a more limited repertoire of driver lines and tools compared to the extensively characterised Gal4-UAS system.

In summary, while alternative gene expression systems offer valuable options for precise control of gene expression in *Drosophila*, they may not fully substitute for the Gal4-UAS

system in the study of ISC-driven tissue dynamics due to specific limitations and potential challenges associated with their use in this context.

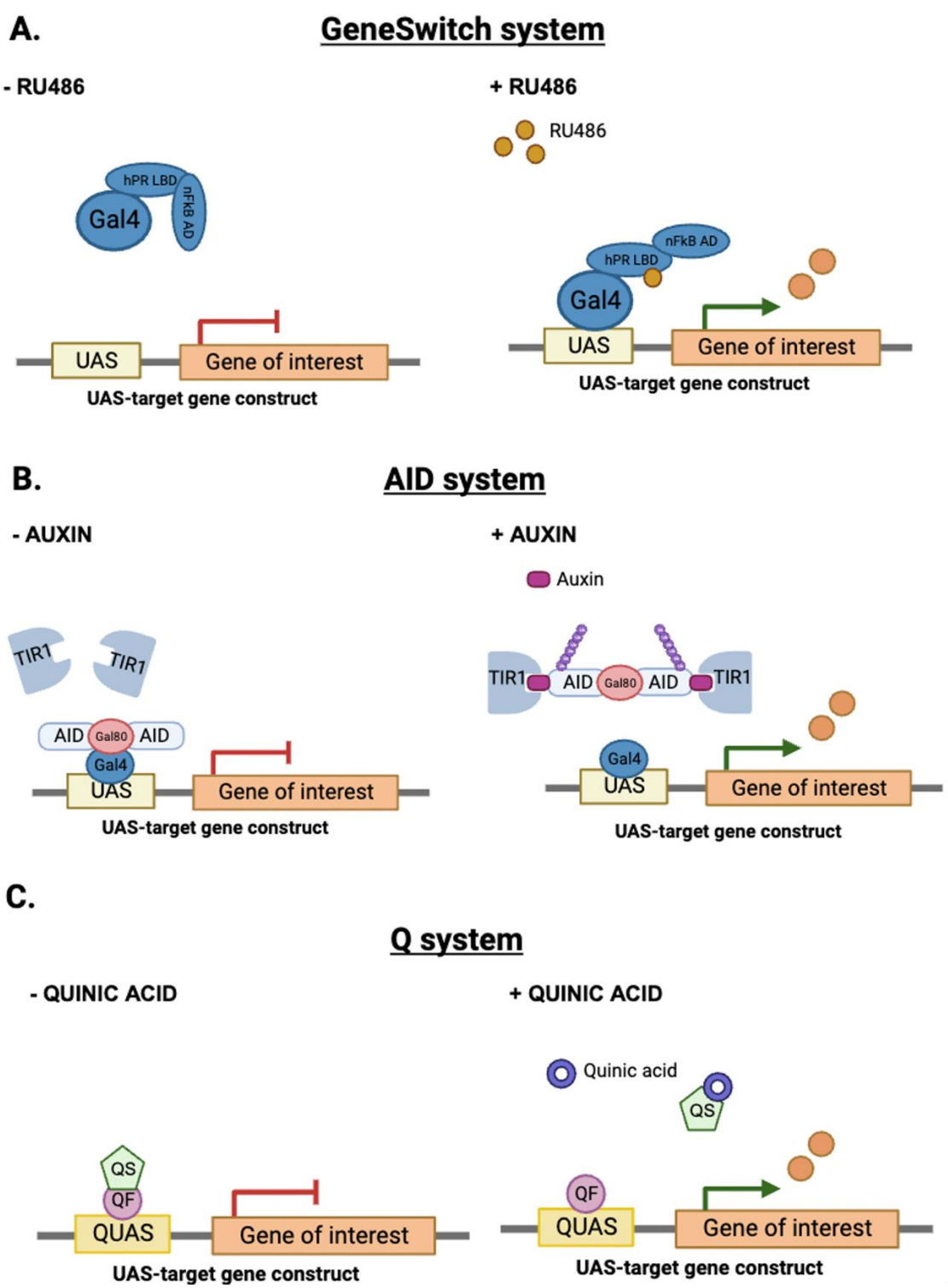

Figure 7. Additional gene expression system in *Drosophila melanogaster*. A. GeneSwitch System: **A. GeneSwitch:** The Gal4-drug domain fusion is inactive without RU486, keeping the target gene off. RU486 induces a conformational change that activates the Gal4 fusion, starting transcription. **B. AID System:** Gal80 with an AID degron is stable without auxin, suppressing gene expression. Auxin triggers SCF-TIR1 to degrade AID-tagged Gal80, allowing Gal4-driven transcription. **C. Q System:** QS repressor binds QF, preventing gene activation. Quinic acid inactivates QS, enabling QF to activate the target gene. *Illustration created with BioRender.com.*

3 Aims of the thesis

This thesis seeks to refine the existing model of neutral competition in the *Drosophila* midgut to accommodate the observed variation in intestinal stem cell (ISC) division rates across different compartments while maintaining consistent rates within the same compartment.

Recognising that homeostasis involves more than balancing division rates, differentiation, and cell loss, this research also aims to elucidate the role of bHLH transcription factors Daughterless (Da) and Scute (Sc) in regulating the differentiation of ISCs into the enteroendocrine lineage.

Furthermore, the study aims to introduce and validate the safety of a new misexpression system designed to enable precise ON/OFF control of gene expression independent of temperature. This system is specifically tailored for investigating midgut homeostasis and is proposed to operate across various Gal4-UAS genetic lines

These three main objectives are further divided into sub-objectives.

1. Proposal and validation of neutral competition model refinement in the *Drosophila* midgut:
    - Propose a new theoretical model to accurately describe the dynamics of ISC division rates.
    - Validate the proposed model through immunohistofluorescence experiments measuring ISC division rates using cell cycle markers.
    - Explore the molecular signals that may support the model using weighted gene correlation network analysis (WGCNA).
2. Investigation of bHLH transcription factors Daughterless and Scute in ISC differentiation into EE:
    - Quantify changes in cell populations across various genetic manipulations involving two bHLH factors, Daughterless and Scute.
    - Compare the outcomes of ISC-EE fate decisions with two theoretical frameworks, the Sc Threshold and Da Titration models.

3. Proposal of an innovative misexpression system:
    - Propose a gene misexpression system that operates independently of temperature conditions.
    - Conduct tests to assess the efficacy and safety of the exogenous ligand, the TMP antibiotic, proposed for use within the misexpression system, ensuring precise ON/OFF gene control.

CHAPTER 2: UNDERSTANDING THE DYNAMIC SHIFT FROM STATIC HOMEOSTASIS TO PULSED TURNOVER IN *DROSOPHILA* MIDGUT TISSUE REPLACEMENT

1 Introduction

The human intestinal tract, the second-largest epithelium in the human body, serves two critical functions: nutrient uptake and protection against environmental challenges (Gehart & Clevers, 2019). Its importance stems from its role as a hub for immune cells, its connection to diet, and its impact on the microbiome (Allaire et al., 2018; W. Li et al., 2022; Okumura & Takeda, 2017). Failures in maintaining intestinal homeostasis can lead to a spectrum of conditions, including cancer, obesity, autoimmune diseases, food intolerances, and even mental disorders (Barker, 2014; Clapp et al., 2017; Maloy & Powrie, 2011; Peterson & Artis, 2014; Winer et al., 2016).

Homeostasis within the intestinal epithelium relies on continuous cell turnover, primarily driven by ISCs. Asymmetric division, where one daughter cell retains stem cell identity while the other specialises, replenishes the stem cell pool and generates differentiated cells for tissue maintenance and repair (Montagne & Gonzalez-Gaitan, 2014a; Sei et al., 2019; Zeng & Hou, 2015). However, asymmetric division is not the only mode of ISC division in the intestine. Symmetric division, where both daughter cells share the same fate—either both becoming differentiated cells or both remaining as ISCs—is also present and plays a central role in maintaining homeostasis (de Navascués et al., 2012; Joly & Rousset, 2020; Lopez-Garcia et al., 2010; Sei et al., 2019).

Maintaining this equilibrium between symmetric and asymmetric stem cell division is essential for tissue maintenance, repair, and disease prevention (Stine & Matunis, 2013). Understanding the mechanisms governing this balance is crucial for unravelling how ISCs maintain homeostasis. *Drosophila* and mammalian intestinal epithelia share genetic and cellular similarities, making flies an excellent model for further studying these ISC dynamics (Jiang & Edgar, 2012; Losick et al., 2011).

Studies in *Drosophila* have indicated that ISC clones expand or contract through neutral competition among symmetrically dividing ISCs (de Navascués et al., 2012; Guisoni et al., 2017). Nonetheless, the mathematical modelling necessary to interpret the clonal behaviour supporting this neutral competition rests on a critical assumption: ISCs within the stem compartment share the same division rate. While the mathematical models can explain the lineage behaviour quantitatively and qualitatively, this assumption of uniform turnover rates is at odds with other observations. Antonello et al. (2017) showed that turnover is not uniform across stem cell compartments; there are areas with different

replacement rates, which, in principle, contradicts the assumption of the neutral competition model.

1.1. The quiescence-division switch model: a refinement for the model of neutral competition

To address these contradicting observations, we propose a refined model for intestinal tissue replacement in the adult *Drosophila* midgut: the quiescence-division switch model. This model proposes that in homeostasis, ISCs could either be quiescent ($\lambda \approx 0$) or dividing ($\lambda > 0$), a duality that the traditional model of neutral competition with constant turnover baseline fails to capture. This new model could potentially revolutionise our understanding of ISC dynamics (de Navascués et al., 2012).

Our model proposes that all ISCs in the same vicinity would have the same λ value, allowing for different division rates ($\lambda \approx 0$ or $\lambda > 0$) as long as the value is shared locally within the stem compartment. This explains the heterogeneity shown in lineage-tracing experiments (Antonello, 2017; Antonello et al., 2015) and provides a practical framework for understanding tissue replacement dynamics. In areas of no tissue replacement, ISCs would remain quiescent, while in areas of rapid cell renewal, ISCs would be dividing at a uniform rate (**Figure 8**).

Our hypothesis raises the question of what triggers the switch from quiescence to division. The technical differences between lineage tracing experiments for single ISC tracing (de Navascués et al., 2012) or compartment tracing (Jiang et al., 2009) can shed some light on this. Specifically, using different induction temperatures (37°C vs 29°C, respectively) suggests that temperature could be critical in this switch. We propose that the inductive heat shock (HS) of 37°C for 60 min used in the lineage-tracing experiment to model the clone size data (de Navascués et al., 2012) could be triggering the ISC switch from quiescence to division (**Figure 8**).

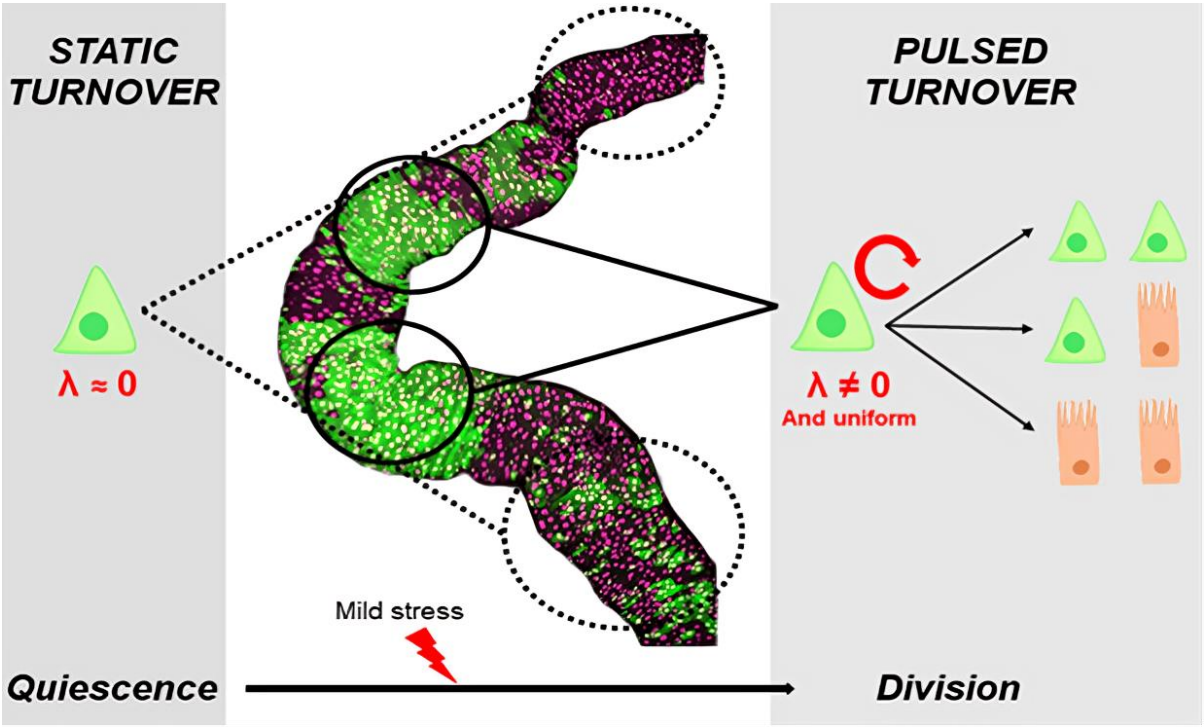

Figure 8. The quiescence-division switch model for ISC dynamics in homeostasis. This theoretical model suggests two states for ISCs under homeostatic conditions: a static state with no division (λ≈0) and a dynamic state where division occurs (λ>0). The model hypothesises that mild environmental stress, such as a sub-lethal heat shock, could trigger the switch from quiescence to division among ISCs.

1.1.1. Exploring the role of the cell cycle in the quiescence-division model

Integrating cell cycle markers into this model provides a valuable tool for testing this hypothesis. This visualizativisualisation the identification and characterisation of actively dividing ISCs, providing empirical evidence for the existence of dual division rates in different regions of the intestinal stem compartment, under homeostatic conditions.

Furthermore, the temporal expression and localisation of these cell cycle markers enable us to assess the correlation between the presence of dividing ISCs and the rate of tissue renewal. If the hypothesis holds true, one would expect to observe a direct relationship between the expression of cell cycle markers and the division rates of ISCs in different intestinal regions. Such empirical data would strengthen the validity of the proposed model, supporting the idea that ISCs can exist in distinct states of quiescence and active division depending on their local microenvironment or stress sensing.

In conclusion, using cell cycle markers to study intestinal stem cell behaviour in homeostasis offers a promising opportunity for validating the hypothesis outlined. By providing a visual and quantitative assessment of ISC division rates in different tissue regions, cell cycle markers can substantiate the existence of the dual division rate phenomenon and, in turn, reinforce the proposed model's explanation for ISC heterogeneity in the context of tissue maintenance and renewal (Liu et al., 2019).

The cell cycle is a highly regulated process consisting of four distinct stages: G1 (Gap 1), S (Synthesis), G2 (Gap 2), and M (Mitosis). These stages are regulated by various proteins, including cyclin-dependent kinases (CDKs), cyclins, and CDK inhibitors (CDKIs). The cell cycle progression is tightly controlled to ensure accurate DNA replication and cell division (He et al., 2022).

In the G1 phase, cells prepare for DNA replication and growth. The key factors during this phase include cyclin-dependent kinases (CDKs), cyclins, and cyclin-dependent kinase inhibitor proteins (CDKI). CDKs are enzymes that regulate the progression of the cell cycle, and cyclins are proteins that bind to CDKs to activate their kinase activity. CDKIs, on the other hand, inhibit the activity of CDKs and act as negative cell cycle regulators. During the G1 phase, CDKs remain inactive, and cell cycle progression is governed by cyclin-dependent kinase inhibitors (CDKIs),ing Dacapo (Bertoli et al., 2013). Dacapo serves a critical CDK inhibitor during G1, effectively inhibiting cell proliferation and inducing cell cycle exit (Kim et al., 2021; Swanson et al., 2015).

During this phase, the chromatin licensing and DNA replication factor 1 (Cdt1) is expressed and is involved in preparing the cell for the next phase, where DNA replication will occur. It is involved in the licensing of DNA replication origins (Matson et al., 2017). Cdt1 is recruited to chromatin-bound proliferating cell nuclear antigen (PCNA) during S phase or after DNA damage, where it is ubiquitinated by the CRL4Cdt2 E3 ubiquitin ligase complex for degradation (Havens & Walter, 2011).

During the S phase, DNA replication takes place, and a key factor involved in this process is indeed PCNA. PCNA is a protein that functions as a processivity factor for DNA polymerase, allowing for efficient and accurate DNA replication (Strzalka & Ziemienowicz, 2011).

After DNA replication, the cell enters the G2 phase, where it prepares for mitosis. As the cell cycle progresses from G2 to the M phase, cyclin-dependent kinase 1 (CDK1), also known as CDC2, assumes a central role in promoting entry into mitosis. CDK1 interacts with cyclin proteins, particularly Cyclin A and Cyclin B, to form active kinase complexes. The Cyclin A/CDK1 complex predominantly operates during the S phase and early mitosis, regulating DNA replication and centrosome duplication (Hégarat et al., 2020; Vigneron et al., 2018). In contrast, the Cyclin B/CDK1 complex becomes prominent during late G2 phasthe e and plays a critical role in initiating various mitotic events, including chromosome condensation, spindle formation, and cell division (Enserink & Kolodner, 2010; Gavet & Pines, 2010; Poon, 2016). These kinase complexes phosphorylate numerous substrates involved in the G2 to M phase transition, including key mitotic regulators such as the anaphase-promoting complex/cyclosome (APC/C), which subsequently promotes the degradation of Cyclin B (Kernan et al., 2018; Zhang et al., 2014).

The critical factors of the M phase, also known as mitosis, include the phosphorylation of histone H3 (PH3) at serine residue 10 (Ser10), which is associated with chromosome condensation and mitotic entry, serving as a marker to distinguish M phase cells from G2 phase cells (Prigent & Dimitrov, 2003; Sawicka & Seiser, 2012).

In some cases, such as the midgut of *Drosophila*, cells, in this case, enterocytes, undergo a modified cell cycle variant known as the endocycle, involving repeated rounds of DNA replication without mitosis, resulting inpolyploidisationn (Fox & Duronio, 2013; Zielke et al., 2011). The endocycle is regulated by factors such as the Cyclin E/CDK2 complex and the CDK inhibitor Dacapo (M. Kim et al., 2021; Zielke et al., 2011). Research has indicated that there is also an increase in PCNA expression during the

endocycle across various fly tissues (Calvi, 2013; M. Kim et al., 2021; Swanson et al., 2015).

1.2. Aim

In our proposed quiescence-division switch model, all ISCs within the same vicinity share the same λ value, i.e., their division rate. The division rate can vary between $\lambda \approx 0$ (no division) and $\lambda > 0$ (division), as long as it is consistent locally within the stem cell compartment.

This hypothesis suggests that the observed heterogeneity in previous lineage-tracing experiments can be explained by the uniform division rate of ISCs in areas of tissue replacement and the quiescent state of ISCs in non-renewing regions.

Additionally, we propose that the switch from quiescence to division in ISCs can be triggered by a sub-lethal stressor, such as a heat shock (HS) of 37°C for 60 minutes, as indicated by differences in induction temperatures between lineage tracing experiments.

The experiments of this chapter aim to characterize the transition from static to dynamic homeostasis in the intestine of adult *Drosophila melanogaster*, specifically focusing on the dynamics of ISCs cell cycle.

2 Materials and methods

2.1. *Drosophila* husbandry

Flies were maintained in plastic tubes containing standard cornmeal medium as food and sealed with cotton bungs. The tubes were placed in fly culture incubators (E-1350-DVL, Ibercex; 1200NP, LMS; 200NP, LSM) with 12-hour light-dark cycles at 25 °C unless otherwise specified.

Fly collection was performed within 24 hours after emergence, and flies were kept in a ratio of 4:3 female/male, with a maximum of 20 female flies per tube. The food was supplemented with dry yeast, and the tubes were flipped every two days. The experiments were conducted using well-fed, 5-days old, mated female flies unless otherwise stated.

2.2. Fly strains

The w^{1118} (BDSC #5905) fly genotype was used to obtain the PH3 data following heat shock (HS). Additionally, the analysis of the different phases of the cell cycle was conducted using the fly strains listed in **Table 1**.

2.3. Heat treatment

To induce heat stress, 3 to 4-day-old, mated female flies in their vials were introduced in a water bath at a temperature of 37°C for 60 minutes and subsequently allowed to recover for 1 day at 25°C before dissection. As a control group, age-matched flies were maintained at a constant temperature of 25°C throughout the entire procedure.

2.4. Gut dissections and immunostaining

Anaesthetised 5-day-old, mated female flies were dissected in a specific PBS formula. Under a dissection microscope (SMZ-2B, Nikon), flies were held ventral side up at the thorax using forceps. The abdominal epidermis was carefully opened and pulled in the direction of the genitalia to expose the intestine, which was subsequently detached from the fly. The gut was then transferred to a 15-minute fixation in 4 % PFA in PBS.

Following fixation, the intestines were transferred to methanol for 15 minutes. After methanol treatment, the guts were rinsed with PBT 0.1 % (PBS + 0.1% Triton) for three rounds and then washed/blocked in PBT: BSA (PBT + 0.1 % BSA) for three rounds of 15

minutes each. The samples were incubated overnight with primary antibodies diluted in PBT: BSA.

Tissue was stained with primary antibodies overnight (16 hours) at 4 degrees with mild rocking (**Table 2**), followed by 15 min washing in PBT (3x rinses and 3x washes). Tissue was stained with secondary antibodies for 2 hours at room temperature with mild rocking (**Table 3**). DNA was stained with Hoescht 33342 (Sigma Aldrich, B2261) at 1:10,000 (10 µg/ml), which was added alongside secondary antibodies. Tissue was washed as before and mounted in a homemade mounting medium (Glycerol: PBS 80:20 with added propyl gallate 4%).

Table 1. Transgenic *Drosophila* strains used for Chapter 2

STRAIN	SOURCE	REFERENCE
PCNA-EMERALD	BDSC #24904	(Swanhart et al., 2007)
POLO-LACZ	BDSC #11543	

Table 2. Primary antibodies used for Chapter 2.

ANTIGEN	HOST SPECIES	DILUTION	SUPPLIER
GFP	Chicken	1:3000	Abcam
DELTA	Mouse	1:200	DSHB
PHOSPHO-HISTONE 3	Rabbit	1:400	Cell Technologies
CYCLIN A	Rabbit	1:2500	Cell Technologies
CLEAVED CASPASE 3	Rabbit	1:200	Cell Technologies
BETA GALACTOSE	Rabbit	1:410000	Cappel

Table 3. Secondary antibodies used for Chapter 2. All secondary antibodies were used at a working dilution of 1:500, and they were purchased from Sigma-Aldrich.

HOST SPECIES	REACTIVITY	ALEXA FLUOROPHORES (REFERENCE)
DONKEY	Rabbit, Mouse	594 (A21207), 594 (A21203)
GOAT	Rabbit, Chicken, Mouse	488 (A11032), 633 (A21071), 633 (A21052)

2.5. Image detection and processing

Images were acquired using a Zeiss LSM710 Confocal Microscope. Image assembly and figure preparation were performed using ImageJ (Schneider et al., 2012). Manual cell counting was conducted using the Cell Counter Plugin within ImageJ.

ImageJ was utilised to generate maximum or average projections from each channel, and the resulting images were saved as individual TIFF or JPEG files.

For cell data counting, custom CellProfiler version 4.2. pipelines were used (Carpenter et al., 2006).

2.6. Statistical analysis

The analyses were conducted using R software version 1.2.5033, with the ggplot2 library employed for data visualisation (Wickham, 2011).

Pairwise comparisons were performed using t-tests with pooled standard deviation to compare PH3 expression at different time points after heat shock (HS). Additionally, the magnitude of changes in PH3+ cell counts between different time points following HS was calculated to quantify them.

For the exploration of non-linear trends in PH3 expression after HS, a Generalized Additive Model (GAM) was applied. GAM is a statistical tool designed to capture non-linear trends in data (Hastie & Tibshirani, 1986). The formula $f(x) = s(x, 5)$, where $s(x, 5)$ represents a smooth term spanning 5 days, was utilised, as it was the maximum number of degrees of freedom chosen. In contrast, under control conditions, it was found that the data best fit a polynomial regression.

Cyclin-A expressing cell counts was analysed using a one-way ANOVA test, which is appropriate for comparing means across different groups.

The Kruskal-Wallis test was employed for Polo expression data, PCNA expression data, and cell density data. This test is suitable for datasets that do not meet the assumptions of parametric tests.

3 Results

3.1. Heat shock triggers a pulse of mitotically-active ISCs

In our investigation of tissue replacement induction under heat stress, we assessed the rate of stem cell proliferation in the gut. Our primary objective was to substantiate prior unpublished lab findings, which, when modelling clonal size data from (de Navascués et al., 2012), indicated a distinct trend in the rate of division—a wave-like pattern with a peak at day 5.

To confirm these findings and ensure we would not overlook the potential division peak, we conducted an 11-day immunostaining study using the anti-phosphohistone H3 antibody (anti-PH3), well-known for its specificity in labelling dividing cells. We chose this duration to account for the possibility of a higher turnover rate of 12 days, as suggested by Jiang (2009), and we performed analysis on days 1, 3, 4, 7, and 11.

We counted mitotically dividing stem cells using an anti-PH3 antibody in both flies given a heat shock (HS) and age-matched control groups. Our results revealed a significant ($p<0.01$) increase in the number of PH3+ cells on day 4 (14-fold increase) and day 7 (8-fold increase) after HS compared to the baseline on day 1 (**Figure 9A and C**). However, by day 11, the number of mitotic figures expressed by PH3+ cells had significantly decreased, returning almost to baseline levels (**Figure 9A and C**).

The data fitting analysis supported these findings, with a peak at day 5 (**Figure 9A**). In contrast, the control group displayed no significant variation in the number of PH3+ cells over the 9-day experimental period (**Figure 9B**).

The findings suggest that HS triggers tissue turnover, causing an increase in the rate of mitotic ISCs.

However, making "dividing cells" mean the same as "mitotic cells" has limitations. While “mitotic cells” precisely refers to cells during mitosis, “dividing cells” can refer to a broader category of cellular division that encompasses various stages of the cell cycle, not just mitosis. Therefore, equating "dividing cells" with "mitotic cells" may overlook other important mechanisms of cell division and limit our understanding of cellular processes.

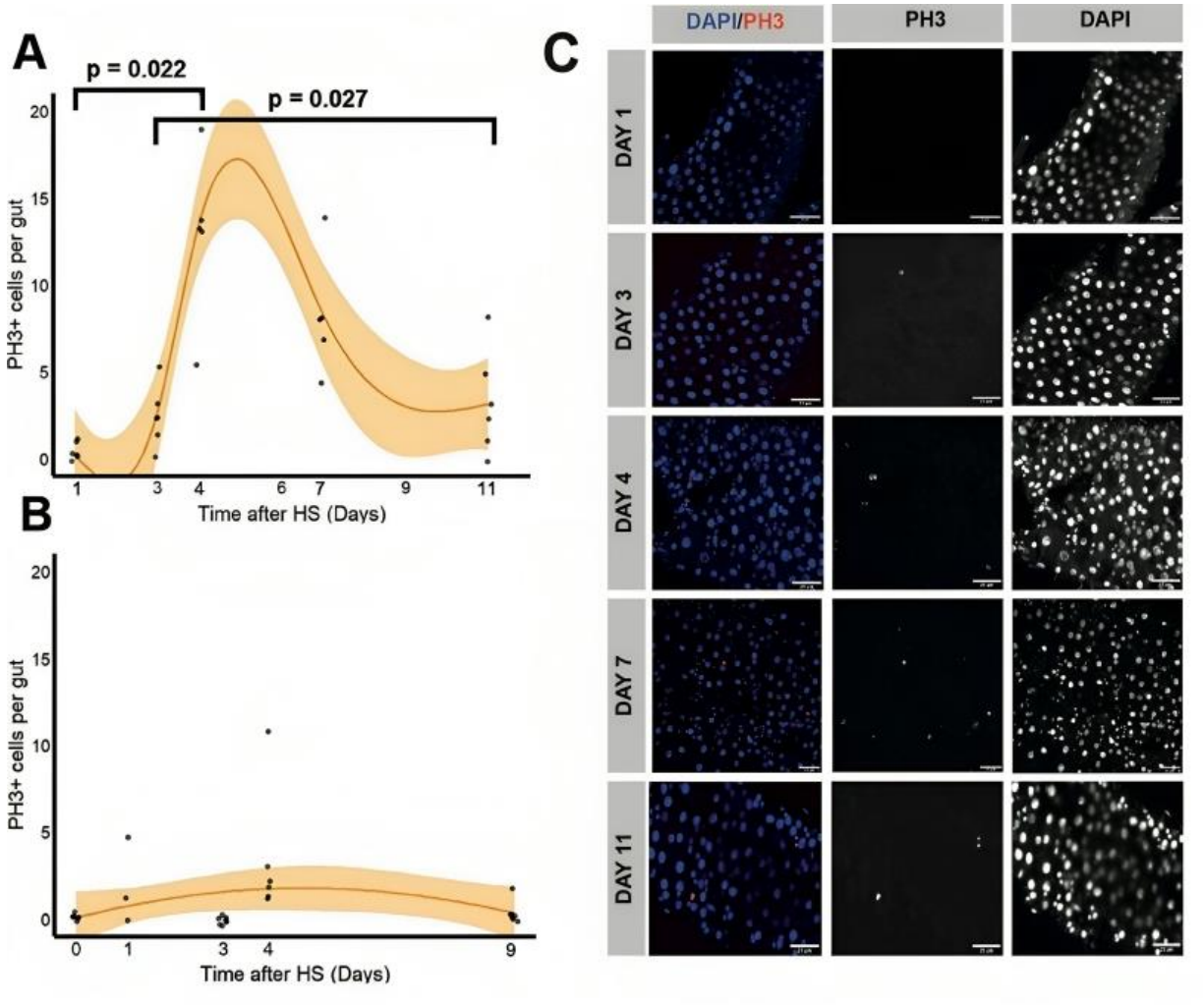

Figure 9. Mitotic figures after HS. A. PH3+ cell quantification after HS: Line plot showing how an increase in PH3+ cells per gut after HS, following a division wave that peaks on day 5. The experimental data after HS was best described by a Generalized Additive Model (GAM) using the formula f(x) = s(x, 5). Each dot represents the number of PH3-positive cells in whole guts (n = 5-7 midguts). Data are presented as the fit ± standard error**. B. Control group PH3+ cell quantification:** Line plot showing PH3+ cell counts in control guts without HS (n= 3-7 midguts), which followed a linear dynamic, best described by the formula f(x) = poly(x, 3). Data are presented as the fit ± standard error**.** Each dot represents the number of PH3 positive cells in whole guts. **C. Immunofluorescence tissue sections:** Tissue sections after HS demonstrate increased PH3-positive cells over time, with a peak between days 4 and 7. Scale bar: 25µm.

3.2. Diverse HS effect dynamics in the different cell-cycle phases

Acknowledging that "dividing cells" span multiple phases throughout the cell cycle is crucial for assessing the rise in cycling cells following heat shock induction (Fendrik et al., 2019; Rhind & Russell, 2012; Wang et al., 2010).

The following analysis extends the scope to include a broader population of actively cycling ISCs, covering S-phase, G2-phase, and M-phase. By considering the proportion of non-quiescent ISCs, we gain a more accurate assessment of overall cell cycle activity.

To evaluate the proportion of cells actively involved in the cell cycle after HS. We examined specific markers, comparing non-heat-shocked and heat-shocked midguts in the 5-day after HS. We chose the 5-day after-stress for our analysis as it coincides with the peak expression of PH3 (**Figure 9A**).

We examined specific markers to better understand the cell cycle stages. We looked at PCNA, which indicates the S-phase, Cyclin-A, related to the G2-M transition, and polo-kinase, which represents the M-phase. We further examined cell identity markers, including Delta (Dl) expression and the S-phase marker PCNA, to identify specifically ISCs going through the S phase. This distinction is vital since PCNA levels also rise in cells undergoing the endocycle, such as enterocytes.

We observed a significant 4-fold increase (p-value<0.05) in the number of cells with high Cyclin-A expression following HS, indicating cell cycle progression from G2 into mitosis (**Figure 10D and E (iv**)). This increase in Cyclin-A levels correlates with the previously observed rise in mitotic figures (PH3+ cells) after HS. However, we did not observe a significant change in the number of Polo+ cells, which represent cells in M-phase, at the peak of the division pulse (5 days after HS) (**Figure 10A and E (i)**).

We anticipated a similar increase in the expression of the S-phase marker PCNA on day 5 after HS. Surprisingly, our results showed decreased PCNA expression following sub-lethal mild stress (**Figure 10B and E (ii)).** Despite the overall decrease in PCNA+ cells, we did not observe a significant variation in PCNA+Dl+ cells (where Dl serves as a marker for ISC cells) following HS (**Figure 10C and E (iii)).**

The expression of these cell cycle markers (Polo, Cyclin-A, and PCNA) exhibited high variability across the tissue, with PCNA being the most pronounced: we observed some areas showing a high density of positive cells while others lacked expression. This

heterogeneity in marker expression may also suggest heterogeneity in stress sensing in the midgut.

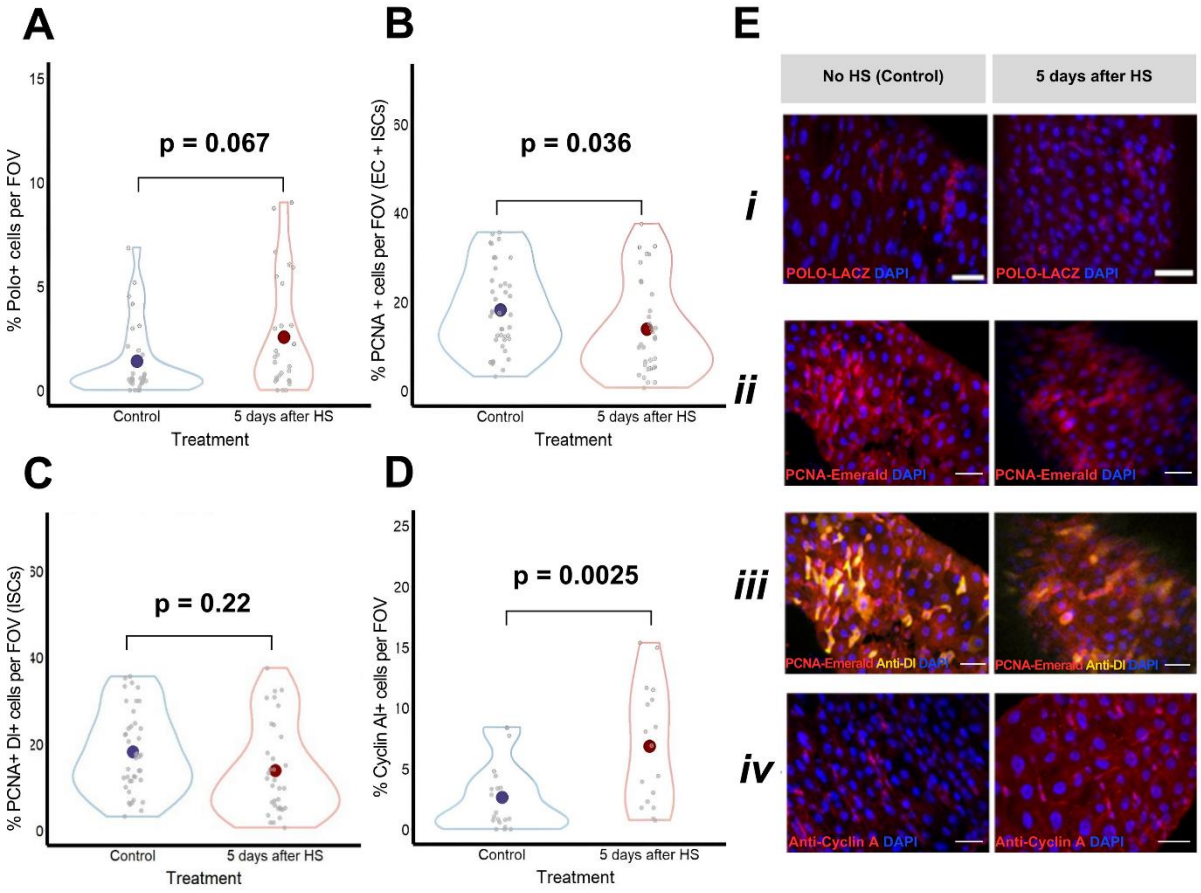

Figure 10. Differential expression of cell cycle markers after HS. Data represented as violin plots overlaid with jittered points for individual field-of-view (FOV) data points and a larger point indicating the mean (n = 5-7 midguts, with all FOVs captured for each midgut). **A. Polo marker analysis:** No significant differences in the M-phase marker after HS. **B. PCNA marker analysis:** Increase in PCNA+ cells 5 days after HS. **C. PCNA and Dl marker analysis:** No variation after HS in the number of ISC PCNA+ cells as Dl serves as a marker of intestinal stem cells. **D. Cyclin A marker analysis:** 50% increase in Cyclin-A^{+} cells after HS. **E. Immunofluorescent tissue-section:** Control and HS-inducted adult fly intestines for the following markers: **i.** polo, **ii.** PCNA, **iii.** PCNA+Delta and **iv.** Cyclin A. Statistical analysis was conducted using a Kruskal-Wallis test for Polo, PCNA, and PCNA-Dl, as well as a one-way ANOVA for Cyclin-A. Scale bar 25µm.

3.3. PCNA+ expression heterogeneity has no spatial specificity

To investigate whether PCNA expression patterns reflect stem compartment differences, we leveraged the findings from independent studies that have extensively characterised the anatomical and functional regions of the gut. These studies have identified five distinct regions in the adult posterior midgut, each exhibiting different regional autonomy of stem cells and diversity in gene expression (**Figure 11A**) (Buchon et al., 2013; Dutta, 2015).

This regional segmentation provides a valuable framework to examine potential variations in PCNA expression across these regions and explore their implications for stem cell behaviour. In examining the expression patterns of PCNA, our goal was to discern whether there is a discernible pattern of PCNA expression that aligns with the regional segmentation of the gut. This would help us understand the spatial aspects of stem cell cycling in relation to tissue homeostasis.

We measured the number of PCNA+ cells across the five regions on day 5 after HS. Although it is noticeable that some areas have a higher number of PCNA+ cells than others, we could not attribute this variation to any midgut regionality. We did not find a correlation between a specific region and a higher density of dividing cells after HS. Overall, the average percentage of PCNA+ cells did not differ significantly across the posterior midgut (**Figure 11B and C**).

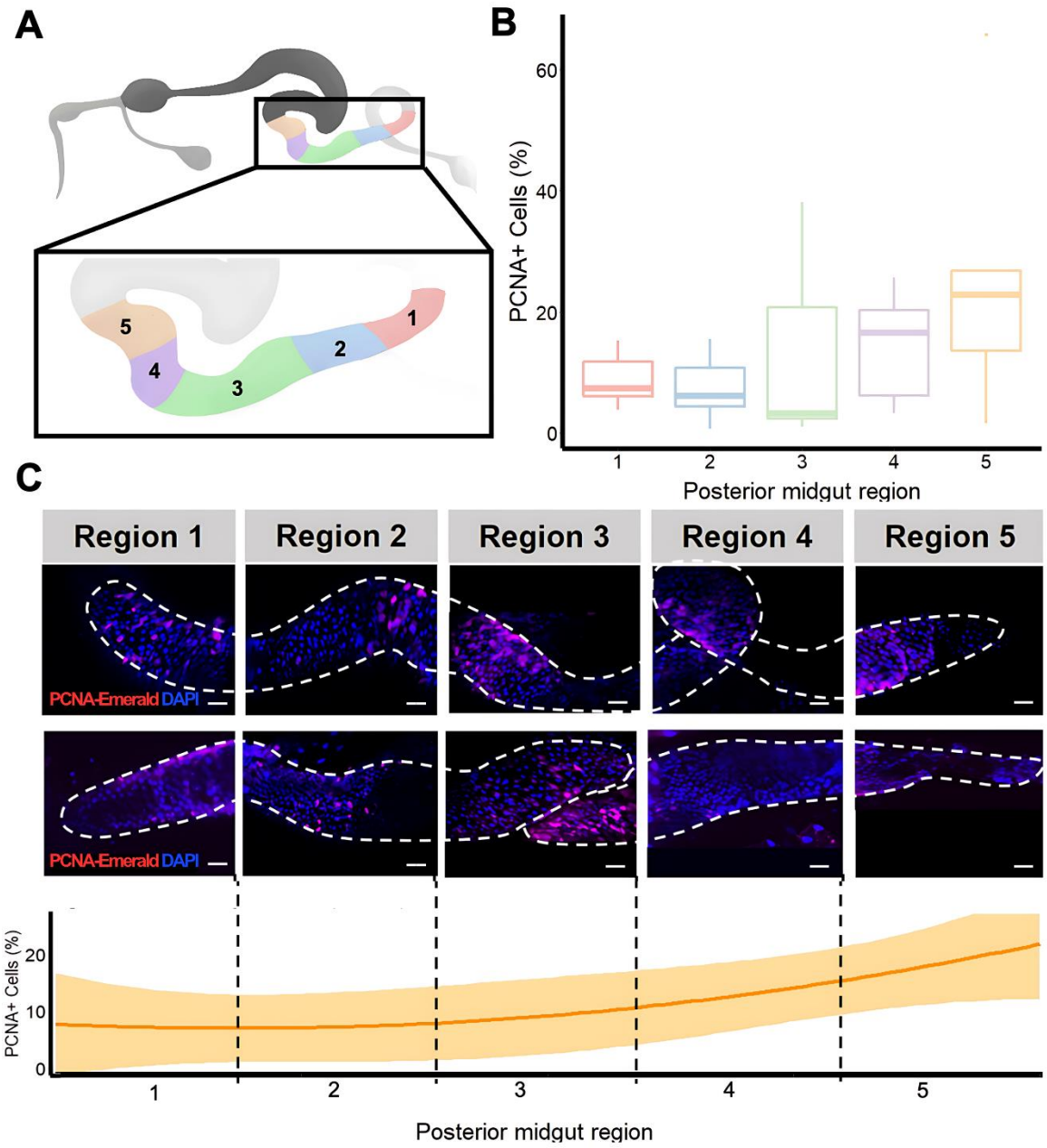

Figure 11. Pulsed turnover heterogeneity has no spatial specificity. A. Midgut compartmentalisation: Schematic of an adult insect intestine, with the posterior midgut emphasised. Detailing of five defined stem cell compartments described by Buchon et al. (2013) and Dutta (2015). **B. PCNA+ cell distribution:** Box plot showing the distribution of PCNA+ cells per FOV across the five regions of the adult fly posterior midgut (n = 5-7 midguts, with all FOVs captured for each midgut). **C. Visualization of PCNA+ cells after HS**: Two representative images of complete adult posterior midguts post-HS, indicating the average percentage of PCNA+ cells in the various compartments. Statistical analysis was conducted using the Kruskal-Wallis test. Scale bar 50 µm.

3.4. HS ISC-response is not regeneration but a homeostatic response: pulsed-turnover

We have observed increased cell cycle markers following heat shock in the adult *Drosophila* midgut. This increase could be interpreted as a typical regenerative response to injury or insult (Amcheslavsky et al., 2009; Buchon et al., 2009; Chatterjee & Ip, 2009; Jiang et al., 2016). However, given our specific focus on studying turnover as a homeostatic state, it becomes crucial to distinguish this surge in ISC division as a turnover response rather than a regenerative one.

Turnover refers to the continuous replacement of cells in a tissue, often driven by a high basal rate of cell division or the capacity for new cell formation following cell loss. This normal physiological process helps maintain tissue homeostasis and functionality (**Figure 12A)** (Blanpain &, 2009; Mannino et al., 2022).

What distinguishes turnover from regeneration in our context is not only the process but also the scale and timeframe of cell replacement. If cell replacement occurs gradually or the damage is extensive enough to significantly change the tissue's structure and size over time, effectively disrupting its normal state, it qualifies as regeneration. On the other hand, if such substantial changes do not occur and the tissue maintains a relatively stable structure and size, it is referred to as homeostatic turnover.

To differentiate between turnover and regeneration, we analysed cell density, quantified by nuclear staining with DAPI per field of view, throughout the 11-day timeline used for PH3 analysis. Additionally, we examined cellular death using caspase-3 expression following HS induction.

Increased caspase-activated cells have been observed after midgut damage, suggesting that EC undergo apoptosis following injury. Several studies have shown that damaged enterocytes produce signals that drive intestinal stem cell proliferation for homeostasis and regeneration in the adult midgut (Buchon et al., 2010; Jiang et al., 2009a)

If HS promotes increased ISC division rates for tissue regeneration, we expect to observe a decrease in cell density (or total tissue size) accompanied by an upregulation of cell death markers following heat stress.

In line with this hypothesis, the rapid surge in mitotic figures observed on day 5 (**Figure 9A**) would coincide with a preceding significant loss of cells, supporting the notion of tissue regeneration. However, our findings reveal that cell density remains relatively unchanged over the 11-day time course following HS (**Figure 12B**). This provides further

evidence that HS does not induce extensive damage followed by regeneration but homeostatic turnover. Furthermore, the analysis of caspase-3 expression as an apoptosis marker on day 5 after HS showed no significant increase (**Figure 12C**).

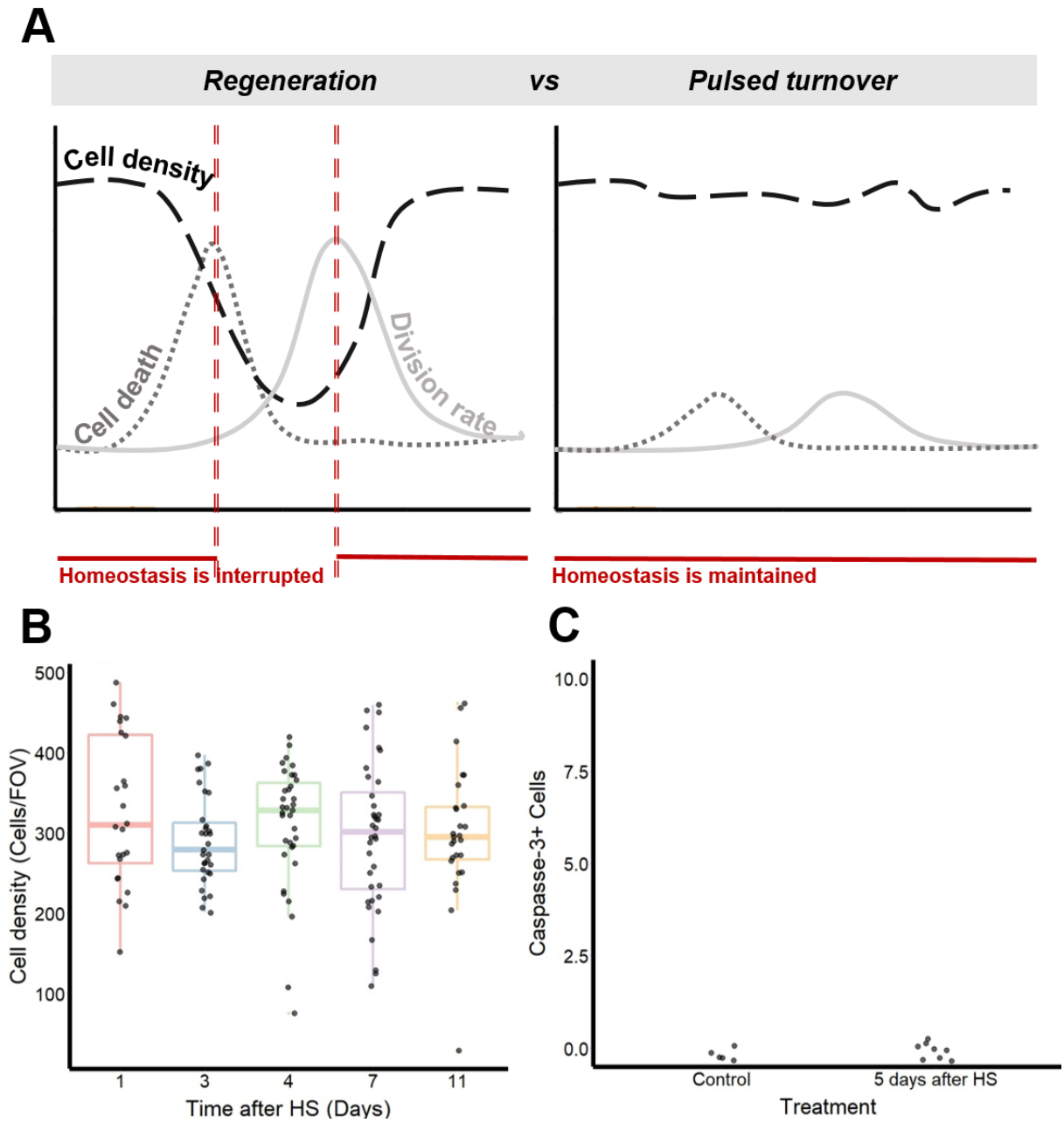

Figure 12. HS ISC-response is not regeneration but pulsed turnover. A. Comparative dynamics: Graphical comparison of cell density and division rates in regeneration versus pulsed turnover following heat shock . **B. Cell density evolution:** Box plot overlaid with jittered points indicating individual FOVs (n = 5-7 midguts, with all FOVs captured for each midgut) demonstrating no changes in cell density over 11 days after HS. **C. Caspase 3 analysis:** Scatter plot comparing caspase 3+ cell counts in control versus 5 days after HS, showing no significant increase in apoptosis. Statistical analysis was conducted using the Kruskal-Wallis test. *Illustration A was created by Biorender.com*

4 Discussion

4.1. Uniting the puzzle: the Quiescence-Division switch model for tissue replacement

Our quiescence-division switch model offers a new perspective on adult *Drosophila* midgut tissue turnover regulated by intestinal stem cells (ISCs). Contrasting division rates reported in prior studies by de Navascués et al. (2012) and Jiang et al. (2009), which were influenced by the temperature of heat shock induction, are reconciled within our framework. It accounts for the variations in cell division rates while explaining the consistency within the ISC compartment, accommodating the compartmental differences observed.

The quiescence-division switch model suggests that in a state of homeostasis, ISCs can exist in one of two states: quiescence, with no division (division rate = 0), or active division at a fixed, non-zero rate (>0) (**Figure 8**). This concept offers a crucial insight into why previous models, such as the neutral competition model proposed by de Navascués et al. (2012), failed to account for this duality. These models relied on cell proliferation for clonal labelling, making it impractical to observe quiescent cells. Detecting quiescence, as we will discuss shortly, is inherently challenging.

Considering our observation that heat shock induces an increase in actively dividing cells, as indicated by PH3 staining, we can lend support to the idea that differences in the temperatures used to induce stress in lineage tracing experiments (**Figure 9A**). This suggests that heat stress can trigger a transition from stem cell quiescence to active division.

This increase in mitotic activity, as marked by PH3-positive cells, does not necessarily indicate a faster division rate, typically associated with regenerative responses. Instead, our hypothesis posits that the observed rise in mitotically active cells reflects the homeostatic rate of ISC division rather than a regenerative response. We base this hypothesis on the notion that the intestinal epithelium experiences continuous but irregular and untimely stress, causing ISCs to transition from quiescence to division. However, this transition is not uniformly distributed, as seen by the two-fold increase in PCNA+ cells from region 1 to 5 in the midgut.

4.2. Homeostatic response and Pulsed Turnover

Our research has unveiled that heat shock triggers an increase in mitotic figures, as detected through PH3 immunostaining (**Figure 9A**). We refer to this phenomenon as

"pulsed turnover," which proposes a new dynamic of cell division under homeostasis, as our quiescence-division switch model suggests. Pulsed turnover is characterised by periodic increases in cell division in response to stress, with cells transitioning from quiescence to active division. This concept is supported by the observed increases in mitotic activity on days 4 and 7 after stress, which return to baseline by day 11 (**Figures 9A and B**).

For our model to be supported, "pulsed turnover" must differ from simple regeneration. We aim to determine whether the observed increase in mitotic figures following heat stress supports our initial hypothesis, thus identifying it as a distinct homeostatic response rather than a regenerative one.

Our findings, including factors like cell density (**Figure 12B**), caspase-3 expression (**Figure 12C**), and the presence of mitotic figures (PH3+ cells) (**Figure 9A and C**), strongly support the existence of distinct homeostatic states: quiescence and pulsed turnover (**Figure 12A**), beyond the regenerative approach.

Firstly, our results support the concept of a homeostatic response following sub-lethal heat stress. What we are observing closely aligns with tissue turnover rather than regeneration. The rise in mitotic figures after HS (**Figure 9A**), without concurrent cell death (**Figure 12**), suggests an adaptive homeostatic response. This interpretation is consistent with prior research showing the initiation of mitotic recombination without simultaneous apoptosis or necrosis in various experimental settings (Bandura et al., 2013; Neophytou & Pitsouli, 2022).

Secondly, in support of the concept of pulsed turnover, our comprehensive study, involving the modelling of PH3+ expression data over 11 days, demonstrates that the increase in mitotically active ISCs follows a wave-like pattern of division (**Figure 9A**), reaching its peak around day 5 after heat shock induction. This pattern aligns with pulsed turnover, as described in prior research (de Navascués et al., 2012). Significantly, this surge in PH3 division, peaking at day 5, corresponds with unpublished lab results which modelled clonal size data from de Navascués' work and showed a distinctive division rate trend resembling a wave, with a peak around day 5 (Morrisey, personal communication, 2018).

Beyond the initial increase in mitotic figures, our PH3 data showed that, by day 11, there was a significant decrease in the number of mitotic figures, returning to baseline levels. This increase, followed by a return to baseline levels could further support our

hypothesis of two homeostatic states in the *Drosophila melanogaster* midgut: cells are either dividing or in quiescence, and stressors such as heat can trigger this transition

4.3. Cycling cells beyond mitosis

PH3 expression, indicating mitotic activity, does not always reflect the full extent of cell cycling, as not all cells in the cycle proceed to mitosis (Flegel et al., 2016). Mitosis constitutes only about 4% of the entire cell cycle. The narrow window for detection may cause us to miss observations, potentially resulting in an underestimate of the true extent of cell cycling. This limitation is crucial as it directly affects the accuracy of our division rate estimates and influences our understanding of ISC behaviour during homeostasis and in response to external factors like heat stress.

To investigate the full spectrum of cell cycle phases, we used markers like PCNA for S phase identification, Cyclin-A for the G2-M transition, and Polo-kinase for M phase. We also made a difference between difivind stem cells (ISCs) and endocycling enterocytes by analysing Delta (Dl) expression alongside PCNA.

After heat shock, we detected an increase in Cyclin A+ cells on day 5, which was indicative of the G2-M transition, suggesting that mild heat stress may trigger ISCs out of quiescence rather than pushing them directly into mitosis because this rise did not coincide with an increase in Polo kinase counts.

The Cyclin A - Polo network is essential in early mitosis and cytokinesis (Liu et al., 2017), and an increase in Polo+ cells after HS would have best integrated previous results (**Figure 10**).

One plausible explanation for the lack of Polo kinase upregulation after heat stress is the existence of a "safeguard" mechanism. In mammalian cells, under stress conditions, stress-induced Polo-like kinase 4 (Plk4) activation promotes centrosome duplication, while stress-induced SAPK activation prevents centrosome duplication (Fu et al., 2015; Nakamura et al., 2013). This balance of opposing signals ensures that centrosome overduplication is avoided in the early phase of the stress response. However, in the late phase of the stress response, p53 downregulates Plk4 expression, preventing sustained Plk4 activity and centrosome amplification (Nakamura et al., 2013)

These findings suggest that under stress conditions, there must be precise control of intestinal stem cell (ISC) proliferation to avoid tumorigenesis, as PLK1 is involved in it (Liu et al., 2016).

Additionally, other studies have shown an increase in Plk3 under stress signals, such as genotoxic stress, hypoxia, and hyperosmotic stress (Wang, Dai, et al., 2014; Wang et al., 2011). However, Plk3 has also been associated with tumorigenesis, as its loss results in increased genomic instability and tumour formation in mice, underscoring the need for precise control and regulation of the Polo-like kinase family under stress conditions to maintain ISC homeostasis and prevention tumorigenesis (Xu et al., 2017).

The lack of an observable increase in Polo kinase expression after heat stress could also be influenced by the post-transcriptional regulation of this mitotic kinase (Pintard & Archambault, 2018). The protein trap strategy used for Polo does not allow for the detection of protein phosphorylation, which could be critical for its activation during the cell cycle. Therefore, the absence of a measurable increase in Polo expression may not necessarily indicate a lack of involvement in the stress-induced mitotic response.

It is also possible that the increase in mitotic activity observed by PH3 staining does not directly correlate with Polo kinase expression. Research by Ghenoiu et al. (2013) suggests that the direct phosphorylation of histone H3, marked by PH3, may involve regulatory mechanisms beyond the activity of Polo-like kinases. This indicates that the increased PH3 staining we observed may not solely be due to Polo kinase activity during mitosis. This suggests that ISCs may not be arrested in G0 (quiescence) but potentially in G2 as well, indicating that an increase in mitosis does not necessarily correspond with an uptick in S phase markers. This could also imply a reduction in the number of cells undergoing endocycling.

4.4. Regional Heterogeneity

We examined the expression of Polo, Cyclin A, and PCNA to better understand the distribution of cell cycle markers in the adult *Drosophila* midgut.

We observed significant spatial heterogeneity in Polo, Cyclin A, and PCNA expression in the *Drosophila* midgut. Some regions exhibited a high density of positive cells, while others showed minimal or no expression of these markers.

PCNA displayed the most significant variability. We analysed PCNA+ expression patterns within the functional regions of the midgut and observed that no specific regions consistently exhibit higher marker expression than others. This observation has led to the hypothesis that cells within the midgut respond to stress in a manner that appears to be more localised and random rather than region-specific.

4.5. Stress Sensing

Building on the observed expression variability of cell cycle markers across the posterior midgut, we propose various mechanisms that could explain this non-region-specific stress sensing, particularly in response to heat shock.

4.5.1. Mechanisms for stress sensing

Understanding the molecules responsible for sensing stress in the midgut is a significant question, primarily due to the intricate relationship the midgut shares with symbiotic organisms, mirroring similar dynamics observed in mammals (Miguel-Aliaga et al., 2018).

The mechanosensing process, where cells or organisms detect and respond to mechanical forces or stimuli, could potentially play a role in the *Drosophila* midgut's response to heat stress (Gong et al., 2023).

In this context, mechanoreceptors emerge as plausible candidates for sensing stress and translating these mechanical cues into biochemical signals that directly influence ISC behaviour. This mechanosensory role may be attributed to specific receptors, including TrpA1, Piezo, Msn (Misshapen), and the Snakeskin-Mesh complex found in smooth septate junctions, the equivalent of tight junctions in mammals.

Proteins like TRP channels and TrpA1 are key in detecting temperature changes under heat stress. These receptors are expressed in larval and adult *Drosophila*, suggesting a widespread role in thermal sensing (Li & Gong, 2016).

For instance, TrpA1 might function as a mechanosensing channel, which, in turn, could regulate ISC proliferation in *Drosophila* (Xu et al., 2017; Zhang et al., 2022). TrpA1's known ability to sense shear stress, heat, and irritant chemicals aligns with its potential role in intestinal growth and homeostasis (De Logu et al., 2017; Viana, 2016; S. R. Wilson et al., 2011).

Piezo, another key mechanoreceptor, could contribute to stem cell mechanosensing within the *Drosophila* midgut, influencing stem cell proliferation and differentiation (He et al., 2018). Furthermore, Msn, predominantly expressed in intestinal stem cells and enteroblasts might play a part in the Snakeskin-Mesh complex, potentially exerting control over the transcriptional coactivator Yorkie, thereby regulating intestinal homeostasis (Chen et al., 2020).

Additionally, peptide hormones, such as Allatostatin C, a *Drosophila* somatostatin homolog, detect stress, subsequently influencing food intake and metabolic homeostasis in response to nutrient-related stress (Kubrak et al., 2022; Veenstra et al., 2008). Alongside these neuropeptides, enteroendocrine peptides like DH31/CGRP could trigger intestinal contractions, aiding in removing opportunistic bacteria, thus impacting ISC dynamics (Zhou et al., 2020).

4.5.2. Communication

To comprehend how certain mechanoreceptors, specifically TrpA1, Piezo, and Msn, trigger specific signalling pathways in response to heat stress and subsequently enhance the proliferation of intestinal stem cells in the *Drosophila* midgut, it's important to examine the process of cellular communication.

For instance, TrpA1 appears to activate the EGFR pathway via a PLC/calcium signalling pathway. This activation leads to an influx of calcium ions and subsequent downstream effects, including activating the EGFR/Ras/MAPK signalling pathway (Jiang & Edgar, 2011).

Piezo's potential impact on ISC proliferation might involve several mechanisms. Piezo activation could increase reactive oxygen species (ROS) concentration, priming stem and progenitor cells for differentiation (Hochmuth et al., 2011). Furthermore, Piezo activation might stimulate EGF signalling, activating the ERK pathway and promoting ISC proliferation (Biteau & Jasper, 2011). Moreover, Piezo activation could enhance signalling via the EGFR pathway (Petsakou & Perrimon, 2023).

Several mechanisms have been explored for Msn's role in ISC proliferation. Msn causes an increase in ROS concentration (Hochmuth et al., 2011). Additionally, Jiang et al. (2016) revealed that nutrient-stimulated intestinal growth in *Drosophila* is mediated by the production of *Drosophila* insulin-like peptide 3 (dILP3) in muscle cells. This peptide acts on ISCs through the *Drosophila* insulin-like receptor (InR) pathway to promote their proliferation. Msn might also interact with the Jak/Stat and EGFR signalling pathways (Puig et al., 2003).

In summary, these insights into the communication process provide a hypothetical framework for how mechanoreceptors like TrpA1, Piezo, and Msn, or other potential candidates, may sense stress, specifically heat stress, and activate specific signalling pathways that contribute to the increase in ISC proliferation in the *Drosophila*, as detailed in Chapter 1, and showed no apparent spatial specificity.

4.6. Potential mechanism for Pulsed Turnover

As we explored in Chapter 1, the Notch/Delta signalling pathways' response to stress is highly context-dependent. We now propose that this pathway could be responsible for the oscillatory pattern of pulsed turnover observed in the *Drosophila* midgut.

Notch is a well-documented regulator of ISC behaviour across various contexts (Mathur et al., 2010; Montagne & Gonzalez-Gaitan, 2014; Shi et al., 2021b). In mouse intestinal ISCs, for instance, the regenerative response marked by the expansion and oscillatory expression of Notch ligands Dll1 and Dll4 follows transient inhibition of the Notch pathway (Bohin et al., 2020). This implies that Notch signalling oscillations might be pivotal in balancing ISC self-renewal and differentiation.

Zhang et al. (2021) observed similar oscillatory behaviour in the Notch signalling of mouse muscle stem cells. Their findings show that the rhythmic expression of the Notch ligand Dll1 is essential for muscle stem cell self-renewal. This suggests that oscillatory Notch signalling may be a universal mechanism to maintain equilibrium between cell states.

In the turnover of the *Drosophila* midgut, Notch signalling might play a crucial role in maintaining the delicate balance between ISC self-renewal and differentiation, and its expression might be tightly regulated through a feedback loop involving its ligand Delta (Montagne & Gonzalez-Gaitan, 2014; Srinivasan et al., 2016). This dynamic regulatory mechanism might underlie the observed wave-like pattern of proliferation when analysing PH3+ cells. The oscillatory nature of Notch signalling suggests that oscillations in Notch ligand expression could influence the behaviour of ISCs in response to stressors such as heat shock. Oscillations in Delta-like ligand expression might serve as a critical factor determining whether ISCs remain quiescent or enter into a proliferative state. Additionally, oscillations in Notch signalling might play a role in coordinating the response of neighbouring ISCs, contributing to the observed wave-like pattern of ISC division.

4.7. Future directions:

4.7.1. Endocycle

The endocycle is pivotal in tissue homeostasis, particularly in the *Drosophila* midgut. This process, characterised by DNA replication without division leading to polyploidy, offers several advantages, including increased cell size, genomic stability, and

resistance to apoptosis. These attributes are critical for maintaining tissue integrity, efficient barrier formation, and homeostasis.

Our unexpected findings regarding the expression of the S-phase marker PCNA on day 5 after HS highlight the complexity of cell cycle regulation in the *Drosophila* midgut. Contrary to our anticipation of an increase, we observed no change in ISC PCNA+ cells. However, there was a notable decrease in overall PCNA+ cells. This finding suggests a potential reduction in EC PCNA+ cells, indicating mechanisms that may prevent endoreplication. (Lee et al., 2009).

To further explore this phenomenon, we propose using geminin as a marker to distinguish cells undergoing the S-G2-M phase from those in the endocycle (Sher et al., 2013). Accurately identifying cells in the endocycle will enhance our understanding of the cellular mechanisms in response to environmental stress (Calvi, 2013; Costa et al., 2022; Øvrebø & Edgar, 2018).

4.7.2. Integrative approaches to quiescence

Our investigation into the dynamics of ISC behaviour in *Drosophila* proposes a model in which ISCs enter and exit quiescence in response to different stresses to proliferate and maintain tissue homeostasis. The quiescence state, characterised by a reversible cell cycle arrest, allows ISCs to remain dormant and potentially re-enter the cell cycle, distinct from terminal differentiation or senescence (Cheung & Rando, 2013).

Our empirical findings have identified actively dividing ISCs through markers like PH3, Cyclin A, and Polo kinase. However, pinpointing the quiescent ISCs has been challenging due to the absence of specific markers.

Reflecting on Otsuki and Brand's (2018) integrative method for characterising quiescence, we have used comparable cell cycle markers to identify non-dividing cells within our studies. Their approach, however, encompasses additional analyses which could enhance ours, particularly the use of gene expression profiling of quiescent ISCs. They have provided insights into the molecular landscape of quiescent stem cells by employing a method similar to Targeted DamID (TaDa) for genome-wide gene expression profiling. Furthermore, the incorporation of reactivation markers, specifically monitoring worniu (wor), has allowed them to track the reactivation process of quiescent neural stem cells (NSCs).

CHAPTER 3: IDENTIFYING KEY GENES AND MODULES IN INTESTINAL TISSUE TURNOVER THROUGH WEIGHTED CORRELATION NETWORK ANALYSIS

1 Introduction

In Chapter 2, we employed immunofluorescence analyses for cell cycle markers in response to stress. Advancing from this foundation, Chapter 2 aims to identify the key molecular mediators that respond to heat stress and could trigger cell division within our proposed model's framework.

Differential expression analysis is a powerful technique for identifying genes that are differentially expressed between different conditions or groups. It involves comparing gene expression levels between two or more experimental conditions to identify genes that show significant changes in expression. This analysis can be performed using various high-throughput techniques, such as RNA sequencing (RNA-Seq) or microarray analysis, which provide a comprehensive view of the transcriptome.

Differential expression analysis is widely used in various research fields, including genomics, transcriptomics, and systems biology. However, it provides a reductionist view of the information contained within large-scale transcriptome datasets. Genes are treated as independent entities in such analyses, whereas in reality, genes interact with other biomolecules within highly complex and intricate systems (de la Fuente, 2010).

Interaction networks, such as weighted gene co-expression network analysis (WGCNA), facilitate the analysis of systems using techniques based on graph theory, including clustering or centrality measures for hub gene detection. (Aittokallio & Schwikowski, 2006).

Weighted Gene Co-expression Network Analysis (WGCNA) aims to identify biologically relevant gene modules and hub genes associated with specific phenotypes or conditions. WGCNA is a powerful bioinformatics method that allows for the construction of gene co-expression networks based on the similarity of gene expression patterns across samples (Langfelder & Horvath, 2008; Li et al., 2018; Pascut et al., 2020).

By clustering genes into modules, WGCNA provides a systematic approach to explore the relationships between genes and phenotypes, such as disease states, treatment responses, or developmental stages (Allen et al., 2012; Chen et al., 2016; Huang et al., 2021).

One of the main advantages of WGCNA is its ability to capture the complex interactions and regulatory relationships between genes within a biological system (Yang et al., 2022). This method accounts for correlation patterns in gene expression across multiple

samples, enabling the identification of co-expressed gene modules with potential functional relationships (Cui et al., 2022). This approach provides a holistic view of gene expression data and can uncover key biological pathways and processes associated with the phenotype of interest (Kowalski et al., 2020; Zhou et al., 2020). Another advantage of WGCNA is its ability to identify hub or highly connected genes within a co-expression module (Chen et al., 2022). Hub genes often play critical roles in biological processes and can serve as potential biomarkers or therapeutic targets (Lin et al., 2021).

By focusing on the relationships between modules and clinical traits, WGCNA can prioritise genes most relevant to the phenotype of interest (Zhang et al., 2022). This approach identifies key genes and pathways involved in disease development, progression, or response to treatment (Shi et al., 2021). WGCNA is also advantageous in integrating different types of omics data, such as gene expression, microRNA expression, or proteomics data, to provide a more comprehensive understanding of biological systems (Liang et al., 2020). Combining multiple data types allows WGCNA to uncover complex regulatory networks and identify potential crosstalk between different molecular layers (Suzuki et al., 2017). This integrative approach can lead to discovering novel biomarkers, therapeutic targets, and mechanistic insights into biological processes (Sánchez-Baizán et al., 2022; Tang & Liu, 2019).

Overall, WGCNA analysis aims to better understand the relationships between genes and phenotypes by constructing gene co-expression networks and identifying biologically relevant modules and hub genes. Its advantages lie in its ability to capture complex interactions, identify key genes and pathways, integrate different omics data types, and provide a holistic view of gene expression data. WGCNA has been widely applied in various research fields and has proven to be a valuable tool for biomarker discovery, therapeutic target identification, and systems-level analysis of biological processes (Ma & Li, 2021; Wu et al., 2020).

1.1. Weighted Gene Co-expression Network Analysis pipeline

The WGCNA pipeline consists of the following steps (**Figure 13**):

1. Construct a gene co-expression network: Pairwise gene expression correlations across samples are calculated, and the correlation matrix is transformed into an adjacency matrix using a chosen soft thresholding parameter. The soft thresholding helps emphasise strong correlations and downweight weak correlations. A suitable soft

threshold will bring the resulting co-expression network closer to scale-free, which is assumed in the WGCNA model.

2. Identify modules: Clustering algorithms, such as hierarchical clustering or dynamic tree cutting, are applied to group genes with similar expression patterns into modules.

3. Module-trait association analysis: Involves correlating module eigengenes (ME), representative expression profiles of gene modules, with external traits or conditions of interest (Hasankhani et al., 2021). ME captures the overall expression pattern of genes within a module and can be correlated with specific phenotypes or conditions to identify significant associations (Gao et al., 2023). Gene significance (GS) and module significance (MS) are other measures used to assess the correlation between individual genes or modules and external traits (Xu et al., 2018). GS quantifies the association between a gene's expression and a specific phenotype, while MS provides an overall measure of the association between a module and a specific condition (Xu et al., 2018). Modules with high MS values are considered to be significantly associated with the studied phenotype or condition.

4. Examine inter-module relationships: WGCNA uses ME as a representative profile of a module and calculates module similarity using eigengene correlation, which assists in determining the relationships between modules.

5. Hub gene identification: Hub genes are highly connected genes and are often considered key regulators or drivers of biological processes (Langfelder & Horvath, 2008). Identifying hub genes is essential for gaining insights into the underlying regulatory network governing gene expression patterns. Two main approaches are used to identify them: **(a)** The intramodular connectivity measure is used to identify genes with the highest number of connections within a module. Genes with high intramodular connectivity values are regarded as hub genes (Langfelder & Horvath, 2008), and **(b)** the module membership (MM) quantifies the correlation between the expression profile of an individual gene and the module eigengene. Genes with high MM values demonstrate strong membership within the module and are considered hub genes (Liu et al., 2016).

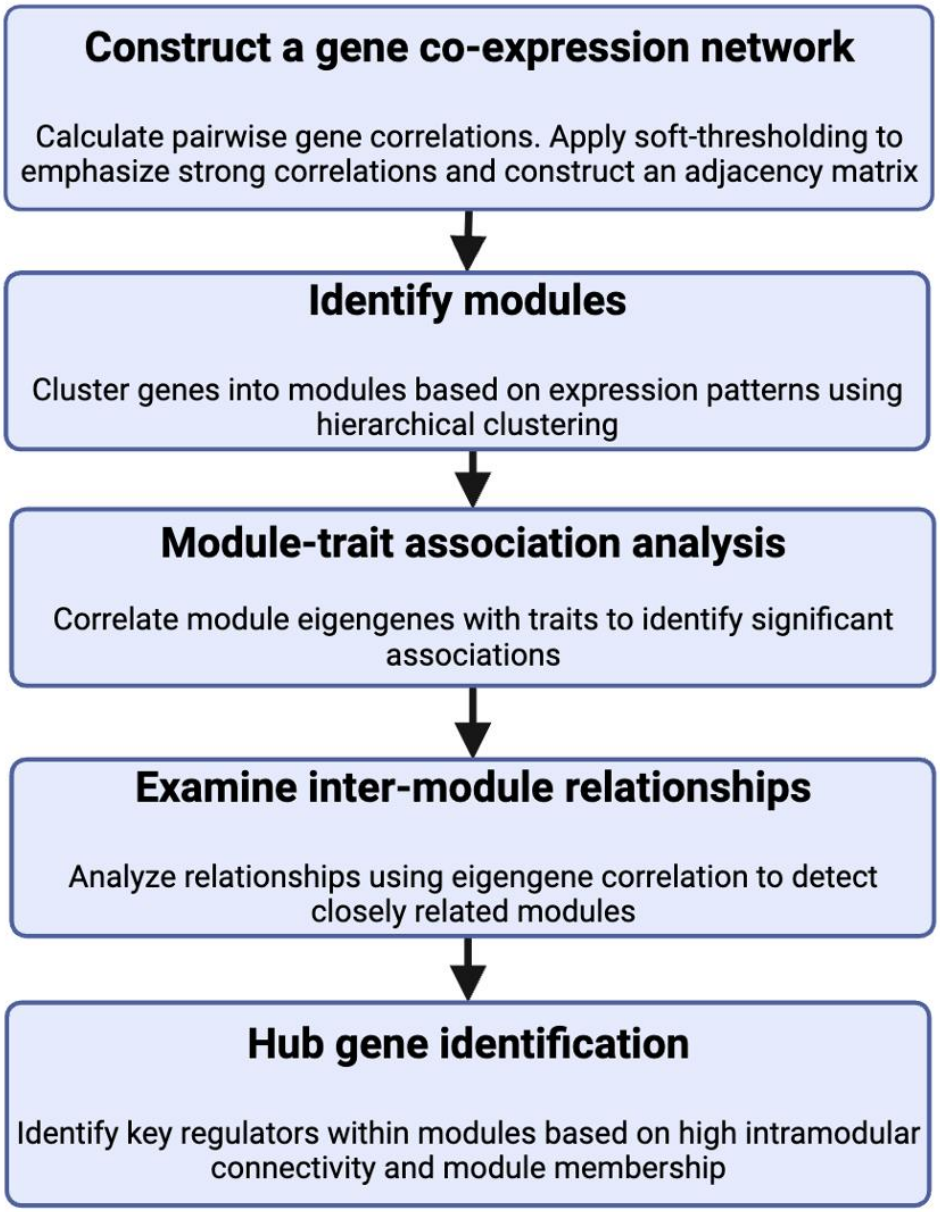

Figure 13. Flowchart of WGCNA. The diagram outlines the sequential steps involved in constructing a gene co-expression network to identify significant gene modules and hub genes.

1.2. Aim

Our chapter employs weighted gene co-expression network analysis (WGCNA) to identify clusters of genes in the *Drosophila* adult midgut that correlate with heat shock responses at various time points.

2 Materials and methods

2.1. Data selection and preprocessing

We conducted our experiments using w^{1118} (BDSC #5905) mated female *Drosophila*, aged 4-5 days. These flies were subjected to heat shock at 37ºC for 60 minutes. Throughout the study, we maintained the *Drosophila* bi-weekly by transferring them to fresh media.to ensure their well-being. After heat stress, on specific post-stress days (1,3, 5 and 7), we dissected the midgut directly into ice-cold PBS pre-treated with DEPC (1:1000) and autoclaved. Each replicate consisted of midgut tissue from 10 female *Drosophila*.

To maintain the integrity of the samples, the dissected midguts were kept on ice. The dissection procedure followed the techniques previously described in **Chapter 2, Section 2.7.**

RNA extraction from the sorted tissues was performed in triplicates. For each replicate, total RNA was extracted from 10 *Drosophila* using the PureLinkTM RNA column extraction kit (Thermo Fisher: 12183018A) as per the manufacturer's instructions. To ensure RNA integrity, we periodically cleaned the equipment and workspace during RNA extraction using the RNAase decontamination solution RNAaseZapTM (Thermo Fisher: AM9780).

The RNA samples were frozen at -80°C overnight prior to transport to the Genome Hub at Cardiff University for sequencing. The Genome Hub at Cardiff University then constructed the cDNA libraries and performed sequencing using Illumina technology, yielding a minimum of 16.7 million paired-end reads, each 150 base pairs in length, for each sample. The libraries were prepared using the Illumina stranded mRNA prep protocol. The quality and quantity of the libraries were assessed using Qubit for quantification and TapeStation for integrity and size distribution analysis.

Data sequence was stored in .fastq format and uploaded to the Galaxy web server (v24.0.3.dev0) for analysis (Afgan et al., 2018). Initial quality checks were conducted with FastQC, as shown in Tables **4, 5 and 6** (Andrews, 2010). We then used Trimmomatic (v0.36.3) (Bolger et al., 2014) to clean the data by trimming sequences of low quality. HISAT2 (v2.0.5.2) (Kim et al.,2015) facilitated sequence alignment to the reference genome. We used featureCounts (v2.0.1) (Liao et al., 2014) before inputting the data into WGCNA for network analysis.

Table 4. Sequencing data overview. The table presents sequencing metrics for 24 samples, detailing chromosome-specific information. For chromosomes 2L, 2R, 3L, and 3R, data include the total length of the chromosome (Length), the number of reads that aligned to the chromosome (Mapped_Reads), and the number of reads that did not align (Unmapped_Reads).

SAMPLE	CHR2L_LENGTH	CHR2L MAPPED_READS	CHR2L UNMAPPED_READS	CHR2R LENGTH	CHR2R MAPPED_READS	CHR2R UNMAPPED_READS	CHR3L LENGTH	CHR3L MAPPED_READS	CHR3L UNMAPPED_READS	CHR3R LENGTH	CHR3R MAPPED_READS	CHR3R_UNMAPPED_READS
1	23513712	6256369	280069	25286936	11524220	477694	28110227	8406432	386416	32079331	9024008	356494
2	23513712	6301224	263953	25286936	9859189	390696	28110227	7918167	343994	32079331	8840689	337827
3	23513712	7145861	310138	25286936	9066768	380121	28110227	7243094	312321	32079331	8662369	348929
4	23513712	6924752	237813	25286936	11614719	373448	28110227	8767980	319657	32079331	9879087	296254
5	23513712	6069981	248564	25286936	10494643	380778	28110227	8039008	341785	32079331	8580323	307953
6	23513712	7294869	278190	23513712	7294869	278190	28110227	8232542	310419	32079331	9477623	318065
7	23513712	7801880	273376	25286936	10197739	345796	28110227	8227173	292301	32079331	9814183	304501
8	23513712	7303969	308098	25286936	11620024	451901	28110227	8599729	371255	32079331	9763619	369500
9	23513712	7369845	249492	23513712	7369845	249492	28110227	9211321	314146	32079331	10309596	298482
10	23513712	6987126	291731	25286936	8866686	352997	28110227	7305604	303867	32079331	9056952	344141
11	23513712	7667917	233229	25286936	10580907	308702	28110227	8629959	263155	32079331	9896221	263213
12	23513712	5785699	280366	25286936	9510132	420365	28110227	7106761	350500	32079331	7487687	327577
13	23513712	7485106	222934	25286936	9193233	254893	28110227	7591343	232120	32079331	9292801	239116
14	23513712	6462346	239449	25286936	10242509	343387	28110227	7998185	296755	32079331	8907992	288322
15	23513712	7030683	239959	25286936	12277146	385185	28110227	9374945	338523	32079331	9623052	282845
16	23513712	5899410	248012	25286936	10103229	375030	28110227	7706479	327480	32079331	8011192	293786
17	23513712	6965488	290793	25286936	10996309	415931	28110227	8625152	360020	32079331	9640908	358480
18	23513712	6400565	274378	25286936	10186964	406058	28110227	8039882	357814	32079331	8166267	319424
19	23513712	6942131	0	25286936	11308630	0	28110227	8573659	0	32079331	10371048	0
20	23513712	6073244	256959	25286936	9218435	364344	28110227	7051156	298783	32079331	7944554	297670
21	23513712	6755152	357274	25286936	11048440	534251	28110227	8438985	449315	32079331	8679649	421546
22	23513712	5499750	420962	25286936	9097148	625204	28110227	6906316	502701	32079331	7165419	507167
23	23513712	6019544	328270	25286936	12515312	599594	28110227	8870242	486085	32079331	9011674	437957
24	23513712	6019544	328270	25286936	12515312	599594	28110227	8870242	486085	32079331	9011674	437957

Table 5. Sequencing data overview. This table summarises the sequencing results for Chromosome 4 and mitochondrial DNA (chrM) across 24 samples. It provides the chromosome length (Length), the number of reads mapped to the chromosome (Mapped_Reads), and the number of reads that failed to map (Unmapped_Reads).

SAMPLE	CHR4_LENGTH	CHR4_MAPPED_READS	CHR4_UNMAPPED_READS	CHRM_LENGTH	CHRM_MAPPED_READS	CHRM_UNMAPPED_READS
1	1348131	337972	11671	19524	344123	12183
2	1348131	296931	9578	19524	630129	22407
3	1348131	516802	17436	19524	554734	19730
4	1348131	407212	10057	19524	420643	11652
5	1348131	295178	8881	19524	1249675	39513
6	1348131	476565	13529	19524	1137272	33253
7	1348131	483720	12267	19524	649252	17681
8	1348131	470705	15163	19524	483071	16367
9	1348131	443042	10565	19524	627850	16160
10	1348131	455975	14699	19524	621848	20758
11	1348131	454244	9574	19524	682817	16645
12	1348131	322021	12074	19524	441659	16794
13	1348131	463514	9759	19524	638867	14988
14	1348131	374948	10085	19524	521759	15752
15	1348131	415503	9690	19524	455460	12041
16	1348131	276016	8392	19524	731200	22564
17	1348131	349522	11363	19524	589212	18766
18	1348131	347422	11504	19524	435951	13965
19	1348131	286994	0	19524	690631	0
20	1348131	389190	11843	19524	1621240	49169
21	1348131	444966	18596	19524	630310	26333
22	1348131	323425	20741	19524	679474	40401
23	1348131	333020	14494	19524	330798	13565
24	1348131	333020	14494	19524	330798	13565

Table 6. Sequencing summary for sampled *Drosophila* genomes. The table provides sequencing metrics for *Drosophila* samples, detailing total sequences obtained, total bases sequenced, sequences flagged as poor quality (indicating robust sequencing quality across samples), sequence length range, and the percentage of GC content in the sequences.

SAMPLES	TOTAL SEQUENCES	TOTAL BASES	SEQUENCES FLAG AS POOR QUALITY	SEQUENCE LENGTH	%GC
1	44244229	3	0	2-76	55
2	44289023	3	0	2-76	54
3	43669090	3	0	2-76	53
4	49085033	3.4	0	2-76	53
5	42698201	2.9	0	2-76	54
6	46903592	3.2	0	2-76	52
7	49489446	3.4	0	2-76	53
8	49782199	3.4	0	2-76	53
9	51378960	3.6	0	2-76	53
10	45630277	3.1	0	2-76	52
11	51802535	3.6	0	2-76	52
12	45852262	3.2	0	2-76	54
13	40211128	2.7	0	2-76	54
14	48545718	3.4	0	2-76	52
15	43818087	3	0	2-76	53
16	52318711	3.6	0	2-76	53
17	50891246	3.5	0	2-76	52
18	46427781	3.2	0	2-76	54
19	42650972	2.9	0	2-76	54
20	46981656	3.3	0	2-76	54
21	43475843	3	0	2-76	51
22	46248083	3.1	0	2-76	53
23	38481696	2.5	0	2-76	54
24	46906151	3.2	0	2-76	55

2.2. Differential gene expression analysis

Differential Expression analysis for Sequence Count data tool (DESeq2, v2.11.40.8), available within the Galaxy web server (Afgan et al., 2018), was used to identify genes that showed differential expression in response to heat shock.

We compared the gene expression of heat-shocked *Drosophila* collected at four different time points (days 1, 3, 5, and 7) with non-heat-shocked flies (control) at the corresponding time points.

Specifically, we conducted intra-group comparisons among heat-shocked flies to analyse the progression of the response over time.

Additionally, we performed inter-group comparisons at each time point by comparing gene expression in heat-shocked flies with control flies. These comparisons included Day 1 heat-shocked flies versus Day 1 control flies, Day 3 heat-shocked flies versus Day 3 control flies, Day 5 heat-shocked flies versus Day 5 control flies, and Day 7 heat-shocked flies versus Day 7 control flies..

2.3. Network construction

For the construction of the Weighted Correlation Network Analysis (WGCNA), additional preprocessing steps were necessary. We utilised featureCounts data obtained from the Galaxy platform to create two crucial Excel files for the subsequent WGCNA analysis in R Studio (**script available in Supplementary Information**):

- Gene expression matrix: Rows in this matrix represent genes, while columns correspond to our samples. The matrix values reflect the feature counts from the RNA sequencing process.
- Trait data matrix: This included the phenotypic data distinguishing between control (non-heat-shocked) and heat-shocked treated flies.

Once these files were uploaded into our R studio script, we used the DESeq2 package to normalise and filter gene expression data, removing genes with low read counts and retaining those with at least 50 reads across the samples (Love et al., 2014). During normalisation and filtering, we removed genes with low read counts, ensuring that only genes with 50 or more reads in total across the samples were retained.

To further enhance the data for WGCNA construction, we applied the variance stabilising transformation (VST) using the vst() function from the DESeq2 package (Love

et al., 2014). This transformation was considered essential, as recommended by the authors of DESeq2, as it helps to improve the accuracy and reliability of subsequent analyses (Love et al., 2014). We opted not to use the rrlog transformation available in DESeq2, as it has the potential to alter the gene order within a sample if neighbouring genes undergo shrinkage of different strengths (Love et al., 2014).

The signed, weighted correlation networks were constructed using WGCNA with a power value of 14, chosen to ensure a scale-free network topology (Langfelder & Horvath, 2008). We utilised the blockwiseModules() function in WGCNA to identify gene co-expression modules, specifying a power value of 14 (Wang et al., 2019). The default maxBlockSize of 5000 was used in this analysis (Wang et al., 2019).

We employed a linear model on each module using the limma package to identify significant associations. We applied multiple testing corrections and considered associations with a Benjamini-Hochberg adjusted p-value < 0.1 and a correlation > 0.3 as significant (Langfelder & Horvath, 2008).

2.4. Module-trait relationship

Utilising a multi-dimensional scaling (MDS) approach with the cmdscale() function, specific thresholds were established based on the scaling dimensions. Subsequently, the Pearson correlation method was employed to determine correlation coefficients between the traits and eigengenes.

2.5. Identification of hub genes

To identify hub genes, we used specific criteria that consider both their module membership (MM) and gene significance (GS) values. Hub genes were selected based on the criteria of (Langfelder & Horvath, 2008): absolute values of module membership (MM) greater than 0.80 and gene significance (GS) greater than 0.20.

2.6. GO Enrichment Analysis and KEGG Pathway Analysis

We utilised the ShinyGO database (Ge et al., 2020) to conduct pathway enrichment analysis. The database offers valuable functionality for gene ontology (GO) functional annotations and draws information from the Kyoto Encyclopedia of Genes and Genomes (KEGG) pathway database. Through this analysis, we aimed to gain a comprehensive understanding of the functional roles and cellular localisation of the hub genes we identified.

The GO enrichment analysis conducted using ShinyGO was divided into three main sections: molecular function (MF), biological process (BP), and cellular component (CC). Each section provided valuable insights into the specific functions and processes associated with the identified hub genes, shedding light on their significance within cellular pathways. This comprehensive analysis enabled us to explore the potential roles and implications of the hub genes in our study, contributing to a deeper understanding of their functional relevance.

2.7. Hub Gene Expression Mapping Using SCope

We visualised hub genes identified WGCNA using the SCope platform (https://flycellatlas.org/scope), which interfaces with single-cell RNA sequencing (scRNA-seq) data from the Fly Cell Atlas (H. Li et al., 2022). For our analysis, we selected the "Stringent" dataset provided by the 10x Genomics platform, ensuring a high-quality, batch-corrected data pool for a more reliable interpretation of gene expression patterns. Uniform Manifold Approximation and Projection (UMAP) was employed as the dimensionality reduction technique to represent the complex, high-dimensional scRNA-seq data in a more interpretable two-dimensional space.

Due to the limitations of the SCope platform, which allows the visualisation of up to three genes at a time, we created composite images representing the expression patterns of approximately 20-25 hub genes per module. This was achieved by capturing individual screenshots for each of the three genes at a time, then layering these images on top of one another after removing the background to retain only the gene expression points.

3 Results

3.1. Differential gene expression analysis results

Our differential gene expression analysis using RNA-seq data (count reads) revealed a limited number of genes with statistically significant changes in expression between heat-shocked flies and controls or across different time points following heat shock. We employed a stringent threshold of adjusted p-value<0.05 to identify significant differentially expressed genes. Notably, a more stringent analysis with fragment reads instead of count reads resulted in no differentially expressed genes for comparisons (data not shown). These findings suggest minimal transcriptional changes in response to heat shock under the conditions tested.

3.1.1. No differentially expressed genes intra-group comparison among heat-shocked flies

We assessed the expression changes in response to heat shock across various time points, comparing days 1, 2, 3, 5, and 7 with each other. The analysis revealed that no genes in the dataset had an adjusted p-value below 0.05.

Significant findings were limited to only two genes with a p-value less than 0.1. The results indicated downregulation of *Chitinase 5* (FBgn0038180) with a log2 fold change of -1.28 and an adjusted p-value of 0.063 and upregulation of *Glycogen Binding Subunit 76A* with a log2 fold change of 0.92 and an adjusted p-value of 0.063.

3.1.2. No differentially expressed genes in intra-group comparison among day 1 heat-shocked flies vs control flies

The gene with the highest differential expression in the dataset was *Neprilysin 3* (FBgn0031081). Its fold change was modest at 0.21, with an adjusted p-value of 0.9999, indicating no significant differential expression.

3.1.3. No differentially expressed genes in intra-group comparison among day 3 heat-shocked flies vs control flies

The DESeq2 analysis conducted to identify differentially expressed genes on Day 3 after HS revealed no genes meeting the adjusted p-value threshold below 0.05.

The gene with the highest expression level on Day 3 was *Spermathecal endopeptidase 1* (FBgn0031406). It showed a log2 fold change of 0.94, indicating moderate upregulation, but with an adjusted p-value of 0.060476.

3.1.4. Only 14 upregulated genes and 6 downregulated genes in intra-group comparison among day 5 heat-shocked flies vs control flies

We identified a few genes showing significant transcriptional changes in the differential expression analysis conducted on Day 5 after heat shock treatment, as analysed using DESeq2. Specifically, only 14 genes were upregulated, and 6 were downregulated under the set criteria of a fold change threshold of 1 (log2) and an adjusted p-value of 0.05, as described in **Table 7**.

3.1.5. Only 20 upregulated genes and 15 downregulated genes intra-group comparison among day 5 heat-shocked flies vs control flies

In the differential expression analysis conducted on Day 7 following the heat shock treatment, as analysed using DESeq2, we observed a more pronounced transcriptional response than earlier. 20 genes were upregulated, while 15 genes were downregulated, adhering to the criteria of an adjusted p-value of 0.05 (**Table 8**).

Table 7. Differential expression analysis on day 7 after heat shock treatment. This table details the transcriptional changes detected on Day 7 following heat shock treatment. The table presents gene identifiers, fold changes, p-values, and adjusted p-values.

GENE ID	GENE NAME	BASE MEAN	LOG2(FC)	STD ERROR	WALD-STATS	P-VALUE	P-ADJ
FBGN0015268	Nap1	298.2166	-2.30212	0.334903	-6.87398	6.24E-12	7.4E-08
FBGN0265525	asRNA:CR44375	71.54277	4.961476	0.738466	6.718626	1.83E-11	1.09E-07
FBGN0039709	Cad99C	311.9406	2.517096	0.41048	6.132087	8.67E-10	3.43E-06
FBGN0263132	Cht6	64.92402	2.438714	0.423371	5.760234	8.4E-09	2.49E-05
FBGN0050031	CG30031	8915.616	-1.8684	0.349431	-5.34696	8.94E-08	0.000212
FBGN0010358	δTrypsin	7106.444	-1.67603	0.319868	-5.23974	1.61E-07	0.000318
FBGN0265680	lncRNA:CR44487	30.60896	6.832913	1.349383	5.06373	4.11E-07	0.000696
FBGN0261584	CG42694	40.70864	2.358584	0.491227	4.801411	1.58E-06	0.002075
FBGN0267572	asRNA:CR45912	17.41437	6.990239	1.450509	4.819163	1.44E-06	0.002075
FBGN0027364	Six4	84.7452	3.74832	0.793602	4.723176	2.32E-06	0.002753
FBGN0050025	CG30025	4416.622	-1.6994	0.365044	-4.65534	3.23E-06	0.003486
FBGN0029856	CG11700	389.1225	1.654244	0.356938	4.634538	3.58E-06	0.003534
FBGN0034950	PAS kinase	40.07133	2.936713	0.642941	4.567625	4.93E-06	0.004331
FBGN0035676	short spindle 6	23.42028	3.933811	0.862668	4.560052	5.11E-06	0.004331
FBGN0038421	CG17931	188.3187	-1.10373	0.243793	-4.52731	5.97E-06	0.004722
FBGN0010359	δTrypsin	11288.15	-1.54916	0.354927	-4.36473	1.27E-05	0.008876
FBGN0058182	CR40182	29.19161	5.353453	1.225739	4.36753	1.26E-05	0.008876
FBGN0035696	Bestrophin 2	1012.106	1.052682	0.252339	4.171694	3.02E-05	0.019914
FBGN0004429	Lysozyme P	21.45312	3.14712	0.764972	4.114032	3.89E-05	0.024262
FBGN0051036	CG31036	17.07266	3.677452	0.896566	4.101709	4.1E-05	0.024311

Table 8. Differential expression analysis on day 5 after heat shock treatment. This table details the transcriptional changes detected on Day 7 following heat shock treatment. The table presents gene identifiers, fold changes, p-values, and adjusted p-values.

GENE ID	GENE NAME	BASE MEAN	LOG2(FC)	STD ERROR	WALD-STATS	P-VALUE	P-ADJ
FBGN0085249	CG34220	10752.36	-5.16561	0.34501	-14.9723	1.11E-50	1.41E-46
FBGN0085353	CG34324	4908.496	-4.82192	0.359825	-13.4007	5.99E-41	3.78E-37
FBGN0036203	Mucin 68D	1181.213	-4.66661	0.356686	-13.0832	4.11E-39	1.73E-35
FBGN0052557	FBGN0052557	112.9294	-4.211	0.347087	-12.1324	7.11E-34	2.25E-30
FBGN0263748	CG43673	580.5071	-4.0062	0.361191	-11.0916	1.38E-28	3.48E-25
FBGN0036232	CG14125	3219.908	-3.73684	0.351378	-10.6348	2.05E-26	4.32E-23
FBGN0036362	CG10725	882.0859	-3.69122	0.367317	-10.0491	9.27E-24	1.67E-20
FBGN0034871	CG3906	2347.355	-3.6551	0.370961	-9.85305	6.65E-23	1.05E-19
FBGN0037563	CG11672	366.7603	-2.79731	0.334896	-8.35278	6.67E-17	9.36E-14
FBGN0051956	Polypeptide N-Acetylgalactosaminyltransferase 4	144.4449	-2.8113	0.351078	-8.00764	1.17E-15	1.48E-12
FBGN0039452	CG14245	2432.81	-2.02459	0.271219	-7.46481	8.34E-14	9.58E-11
FBGN0034580	Chitinase 8	343.132	-2.25428	0.373478	-6.03591	1.58E-09	1.66E-06
FBGN0025583	Bomanin Short 2	5312.484	-1.46126	0.287362	-5.08509	3.67E-07	0.000357
FBGN0035743	Acyl-CoA binding protein 6	1947.399	-1.17596	0.232775	-5.0519	4.37E-07	0.000395
FBGN0028523	CG5888	153.9456	-1.68407	0.344047	-4.8949	9.84E-07	0.000828
FBGN0040653	Daisho1	6201.839	-1.29752	0.276965	-4.68478	2.8E-06	0.002213
FBGN0040734	Bomanin Short 5	921.7726	-1.47118	0.318649	-4.61691	3.89E-06	0.002895
FBGN0264479	long non-coding RNA:CR43887	81.66316	-1.6915	0.374437	-4.51745	6.26E-06	0.004393
FBGN0038150	yellow-e3	40.96676	-1.67226	0.371898	-4.49656	6.91E-06	0.004592

FBGN0067905	Daisho2	1676.173	-1.27375	0.285179	-4.4665	7.95E-06	0.005023
FBGN0266631	long non-coding RNA:CR45138	14.94086	-1.65681	0.372185	-4.45158	8.52E-06	0.005128
FBGN0003448	snail	48.67251	-1.64385	0.371566	-4.42411	9.68E-06	0.005561
FBGN0034317	CG14499	351.3903	-1.44843	0.329621	-4.39424	1.11E-05	0.006106
FBGN0261434	huckebein	15.16668	-1.56415	0.364537	-4.29079	1.78E-05	0.009372
FBGN0038180	Chitinase 5	84.08034	-1.35866	0.326031	-4.16725	3.08E-05	0.015117
FBGN0038431	CG10405	54.551	-1.34248	0.322309	-4.16518	3.11E-05	0.015117
FBGN0028855	CG15282	33.94868	-1.53449	0.369855	-4.1489	3.34E-05	0.015632
FBGN0034328	Bomanin Bicipital 1	689.9426	-1.41033	0.348005	-4.05263	5.06E-05	0.022852
FBGN0036350	CG14111	14.41806	-1.43945	0.361033	-3.98703	6.69E-05	0.029147
FBGN0085243	CG34214	90.94282	-1.43914	0.365146	-3.94128	8.1E-05	0.034132
FBGN0001230	Heat shock protein 68	380.1645	-1.45082	0.374131	-3.87783	0.000105	0.04161
FBGN0085294	CG34265	152.495	-1.43607	0.369837	-3.88297	0.000103	0.04161
FBGN0031632	CG15628	131.3915	-1.31741	0.340703	-3.86674	0.00011	0.042228
FBGN0032285	CG15628	4581.321	-1.20347	0.314398	-3.82784	0.000129	0.046664
FBGN0020377	Scavenger receptor class C, type II	88.25463	-1.38797	0.362598	-3.82786	0.000129	0.046664
FBGN0000473		7317.584	1.11744	0.292498	3.820335	0.000133	0.046771
FBGN0039286	distal antenna	79.32764	-1.4269	0.374526	-3.80989	0.000139	0.047472
FBGN0003430	sloppy paired 1	82.41038	-1.42197	0.373997	-3.8021	0.000143	0.047702

3.2. WGCNA network construction

As differential gene expression analysis yields very few results, we decided to use the weighted Gene Coexpression Network Analysis approach. We used featureCounts to process the data before inputting it into WGCNA for network analysis. From these feature counts, we created two Excel files that served as the primary inputs for the WGCNA analysis:

- A gene expression matrix, where rows correspond to genes and columns correspond to our samples. The values in the matrix represent the feature counts.
- A trait data matrix included the phenotypic data (i.e., control or heat-shocked treated flies).

The expression data was then converted to integers, and genes of low quality were filtered out. This expression data is also normalised and transformed.

Following these initial preparations, the next step involved constructing the network structure.

We first calculated the pairwise correlation between genes using a Pearson correlation to generate the adjacency matrix. Subsequently, we transformed the correlation matrix with a power adjacency function to prioritise stronger correlations.

The selection of the soft thresholding power, β, is critical. We chose a β value of 14, guided by the scale-free fit index where an R^2 value greater than 0.8 suggested a robust fit to a scale-free topology (**Figure 14A**). This means that the degree distribution, showing the proportion of nodes with a certain number of connections, forms a straight line with a negative slope when plotted on a log-log scale (**Figure 14C**). Moreover, a mean connectivity above 1 indicated adequate network robustness (**Figure 14B**). These parameters confirm that our network has a scale-free topology typified by a few highly connected nodes amongst many lesser-connected ones. The suitability of β=14 and the network's topological accuracy are further evidenced by the visual analyses presented in **Figure 15**.

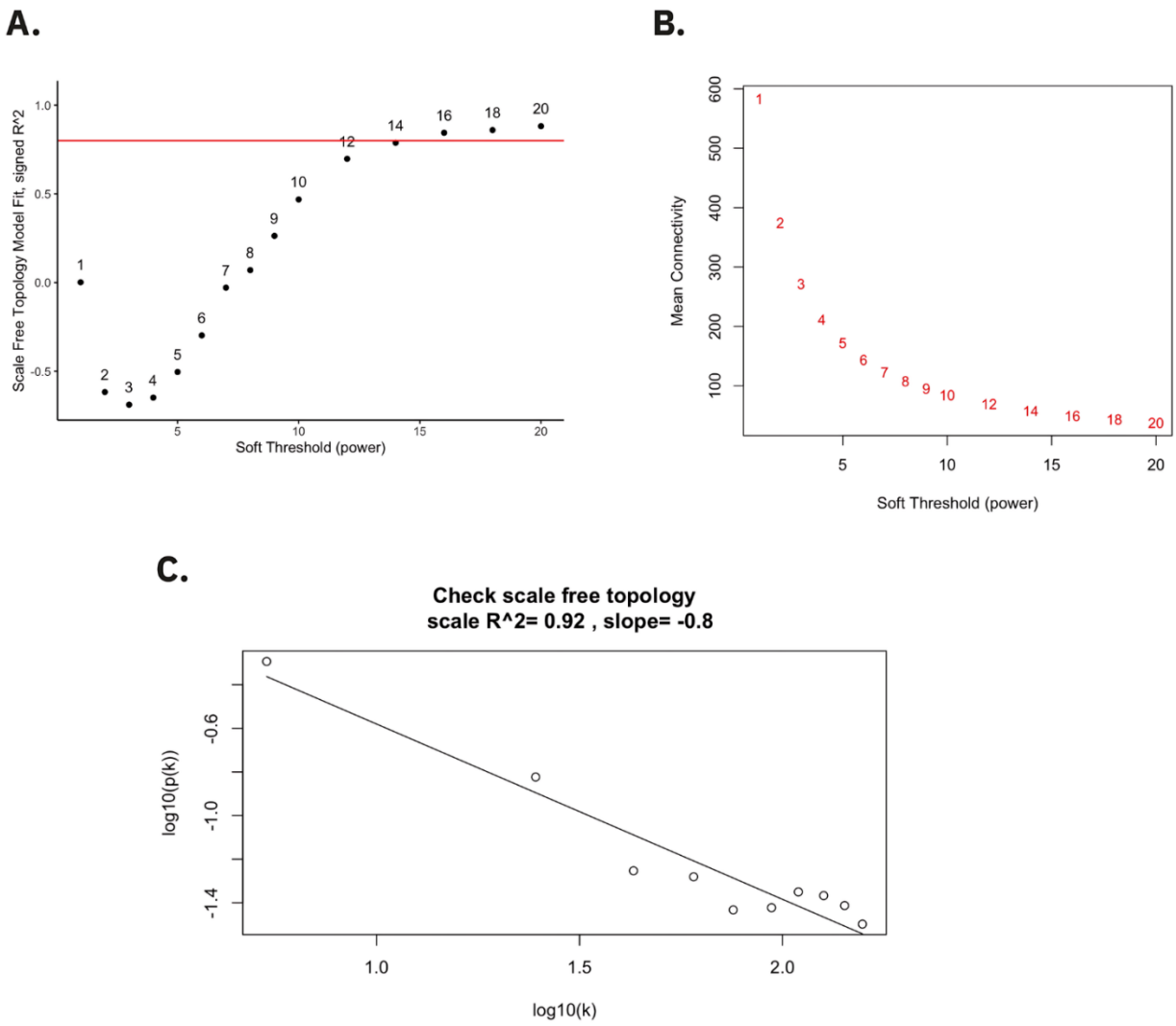

Figure 14. Soft threshold determination for WGCNA. A. Scale-free fit index: The plot shows the free-scale fit index across a range of soft thresholding powers. **B. Mean connectivity:** The plot displays the average connectivity within the network for different soft thresholding powers. **C. Log-Log degree distribution plot:** Validates the scale-free topology of the network at the selected β value, where network connectivity (K) and corresponding frequency distribution (p(k)) are plotted on a log10 scale, resulting in a linear relationship with a negative slope.

3.3. Identification of network modules

To define the network modules, we converted the adjacency matrix, representing the strength of connections between gene pairs, into a topological overlap matrix (TOM). The TOM captures the similarity of expression patterns between genes to identify robust and biologically meaningful modules (Dang et al., 2022).

The hierarchical clustering algorithm is then applied to the TOM to group genes into modules based on their topological overlap. Hierarchical clustering relies on the topological overlap measure to assign genes with similar expression patterns to the same module (**Figure 15A**) (H.-J. Lee et al., 2022). This approach ensures that genes within a module are highly interconnected and share similar co-expression patterns, while genes in different modules have distinct expression profiles (Saelens et al., 2018; Yu et al., 2022).

A dendrogram was produced to present the hierarchical structure of the modules (**Figure 15A).** Using the dynamic tree-cutting algorithm, we merged the branches of the clustering tree into different gene modules, each assigned a unique colour identifier (**Figure 15A**). The branches are the modules, and they are visualised and labelled using colours for more straightforward interpretation. Larger branches represent higher-level groupings, and smaller branches represent more specific subgroups.

Once the modules are defined, genes within these modules are evaluated for their co-expression strength. Genes with high co-expression, indicating strong correlation in their expression patterns, are merged based on their similarity or dissimilarity. By merging genes with high co-expression, the resulting modules become more robust and representative of specific biological processes or functional pathways. This facilitates the interpretation and analysis of gene expression data, as it allows for the identification of groups of genes that work together in a coordinated manner. This process resulted in identifying 9 distinct modules (**Figure 15B**).

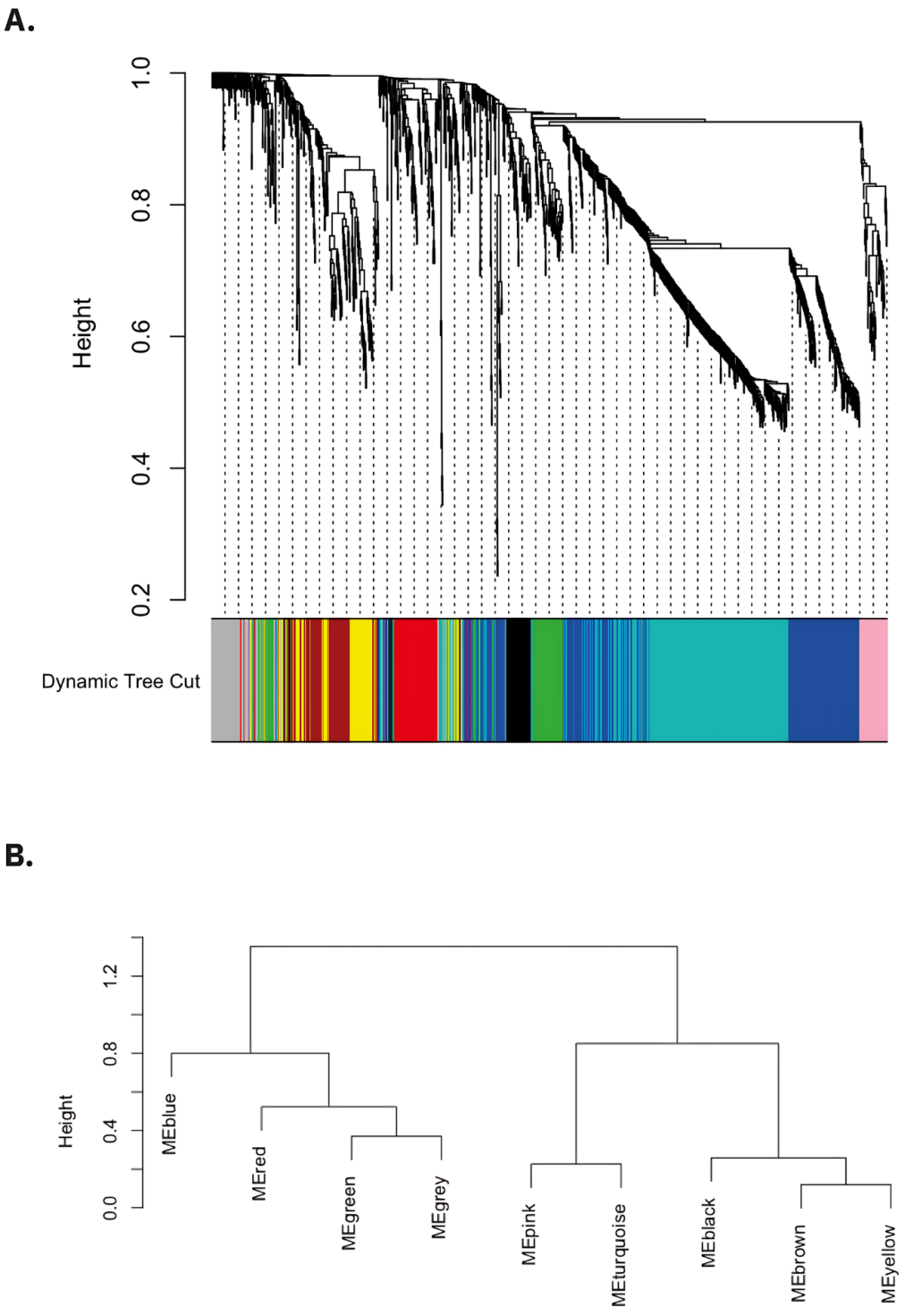

Figure 15. Gene co-expression analysis and module detection. **A. Gene clustering dendrogram:** Hierarchical clustering results based on gene expression similarity, revealing 11 distinct co-expression clusters. Each cluster is represented by a unique colour, with the grey module indicating genes that do not cluster significantly**. B. Grouping of modules:** Modules with similar gene expression patterns are grouped, with the vertical linkage distance reflecting their expression similarity levels. This process resulted in the identification of 9 distinct modules.

3.4. Related modules with traits of interest

In order to discern modules that exhibit significant associations with the traits following heat stress treatment, correlations were drawn between nine module eigengenes and external traits.

The module-trait correlations are detailed in a colour-coded table, as shown in **Figure 16A**. From this analysis, specific pronounced module-trait associations were observed. The black module, associated with the heat shock treatment, demonstrated a strong positive correlation. This module had a correlation coefficient (r) of 0.49, indicating a statistically significant association (p-value = 0.02). This points to the upregulation of genes in response to the heat shock treatment. In contrast, the blue module exhibited a negative correlation. The correlation coefficient (r) was -0.38, with a p-value of 0.09. This hints at a certain degree of gene downregulation following the treatment. The brown module stood out with a positive correlation. The correlation coefficient (r) reached 0.47, with a p-value of 0.03. This indicates gene upregulation linked to our trait of interest, heat stress.

Gene significance within these modules, which provides insights into the impact of each gene on the module's response to heat stress, is visually shown in the bar plot in **Figure 16B.**

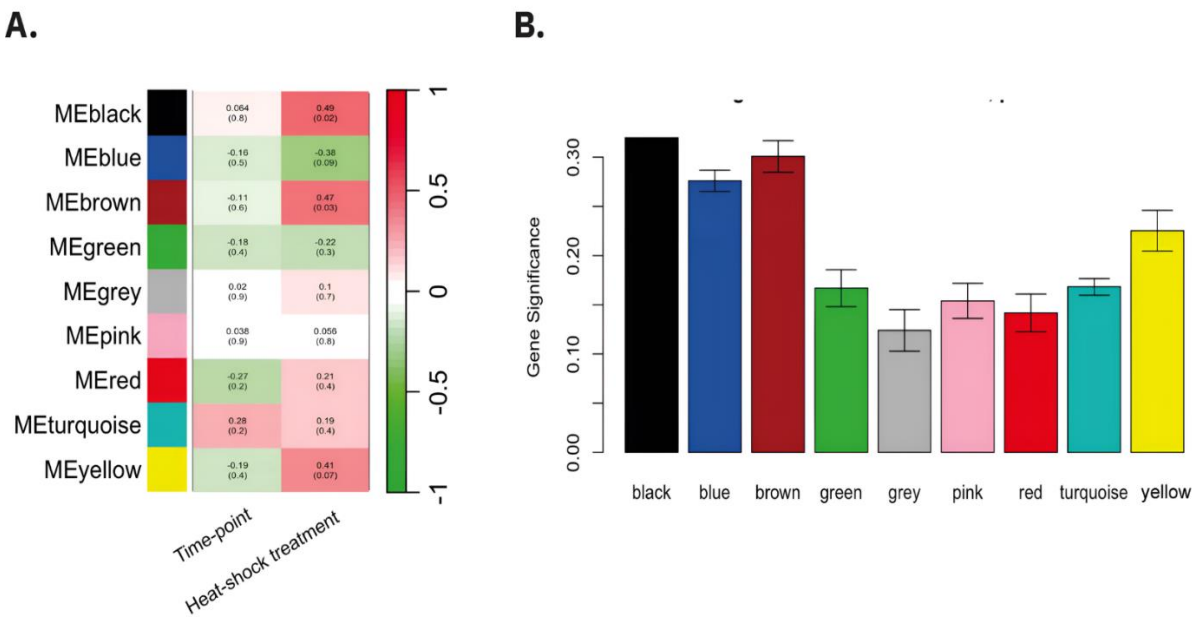

Figure 16. Module-Trait associations and gene significance in heat shock response. A. Correlation matrix of Module Eigengenes (ME) and traits: Heat map displaying the correlation between ME and two traits: time point and HS. The rows correspond to the MEs of various colours, while the columns represent the traits. Each cell within the matrix provides the correlation coefficient and p-value, indicating the strength and significance of the association. **B. Gene significance by module:** Bar plot showing GS for each module, colour-coded bars to match the corresponding module colours. The GS values reflect the association of individual genes with the heat shock response, where higher values indicate stronger relationships.

To further explore the relationship between Gene Significance (GS) and Module Membership (MM), we generated scatterplots for visualisation (**Figure 16**). Each plot point represents an individual gene, denoted by its GS and MM metrics. (**Figure 16**).

The correlation between GS and MM is pivotal in WGCNA. A robust positive correlation implies that genes within a module are significantly related to the trait of interest, denoting a pivotal biological influence. Conversely, a negative correlation suggests a weaker connection to heat stress for genes within a module (Lu et al., 2019; Wang et al., 2017).

Analysis revealed notable correlations with the heat shock treatment in the black (cor = 0.56, p-value = 0.1) (**Figure 17A**), brown (cor = 0.48, p-value = 0.1) (**Figure 17B**), and blue (cor = 0.32, p-value = 0.1) (**Figure 17C**) modules. If there is a high positive correlation between GS and MM for a particular module, this means genes that are central to that module (high MM) also have strong associations with the trait (high GS) (Chen et al., 2016).

Conversely, scatterplots in **Figures 17D, E, and F** depict the turquoise, red, and green modules, where the correlations are either negative or non-significant. The turquoise module shows a negative correlation (cor = -0.55, p-value = 0.00016), indicating an inverse relationship between GS and MM. Meanwhile, the red and green modules show negligible correlations (cor = -0.0087, p-value = 0.96; cor = 0.0012, p-value = 0.99), suggesting these genes are not strongly associated with the heat shock response within their modules.

For subsequent analyses, we will specifically target the black, blue, and brown modules (**Figure 18A-C**).

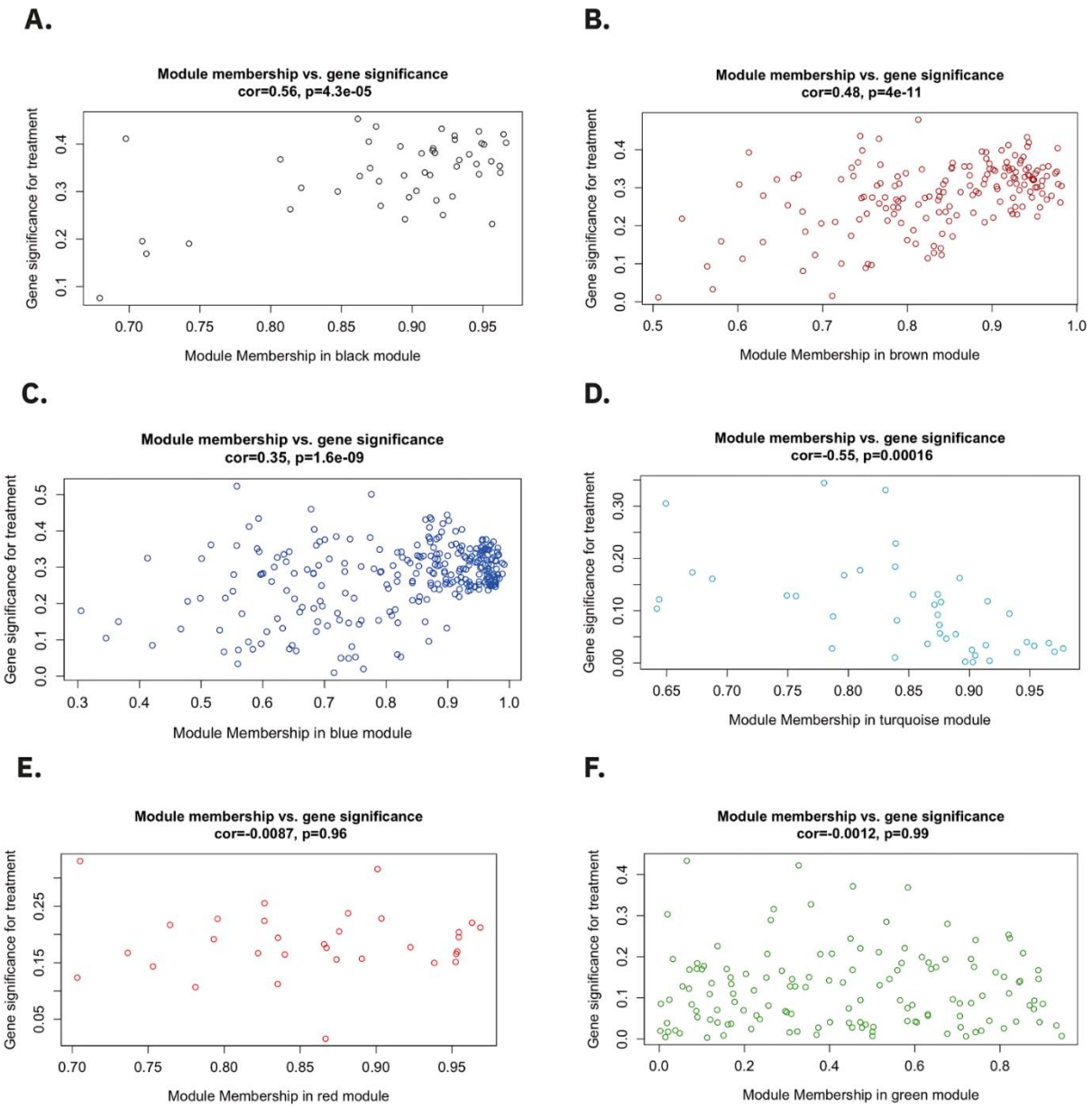

Figure 17. Correlation of GS and MM across modules. **A-C**. Scatterplots illustrating significant positive correlations of Gene Significance (GS) with Module Membership (MM) in black (A), brown (B), and blue (C) modules, indicative of genes crucial to the heat shock response (black module: cor = 0.56, p-value = 4.3e-05; brown module: cor = 0.48, p-value = 4e-11; blue module: cor = 0.35, p-value = 1.6e-09). **D-F.** Scatterplots for turquoise (D), red (E), and green (F) modules show negative or non-significant correlations, suggesting a weaker or non-existent relationship to the trait of heat shock (turquoise module: cor = -0.55, p-value = 0.00016; red module: cor = -0.0087, p-value = 0.96; green module: cor = 0.0012, p-value = 0.99).

3.5. Hub genes and identification of key modules

We focused on three modules, black, brown, and blue, selected for their high Gene Significance (GS) and correlation with module membership. Using a threshold of GS >|0.2| and Module Membership (MM) >|0.8|, we identified hub genes within these modules (Langfelder & Horvath, 2008).

GO enrichment analysis was performed for all hub genes from the three target modules. Please refer to **Table 7** for hub genes in the black module, **Table 8** for the brown module, and **Table 9** for the blue module. In the Biological Process category, 'nuclear division' was notably associated (**Figure 18A**). Enrichments in the Cellular Component category included components such as the 'cyclin-dependent protein kinase holoenzyme complex' (**Figure 18C**). In the Molecular Function category, 'translation repressor activity' emerged as a significant term (**Figure 18B**). Furthermore, the KEGG pathway enrichment analysis identified key pathways, including the 'Fanconi anaemia pathway' and the 'MAPK signalling pathway', highlighting a broad spectrum of cellular activities influenced by heat stress (**Figure 18D**).

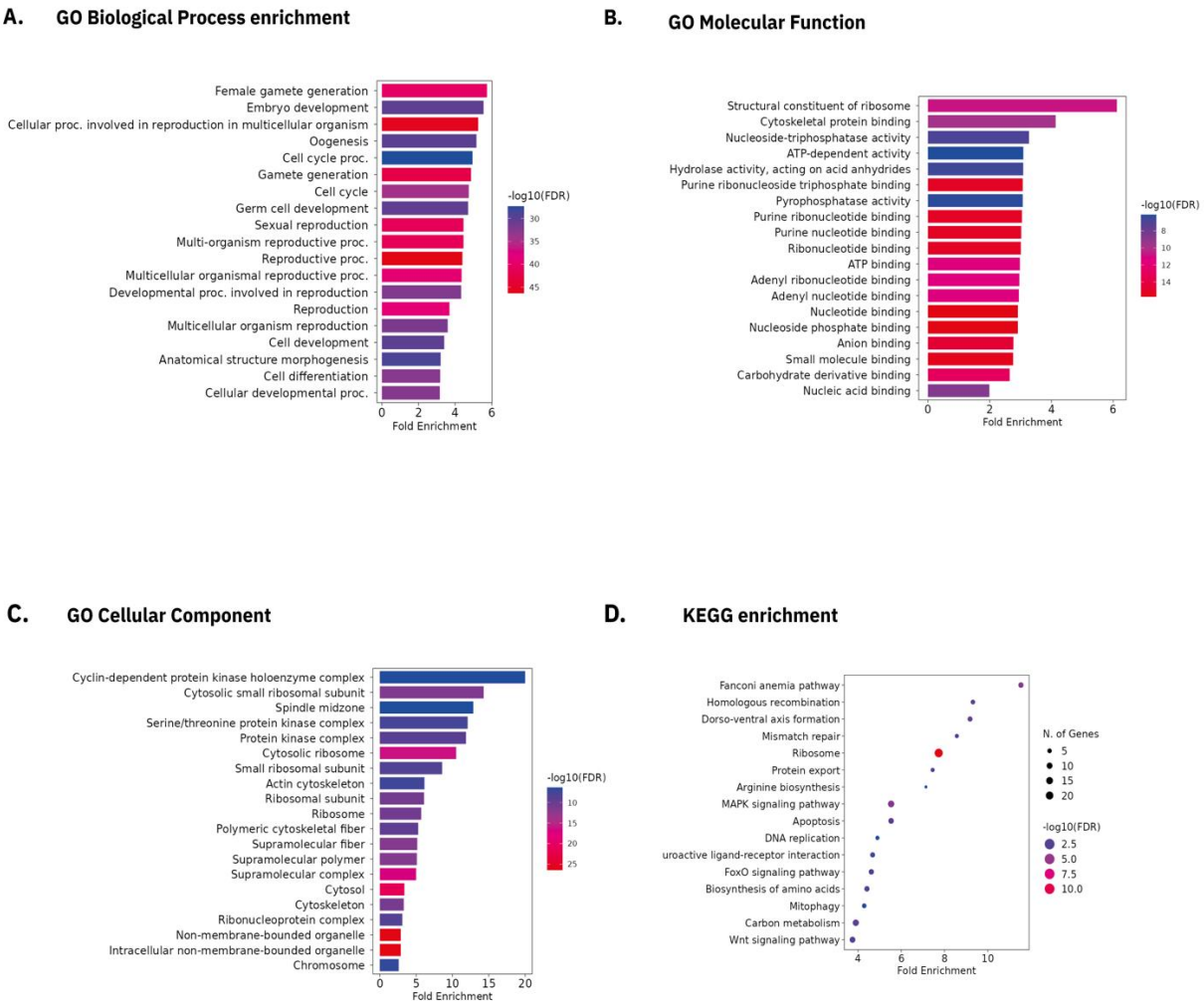

Figure 18. Gene Ontology (GO) enrichment analysis of hub genes from the three targeted modules (black, brown and blue). **A. Biological process enrichment:** Bar chart illustrating significant GO terms in the biological process category for hub genes. **B. KEGG pathway enrichment analysis:** Scatter plot showing the enrichment of KEGG pathways, with the size of each point indicating the number of genes involved and colour denoting the significance level (-log10 FDR). **C. Cellular component enrichment:** Bar chart displaying significant GO terms in the Cellular component category for hub genes, with fold enrichment on the x-axis. **D. Molecular Function Enrichment:** Bar chart of significant GO terms in the molecular function category for hub genes, sorted by fold enrichment.

3.6. Functional annotation of hub genes in the black module

We identified 42 hub genes in the black module, each characterised by their module membership (MM) and gene significance (GS), as detailed in Table 7.

3.6.1. Gene Ontology (GO) Enrichment Analysis:

GO Biological Process (BP) Enrichment:

The GO BP enrichment for the black module, illustrated in **Figure 19A**, predominantly associated it with DNA repair, such as 'reciprocal homologous recombination' and 'cell cycle', along with a response to DNA damage stimuli (**Supplementary Table 10)**.

GO Molecular Function (MF) Enrichment:

As shown in **Figure 19B**, the MF enrichment analysis of the black module exhibited significant involvement with n with activities related to DNA polymerase function, indicative of a robust involvement in DNA synthesis and repair. Key functions such as 'DNA-directed DNA polymerase activity' and 'ATP-dependent activity, acting on DNA' are highlighted, suggesting active participation in DNA damage repair (**Supplementary Table 11)**.

3.6.2. KEGG Pathway Enrichment Analysis:

As depicted in **Figure 19C** and Supplementary Table 12, the KEGG pathway analysis emphasises the black module's engagement in critical DNA repair pathways, including the 'Homologous Recombination' and 'Fanconi Anemia' pathways. '

3.6.3. Hub Gene Specific Analysis:

In our analysis of the black module, we focused on identifying genes with GS, irrespective of whether the values are positive or negative, and MM, which is as close as possible to positive 1. GS is crucial as it indicates the correlation of each gene with heat stress; positive values imply a positive correlation, while negative values indicate a negative correlation. Conversely, MM reveals the degree of association of each gene with the black module. Values close to 1 suggest a strong association with the module, whereas values closer to -1 indicate a weaker one.

Several genes stand out due to their high GS and MM values, suggesting they are upregulated in response to heat stress. These include gd (GS =0.35 and MM of 0.96), mus101 (GS = 0.40, MM = 0.96), okr (GS= 0.36, MM=0.96), snk (GS=0.34 and MM =0.96), spn-B (GS=0.12, MM=0.96), and *zfh1* (GS=0.42, MM=0.96).

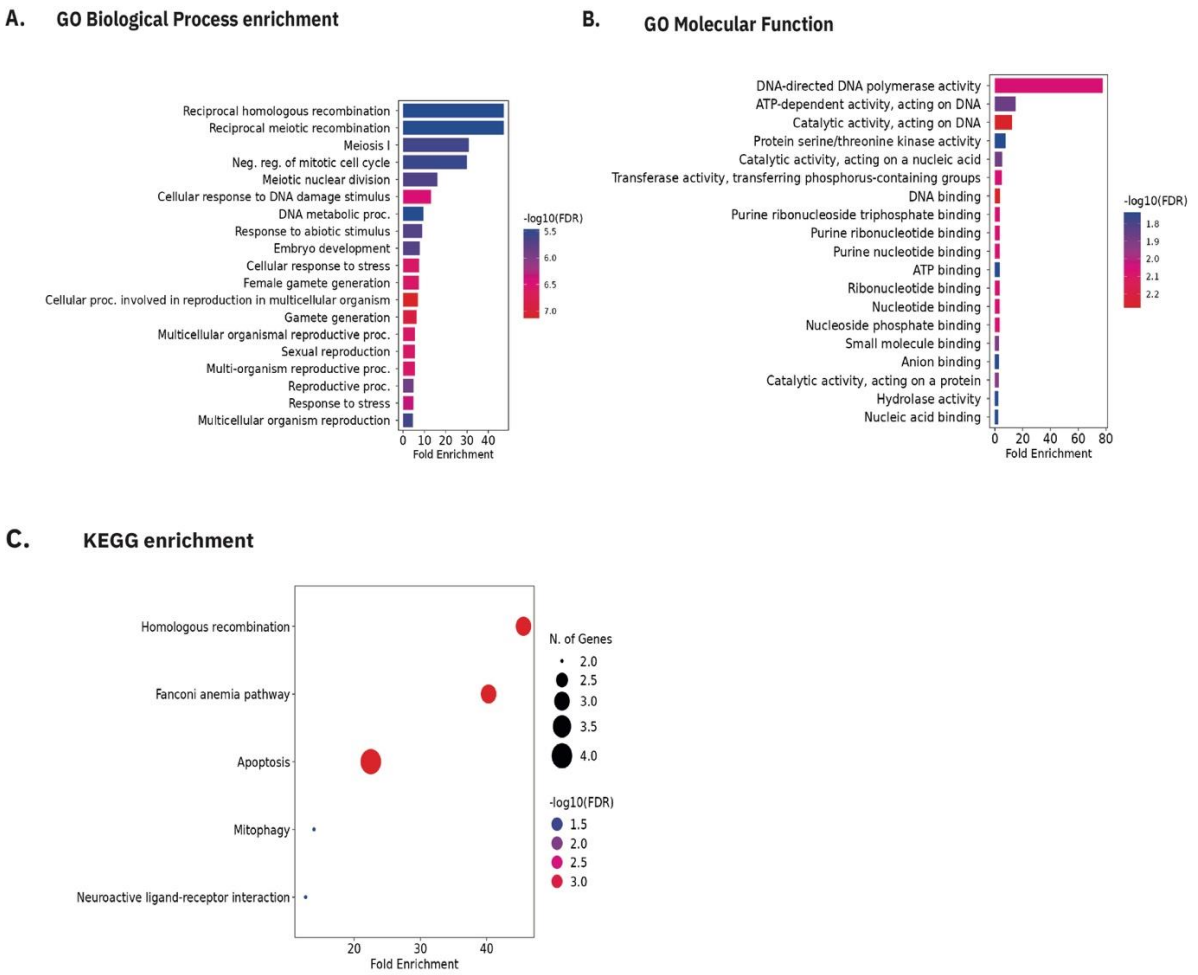

Figure 19. Gene Ontology and KEGG pathway analysis of the black module. A. Biological process enrichment: Bar chart illustrating the significant GO terms associated with biological processes for genes within the black module, with fold enrichment represented on the x-axis. **B. Molecular function enrichment:** Bar chart detailing significant GO terms related to molecular functions for genes in the black module, sorted by fold enrichment. **C. KEGG pathway enrichment** analysis: Scatter plot showing the enriched KEGG pathways for genes in the black module. The size of each point indicates the number of genes involved, and the colour denotes the significance level, with darker shades representing higher −log10 (p-value) values.

Table 9. List of genes identified in the black module from WGCNA analysis, with a focus on their significance and association within the module. The 'Flybase ID' column provides unique identifiers for each gene, while the 'Gene Name' column specifies the common names. Gene Significance indicates the correlation of each gene with heat stress, where positive values imply a positive correlation and negative values indicate a negative correlation. Module Membership shows the degree of association of each gene with the black module, with values close to 1 suggesting a strong association and values close to -1 indicating a weaker association.

FLY BASE ID	GENE NAME	GENE SIGNIFICANCE (GS)	MODULE MEMBERSHIP (MM)
FBGN0000229	bsk	-0.4176257	-0.9300133
FBGN0000244	by	-0.3363752	-0.9472167
FBGN0000256	capu	-0.2999264	-0.8473436
FBGN0010501	Dcp-1	-0.3862748	-0.9144869
FBGN0000588	esc	0.30117883	0.90296434
FBGN0004510	Ets97D	0.30778103	0.82160298
FBGN0000320	eya	0.45291934	0.86150896
FBGN0000808	gd	0.3538284	0.96183866
FBGN0001123	Gαs	-0.4012979	-0.9491007
FBGN0001189	hfw	-0.3323685	-0.8629655
FBGN0001202	hook	-0.408994	-0.9301668
FBGN0001168	hry	-0.2627953	-0.8138192
FBGN0011603	ine	-0.3344765	-0.9126106
FBGN0001291	Jra	-0.3527247	-0.9314168
FBGN0002578	Kaz-m1	-0.4266407	-0.9471482
FBGN0001234	lncRNA:Hsrω	-0.357814	-0.9454673
FBGN0010398	Lrr47	0.25057187	0.92177292
FBGN0004512	Mdr49	-0.2698566	-0.8777781
FBGN0004367	mei-41	0.43199493	0.92078641
FBGN0002707	mei-9	0.2877549	0.89776453
FBGN0002715	mei-S332	0.34020855	0.90889742
FBGN0000063	Mps1	0.38022917	0.90661235
FBGN0002878	mus101	0.39888144	0.9507067
FBGN0002901	mus304	0.28133628	0.91704857
FBGN0002989	okr	0.36367493	0.9558764
FBGN0011754	PhKγ	-0.2894567	-0.9284044
FBGN0010309	pigeon	0.24159766	0.89486567
FBGN0002905	PolQ	0.38138767	0.91609218
FBGN0002891	PolZ1	0.36746506	0.80684377
FBGN0011762	Prim1	0.37830771	0.94029736

FBGN0003292	rt	0.39099624	0.91479998
FBGN0011020	Sas-4	0.32147109	0.87659753
FBGN0003321	sbr	-0.3337598	-0.8942377
FBGN0003444	smo	0.39508495	0.89165935
FBGN0002878	Mus101		
FBGN0003450	snk	0.33976588	0.96225001
FBGN0003480	spn-B	0.23151291	0.95654555
FBGN0001990	wek	0.34930601	0.8702001
FBGN0004606	zfh1	0.42039889	0.96456248
FBGN0003890	βTub97EF	-0.4027514	-0.9663799
FBGN0010359	γTry	-0.4049356	-0.8693224
FBGN0010358	δTry	-0.4367917	-0.8745214
FBGN0010425	εTry	-0.3662955	-0.9332473

3.7. Functional annotation of hub genes in the brown module

We identified 102 hub genes in the brown module, characterised by high gene significance (GS < |0.2|) and high module membership (MM) (MM < |0.8|), detailed in **Table 10**.

3.7.1. Gene Ontology (GO) Enrichment Analysis:

GO Biological Process (BP) Enrichment:

The GO BP enrichment for the brown module, illustrated in **Figure 20A and Supplementary Table 13**, highlighted significant activities such as 'nuclear division' and 'organelle fission,' as well as various reproductive functions, including 'female gamete generation' and 'oogenesis.'

GO Molecular Function (MF) Enrichment:

As shown in **Figure 20B and Supplementary Table 14,** the MF enrichment analysis of the brown module revealed a strong correlation with functions related to 'translation repressor activity' and 'cyclin-dependent protein serine/threonine kinase activity.'

3.7.2. KEGG Pathway Enrichment Analysis:

The KEGG pathway enrichment (**Figure 20C and Supplementary Table 15)** demonstrated the module´s association with critical DNA repair pathways, such as 'mismatch repair' and 'Fanconi anaemia pathway,' and processes vital for development like 'dorsoventral axis formation.' Moreover, the enrichment in 'DNA replication' and 'FoxO signalling pathway' underscores the module's involvement in maintaining cellular homeostasis and orchestrating responses to environmental stress.

3.7.3. Hub Gene Specific Analysis:

In our detailed analysis of the brown module hub genes, we concentrated on identifying genes with high Gene Significance (GS), either positively or negatively, coupled with a strong Module Membership (MM).

Key genes that stand out in the brown module, all being upregulated in response to HS include: *hsp26* (GS = 0.22 and MM = 0.90), *hsp27* (GS = 0.23, MM = 0.93), *grip91* (GS = 0.30, MM = 0.91), In the context of cell cycle regulation, we highlight hub genes including *cdk1* (GS = 0.36, MM = 0.92) and *cdk2* (GS = 0.36, MM = 0.97) are particularly noteworthy. They are accompanied by various cyclin genes such as *cycA* (GS = 0.30, MM = 0.87), *cycB* (GS = 0.28, MM = 0.86), *cycD* (GS = 0.21, MM = 0.89), *cycE* (GS =

0.29, MM = 0.93). There is an upregulation of other genes of interest for the cell cycle, including *polo* (GS = 0.35, MM = 0.90), *stg* (GS = 0.39, MM = 0.93), *PCNA* (GS = 0.32, MM = 0.89), *asp (*GS = 0.32, MM = 0.95), *pav* (GS = 0.35, MM = 0.94), and *pbl* (GS = 0.41, MM = 0.94). The module's linkage to structural components like the spindle midzone and mitotic spindle is further highlighted by genes such as *blm* (GS = 0.33, MM = 0.91), and *rrp1* (GS = 0.38, MM = 0.89) (**Table 8**).

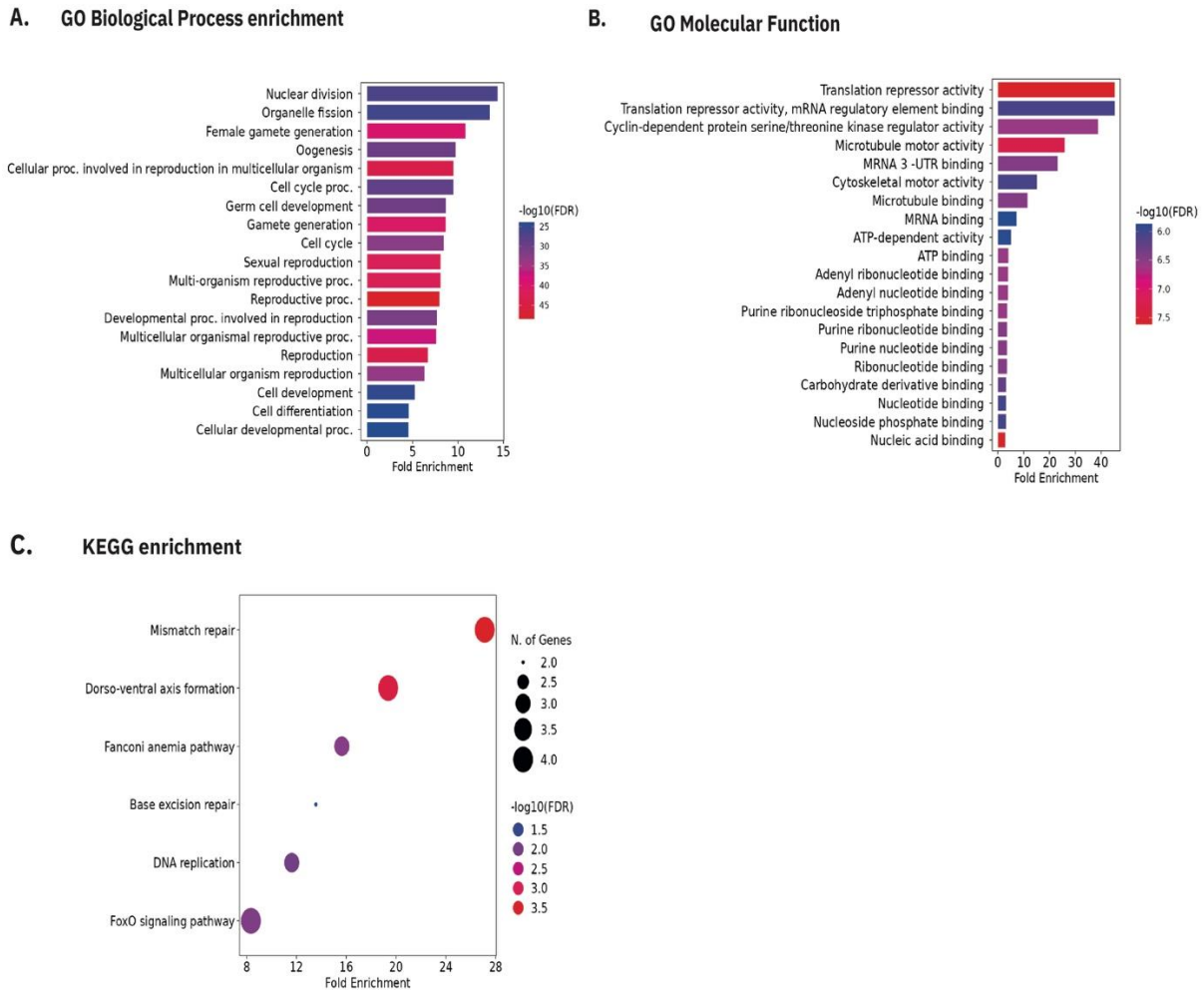

Figure 20. Gene Ontology and KEGG pathway analysis of the brown module. A. Biological process enrichment: Bar chart with the significant GO terms associated with biological processes for genes within the brown module, with fold enrichment represented on the x-axis. **B. Molecular function enrichment:** Bar chart detailing significant GO terms related to molecular functions for genes in the brown module, sorted by fold enrichment. **C. KEGG pathway enrichment analysis:** Scatter plot showing the enriched KEGG pathways for genes in the brown module. The size of each point indicates the number of genes involved, and the colour denotes the significance level, with darker shades representing higher −log10 (p-value) values.

Table 10. List of genes identified in the brown module from WGCNA analysis, with a focus on their significance and association within the module. The 'Flybase ID' column provides unique identifiers for each gene, while the 'Gene Name' column specifies the common names. Gene Significance indicates the correlation of each gene with heat stress where positive values imply a positive correlation and negative values indicate a negative correlation. Module Membership shows the degree of association of each gene with the brown module, with values close to 1 suggesting a strong association and values close to -1 indicating a weaker association.

FLY BASE ID	GENE NAME	GENE SIGNIFICANCE (GS)	MODULE MEMBERSHIP (MM)
FBGN0010223	Gαf	-0.3483171	-0.8172103
FBGN0004580	Cbp53E	-0.3183594	-0.8449278
FBGN0004910	Eip63F-1	-0.2862117	-0.8841034
FBGN0005771	noc	-0.255947	-0.8131066
FBGN0004057	Zw	-0.2200344	-0.8221071
FBGN0010315	CycD	0.20912742	0.89115331
FBGN0005695	gcl	0.21222157	0.84934648
FBGN0001225	Hsp26	0.22112497	0.90130549
FBGN0010431	mtrm	0.22439661	0.95346041
FBGN0011761	dhd	0.22758893	0.8581163
FBGN0001226	Hsp27	0.22975146	0.92949006
FBGN0000615	exu	0.23120708	0.92426671
FBGN0003165	pum	0.23373512	0.87787515
FBGN0004913	Gnf1	0.23539463	0.83745166
FBGN0003598	Su(var)3-7	0.23644135	0.84502469
FBGN0000114	bru1	0.23986521	0.92199314
FBGN0001120	gnu	0.24819627	0.95648129
FBGN0010300	brat	0.24919836	0.92729229
FBGN0011703	RnrL	0.24986743	0.93582927
FBGN0004598	Fur2	0.25063992	0.84976147
FBGN0010097	γTub37C	0.26105214	0.98062009
FBGN0004649	yl	0.26300501	0.90945892
FBGN0004666	sim	0.26700675	0.83645194
FBGN0003655	swa	0.26896096	0.96449465
FBGN0010278	Ssrp	0.2732345	0.8207605
FBGN0005596	yem	0.27345816	0.92468422
FBGN0002542	lds	0.27438611	0.94708623
FBGN0003346	RanGAP	0.27620519	0.83789377
FBGN0010313	corto	0.27658332	0.82593097
FBGN0003023	otu	0.27861476	0.97008687

FBGN0000166	bcd	0.28087027	0.87702846
FBGN0000927	fs(1)Ya	0.2847844	0.95923807
FBGN0000405	CycB	0.28839018	0.86278379
FBGN0010113	heca	0.28839462	0.84259365
FBGN0000246	c(3)G	0.28951234	0.9449406
FBGN0002926	ndl	0.29044277	0.88098255
FBGN0011474	Set8	0.29099038	0.83711759
FBGN0010382	CycE	0.29363304	0.93214312
FBGN0001612	Grip91	0.29675553	0.90624295
FBGN0003495	spz	0.30101331	0.95102368
FBGN0004650	fs(1)N	0.30119103	0.9532513
FBGN0011802	Gem3	0.3031026	0.90548345
FBGN0003187	qua	0.30427063	0.9584813
FBGN0002962	nanos	0.3046518	0.98191406
FBGN0000404	CycA	0.3054313	0.87397997
FBGN0002673	twe	0.30782788	0.93799814
FBGN0003410	sina	0.3092283	0.84242103
FBGN0000376	crm	0.30932959	0.89025561
FBGN0003483	spn-E	0.30940886	0.97792278
FBGN0005390	fs(1)M3	0.3106267	0.92882097
FBGN0005683	pie	0.31183357	0.92111623
FBGN0000147	aurA	0.31813869	0.95921064
FBGN0011666	msi	0.3199262	0.94840009
FBGN0011606	Klp3A	0.32063267	0.94937564
FBGN0000140	asp	0.32184352	0.94895148
FBGN0003268	rod	0.32289898	0.94724758
FBGN0005655	PCNA	0.32316134	0.8916538
FBGN0003044	Pcl	0.32411561	0.92709422
FBGN0011660	Pms2	0.32677773	0.92537667
FBGN0004872	piwi	0.32837204	0.93847797
FBGN0002948	nod	0.330325	0.96465138
FBGN0002906	Blm	0.33108535	0.91407252
FBGN0000146	aub	0.33185137	0.94391647
FBGN0011818	oaf	0.33233497	0.8736437
FBGN0003114	plu	0.33376111	0.94248735
FBGN0000996	dup	0.33496644	0.89422619
FBGN0000826	png	0.33754857	0.95111411
FBGN0003028	ovo	0.33808246	0.97459953
FBGN0002899	mus301	0.34112955	0.92794863
FBGN0003447	sn	0.34248681	0.97635092

FBGN0003087	pim	0.3445181	0.90344339
FBGN0011224	heph	0.34455478	0.95322283
FBGN0003545	sub	0.34548434	0.92026615
FBGN0004882	orb	0.34761367	0.93974526
FBGN0003124	polo	0.34778592	0.90120183
FBGN0000158	bam	0.3495924	0.8971245
FBGN0010314	Cks30A	0.34984045	0.92374838
FBGN0000964	tj	0.35049563	0.85204285
FBGN0001085	fz	0.35241713	0.91926754
FBGN0003527	stil	0.3527222	0.91561801
FBGN0000352	cos	0.35346452	0.85285119
FBGN0003733	tor	0.35362535	0.959851
FBGN0011692	pav	0.35363784	0.9432262
FBGN0011659	Mlh1	0.3558298	0.86738715
FBGN0004400	rhi	0.35613628	0.87349418
FBGN0004107	Cdk2	0.35648029	0.96631551
FBGN0003701	thr	0.36307584	0.89686412
FBGN0003401	shu	0.36473943	0.93305987
FBGN0000547	ed	0.36520092	0.85352613
FBGN0004106	Cdk1	0.3674728	0.91735459
FBGN0003015	osk	0.37167479	0.93408434
FBGN0004584	Rrp1	0.37660465	0.89315542
FBGN0000351	cort	0.38141511	0.93698665
FBGN0003525	stg	0.38549391	0.92698033
FBGN0010317	CycJ	0.3934232	0.89304446
FBGN0003310	S	0.39529778	0.88796172
FBGN0002924	ncd	0.39845317	0.91127562
FBGN0002872	mu2	0.4039432	0.97744474
FBGN0003041	pbl	0.40837264	0.94182228
FBGN0004378	Klp61F	0.41205086	0.91920508
FBGN0005696	PolA2	0.41892863	0.94330694
FBGN0004379	Klp67A	0.4328828	0.94138349
FBGN0001180	hb	0.47900371	0.81284787

3.8. Functional annotation of hub genes in the blue module

We identified 87 hub genes in the blue module, with their specifics detailed in Table 9.

3.8.1. Gene Ontology (GO) Enrichment Analysis

GO Biological Process (BP) Enrichment:

As shown in **Figure 21A** and Supplementary Table 16, the GO BP enrichment for the blue module revealed significant involvement in processes such as 'cytoplasmic translation' and various developmental processes, including 'embryo development ending in birth or egg hatching' and 'system development.'

GO Molecular Function (MF) Enrichment:

The blue module's MF enrichment analysis showed a strong association with activities involving 'myosin heavy chain binding' and 'GTPase activity,' among others (**Figure 21B and Supplementary Table 17**).

3.8.2. KEGG Pathway Enrichment Analysis:

The KEGG pathway enrichment (**Figure 21C and Supplementary Table 18**) highlighted the blue module's significant contribution to pathways involved in 'ribosome' and 'protein export', as well as metabolism-related pathways such as 'alanine, aspartate and glutamate metabolism' and 'biosynthesis of amino acids'.

3.8.3. Hub Gene Specific Analysis:

We paid attention to hub genes (**Table 9**) that exhibited high correlation within the module, we found out a clear downregulation of genes following heat stress: *catsup* (GS = -0.38, MM = 0.96), *jon99ciii* (GS = -0.38, MM = 0.96), *jon99cii* (GS = -0.37, MM = 0.96), *syb* (GS = -0.37, MM = 0.97), *fkbp14* (GS = -0.36, MM = 0.97), *arp1* (GS = -0.36, MM=0.97), *ifc* (GS = -0.36, MM = 0.96), *θtry* (GS = -0.35, MM = 0.95), *nd-acp* (GS = -0.35, MM = 0.98) and *mtna* (GS = -0.35, MM = 0.96).

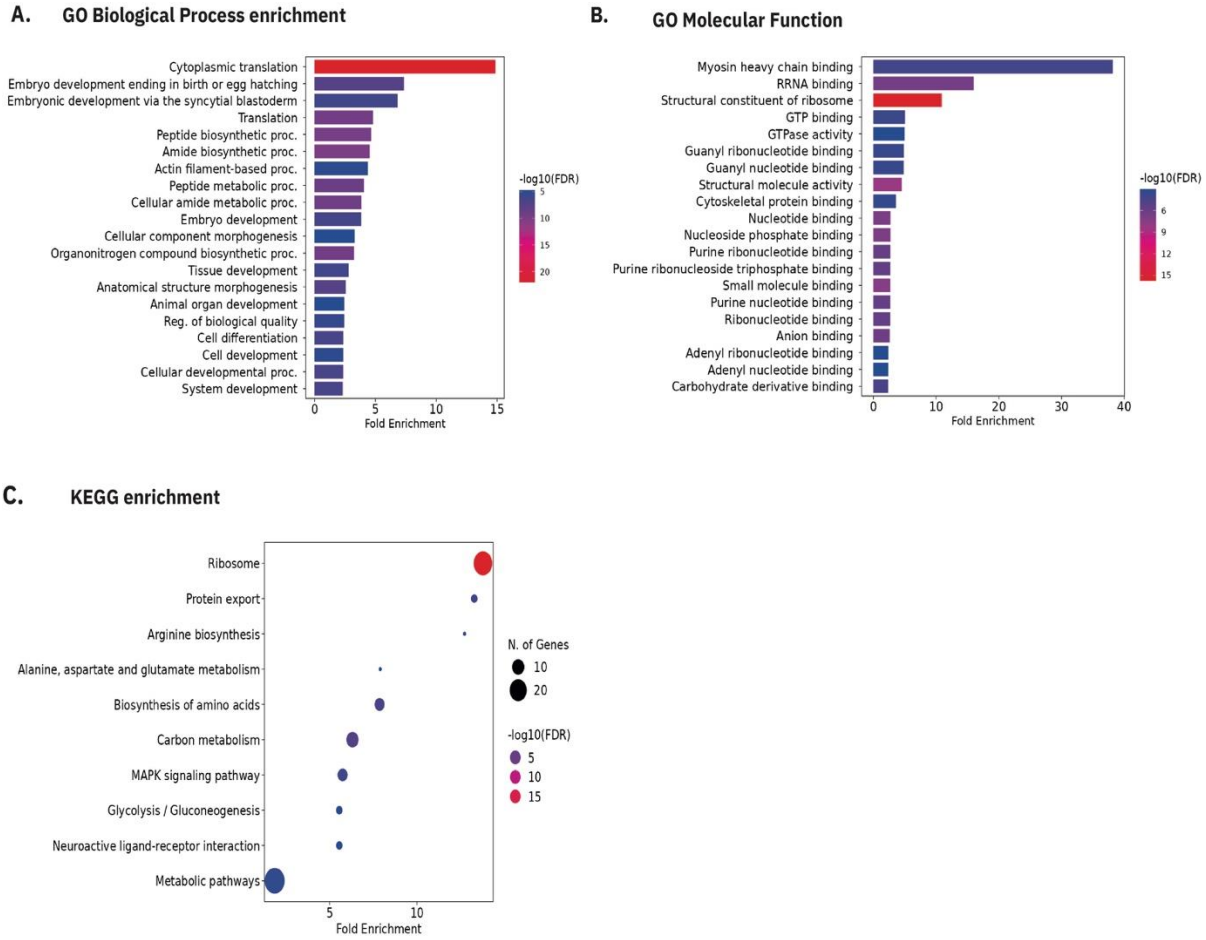

Figure 21. Gene Ontology and KEGG Pathway Analysis of the blue module. **A. Biological process enrichment:** Bar chart illustrating the significant GO terms associated with biological processes for genes within the blue module, with fold enrichment represented on the x-axis. **B. Molecular function enrichment:** Bar chart detailing significant GO terms related to molecular functions for genes in the blue module, sorted by fold enrichment**. C. KEGG pathway enrichment analysis:** Scatter plot showing the enriched KEGG pathways for genes in the blue module. The size of each point indicates the number of genes involved, and the colour denotes the significance level, with darker shades representing higher −log10 (p-value) values.

Table 11. List of genes identified in the blue module from WGCNA analysis, with a focus on their significance and association within the module. The 'Flybase ID' column provides unique identifiers for each gene, while the 'Gene Name' column specifies the common names. Gene Significance column indicates the correlation of each gene with heat stress where positive values imply a positive correlation and negative values indicate a negative correlation. Module Membership shows the degree of association of each gene with the brown module, with values close to 1 suggesting a strong association and values close to -1 indicating a weaker association.

FLY BASE ID	GENE NAME	GENE SIGNIFICANCE (GS)	MODULE MEMBERSHIP (MM)
FBGN0011705	ROST	-0.444139	0.89902025
FBGN0000339	cni	-0.4367711	0.87147748
FBGN0004228	mex1	-0.4322454	0.87338655
FBGN0011509	SrpRβ	-0.4313557	0.86392463
FBGN0011822	Pgcl	-0.4283355	0.90170328
FBGN0011227	ox	-0.420183	0.89207957
FBGN0005670	Cyp4d1	-0.409782	0.87045326
FBGN0011554	ηTry	-0.4041994	0.92291623
FBGN0010228	HmgZ	-0.3990724	0.91284023
FBGN0001989	ND-B17	-0.3972743	0.89007379
FBGN0002524	lace	-0.3836097	0.86910816
FBGN0010387	Acbp2	-0.3825536	0.88560481
FBGN0010504	kermit	-0.3790046	0.87067168
FBGN0002174	CG5504	-0.3778712	0.88152652
FBGN0002022	Catsup	-0.3765795	0.96225394
FBGN0003357	Jon99Ciii	-0.3765688	0.95627251
FBGN0003356	Jon99Cii	-0.3728144	0.95606193
FBGN0003660	Syb	-0.3702023	0.97416991
FBGN0004465	Su(P)	-0.364333	0.91334026
FBGN0010470	Fkbp14	-0.3624039	0.96997899
FBGN0010397	LamC	-0.3613948	0.85061589
FBGN0001285	Jon44E	-0.3612791	0.90607473
FBGN0002789	Mp20	-0.358885	0.92305441
FBGN0011745	Arp1	-0.358049	0.96745921
FBGN0001941	ifc	-0.3576798	0.95688923
FBGN0011555	θTry	-0.3541863	0.95402388
FBGN0002772	Mlc1	-0.3540638	0.87707419
FBGN0011708	Syx5	-0.3534757	0.91921221
FBGN0011361	ND-ACP	-0.3528939	0.98126392
FBGN0002868	MtnA	-0.3514444	0.9603437

FBGN0004574	Rop	-0.3507161	0.93596452
FBGN0005322	nmd	-0.3497403	0.96202043
FBGN0010808	Chchd3	-0.3486255	0.95950695
FBGN0004687	Mlc-c	-0.3483136	0.96487253
FBGN0004921	Gγ1	-0.3480475	0.96684501
FBGN0004179	Csp	-0.3462755	0.92172479
FBGN0003514	sqh	-0.3441887	0.95538045
FBGN0000253	Cam	-0.3436486	0.95784884
FBGN0003721	Tm1	-0.342121	0.98054855
FBGN0010235	Klc	-0.3410465	0.97161505
FBGN0001961	Arpc1	-0.340275	0.95381444
FBGN0000318	cl	-0.3391283	0.94538683
FBGN0010803	TrpRS	-0.3376005	0.88669302
FBGN0004654	Pgd	-0.3353534	0.95176799
FBGN0003863	αTry	-0.3343977	0.98283455
FBGN0011455	ND-SGDH	-0.3328945	0.98107097
FBGN0004117	Tm2	-0.3315487	0.89987638
FBGN0002567	Rab32	-0.3311755	0.87265351
FBGN0010638	Sec61β	-0.3306478	0.92718643
FBGN0010741	Pfdn2	-0.3301666	0.85378829
FBGN0004436	Ubc6	-0.3298399	0.93908395
FBGN0000115	Arl1	-0.3272676	0.82662577
FBGN0010497	dmGlut	-0.3270276	0.85601873
FBGN0010611	Hmgs	-0.3258615	0.92913148
FBGN0010357	βTry	-0.3249923	0.95882649
FBGN0010246	Myo61F	-0.3245491	0.93601747
FBGN0004636	Rap1	-0.3238859	0.87922252
FBGN0001247	Ide	-0.3216994	0.88370405
FBGN0010612	ATPsynG	-0.3199862	0.97026227
FBGN0010213	Sod2	-0.3199485	0.96383791
FBGN0010339	128up	-0.3194065	0.83462999
FBGN0010348	Arf1	-0.3190549	0.97736495
FBGN0010341	Cdc42	-0.3181437	0.94992979
FBGN0002773	Mlc2	-0.3168622	0.93512097
FBGN0000116	Argk1	-0.3165067	0.97845862
FBGN0011016	SsRβ	-0.3135731	0.94529435
FBGN0010391	SrpRα	-0.3134376	0.94819656
FBGN0003139	PpV	-0.3117279	0.83889408
FBGN0004907	14-3-3ζ	-0.3114697	0.98847149
FBGN0000308	chic	-0.3095204	0.96568914

FBGN0001187	Hex-C	-0.3093877	0.89539987
FBGN0010516	wal	-0.3073079	0.99156616
FBGN0003169	put	-0.3072709	0.87955876
FBGN0004926	eIF2β	-0.3060839	0.97085288
FBGN0003462	Sod1	-0.3060258	0.96025754
FBGN0010333	Rac1	-0.3057096	0.93448929
FBGN0011586	e(r)	-0.3045842	0.81133641
FBGN0011570	cpb	-0.3035145	0.88350892
FBGN0004427	LysD	-0.3031905	0.85315712
FBGN0011336	Stt3B	-0.3000629	0.95510188
FBGN0011726	tsr	-0.2984445	0.95322514
FBGN0010100	mAcon1	-0.2967884	0.96594117
FBGN0001124	Got1	-0.2950429	0.9791637
FBGN0000536	eas	-0.2946622	0.92007851
FBGN0008635	βCOP	-0.294267	0.92970028
FBGN0000611	exd	-0.2913774	0.87052211
FBGN0005671	Vha55	-0.2911095	0.96047122
FBGN0002031	Phb1	-0.2901401	0.9635399
FBGN0004404	RpS14b	-0.2890559	0.966226
FBGN0010590	Prosβ1	-0.2888302	0.89486287
FBGN0001145	Gs2	-0.2888199	0.9188235
FBGN0000044	Act57B	-0.2849021	0.87573729
FBGN0010352	Ogdh	-0.2844112	0.89489308
FBGN0005411	U2af50	-0.28303	0.84875269
FBGN0004169	up	-0.2821997	0.87760174
FBGN0002590	RpS5a	-0.2817032	0.988709
FBGN0010217	ATPsynβ	-0.2815281	0.97396916
FBGN0004363	porin	-0.2804117	0.9638281
FBGN0000083	AnxB9	-0.2804065	0.95098475
FBGN0002626	RpL32	-0.279278	0.98145118
FBGN0011640	lark	-0.2789737	0.90519736
FBGN0011584	Trp1	-0.2781458	0.97287287
FBGN0010198	RpS15Aa	-0.2775112	0.97372246
FBGN0010078	RpL23	-0.2736664	0.97693197
FBGN0004888	Scsα1	-0.2732462	0.97493486
FBGN0005585	Calr	-0.2731629	0.96592066
FBGN0000455	Dip-C	-0.2719208	0.92146439
FBGN0010408	RpS9	-0.2713599	0.96489525
FBGN0002593	RpLP1	-0.2709501	0.9801381
FBGN0003941	RpL40	-0.2690899	0.98364333

FBGN0001128	Gpdh1	-0.2682945	0.96298605
FBGN0003358	Jon99Ci	-0.2663512	0.89698209
FBGN0000370	crc	-0.2654233	0.91547532
FBGN0002622	RpS3	-0.2639968	0.97645266
FBGN0005533	RpS17	-0.2626411	0.96922337
FBGN0003134	Pp1α-96A	-0.2618676	0.8428468
FBGN0000251	cad	-0.2606955	0.81786234
FBGN0003231	ref(2)P	-0.260503	0.95068597
FBGN0005593	RpL7	-0.2599821	0.97647544
FBGN0000566	Cth	-0.2595864	0.96031527
FBGN0001565	Ddx56	-0.2591136	0.90799485
FBGN0010548	Aldh-III	-0.2590061	0.92213529
FBGN0004856	Bx42	-0.2583859	0.89774417
FBGN0004867	RpS2	-0.2583254	0.96622947
FBGN0003942	RpS27A	-0.2578985	0.97822416
FBGN0010265	RpS13	-0.2578855	0.97572431
FBGN0002284	Prosβ6	-0.2572476	0.84267829
FBGN0000150	awd	-0.2547205	0.93116501
FBGN0010412	RpS19a	-0.2544179	0.97021387
FBGN0001098	Gdh	-0.2543044	0.90361252
FBGN0010602	lwr	-0.2539013	0.88369437
FBGN0004403	RpS14a	-0.2537226	0.97172634
FBGN0010225	Gel	-0.2526577	0.93656872
FBGN0010409	RpL18A	-0.2526488	0.97753074
FBGN0000064	Ald1	-0.2522187	0.97588542
FBGN0003149	Prm	-0.2519458	0.80123021
FBGN0000100	RpLP0	-0.2519222	0.97124873
FBGN0010551	Phb2	-0.2518208	0.95090766
FBGN0002579	RpL36	-0.251536	0.96296867
FBGN0001942	eIF4A	-0.2504576	0.97447367
FBGN0010411	RpS18	-0.2502852	0.96787364
FBGN0004638	drk	-0.2500095	0.87265261
FBGN0004045	Yp1	-0.2493492	0.93739503
FBGN0003517	sta	-0.2487912	0.97067616
FBGN0011272	RpL13	-0.2482623	0.9692586
FBGN0003748	Treh	-0.2471588	0.94430934
FBGN0001248	Idh	-0.2469996	0.93414492
FBGN0011284	RpS4	-0.2464901	0.97751283
FBGN0010747	Srp54k	-0.2454126	0.94397618
FBGN0011672	Mvl	-0.2395012	0.91912046

FBGN0003274	RpLP2	-0.239043	0.95057963
FBGN0011695	EbpIII	-0.238849	0.88636621
FBGN0001091	Gapdh1	-0.2370618	0.93655693
FBGN0003279	RpL4	-0.2366855	0.96554528
FBGN0000181	bic	-0.234476	0.93301532
FBGN0004047	Yp3 4	-0.2262391	0.91196213
FBGN0011289	TfIIA-L	-0.211203	0.86611895
FBGN0011746	ana	0.20600038	-0.8529429
FBGN0003091	Pkc53E	0.20923748	-0.842888
FBGN0003435	sm	0.21862388	-0.8544119
FBGN0003042	Pc	0.21893789	-0.9185541
FBGN0003997	hid	0.24043842	-0.877874
FBGN0004832	Xpac	0.24152481	-0.8037293
FBGN0000346	comt	0.25325045	-0.8963758
FBGN0004957	por	0.2573611	-0.872251
FBGN0003751	trk	0.26010175	-0.934863
FBGN0003353	sei	0.26626529	-0.928952
FBGN0003227	rec	0.274434	-0.9668346
FBGN0000279	CecC	0.27903755	-0.8187782
FBGN0011259	Sema1a	0.29566342	-0.9251836
FBGN0004860	ph-d	0.30575516	-0.8870019
FBGN0000274	Pka-C2	0.32251101	-0.9543239
FBGN0000928	fs(1)Yb	0.32339799	-0.9367368
FBGN0003482	spn-D	0.32377111	-0.9718468
FBGN0004837	Su(H)	0.33121913	-0.8607047
FBGN0003312	sad	0.33217155	-0.8508578
FBGN0003950	unc	0.3330674	-0.9559411
FBGN0004959	phtm	0.33642012	-0.8819899
FBGN0010549	l(2)03659	0.33784948	-0.9164846
FBGN0003174	YVBN	0.3408901	-0.8185596
FBGN0010194	Wnt5 AGH	0.34239397	-0.8248395
FBGN0010768	sqz	0.35097633	-0.9466368
FBGN0005624	Psc	0.3694814	-0.8714685

3.9. Integration of WGCNA modules with single-cell expression data

We further integrated the results from the WGCNA analysis, i.e. the hub genes from each module, with high-resolution single-cell expression data of the *Drosophila* midgut provided by the Fly Cell Atlas (Li et al., 2022). Using Uniform Manifold Approximation and Projection (UMAP), we visualised the spatial distribution of these hub genes within identified cellular clusters across our three modules of analysis **(Figure 22A-C)**:

3.9.1. Black module:

Figure 22A presents the composite mapping of hub genes from the black module, as listed in **Table 7**, onto single-cell expression data of the *Drosophila* midgut. This overlay highlights the genes' distribution, notably including enterocyte-like cells and enterocytes situated in the midgut's posterior and anterior regions.

3.9.2. Brown module:

Figure 22B illustrates the localised expression patterns of the brown module hub genes, detailed in **Table 8**, within a distinct cell population. This cluster, currently unannotated and referred to as Cluster 39, is situated near cell types identified as intestinal stem cells and enteroblasts—progenitor cells of the midgut.

3.9.3. Blue module:

Figure 22C shows the expression of hub genes from the blue module. These genes are observed to have a concentrated expression in the midgut's large flat cells and enterocytes, exhibiting a distribution pattern like that seen with the black module (**Figure 24A**).

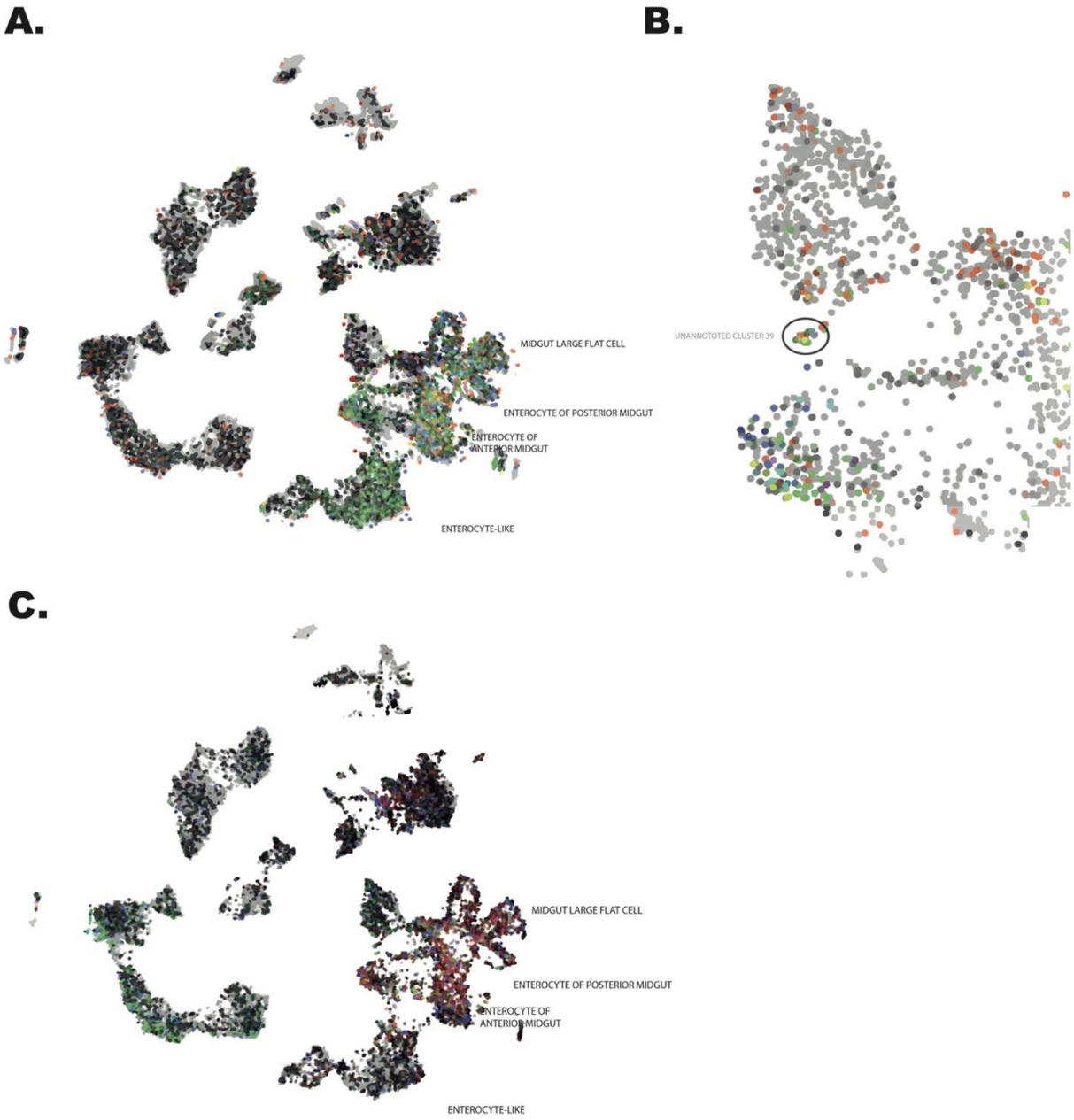

Figure 22. Single-cell UMAP expression mapping of hub genes in the *Drosophila* midgut from the Fly Cell Atlas. A. Black module hub genes: UMAP plot representing a composite visualisation of the expression of multiple hub genes across various cell types, with node size and colour intensity indicating gene centrality in the network**. B. Brown module hub genes:** Composite UMAP visualisation focusing on the collective expression profile of hub genes in the brown module, particularly within Cluster 39. **C. Blue module hub genes:** Composite UMAP image showing the expression of blue module hub genes in large flat and enterocyte cells. Each panel represents a composite image constructed by superimposing multiple individual gene expression maps.

4 Discussion

In our differential gene expression analysis using RNA sequencing (RNA-seq) data, we found only minimal transcriptional changes in response to heat shock. Using stringent criteria (adjusted p-value < 0.05), our initial analysis with count reads identified a limited number of significantly differentially expressed genes, and a more rigorous analysis with fragment reads identified none. These findings suggest that the transcriptional response to heat shock under our experimental conditions is relatively modest.

Given our hypothesis that we were observing a homeostatic rather than regenerative state, it seemed plausible that differential expression analysis would not highlight genes, as it is traditionally employed to identify those that show significant changes in expression levels under different conditions (Langfelder & Horvath, 2008). Differential expression analysis is particularly valuable for identifying genes associated with distinct phenotypes or conditions. However, it may be less effective for subtle homeostatic changes without substantial cell loss or dramatic alterations.

Consequently, we shifted our approach to Weighted Gene Co-expression Network Analysis (WGCNA). WGCNA identifies clusters of genes with high correlation across samples. This approach can pinpoint key gene modules related to sample traits and offer insights into gene interactions and regulatory networks. It is especially adept at unravelling complex gene relationships and identifying gene groups functioning together within biological processes (Langfelder & Horvath, 2008; Liang et al., 2020; Wu et al., 2020; Yu et al., 2022).

Utilising WGCNA, we explored the intricate gene expression patterns triggered by heat stress. We aimed to detect central hub genes, integrate them within the GO framework, and correlate these findings with single-cell data. We identified specific modules—black, brown, and blue—that strongly correlated with the effects of heat shock, yet none correlated with changes over time. This lack of time-specific correlation suggests that the analysis did not distinguish between the day-to-day responses of heat-shocked flies and control groups (**script in Supplementary Information**). Consequently, the temporal dynamics of the response to heat shock — particularly the upsurge in cell cycle markers exclusive to heat-shocked flies as modelled in Chapter 2 — may have been obscured. Isolating the day variable only in heat-shocked flies could support the modelling seen in Chapter 2 of pulsed turnover.

We did see differences between heat-shocked and control flies, and we uncovered specific dynamics in enterocytes and what we hypothesised were progenitor cells.

4.1. Enterocyte contribution to homeostatic turnover

Our analysis revealed that the hub genes in black and blue modules are best mapped to enterocytes, as shown in **Figures 22A and C**. The analysis of hub genes within these modules helps elucidate the potential responses of enterocytes, which are crucial for maintaining homeostasis following heat stress.

We provide a possible understanding of the cellular dynamics in enterocytes under heat stress conditions by examining the gene expression changes in two distinct modules - the black module, which shows upregulated genes, and the blue module, which marks downregulated genes.

Upregulated Responses in Black Module

Our GO and KEGG analyses of the black module revealed an upregulation in processes related to DNA repair and reproductive functions when subjected to heat stress. Key upregulated processes include reciprocal homologous recombination, meiotic recombination, Meiosis I, and the cellular response to a DNA damage stimulus. These changes could indicate a state of DNA repair and cell cycle regulation, ensuring genomic integrity following environmental stress such as heat stress.

Downregulated Responses in Blue Module

The blue module demonstrated significant downregulation in genes involved with GO processes predominantly related to protein synthesis and developmental activities. This encompasses decreased cytoplasmic translation, embryonic development, and tissue development. Such downregulation could indicate a cellular strategy to conserve resources under stress conditions.

This dynamic is further observed by examining hub genes with the highest GS and strong module correlation (MM values closest to 1) in both modules. This provides a more detailed understanding of the cellular responses that may be occurring in enterocytes subjected to heat stress conditions.

4.1.1. Increased focus on DNA repair

Heat stress compromises DNA integrity by inducing double-stranded breaks (DSBs) in DNA (Morrow & Tanguay, 2003; Velichko et al., 2012). The DNA Damage Response (DDR) of enterocytes plays an integral role in preserving the intestinal homeostasis of

the *Drosophila* midgut after such DSBs (Park et al., 2015). Enterocytes, continuously exposed to various external factors, are prone to stress-induced DNA damage, which explains the importance of the DDR, which is particularly significant in cells undergoing endoreplication.

We observed an increase in this DDR response with the upregulation of gene *mei-41*, the *Drosophila* equivalent of human ATR kinase. This enzyme plays a crucial role in the DNA damage response and repair processes (Bayer et al., 2018; LaRocque et al., 2007). Its increased expression highlights an intensified focus on maintaining genomic integrity and supporting the proliferation of intestinal stem cells (ISCs), vital for gut homeostasis and regeneration. Additionally, the genes *mus101* and *meiS332*, encoding a protein involved in DNA damage response and meiotic chromosome segregation, respectively, also show increased expression, further emphasising the cell's commitment to DNA repair (Sekelsky, 2017).

The *okr* gene, encoding the 6-4 photolyase in *Drosophila melanogaster*, is crucial for repairing UV-induced DNA lesions. Its significant upregulation aligns with a suggested cell's enhanced capacity to respond to DNA damage under stress (Koval et al., 2020; Sekelsky, 2017).

4.1.2. Enhanced immune response to stress

Enterocytes in *Drosophila* have also been demonstrated to adaptively respond to stress by modulating immune signalling pathways (Shin et al., 2022)

Our study identified a significant upregulation in the Hedgehog (Hg) pathway, evidenced by increased expression of the *smo* gene. This pathway is integral to immune regulation and promotes ISC proliferation in *Drosophila* (Jing et al., 2023; Shin et al., 2022; Tian et al., 2015).

Furthermore, the activation of the Toll pathway was observed, particularly through the enhanced gene expression of the proteases genes *snake* (*snk*) and *gastrulation defective* (*gd*) (Patterson et al., 2013). Both Hg and Toll pathways are involved in the immune response in the *Drosophila* midgut (Buchon et al., 2014).

Interestingly, we also noted an unexpected upregulation of the *zfh1* gene*. Zfh1* is a transcription factor that typically acts as a negative regulator in the Imd signalling pathway (Postigo & Dean, 2000). This may suggest a strategic shift in the enterocytes' immune response, with zfh1 downregulating antimicrobial peptide (AMP) gene expression, thereby recalibrating the balance between the Imd, Hedgehog, and Toll.

The suppression of AMP genes within the Imd pathway aligns with previous findings that such downregulation can enhance stress resistance and extend lifespan in fruit flies (Lin et al., 2018). Conversely, the activation of the Toll pathway, particularly in neuronal contexts, has been linked to a reduction in fly longevity. This contrast may suggest a complex interplay between various immune signalling pathways in *Drosophila*, especially under stress conditions.

4.1.3. Increased emphasis on cell cycle regulation

Apart from the increased DNA damage response and immune system activation, our analysis also highlights a significant upsurge in cell cycle regulation activities in enterocytes under heat stress.

Hub genes such as *prim1*, *polQ*, *polz1*, and *sas4* are notably upregulated, underlining an active cellular environment committed to DNA repair and replication (Marygold et al., 2020; Conduit et al., 2015; Novak et al., 2016).). Additionally, we observed an upregulation of genes *monopolar spindl*e 1 (*MPS1*) and *spindle B* (*spn-b*), which encode for crucial components of the spindle apparatus in *Drosophila*, which reinforces the idea of an increase in the cell cycle machinery following HS.

4.1.4. Decrease in metabolism and development processes

Like many other species, *Drosophila* also responds to heat stress by slowing down its metabolism and development.

In our analysis of hub genes in the blue module, we noticed a decrease in the activity of the *syb* gene, which plays a critical role in synaptic vesicle exocytosis (Quiñones-Frías & Littleton, 2021). This reduction could suggest a decreased emphasis on synaptic transmission and neural communication, a likely adaptation to conserve energy under stress conditions.

We also observed that *nd-acp,* a gene involved in fatty acid metabolism and electron transfer in the respiratory chain, is less expressed following heat shock. Additionally, the activity of *metallothionein A*, which is integral to metal ion regulation (Wang et al., 2022), is also reduced. Another interesting finding is the decreased activity of gene *FKBP13*. The FKBP family of proteins involves many cellular processes, including protein folding, trafficking, and signalling (Ghartey-Kwansah et al., 2018).

4.2. Cluster 39 cells contribution to homeostatic turnover

Our comprehensive GO and KEGG analysis, as outlined in **Table 10** and **Table 11**, underlines the significant upregulation in cellular processes and molecular activities in cells from Cluster 39.

Despite this unannotated cluster, we suggest these cells likely correspond to progenitor cells. This inference is drawn from their distinct response patterns, particularly the dramatic increase in cell cycle activities, which we believe is a strategic response to enhance cell division and maintain homeostasis under sublethal stress conditions. These have been stated by several studies showing that various signalling pathways are activated in response to midgut stress, promoting ISC division and proliferation (Jin et al., 2015).

In this annotated cluster 39, we observed an increase in:

- Cellular Processes (**Table 10**): associated with nuclear division, organelle fission and various aspects of reproduction biology. Including female gamete generation and oogenesis.
- Molecular Activities (**Table 11**): related to translation repression, cyclin-dependent serine/threonine kinase activity, and ATP production.

4.2.1. Great increase in cell cycle

In response to stress, several signalling pathways are activated to directly increase ISC proliferation and enterocyte production, thereby restoring tissue homeostasis (Choi et al., 2011; Deng et al., 2015; Guo et al., 2016). This aligns with what we observe in this brown module, mapping to uncluster 39.

We observed a marked increase in the expression of genes *klp67A* and *klp61F*. These genes are crucial for chromosome separation and spindle formation. The elevated levels of these genes suggest an active cellular response to heat stress, preparing the cells for division (Radford et al., 2017; Savoian & Glover, 2010; Sharp & Rath, 2009).

There was also an upregulation in the expression of *polα2*, the gene encoding the DNA polymerase alpha complex accessory subunit (Marygold et al., 2020). This increase indicates an accelerated progression through the cell cycle, hinting at a rapid cellular response to initiate DNA replication and cell division in the wake of heat stress.

Genes involved in reorganising the actin cytoskeleton and chromatin structure, such as *pebble* (*pbl*), were also upregulated. This underscores the cells' preparation for

differentiation and division, a crucial step in responding to environmental stressors (Dronamraju & Mason, 2009).

There was a significant increase in the expression of genes for cyclin-dependent kinases (*cdk1* and *cdk2*) and mostly all genes encoding for cyclins, including *cycA*, *cycB*, *cycD*, *cycE* and *cycJ*. This rise suggests a robust increase in the cell division process. Cyclin J, especially, is known for its role in oogenesis and is expressed exclusively in females (Althoff et al., 2009; Ruiz-Losada et al., 2022).

Further, genes like *polo* (Wong et al., 2022), *stg* (Jin et al., 2015), *PCNA* (Xiang et al., 2017), *aurA* (Zhang et al., 2023) or *pav* (DeBruhl et al., 2013) were also found to have increased expression. These genes play integral roles in various aspects of cell cycle regulation.

Finally, the *grip91* gene, encoding the Gamma-tubulin ring protein 91 crucial for microtubule organisation within the cell, showed a very important increased expression. This, alongside the upregulation of other cell division-related genes, confirms that these cells are actively preparing for division in response to heat stress.

4.2.2. Enhanced stress response:

Our analysis also revealed an enhanced response to stress, particularly through the upregulation of genes encoding for small heat shock proteins (sHsps) like *hsp26* and *hsp27*. These proteins act as molecular chaperones, involved in preventing protein aggregation, assisting in protein refolding, and protecting cells from stress-induced damage (Dwivedi et al., 2022; Morrow & Tanguay, 2015). Their functions are crucial across various cellular processes, including ageing, immunity, proteotoxicity, apoptosis, and cargo movement, thus underscoring their importance in maintaining cellular homeostasis.

Gene *mu2* was also upregulated. MU2 protein in *Drosophila melanogaster* plays a crucial role in recognising and repairing double-strand DNA breaks (DSBs) induced by ionising radiation. It is involved in the formation of repair foci, particularly in conjunction with the phosphorylated histone variant H2Av, and affects the kinetics of foci formation (Dronamraju & Mason, 2009)

Furthermore, *cortex* (*cort*) and *rrp1* were upregulated, contributing to the activation of the Anaphase Promoting Complex and DNA repair, respectively, which are vital for genomic stability (Sivakumar & Gorbsky, 2015).

4.2.3. Increased focus on reproductive processes:

Nevertheless, we observed an upregulation of genes typically linked to reproductive processes. Initially, we could have attributed this to potential contamination from ovarian tissue, a common issue during dissection, especially since our experiments were conducted on mated females. However, we confirmed that these genes were also expressed in males by examining data from the Fly Cell Atlas in Scope, where gene expression was analysed separately in males and females. This finding indicates that the upregulation is a general response to heat stress rather than a sex-specific phenomenon or a result of contamination in our female samples.

The significant increase in *nanos* expression, known for its role in inhibiting apoptosis in pole cells, aligns with our findings that heat stress does not necessarily lead to increased apoptosis but may induce alterations in the cell cycle (Asaoka et al., 2019). This adaptation could be a strategic response to ensure the survival and integrity of germ cells under stressful conditions.

The upregulation of *png* also supports this idea, as they are pivotal in regulating the embryonic cell cycles, particularly during the critical phase of egg activation (Vardy & Orr-Weaver, 2007).

Furthermore, we observed an upsurge in the expression levels of the *otu* and *ovo* genes, both known for their pivotal roles in sex determination and germline development. Nevertheless, *otu* has been implicated in a wide array of stress responses, including heat shock and oxidative stress, and plays a role in modulating apoptosis through the JNK signalling pathway (Roxström-Lindquist et al., 2004).

An increase in *bam* (bag of marbles) expression has also been seen. Notably, *bam* is implicated in the regulation of metabolic homeostasis through the modulation of the gut microbiota, highlighting its role in organismal response to environmental stressors (Wang et al., 2022).

Lastly, *spn-E* and *qua* have been identified as genes with essential functions in reproductive tissue development. spn-E is likely an ATP-binding RNA helicase integral to both spermatogenesis and oogenesis. qua is involved in wing hair development and oogenesis, underscoring the multifunctionality of these genes in development and reproduction. However, quail has been shown to bundle actin filaments in apoptotic nurse cells, indicating its involvement in cytoskeletal reorganisation during apoptosis (Matova et al., 1999).

These findings suggest a possible shift in cellular priorities from apoptosis to cell cycle progression under heat stress conditions. Such a shift could be a homeostatic response to preserve cellular and tissue integrity in the face of environmental challenges. This strategy might not only ensure reproductive continuity under adverse conditions but also align with the hypothesis of a pulse turnover homeostatic response in the *Drosophila* midgut.

5 Supplementary tables

Table 12. Biological processes associated with the black module. The table summarises the GO biological processes enriched in the black module. It presents the FDR, number of genes in the module and those related to each biological process, and the fold enrichment.

ENRICHMENT FDR	NGENES	PATHWAY GENES	FOLD ENRICHMENT	PATHWAYS
3.5E-06	5	37	47.2	Reciprocal homologous recombination
3.5E-06	5	37	47.2	Reciprocal meiotic recombination
2.5E-06	6	68	30.8	Meiosis I
2.9E-06	6	70	29.9	Neg. reg. of mitotic cell cycle
2.1E-06	8	173	16.1	Meiotic nuclear division
3.4E-07	10	266	13.1	Cellular response to DNA damage stimulus
3.5E-06	10	369	9.5	DNA metabolic proc.
2.0E-06	11	433	8.9	Response to abiotic stimulus
1.9E-06	12	540	7.8	Embryo development
2.7E-07	14	651	7.5	Cellular response to stress
2.7E-07	14	664	7.4	Female gamete generation
7.4E-08	17	872	6.8	Cellular proc. involved in reproduction in multicellular organism
1.2E-07	17	942	6.3	Gamete generation
2.7E-07	17	1073	5.5	Multicellular organismal reproductive proc.
2.7E-07	17	1077	5.5	Sexual reproduction
2.7E-07	17	1077	5.5	Multi-organism reproductive proc.
1.3E-06	17	1228	4.8	Reproductive proc.
4.5E-07	18	1304	4.8	Response to stress
2.5E-06	17	1311	4.5	Multicellular organism reproduction

Table 13. Molecular functions of the black module. This table outlines the molecular functions associated with the brown module based on GO analysis. It provides the FDR, gene counts, pathway gene counts, and fold enrichment.

ENRICHMENT FDR	NGENES	PATHWAY GENES	FOLD ENRICHMENT	PATHWAYS
8.6E-03	2	9	77.6	DNA-directed DNA polymerase activity
1.4E-02	3	70	15	ATP-dependent activity, acting on DNA
5.3E-03	5	141	12.4	Catalytic activity, acting on DNA
1.8E-02	4	182	7.7	Protein serine/threonine kinase activity
1.3E-02	6	404	5.2	Catalytic activity, acting on a nucleic acid
8.6E-03	7	484	5.1	Transferase activity, transferring phosphorus-containing groups
5.3E-03	12	1140	3.7	DNA binding
8.6E-03	10	991	3.5	Purine ribonucleoside triphosphate binding
8.6E-03	10	1013	3.4	Purine ribonucleotide binding
8.6E-03	10	1021	3.4	Purine nucleotide binding
1.8E-02	8	820	3.4	ATP binding
8.6E-03	10	1025	3.4	Ribonucleotide binding
8.6E-03	11	1177	3.3	Nucleotide binding
8.6E-03	11	1177	3.3	Nucleoside phosphate binding
1.2E-02	11	1304	2.9	Small molecule binding
1.8E-02	10	1207	2.9	Anion binding
1.2E-02	12	1500	2.8	Catalytic activity, acting on a protein
1.8E-02	13	1875	2.4	Hydrolase activity
1.8E-02	13	1917	2.4	Nucleic acid binding

Table 14. KEGG pathway enrichment in the black module The table illustrates the KEGG pathways enriched within the brown module, including the FDR, number of genes involved, and fold enrichment.

ENRICHMENT FDR	NGENES	PATHWAY GENES	FOLD ENRICHMENT	PATHWAYS
4.3E-04	3	23	45.5	Homologous recombination
4.3E-04	3	26	40.3	Fanconi anemia pathway
4.3E-04	4	62	22.5	Apoptosis
4.3E-02	2	50	14	Mitophagy
4.3E-02	2	55	12.7	Neuroactive ligand-receptor interaction

Table 15. Biological processes associated with the brown module. This table enumerates the significantly enriched biological processes associated with the black module as identified by Gene Ontology (GO) analysis. For each process, the False Discovery Rate (FDR) of enrichment, the number of genes (NGENES) within the module, the number of genes associated with the pathway (PATHWAY GENES), and the fold enrichment are presented.

ENRICHMENT FDR	NGENES	PATHWAY GENES	FOLD ENRICHMENT	PATHWAYS
1.5E-27	33	312	14.3	Nuclear division
1.1E-26	33	332	13.5	Organelle fission
1.8E-40	53	664	10.8	Female gamete generation
1.3E-30	44	614	9.7	Oogenesis
2.9E-44	61	872	9.5	Cellular proc. involved in reproduction in multicellular organism
2.2E-29	43	615	9.5	Cell cycle proc.
9.3E-31	47	737	8.6	Germ cell development
2.7E-41	60	942	8.6	Gamete generation
2.7E-33	51	822	8.4	Cell cycle
6.4E-43	64	1077	8.1	Sexual reproduction
6.4E-43	64	1077	8.1	Multi-organism reproductive proc.
3.2E-49	72	1228	8	Reproductive proc.
4.4E-32	52	921	7.7	Developmental proc. involved in reproduction
4.3E-38	60	1073	7.6	Multicellular organismal reproductive proc.
2.9E-44	72	1463	6.7	Reproduction
2.8E-34	61	1311	6.3	Multicellular organism reproduction
2.1E-25	54	1399	5.2	Cell development
9.3E-25	58	1723	4.6	Cell differentiation
1.2E-24	58	1734	4.5	Cellular developmental proc.

Table 16. Molecular functions of the brown module. This table outlines the molecular functions associated with the brown module based on GO analysis. It provides the FDR, gene counts, pathway gene counts, and fold enrichment.

ENRICHMENT FDR	NGENES	PATHWAY GENES	FOLD ENRICHMENT	PATHWAYS
2.4E-08	7	21	45.2	Translation repressor activity
8.9E-07	5	15	45.2	Translation repressor activity, mRNA regulatory element binding
2.6E-07	6	21	38.7	Cyclin-dependent protein serine/threonine kinase regulator activity
5.4E-08	8	42	25.8	Microtubule motor activity
3.4E-07	7	41	23.2	MRNA 3 -UTR binding
8.9E-07	8	72	15.1	Cytoskeletal motor activity
3.4E-07	10	119	11.4	Microtubule binding
1.3E-06	12	227	7.2	MRNA binding
1.3E-06	16	430	5	ATP-dependent activity
2.6E-07	24	820	4	ATP binding
2.6E-07	24	839	3.9	Adenyl ribonucleotide binding
2.6E-07	24	844	3.9	Adenyl nucleotide binding
2.6E-07	26	991	3.6	Purine ribonucleoside triphosphate binding
3.4E-07	26	1013	3.5	Purine ribonucleotide binding
3.4E-07	26	1021	3.5	Purine nucleotide binding
3.4E-07	26	1025	3.4	Ribonucleotide binding
5.7E-07	28	1214	3.1	Carbohydrate derivative binding
9.5E-07	27	1177	3.1	Nucleotide binding
9.5E-07	27	1177	3.1	Nucleoside phosphate binding
2.4E-08	40	1917	2.8	Nucleic acid binding

Table 17. KEGG pathway enrichment in the brown module. The table illustrates the KEGG pathways enriched within the brown module, including the FDR, number of genes involved, and fold enrichment.

ENRICHMENT FDR	NGENES	PATHWAY GENES	FOLD ENRICHMENT	PATHWAYS
3.1E-04	4	20	27.1	Mismatch repair
6.2E-04	4	28	19.4	Dorso-ventral axis formation
7.5E-03	3	26	15.6	Fanconi anemia pathway
3.9E-02	2	20	13.6	Base excision repair
1.1E-02	3	35	11.6	DNA replication
8.4E-03	4	65	8.3	FoxO signalling pathway

Table 18. Biological processes associated with the blue module. The table summarises the GO biological processes enriched in the black module. It presents the FDR, number of genes in the module and those related to each biological process, and the fold enrichment.

ENRICHMENT FDR	NGENES	PATHWAY GENES	FOLD ENRICHMENT	PATHWAYS
9.8E-23	29	149	14.9	Cytoplasmic translation
3.9E-08	17	177	7.3	Embryo development ending in birth or egg hatching
8.1E-07	15	168	6.8	Embryonic development via the syncytial blastoderm
4.3E-10	30	478	4.8	Translation
2.1E-10	32	526	4.6	Peptide biosynthetic proc.
1.1E-10	34	574	4.5	Amide biosynthetic proc.
9.1E-06	19	332	4.4	Actin filament-based proc.
1.6E-09	33	622	4	Peptide metabolic proc.
8.2E-10	36	716	3.8	Cellular amide metabolic proc.
3.4E-07	27	540	3.8	Embryo development
1.8E-05	25	582	3.3	Cellular component morphogenesis
4.4E-10	45	1063	3.2	Organonitrogen compound biosynthetic proc.
8.1E-07	38	1040	2.8	Tissue development
3.9E-08	51	1523	2.6	Anatomical structure morphogenesis
1.4E-05	39	1219	2.4	Animal organ development
3.7E-06	43	1350	2.4	Reg. of biological quality
2.7E-07	53	1723	2.3	Cell differentiation
9.1E-06	43	1399	2.3	Cell development
2.9E-07	53	1734	2.3	Cellular developmental proc.
2.9E-07	54	1788	2.3	System development

Table 19. Molecular functions of the blue module. This table outlines the molecular functions associated with the brown module based on GO analysis. It provides the FDR, gene counts, pathway gene counts, and fold enrichment.

ENRICHMENT FDR	NGENES	PATHWAY GENES	FOLD ENRICHMENT	PATHWAYS
6.6E-05	4	8	38.2	Myosin heavy chain binding
2.7E-07	9	43	16	RRNA binding
1.7E-16	25	175	10.9	Structural constituent of ribosome
1.6E-04	12	182	5	GTP binding
8.6E-04	10	154	5	GTPase activity
2.1E-04	12	189	4.8	Guanyl ribonucleotide binding
2.2E-04	12	191	4.8	Guanyl nucleotide binding
5.4E-09	28	477	4.5	Structural molecule activity
2.9E-04	16	342	3.6	Cytoskeletal protein binding
1.3E-07	42	1177	2.7	Nucleotide binding
1.3E-07	42	1177	2.7	Nucleoside phosphate binding
1.7E-06	36	1013	2.7	Purine ribonucleotide binding
2.3E-06	35	991	2.7	Purine ribonucleoside triphosphate binding
4.1E-08	46	1304	2.7	Small molecule binding
1.8E-06	36	1021	2.7	Purine nucleotide binding
1.8E-06	36	1025	2.7	Ribonucleotide binding
6.3E-07	41	1207	2.6	Anion binding
8.6E-04	26	839	2.4	Adenyl ribonucleotide binding
9.0E-04	26	844	2.4	Adenyl nucleotide binding
3.4E-05	37	1214	2.3	Carbohydrate derivative binding

Table 20. KEGG pathway enrichment in the blue module. The table illustrates the KEGG pathways enriched within the brown module, including the FDR, number of genes involved, and fold enrichment.

ENRICHMENT FDR	NGENES	PATHWAY GENES	FOLD ENRICHMENT	PATHWAYS
5.2E-19	24	133	13.8	Ribosome
3.3E-03	4	23	13.3	Protein export
1.7E-02	3	18	12.7	Arginine biosynthesis
4.8E-02	3	29	7.9	Alanine, aspartate and glutamate metabolism
7.4E-04	7	68	7.9	Biosynthesis of amino acids
1.6E-04	10	121	6.3	Carbon metabolism
3.3E-03	7	93	5.7	MAPK signalling pathway
4.8E-02	4	55	5.6	Glycolysis / Gluconeogenesis
4.8E-02	4	55	5.6	Neuroactive ligand-receptor interaction
1.3E-02	28	1153	1.9	Metabolic pathways

CHAPTER 4: INSIGHTS INTO BHLH TRANSCRIPTION FACTORS SCUTE AND DAUGHTERLESS IN INTESTINAL STEM CELL DIFFERENTIATION

1 Introduction

Maintaining homeostasis is a multifaceted process, not limited to balancing rates of division, differentiation, and cell loss (Nakamuta et al., 2022; O'Brien, 2022; Weterings et al., 2021). Equally critical is ensuring the appropriate differentiation proportion into various mature cell types. This delicate balance is crucial for properly functioning biological systems (Komarova, 2013; Morrison & Kimble, 2006).

The control of stem cell fate is tightly linked to transcription regulation, where gene regulatory networks are essential in guiding cells through specific differentiation pathways. These pathways are often a result of binary decisions directed by opposing actions of transcription factor pairs and are even more complex for multipotent stem cells, which have several potential fate options (Graf & Enver, 2009; Levine & Davidson, 2005; Moris et al., 2016).

In the adult tissues of both *Drosophila* and mammals, intestinal stem cells exemplify multipotency, facing a tripartite decision: self-renewal or differentiation into one of two mature lineages—secretory or absorptive (Jiang et al., 2016; Liu & Jin, 2017; Ohlstein & Spradling, 2006). BHLH transcription factors profoundly influence the decision-making process of ISCs. This family of factors is known for its developmental versatility, playing regulatory roles in processes ranging from sex determination to neurogenesis (Bertrand et al., 2002; Murre, 2005; Murre et al., 1994).

bHLH transcription factors are central to regulating stem cell fate due to their unique structural motif, allowing various dimer configurations to form (de Martin et al., 2021; Jones, 2004; Michael et al., 2023). This flexibility is conferred by the basic Helix-Loop-Helix (HLH) domain, enabling dimer formation with a basic region that binds to specific DNA sequences, thereby directing the transcriptional outcomes necessary for cell differentiation (Imayoshi et al., 2015; Massari & Murre, 2000). Their involvement in the binary fate decisions of ISCs—whether to continue self-renewing or to embark on a path toward becoming a secretory or absorptive cell—is a critical aspect of intestinal homeostasis and reflects the broader significance of these transcription factors in cellular differentiation (Bardin et al., 2010; Puig Barbe, 2018).

Based on structural and functional traits, HLH proteins are categorised into six classes: Class I through Class VI (Murre, 2019).

- Class I: These HLH proteins, such as E12, E47, E2-2, and Daughterless, are widely expressed and can form both homo- and heterodimers.
- Class II: Tissue-specific HLH proteins, such as MyoD, myogenin, myf-5 and Scute.
- Class III: This class, with proteins like c-myc, N-myc, and L-myc, is associated with growth control.
- Class IV: These HLH proteins, including mad and max, interact with myc proteins.
- Class V: Unique HLH proteins in this category, like emc and Id, do not possess a DNA binding domain.
- Class VI: HLH proteins in this class, such as hairy and enhancer of split, are defined by having a proline in their basic region.

In our lab's ongoing exploration of the tissue homeostasis of the *Drosophila* adult midgut, experiments conducted by Puig-Barbe et al. (2023) have been instrumental in uncovering the roles of bHLH transcription factors in regulating the fate of ISCs in the *Drosophila* midgut. These studies revealed that Class I bHLH factors, such as Daughterless (Da), possess the capacity to form homodimers and heterodimers with other bHLH factors like Scute (Sc) and Extramacrochaetae (Emc). Such dimerisation events significantly impact the fate decisions of ISCs (Puig-Barbe et al., 2023).

Building upon these findings, our research aims to delve deeper into the intricate dynamics of these bHLH factors, with a particular focus on the interplay between Da and Sc, which is crucial for EE differentiation in the adult *Drosophila* midgut. The ability of these transcription factors to form a variety of homo- and heterodimers enables them to coordinate complex transcriptional changes within the cells. These interactions can operate in diverse ways—synergistically, antagonistically, or even combinatorially—thereby effectively regulating the multipotent nature of adult stem cells, which require a transition between states of self-renewal and multiple differentiation pathways (Puig-Barbe et al., 2023).

Building on previous studies, including those by Puig-Barbé, we understand that Da:Sc heterodimers play a crucial role in initiating pre-entroendocrine (pre-EE) cell formation. However, their role extends beyond this; Da:Sc heterodimers also contribute to maintaining ISCs in an undifferentiated state and facilitate the conversion of EBs into ISCs.

In contrast, Da:Da homodimers are primarily responsible for maintaining both ISCs and EBs in an undifferentiated state, and additionally, they inhibit the formation of EE cells. This dichotomy in function between Da:Da and Da:Sc dimers raises an essential question for our research: How does an increase in Sc function override the differentiation-inhibiting effect of Da:Da dimers? In other words, we aim to explore how the ratio and balance between Da:Da and Da:Sc are modulated and interpreted within the cells, leading to a shift from maintaining ISC renewal towards promoting differentiation.

This consideration led us to propose two possible Scenarios:

- **Sc Threshold Scenario:** In this model, the key factor is the concentration of Da:Sc dimers. When Da:Sc reaches a certain threshold level, it triggers the differentiation of ISCs into EE cells, independent of Da:Da concentration (**Figure 23A**). This suggests a mechanism where a critical level of Da:Sc activation is sufficient to initiate the differentiation process, overriding the inhibitory influence of Da:Da (**Figure 23A**).
- **Da Titration Scenario:** Here, the focus is on the ratio of Da:Sc to Da:Da dimers. As Sc concentration increases, it not only promotes the formation of more Da:Sc dimers but also effectively decreases the concentration of Da: Da dimers (**Figure 23B**). This change in ratio is hypothesised to be crucial for determining EE cell differentiation. In this scenario, the relative decrease in Da:Da alongside an increase in Da:Sc shifts the cellular equilibrium towards differentiation (**Figure 23B**).

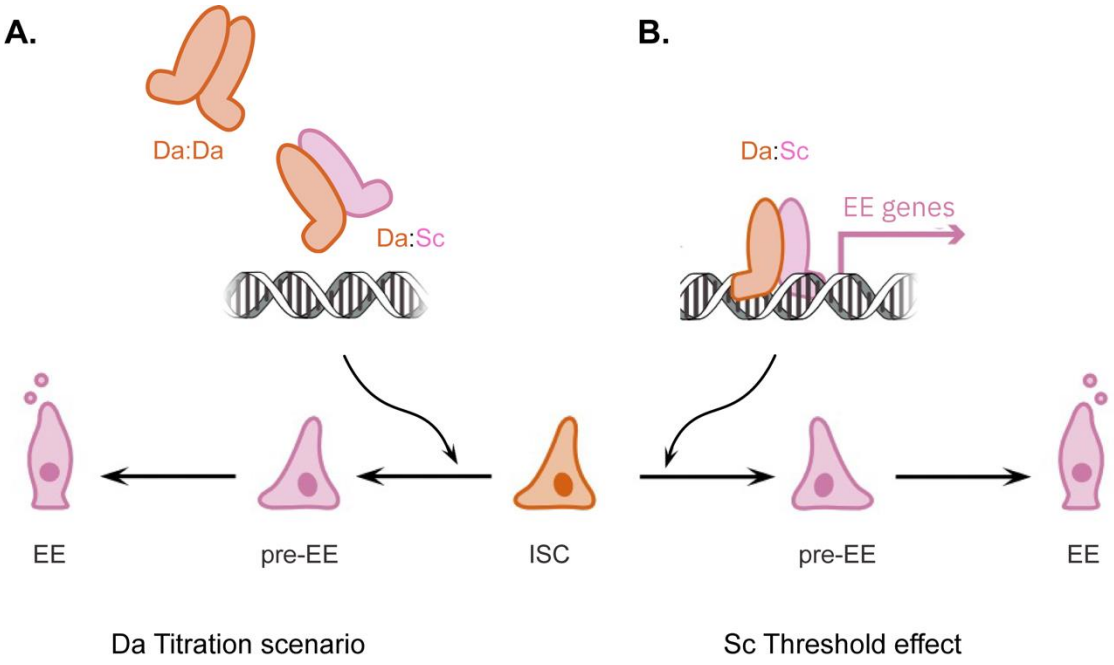

Figure 23. Illustration of Da Titration and Sc Threshold Hypotheses in ISC differentiation into EE. **A. Da Titration hypothesis:** Increasing Sc expression leads to a higher formation rate of Da:Sc heterodimers. As a result, Da is titrated away from Da:Da homodimers, decreasing their concentration. This shift in the balance towards Da:Sc dimers favours the progression from ISC to pre-EE and eventually to mature EE cells, highlighting the role of the Da: Sc to Da: Da ratio in determining cell fate. **B. Sc Threshold hypothesis:** A critical concentration of Da: Sc heterodimers activates EE gene expression, independent of Da: Da homodimer levels. Once the threshold level of Da :Sc is reached, it triggers the differentiation of ISCs into pre-EE c and, with sustained expression, into EE cells without the involvement of Da:Da homodimers.

To distinguish between these two possibilities and understand the triggers for ISC EE differentiation, our collaborators in Garcia Ojalvo's lab (Martinez-Corral, personal communication.) theoretically predicted that irrespective of their affinity constants, an increase in the Da concentration, for any given Sc concentration, would invariably lead to a rise in the total amount of Da:Sc. This increase is accompanied by a proportional rise in the ratio [Da:Da] to [Da:Sc]. Consequently, the more critical ratio, Da:Sc to Da:Da, would witness a decline. This prediction is visually represented in **Figure 24**.

Given this prediction, the balance between these dimers is expected to be sensitive to the relative concentrations of Da and Sc, whose expression can be independently manipulated thanks to genetic tools available in *Drosophila*.

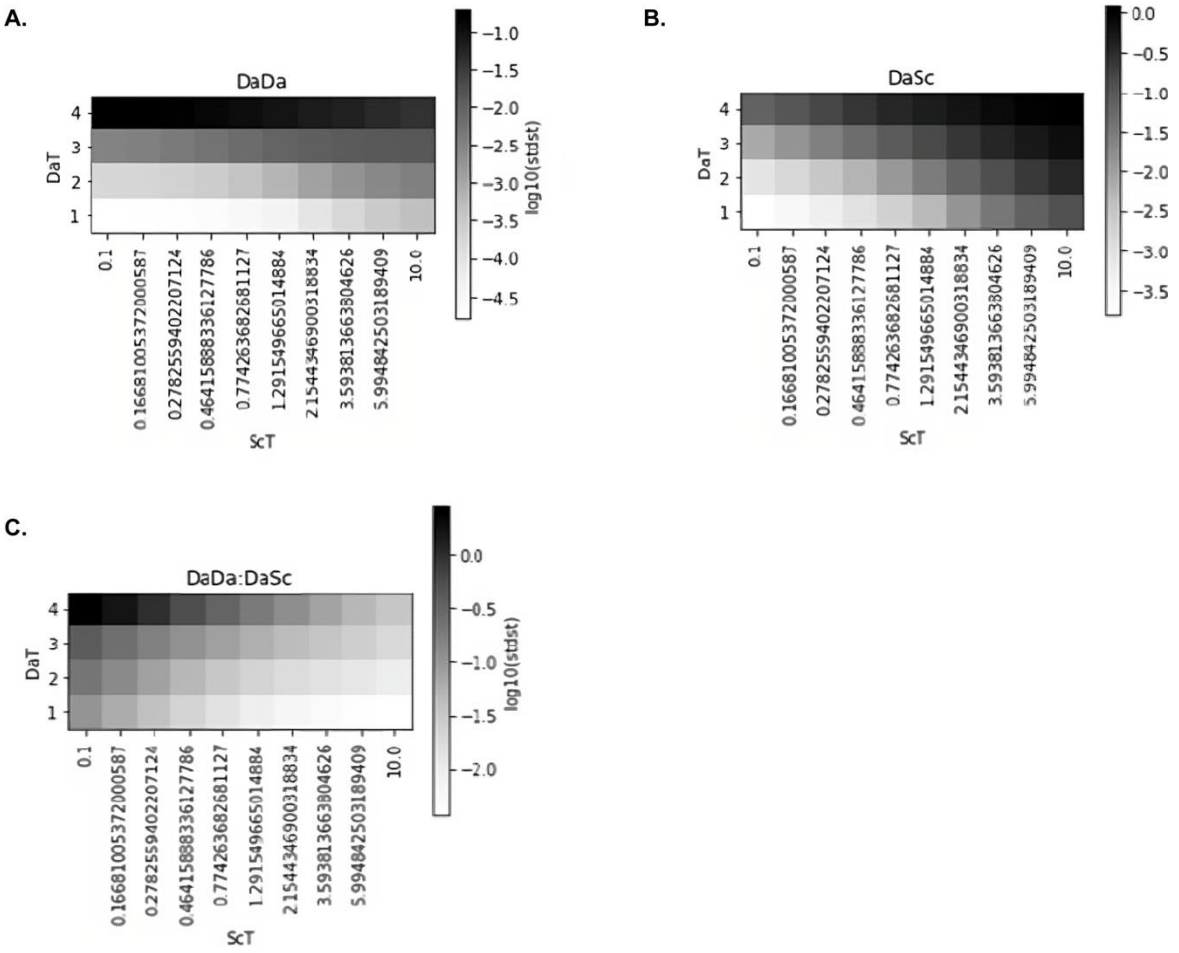

Figure 24. The theoretical framework of Da Titration Hypothesis and Sc Threshold Effect. A. Heatmap visualisation of Da homodimer (DaDa) concentrations against a range of Sc concentrations: The intensity of colouration correlates with the log-transformed concentration values of DaDa, with darker shades indicating higher levels. **B. Heatmap for DaSc heterodimer concentrations against Sc concentration:** The colour gradient represents the log-transformed concentrations of DaSc complexes, with darker tones signifying increased abundance. **C. Heatmap of the ratio between Da homodimers and DaSc heterodimers:** Map illustrates the predicted decrease in the ratio of Da:Sc to Da:Da as the concentration of Da increases, despite constant Sc concentration levels. Darker colours represent higher log-transformed ratio values, indicating a shift in the balance towards Da homodimer formation. *Prediction done by Rosa Martínez Corral from the Garcia-Ojalvo Lab* (Martinez-Corral, personal communication).

1.1. Aim

Building upon the genetic manipulations already executed by previous members of the lab, which involve the genetic manipulation of Daughterless (Da) and Scute (Sc) expression levels, this chapter focuses on the subsequent analysis phase, whose primary objectives are:

- To perform detailed cell counts across various Da and Sc expression conditions, providing quantifiable Data on ISC, pre-EE, and EE cell populations.
- To compare the observed Data against the previously outlined theoretical Scenarios: the Sc Threshold and Da Titration Scenarios.

2 Materials and methods

2.1. Experimental acknowledgments for data acquisition, gut dissection and immunofluorescence

Fly husbandry practices, along with procedures for fly crosses, and gut dissections and immunostaining and confocal microscopy, were performed by Joaquin de Navascués and Carlos de la Torre, adhering to the protocols detailed in Chapter 2.

To ascertain the effec[ts] of genetic variations on cellular differentiation, **Table 19** provides an overview of the *Drosophila* genotypes used in our study. Each genotype, carrying single, double, or quadruple copies of the Da gene and heat shock-inducible Sc expression, was subjected to a heat shock treatment and dissected the subsequent day for analysis. Our experimen[ts] included conditions with no heat shock (0 minutes) as a baseline and a moderate heat shock duration of 30 minutes, essential for inducing Sc expression via the HS-Gal4, UAS-Sc42 system.

Table 20 presents detailed descriptions of the specific crosses, outlining the genotypes involved and their significance in our experiments.

The primary antibodies used are listed in **Table 21**, while **Table 22** details the secondary antibodies, including their dilutions and suppliers.

Table 21. Overview of *Drosophila* genotypes used. Table details their genetic composition and its role in the experimental design, including single, double and quadruple copies of Da gene and the heat shock-induce Sc expression.

GENOTYPE	DESCRIPTION	DETAILS
DAX1	w; Da[10] / CyO; +	Used rescue fragment[ts] of the genomic region of Daughterless and null mutations to generate flies with 1, 2, or 4 copies of Da.
DAX2 (VALLECAS)	Vallecas (WT)	
DAX4	w; P{Da[+]} / CyO; P{Da[+]} / TM6B	
HS-SC	w; UAS-Sc / CyO; HS-Gal4	Used HS-Gal4, UAS-Sc42 system to increase Sc abundance at different levels with treatment[ts] at 37ºC for 0, and 30.

Table 22. Genotypic variations for Scute inductions experiment[ts]. Table categories *Drosophila* strains used to assess the impact of Da gene copy number and Scute in EE differentiation.

CROSS DESCRIPTION	GENOTYPES INVOLVED	HEAT SHOCK DURATION	SIGNIFICANCE
DAX1, DAX2, DAX4 × HS-SC (0, 30)	DAX1, DAX2, DAX4, HS-SC	0, 30	Explores the impact of Scute (Sc) induction via a 30-minute heat shock on different Daughterless (Da) genotypes (DAX1, DAX2, DAX4). Evaluates the influence of varying Da copy numbers on EE/ISC abundance.

Table 23. Primary antibodies used for Chapter 4.

ANTIGEN	ANTIBODY	HOST SPECIES	DILUTION	SUPPLIER
DELTA	MONOCLONAL	MOUSE	1:100	DSHB (C594.9B)
PROSPERO	MONOCLONAL	MOUSE	1:200	DSHB (MR1A)
PROSPERO	POLYCLONAL	RABBIT	1:1000	Yuh Nung Jan

Table 24. Secondary antibodies used for Chapter 2. All secondary antibodies were used at a working dilution of 1:500 and purchased from Sigma-Aldrich. Table includes the host species reactivity information as you specified.

HOST SPECIES	REACTIVITY	ALEXA FLUOROPHORES (REFERENCE)
DONKEY	RABBIT, MOUSE	594 (A21207), 594 (A21203)
GOAT	RABBIT, CHICKEN, MOUSE	488 (A11032), 633 (A21071), 633 (A21052)

2.2. Data handling and cell annotation

Cell Data from microscopy images was handled using the CellCounter plugin of FIJI/ImageJ, which exports the results as XML files. Each XML file corresponds to an image or field of view (FoV) and contains the X-Y coordinates of each identified cell, the type of cell based on specific criteria, and the corresponding image file name.

Within the CellCounter plugin of FIJI/ImageJ (REF), we categorised cells into six different types based on the following criteria:

- EB/EC: Identified by a DAPI nucleus, which could be polyploid or diploid and lack both Pros and Dl.
- EC Pros+: DAPI polyploid nucleus with the presence of Pros but lack of Dl.
- EE: DAPI diploid nucleus with the presence of Pros but lack of Dl.
- preEE: DAPI diploid nucleus with both Pros and Dl presence.
- ISC: DAPI diploid nucleus, absent of Pros but presence of Dl.
- Weak Pros+: Ambiguous DAPI nucleus (potentially diploid) with weak presence of Pros but absence of Dl.

2.3. Data Extraction from XML Files

The XML files were parsed to create a Pandas DataFrame. A Python script was developed to read and extract the necessary data from these XML files (**script available in Supplementary Information**). The Script utilised the ElementTree module to parse the XML content. It systematically extracted the cell type, coordinates, and associated image filename for every cell in each XML file.

These extracted data were compiled into a singular data frame, serving as the primary Data structure for subsequent analysis. To extract the information about the genotype and treatment conditions associated with each cell, the image file names were analysed as they contained encoded details and experimental conditions. To automate the extraction process, a Python Script was developed that analysed each unique image file name and used predefined dictionaries of substrings to determine the genotype and treatment conditions. The two Datasets were merged after extracting the cellular data and associated genotypes and treatments. The final DataFrame contained information about each cell, its associate genotype its treatment conditions.

2.4. Statistical analysis and visualisation

The statistical analysis used R software and the following libraries: ggplot2, readxl, dplyr, car, and emmeans.

Linear modelling was used to understand how heat shock-induced Sc expression relates to Daughterless copies.

For assessing the effect of Scute and Daughterless, linear regression model was applied. ANOVA was used to assess differences in ratios across Daughterless and Scute levels followed by Tukey's HSD for specific group distinctions.

3 Results and discussion

3.1. Different effects of Scute presence and Da copies on midgut cell types

In our investigation, we aimed to understand the dynamics of midgut cell type differentiation with respect to Daughterless (Da) copy numbers, the induction of Scute (Sc) via a 30-minute heat shock (HS), and their potential interaction. To comprehensively dissect these relationships, we employed a statistical approach known as a generalised linear model (GLM).

The GLM, a versatile modelling technique, offers a robust framework to examine complex relationships within datasets. In our specific study, the model:

Percentage of cells∼Cell Type×Da+Cell Type×HS

allows us to explore not only the individual effects of Daughterless copies and heat shock but also how these effects may depend on one another. In the formula, “percentage of cells” is the dependent variable and indicates that we are modelling the percentage of cells based on 1) Cell type X Da, which suggests an interaction between which cell type there is and the number of copies of the Da gene copies and 2) Cell type X HS which suggests an interaction between the type of cell and the heat shock treatment, this is, the presence of Scute.

In our specific findings, a significant decrease in the total percentage of EB/EC cells was shown under a 30-minute heat shock, irrespective of Daughterless copy numbers (p-values< 0.0001) (**Figure 25 & Figure 26**). This decrease could imply that heat shock, which induces Scute expression, has a down-regulating effect on these cell types, potentially independent of Da copies.

EC Pros cell numbers remained stable across all experimental conditions ($p > 0.05$) (**Figures 25 & 26**), aligning with studies which show EC differentiation is largely Sc-independent (Bardin et al., 2010; Tian et al., 2022). Scute´s primary role is in EE cell specification from ISCs, and its influence on EC differentiation may be indirect through its regulatory effects on EE cell differentiation pathways.

ISC showed no significant changes in frequency concerning heat shock duration or Daughterless copy numbers (p-values > 0.05) (**Figure 3 & Figure 4**). The consistent ISC numbers across different experimental conditions align with the concept that Sc is not directly involved in regulating ISC themselves. There is an intrinsic balance between Da homodimers, known to maintain ISC self-renewal,

and Da-Sc heterodimers, which promote differentiation. Our findings align with models proposing that Da-Sc heterodimers do not disrupt the homeostasis of ISC populations but instead signal differentiation pathways at a threshold level without further affecting ISC self-renewal (Jiang et al., 2016; Puig-Barbé & Navascués, 2019).

Following the induction of Scute, we observed a significant increase (p-values < 0.05) (**Figure 25 and Figure 26**) in pre-enteroendocrine cell populations, which did not vary with the number of Daughterless copies. This observation indicates that a critical level of Da: Sc heterodimers is sufficient to initiate the differentiation of intestinal stem cells into pre-EE cells. The rise in pre-EE cells seems to be a direct response to the Scute presence rather than the amount of Da available, suggesting that reaching a specific threshold of Da:Sc concentration is the key to triggering this initial step in differentiation (**Figure 25 and Figure 26**).

As seen in **Figure 25 and Figure 26**, the number of mature enteroendocrine cells remained unchanged across all tested conditions of Da copy numbers and Scute presence (p-values>0.5), suggesting a complex regulation at later stages of differentiation that may reach a saturation point where additional Scute does not equate to an increase in mature EE cells. However, it does so by initiating the differentiation pathway.

This underlines the regulated nature of the differentiation process, where a multitude of factors contribute to the outcome, ensuring the proper lineage commitment within the *Drosophila* midgut, including the Notch signalling pathway and transcriptional regulators such as Prospero (Pros) and Scute, intricately balance the differentiation of progenitor enteroblast cells into mature secretory EE cells (Bardin et al., 2010; Singh et al., 2012).

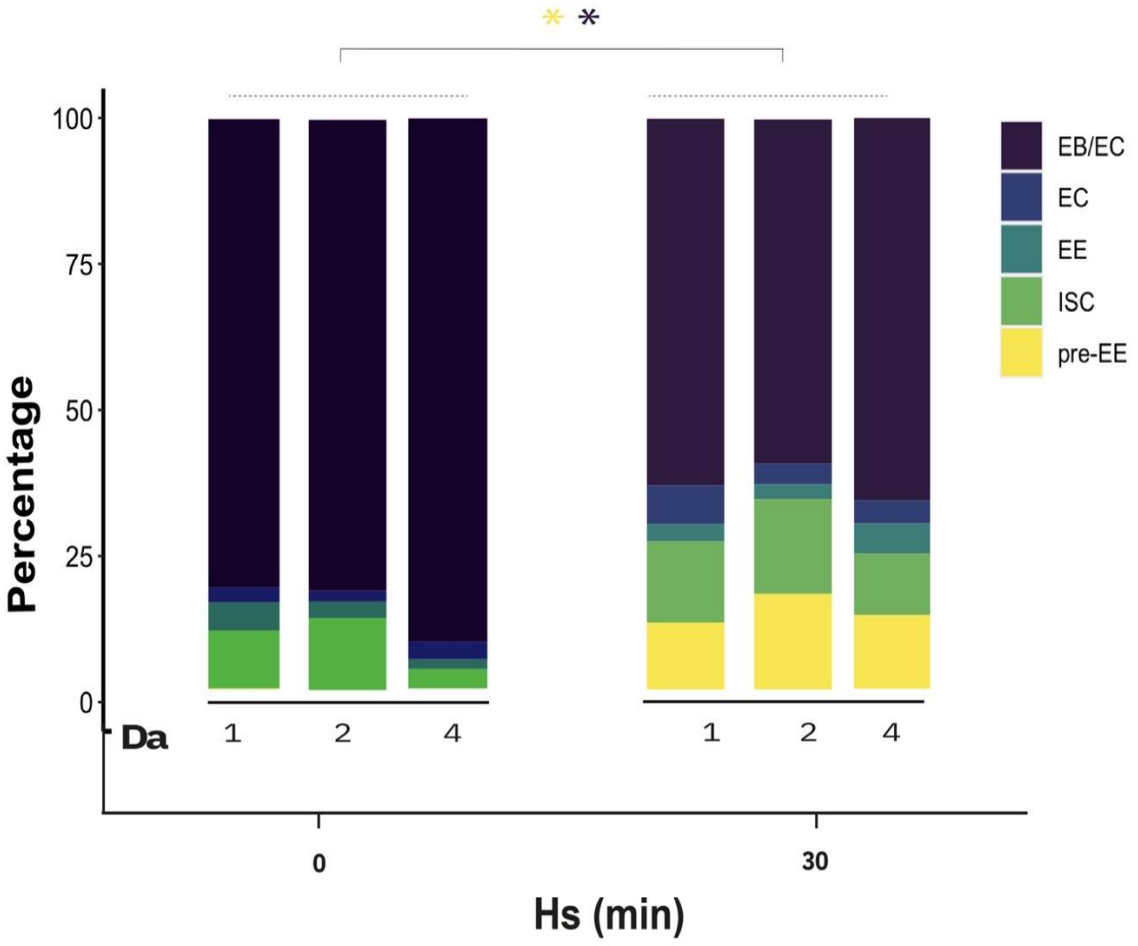

Figure 25. Different effects of Scute and Da copies on midgut cell types. Bar graphs showing the percentage distribution of cell types in response to different Daughterless (Da) and Scute (Sc) conditions post a 30-minute heat shock treatment. Cell types are categorised as EB/EC (enteroblast/enterocyte), EC (enterocyte), ISC (intestinal stem cell), EE (enteroendocrine cells), and pre-EE (pre-enteroendocrine). Heat shock (HS) in the y-axis means the presence or absence of Scute induction via the HS-Gal4, UAS-Sc42 system. The Generalized Linear Model (GLM) with Bonferroni-adjusted pairwise comparisons indicate a significant decrease in EB/EC cells and an increase in pre-EE cells under Scute induction (p-value < 0.05). Asterisks are colour-coded to indicate cell type differences, with significance denoted by * (p-value <0.05).

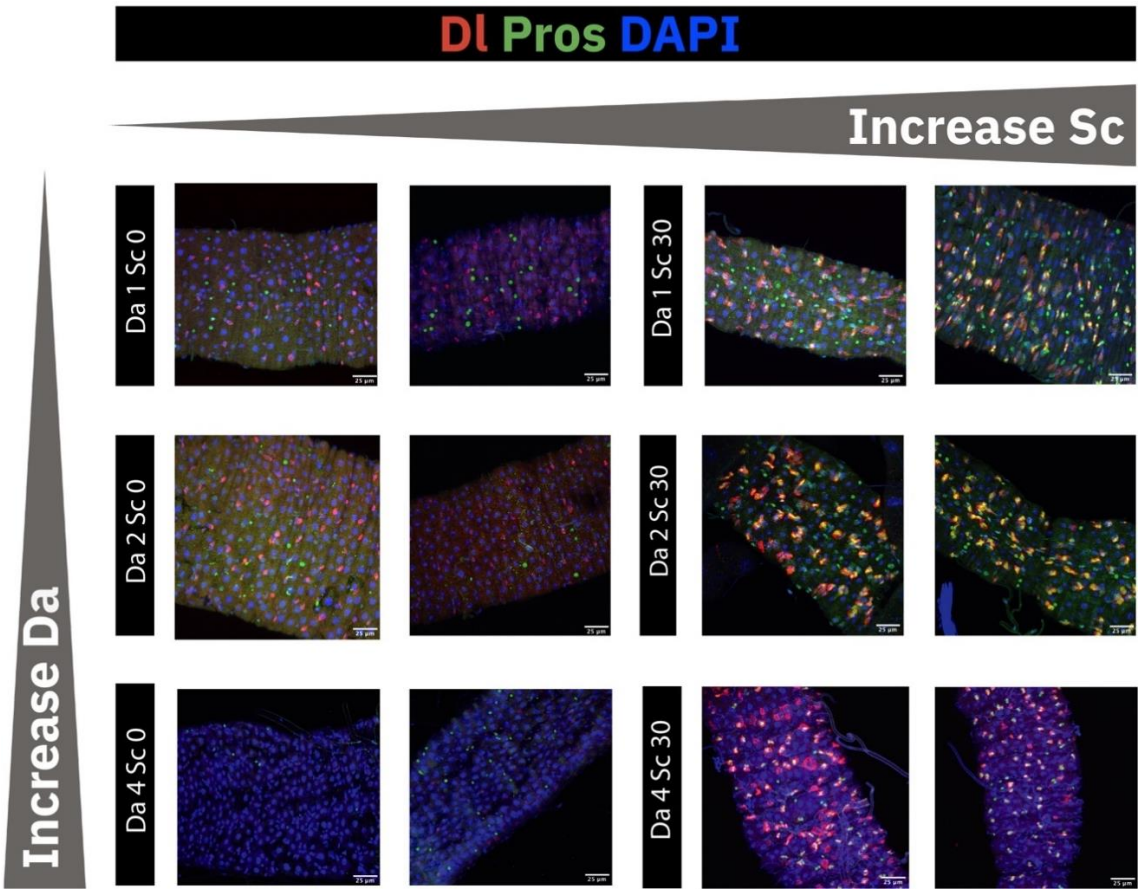

Figure 26. Different effects of Scute and Da copies on midgut cell types. Immunofluorescent tissue sections, showing two representative examples for each condition, to illustrate the differential effects of Scute and Daughterless (Da) on midgut cell types. Sections are stained with Delta (Dl), Prospero (Pros), and DAPI. Scale bar 25 µm.

3.2. Da: Sc heterodimers do not affect ISC percentage

After examining the collective trends among all cell types, we focused on the specific trend of cell types within the EE differentiation pathway. In the differentiation pathway of ISC to mature EE cells, we first focus on ISC percentage across the different conditions of Da and Sc. This analysis aimed to isolate the ISC population to discern patterns that might be overshadowed when considering all cell types collectively.

Linear modelling yielded no significant variables affecting ISC percentages, which is consistent with our broader Generalized Linear Model (GLM) assessment: neither the heat shock to induce Scute expression nor the Daughterless copies.

Nonetheless, a trend emerged within the data: irrespective of the Daughterless copies – one (1), two (2) or four (4) – the presence of Scute was consistently correlated with an increase in ISC concentration (**Figure 28**).

However, this correlation was nonlinear, as we found that the higher concentration of ISC was seen when Da was present in two copies and not when there were four copies of Daughterless (**Table 23 and Figure 28**).

Puig-Barbe et al. (2023) showed a complex interplay between Da homodimers and Sc-Da heterodimers in regulating ISC identity. Da homodimers are pivotal for ISC self-renewal, while the Da-Sc heterodimers promote differentiation-related characteristics, including ISC proliferation and the upregulation of ISC-specific genes like Delta (Dl). These findings indicate that Da:Da and Da:Sc dimers work collaboratively yet exert opposing influences on ISC fate, maintaining a delicate equilibrium between self-renewal and the onset of differentiation within the ISC population (Puig Barbe, 2018; Puig-Barbe et al., 2023).

This balance of dimerisation forms underpins a finely tuned regulatory mechanism governing ISC behaviour. The consistent ISC numbers, despite Scute induction, suggest that while Da:Sc heterodimers are critical to triggering differentiation, they do not diminish the role of Da:Da dimers in sustaining ISC self-renewal.

Table 25. Average percentage of ISC per different Sc and Da conditions. Effects of heat shock (HS) duration on the average percentage of intestinal stem cells (ISCs) across varying copies of the daughterless (Da) gene. Data poin[ts] reflect ISC abundance in the *Drosophila* midgut per total number of cells per field of view (FOV) under control conditions (0 minutes of HS) and after a 30-minute HS induction.

DA (COPIES)	HS (MIN)	AVERAGE ISC PERCENTAGE (PER TOTAL NUMBER OF CELLS PER FOV)
1	0	10.1
1	30	14.1
2	0	12.6
2	30	16.6
4	0	3.30
4	30	10.7

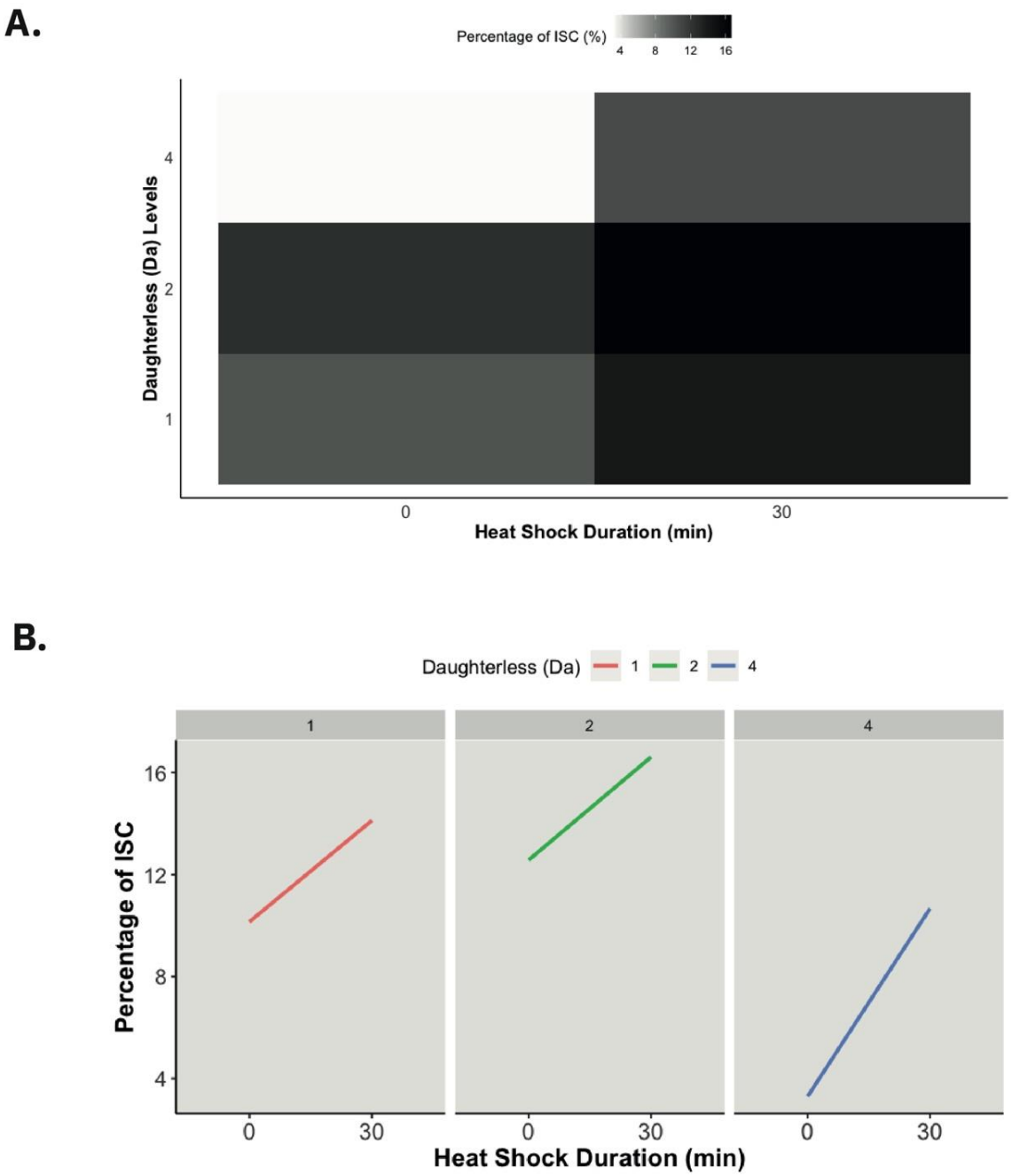

Figure 27. Impact of Sc and Da levels on ISC percentage. A. ISC percentage across different Sc and Da levels: Heat map showing the percentage of ISC at different Da and Sc levels (inducted by HS). Darker shades indicate higher percentages**. B. Interaction plot for ISC percentage: Interaction between Da copies and Sc expression.** Each line represents a different number of Da copies (1, 2, or 4) and how the ISC percentage changes with the duration of heat shock, indicative of Sc induction. Statistical analysis involved linear regression.

3.3. Da:Sc heterodimers drive pre-EE increase

Continuing our exploration of midgut cell dynamics, we now shifted our attention to precursor Enteroendocrine cells—an intermediate stage in ISC differentiation into EE cells.

The findings indicate that, for any given number of Daughterless copies, the expression of Scute as a result of a 30-minute heat shock consistently translated to an increase in the percentage of pre-EE cells. When Scute was present, the percentage of pre-EE increased from 0.102 to 11.77, where the number of Das copies did not have any notable effect (**Table 24**).

The heatmap in **Figure 29** shows that the induction of Scute through a 30-minute heat shock significantly increases the percentage of pre-EE cells across all levels of Da copies. This significant rise in pre-EE cells, particularly from a low baseline in the absence of heat shock, demonstrates the potent effect of Scute in driving the initiation of the differentiation process from ISCs to EE cells (**Figure 29**).

It seems that reaching a critical level of Sc activation triggers the differentiation pathway, a process not significantly enhanced by additional Da copies, indicating a saturation point in the pathway.

The number of Da copies does not seem to significantly alter the increase in pre-EE induced by Scute. This observation suggests that once the required Scute level is achieved, the system reaches a state conducive to pre-EE cell differentiation, regardless of the Da levels.

Table 26. Average percentage of pre-EE per different Sc and Da conditions. Effects of heat shock (HS) duration on the average percentage of intestinal stem cells (ISCs) across varying copies of the daughterless (Da) gene. Data poin[ts] reflect ISC abundance in the *Drosophila* midgut per total number of cells per field of view (FOV) under control conditions (0 minutes of HS) and after a 30-minute HS induction.

DA (COPIES)	HS (MIN)	AVERAGE PRE-EE PERCENTAGE (PER TOTAL NUMBER OF CELLS PER FOV)
1	0	0.10
1	30	11.77
2	0	0.06
2	30	16.6
4	0	0.02
4	30	12.98

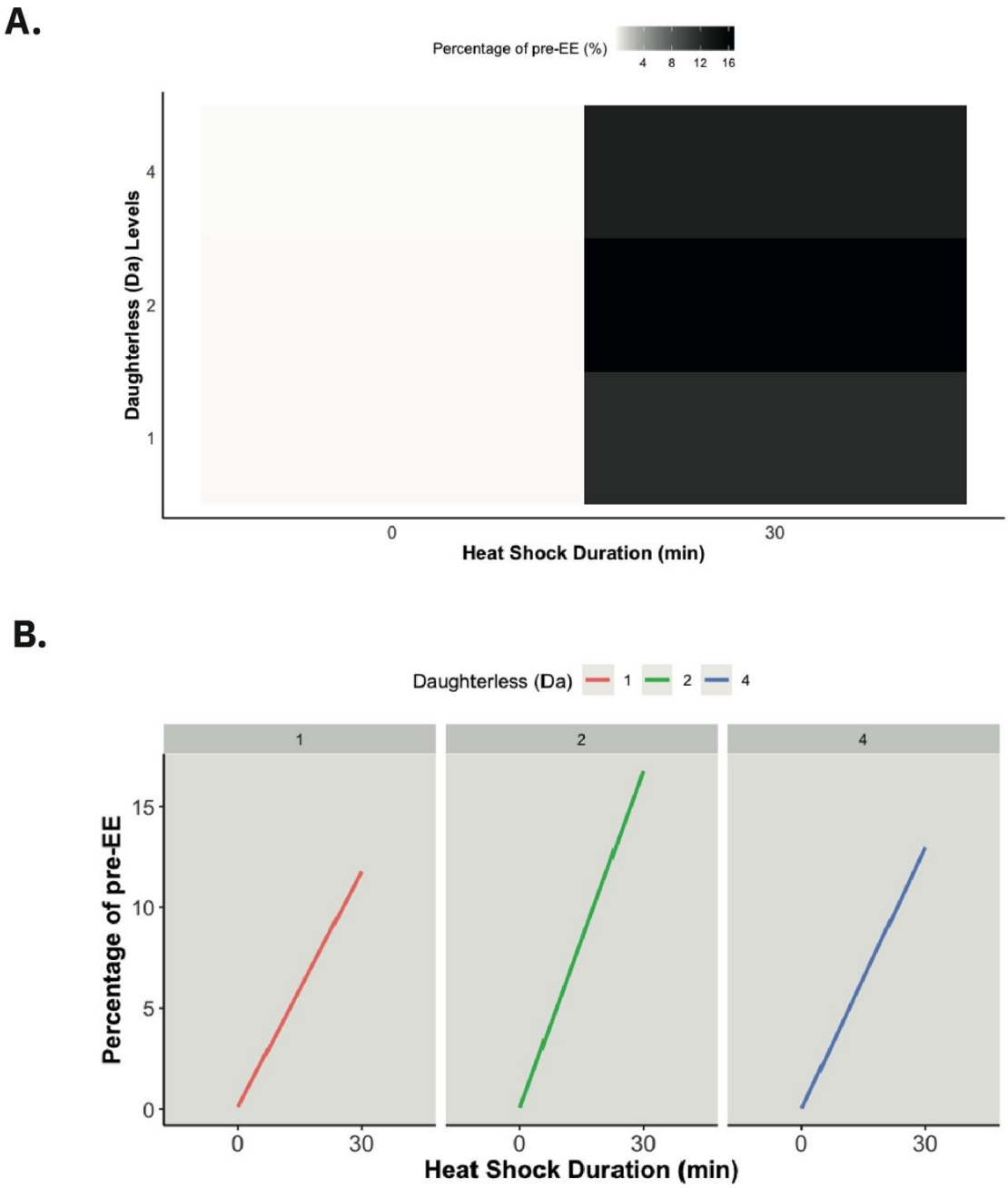

Figure 28. Figure 28. Impact of Sc and Da levels on pre-EE percentage. **A. pre-EE percentage across different Sc and Da levels:** Heat map showing the percentage of pre-EE at different Da and Sc levels (inducted by HS). Darker shades indicate higher percentages. **B. Interaction plot for pre-EE percentage:** Interaction between Da copies and Sc expression. Each line represents a different number of Da copies (1, 2, or 4) and how the pre-EE percentage changes with the duration of heat shock, indicative of Sc induction. Statistical analysis involved linear regression.

3.4. Da:Sc heterodimers modulate EE cell percentage in a non-linear manner

We centred our attention on the concentration of enteroendocrine (EE) cells, the final phase of the differentiation of ISCs.

Our heatmap analysis (**Figure 29A**) revealed a pattern: in the absence of Scute, an increase in the copies of Daughterless correlated with a decrease in the EE cell percentage per total cell, decreasing from 5% with one copy of Da to 1.8% with four copies of Da (**Table 25**). This trend suggests that the formation of Da:Da homodimers is associated with a reduced concentration of EE cells.

Conversely, the trend is reversed when a 30-min heat shock induces the Sc transgene. As Daughterless levels increase, so does the percentage of EE per total cells (**Figure 29A**). With one copy of Da, EE percentages decrease from 5.00% to 3.09% after a 30-minute heat shock. For two copies, the percentages are consistently lower (around 2.81% to 2.62%), regardless of heat shock. However, the EE percentage significantly increases with four copies from 1.84% to 5.29% following a 30-minute heat shock (**Table 25**).

Despite the observed trends, linear modelling did not yield significant differences when considering Scute presence and Da copy numbers in isolation. However, examining the interaction between Sc and Da, we found that Scute presence decreased EE cell percentages with just one copy of Da. In contrast, EE levels remained stable with two copies. Remarkably, at four copies, Scute's presence boosted EE cell percentages above baseline levels without heat shock (**Figure 29B**).

These observations suggest that the mere presence of Scute influences EE cell percentages, but the extent of this influence is modulated by Da's availability to form heterodimers. The differential effect based on Da copy number underscores the delicate balance required between Da homodimers, which maintain ISC self-renewal, and Da:Sc heterodimers, which promote EE differentiation.

The findings by Puig-Barbe et al. (2023) complement this, elucidating the roles of Sc and Da in enteroendocrine (EE) cell differentiation within the *Drosophila* adult intestine. It is speculated that for successful initiation of EE differentiation, Sc:Da heterodimers must outcompete Da:Da homodimers. Furthermore, Emc, a helix-loop-helix (HLH) factor, modulates Da and Sc levels to fine-tune the balance

between absorptive and secretory cell fates. This delicate regulation is essential for managing the transition from ISC self-renewal to differentiation and the subsequent specification of EE cells (Puig Barbe, 2018; Puig-Barbe et al., 2023).

Table 27. Average percentage of EE per different Sc and Da conditions. Effects of heat shock (HS) duration on the average percentage of intestinal stem cells (ISCs) across varying copies of the daughterless (Da) gene. Data points reflect ISC abundance in the *Drosophila* midgut per total number of cells per field of view (FOV) under control conditions (0 minutes of HS) and after a 30-minute HS induction.

DA (COPIES)	HS (MIN)	AVERAGE EE PERCENTAGE (% PER TOTAL NUMBER OF CELLS PER FOV)
1	0	5.00
1	30	3.09
2	0	2.81
2	30	2.62
4	0	1.84
4	30	5.29

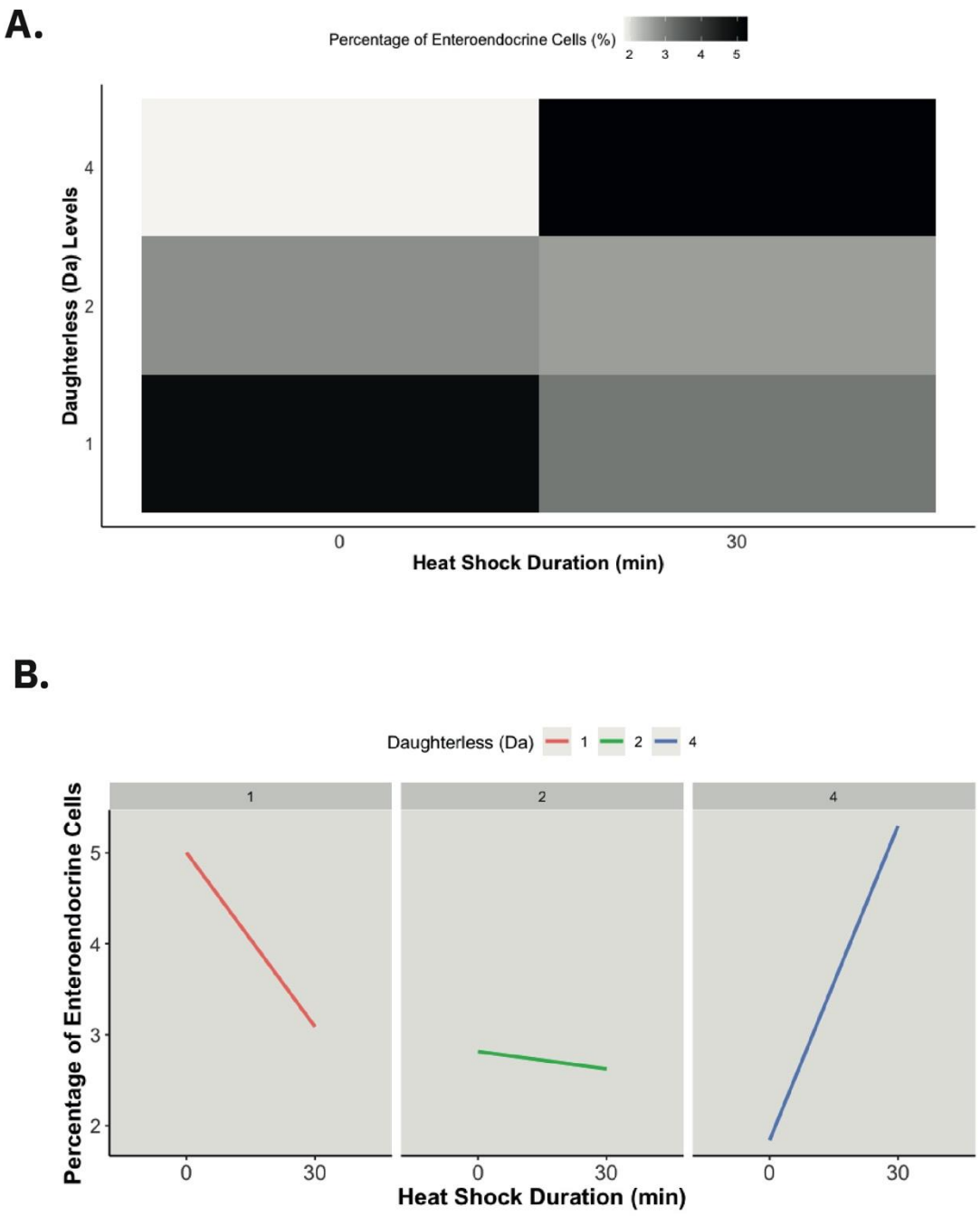

Figure 29. Impact of Sc and Da levels on EE percentage. A. EE percentage across different Sc and Da levels: Heat map showing the percentage of EE at different Da and Sc levels (inducted by HS). Darker shades indicate higher percentages**. B. Interaction plot for EE percentage:** Interaction between Da copies and Sc expression. Each line represents a different number of Da copies (1, 2, or 4) and how the EE percentage changes with the duration of heat shock, indicative of Sc induction. Statistical analysis involved linear regression.

3.5. Da:Sc heterodimers trigger an increase in EE-to-pre-EE ratio

In our analysis of the relationship between ISC, EE, and pre-EE, we observed that ISC and EE remained relatively unchanged, while pre-EE exhibited changes when expression of Scute was induced.

Our previous findings showed that: **1)** Even with Scute activation, Da:Da homodimers maintain ISC self-renewal, suggesting Da:Sc heterodimers may drive differentiation without compromising the maintenance of ISCs, **2)** the notable rise in pre-EE cell numbers following Scute induction, regardless of the number of Da copies, indicates a Scute-mediated threshold mechanism that triggers EE differentiation and **3)** while Scute is implicated in EE cell differentiation, its impact may be modulated by the ability of Da to form heterodimers, thereby intricately influencing EE cell outcomes under different Scute conditions.

To gain a deeper understanding of these dynamics, we focused on analysing the ratios between these cell types, providing additional insigh[ts] into how changes in one cell type might influence the others.

Our research highlighted two ratios: the first ratio, Ratio 1 (pre-EE to the sum of pre-EE and ISC) and the second ratio, Ratio 2 (ISC to the sum of pre-EE and ISC) (**Figure 30A**). In the absence of Scute, there is a notable difference between Ratio 1 and Ratio 2, with the latter being substantially higher (**Figure 30A**). This aligns with earlier results that identified Scute as crucial for initiating the differentiation process. In its absence, ISCs do not commit to the pre-EE pathway, as indicated by the higher Ratio 2.

However, following Scute induction, Ratios 1 and Ratio 2 become similar and do not vary with the number of Da copies (**Figure 30A**). This uniformity suggests a threshold effect of Scute induction, where a certain level of Sc activation is sufficient to initiate the differentiation process.

Further, we examined three additional ratios: Ratio 3 (EE to pre-EE), Ratio 4 (EE to ISC), and Ratio 5 (EE to the sum of pre-EE and ISC) (**Figure 30B**).

Our results show that when Sc is expressed, there is a significant decrease in the ratio between EE and pre-EE cells (p-value=0.0018), and this is because Sc favours the differentiation towards pre-EE. However, it appears not to promote the subsequent differentiation of pre-EE into EE cells to the same extent (**Figure 30B**).

The interactions between the ratios and Da, as well as the ratios and Scute, particularly point out the importance of Sc expression for Ratio 3 (p-value= 0.0018).

The effect of Scute induction on Ratio 3 reinforces the Sc Threshold Scenario, suggesting that induction directly contributes to the differentiation into pre-EE, irrespective of the Da concentration.

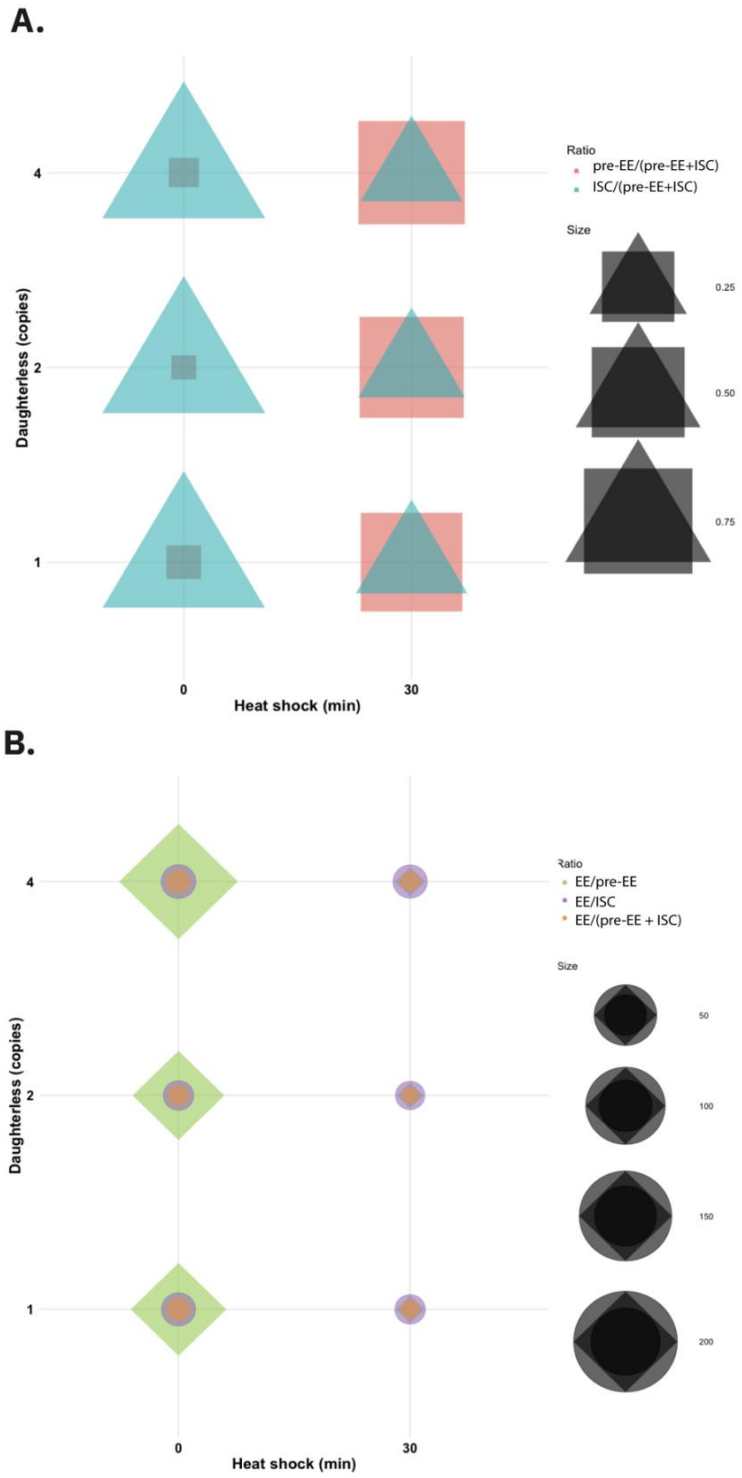

Figure 30. Cell type ratios in response to Sc induction and Da copy numbers. **A. Ratio 1 and Ratio 2:** Bubble plot illustrating the relationship between HS duration and Da copies. Bubble sizes represent the values of Ratio 1 and Ratio 2, with distinct colours indicating each ratio. **B. Ratios 3, 4, and 5:** Bubble plot showing associations among HS duration, Da copies, and Ratios 3, 4, and 5. Bubble sizes correspond to the values of each ratio, with unique colours for differentiation. Ratio value is represented by each bubble size. Statistical analysis was conducted using ANOVA, followed by Tukey's HSD.

4 Conclusion

Maintaining homeostasis, a complex and multifaceted process, involves more than just balancing cell division, differentiation, and loss (Nakamuta et al., 2022a; O'Brien, 2022; Weterings et al., 2021). An equally critical aspect is ensuring the appropriate proportion of differentiation into various mature cell types (Morrison & Kimble, 2006; Shahriyari & Komarova, 2013).

Building upon the foundation laid by previous research conducted by Puig-Barbé (2019), we specifically investigated the function of Da:Sc bHLH heterodimers in driving ISC differentiation into EE cells.

The primary objective was to elucidate how an increase in Sc expression can counteract the differentiation-inhibitory effects of Da:Da homodimers. We explored how the balance between Da:Da and Da:Sc heterodimers is regulated within cells and how shifts in this balance can influence the transition from ISC maintenance to EE differentiation.

This chapter delved into the pivotal role of Da:Sc heterodimers in ISC differentiation, exploring two distinct hypotheses – the Sc Threshold Scenario and the Da Titration Scenario.

Our findings lean towards the Sc Threshold model, suggesting that a specific concentration of Da:Sc is essential for triggering ISC differentiation into pre-EE cells, irrespective of Da:Da levels.

4.1. Support for Sc Threshold Scenario:

Our results seem to better align with the Sc Threshold Scenario: a significant increase in pre-EE cells was observed following Scute induction, which occurred irrespective of Da copy number (**Figure 29**). This finding strongly supports the hypothesis that a critical level of Da:Sc heterodimers is crucial for initiating differentiation.

Furthermore, we found that Ratio 1 (the proportion of pre-EE cells relative to the sum of pre-EE cells and ISCs) significantly increased upon Scute induction. This indicates a higher proportion of pre-EE cells when Sc is present, a key indicator supporting the Sc Threshold Scenario (**Figure 30A**).

The consistency of the proportion of ISCs relative to the sum of pre-EE cells and ISCs (Ratio 2) with varying Da copy numbers further reinforces the Sc Threshold

Scenario. The non-variability of this ratio suggests that the level of Scute activation is the primary determinant of initiation of differentiation into pre-EE cells (**Figure 30A**). When the threshold of Scute is achieved, the differentiation process is triggered, seemingly independent of Da copy number variations.

Overall, these findings provide evidence for the threshold effect of the Scute transcription factor, which, when forming heterodimers with Da, drives the differentiation pathway into pre-EE cells.

4.2. More intricate scenario than just a Sc Threshold for EE differentiation

The Sc Threshold Scenario proposes that a critical level of Da:Sc heterodimers can trigger ISC differentiation into pre-EE cells. Our results confirm that these heterodimers can initiate differentiation, leading to a noticeable increase in pre-EE cells. However, this increase may not be sufficient for further differentiation into mature EE cells.

The observed non-linear modulation in EE cell percentages suggests that while the threshold mechanism is significant, it may not be the sole determinant of EE cell fate. Additional layers of regulation could be at play, including feedback loops (Biteau & Jasper, 2014; Chen et al., 2016; Sallé et al., 2017), interactions with other signalling pathways, or the influence of the microenvironment (Zhu et al., 2021). These factors are not comprehensively explained by the Sc Threshold Scenario alone.

The Sc Threshold Scenario may be more applicable to the initial stages of differentiation, such as the formation of pre-EE cells. However, as cells progress toward becoming mature EEs, other factors and signalling pathways may come into play, exerting influence on the final stages of differentiation in ways that extend beyond the scope of the Sc Threshold Scenario.

4.3. Future directions:

Another plausible explanation for the non-linear dynamics observed in EE cell expression could be attributed to the timing of our experimental analysis.

After inducing Scute expression through heat shock, flies were dissected only a day later. This short interval likely captured an increase in pre-EE cells but may not have allowed sufficient time for these cells to further differentiate into EE cells.

For future studies, conducting a time-course analysis after heat shock would be insightful. This would enable us to observe the evolution of cell types over time and better understand the differentiation process in the presence of Sc and Da.

Additionally, exploring the entire spectrum of Sc and Da parameters could provide deeper insights. This exploration should include varying the heat shock duration (specifically 15 and 60 minutes) to determine how different levels of Scute influence the outcomes. Incorporating a negative control for the Sc transgene using a non-inducible transgene would also help delineate the specific effects of induced Scute expression.

CHAPTER 5: EXPLORING TRIMETHOPRIM (TMP) SAFETY AND GUT APPLICABILITY IN *DROSOPHILA* FOR NOVEL DESTABILISING DOMAINS -BASED MISEXPRESSION SYSTEM

1 Introduction

In this thesis, we have consistently explored the use of heat shock in *Drosophila* research, applying it across various contexts and methodologies.

Chapters 2 and 3 focused on employing HS to study midgut tissue turnover. This was built on the hypothesis that HS might trigger a homeostatic response in ISCs, as proposed in our quiescence-division switch model.

In Chapter 4, the scope of HS expanded to its use as a genetic tool. We used HS to induce the expression of the Scute gene through the HS-Gal4, UAS-Sc42 system. This application underscored the broader roles of HS and temperature in general in *Drosophila* research as a common strategy for temporal control of gene expression.

However, this approach also illuminated a critical challenge: temperature, while a useful tool in gene expression control on the fly, can influence cellular dynamics, as seen in Chapters 2 and 3. This is particularly relevant in studies where temperature variations could confound the interpretation of stem cell behaviour turnover. Therefore, there is an emerging need for advanced genetic tools that offer precise control over gene expression, dependent on temperature fluctuations. Such tools would enable us and other researchers to more accurately dissect temperature-influenced dynamics in *Drosophila*.

Researchers have explored various alternative systems to address the limitations of the Gal4-UAS system in *Drosophila* and its temperature-sensitive variant, Gal80ts.

These alternatives include chemically inducible gene expression systems, such as tetracycline-inducible systems (Bello et al., 1998; Stebbins et al., 2001), steroid hormone-induced systems, and the quinic acid-responsive QS/QF/QUAS systems (Potter et al., 2010; Potter & Luo, 2011; Riabinina & Potter, 2016).

The Tetracycline-Transactivator system introduces the tetracycline transactivator (tTA) to regulate gene expression based on the presence or absence of tetracycline or its derivatives (Stebbins et al., 2001).

The tet-on system is an example where tTA is engineered to activate transcription in the presence of tetracycline, which triggers tTA to bind to specific promoter sequences, leading to the activation of the target gene (Cuperus et al., 2015). It has been employed effectively for tissue-specific and stage-specific gene regulation

(White-Cooper, 2012), and it has significantly contributed to understanding various biological processes such as ageing, behaviour, and development (**Table 26**) (Burnett et al., 2011; Robles-Murguia et al., 2019).

In contrast, the Tet-Off system operates on the opposite principle. When tetracycline is present, it binds to tTA, causing a conformational change that prevents tTA from binding to DNA, thereby turning off-target gene expression (Bieschke et al., 1998).

However, tetracycline has been linked to decreased mitochondrial function, potentially introducing biases in experimental outcomes (**Table 26**) (Chatzispyrou et al., 2015; Moullan et al., 2015).

Ligand-inducible Gal4 Chimeras, such as Gal4-ER and GeneSwitch, also fuse Gal4 with estrogen or progesterone receptors, responding to specific ligands for controlled gene expression. This approach allows tissue-specific expression of UAS-based transgenes with precise temporal regulation.

Other systems, as we explored in Chapter 1, include the GeneSwitch system. The Gal4 DNA-binding domain is fused to the human progesterone receptor, enabling RU486-induced gene expression (**Figure 7A**). While this method achieves a high level of spatial-temporal expression control, the fitness of flies can be negatively impacted by using the hormone RU48 at concentrations as low as 10 ug/ml of mifepristone (Landis et al., 2015; Yamada et al., 2017). RU486 has also been shown to cause developmental lethality in flies at concentrations greater than 25 mM (Li & Stavropoulos, 2016) (**Table 26**).

Another method we referred to in the introductory Chapter 1, the quinic acid-inducible QS/QF/QUAS system, can also efficiently control expression (Potter & Luo, 2011). A limitation of the QS/QF/QUAS system is leakiness in the expression of the transgene downstream of the QUAS promoter, which can occur even in the absence of the QF protein. This can result in low-level transgene expression when it is not desired. This leakiness can affect the specificity and precision of gene expression control. Another limitation is the requirement for exogenous quinic acid as an inducer for the Q system (**Table 26**) (Riabinina & Potter, 2016).

Lastly, the auxin-inducible degron (AID) system offers another chemical approach for controlled protein depletion in *Drosophila*, which employs an AID tag fused to a protein targeted for depletion. The AID system is not without limitations. Off-target

effects may occur, with auxin potentially causing the degradation of non-target proteins interacting with TIR1 (Bence et al., 2017). The necessity for genetic modification to integrate the AID tag into the target protein also limits its applicability in some experiments (**Table 26**) (Tanaka et al., 2015).

A new approach, also based on degrons, has gained attention in the last decade: the use of destabilising domains (DDs) to control gene expression. In this method, destabilising domains are used to induce the degradation of fused proteins. Introducing specific ligands can precisely regulate this destabilisation (**Table 26**) (Iwamoto et al., 2010). By introducing these ligands, gene expression can be controlled by modulating the stability and degradation of the fused protein (Quintino et al., 2018).

1.1. Destabilisation domains (DDs)

When incorporated into fusion proteins, DDs cause destabilisation, leading to the rapid degradation of the entire protein (Cho et al., 2013; Wilmington & Matouschek, 2016). This destabilisation occurs through targeting the fusion protein for proteasomal degradation (Egeler et al., 2011).

Nevertheless, the destabilisation of the fusion protein can be stopped when specific ligands are introduced, effectively preventing further degradation (Iwamoto et al., 2010; Senturk et al., 2017). This property allows researchers to exercise precise control. Ligands can vary widely and may include small molecules, natural compounds, or even endogenous molecules. The ligand-binding interaction with the DD can induce conformational changes that stabilise the fusion protein, preventing proteasome degradation (Rakhit et al., 2011).

When ligands are present, the fusion protein remains intact and functional, determining when and how much of the specific protein is present within a cell (Banaszynski et al., 2006; Cho et al., 2013; Maynard-Smith, 2007).

The origins of DD technology can be traced back to identifying specific destabilising mutations in the human FKBP12. This discovery led to the development of a family of highly specific synthetic FKBP12 ligands. One such ligand, Shield-1, could bind to mutant FKBP12 and prevent proteasome-induced degradation of DD-GFP and other fusion proteins (Banaszynski et al., 2006; Senturk et al., 2017).

Expanding upon the potential of the FKBP12-based DD architecture, Iwamoto et al. (Iwamoto et al., 2010) engineered a similar destabilising domain, the *E. coli*

dihydrofolate reductase (ecDHFR). This 159-residue enzyme plays a pivotal role in catalysing the conversion of dihydrofolate to tetrahydrofolate, which is essential for various steps in prokaryotic primary metabolism. In this system, ligands such as the antibiotic trimethoprim (TMP) have been used to stabilise fusion proteins containing the ecDHFR destabilising domain, which prevents the degradation and maintains the stability of the fusion protein (Matthews et al., 1985; Schweitzer et al., 1990).

1.2. Use of destabilising domains in *Drosophila*

Over the past decade, the TMP and DD system has become increasingly popular in their applications (Kogenaru & Isalan, 2018; Peng et al., 2022; Sethi & Wang, 2017).

In 2017, Sethi et al. (2017) broke new ground by applying this system to *Drosophila melanogaster*. They introduced the Gal80-DD technique by fusing Gal80, a suppressor in the GAL4-UAS system, with a DD. The presence of TMP effectively modulates Gal80 activity, making gene expression contingent upon chemical induction. The removal of TMP induces Gal80 degradation, thus allowing for reversible and dynamic control of gene expression.

The Gal80-DD technique has successfully been employed in *Drosophila* neural system to achieve post-translational control of gene expression, demonstrating its versatility and potential for genetic manipulations (Sethi & Wang, 2017). By controlling protein stability in a ligand-inducible manner, the Gal80-DD technique allows for the temporal manipulation of gene expression within neural circuits (Sethi & Wang, 2017). The technique demonstrated a wide dynamic range, as GFP expression increased up to 45 times with 1 mM TMP and varied across TMP concentrations (0–5 mM), reaching a plateau within 36 hours. Additionally, it showed reversibility, with GFP intensity decreasing by 73% within 24 hours after switching from 1 mM TMP to regular food. Notably, these features were achieved without any detectable side effects on the lifespan or behaviour of the flies (Sethi & Wang, 2017).

In 2018, Kogenaru & Isalan also achieved success by developing a Gal4 protein fused to two ecDHFR domains, which functions *in vivo* in the format of the Gal4-UAS bipartite system (Kogenaru & Isalan, 2018). These domains make the Gal4 protein unstable, leading to its degradation under normal conditions. However, exposure to TMP stabilises the ecDHFR domains, thereby preventing the

degradation of the Gal4 protein. This stabilisation allows the Gal4 protein to function as a transcriptional activator in the Gal4-UAS bipartite system, enabling controlled gene expression. The dual-domain architecture used by the authors was particularly effective in completely suppressing the protein's function in an uninduced state while allowing for tunable activation upon TMP addition. By integrating the destabilising domains with the Gal4-UAS framework, this approach offers precise control over gene expression, enabling the activation or suppression of potentially lethal genes in a regulated, drug-responsive manner.

However, both systems have important limitations which have prevented broader uptake by the *Drosophila* community.

One limitation of using Gal80 for degradation is that it only facilitates an "OFF" strategy, implying that gene expression only occurs when TMP is removed, as Gal80 is degraded and no longer recruits Gal4 to bind to the UAS promoter sequence. Consequently, the presence of TMP suppresses gene expression.

This implies that flies would have to be raised in a TMP-containing medium and then removed from it to activate gene expression. Maintaining flies in TMP food for extended periods of time may compromise their well-being and normal development. The full range of potential implications remains uncertain because standard protocols do not involve such conditions.

Similarly, the Gal4-DD system's incompatibility with existing UAS lines presents a challenge. The UAS lines are designed to work with the unmodified Gal4 protein and may not efficiently respond to the modified Gal4-DD protein.

This limitation highlights the need for compatibility and flexibility when considering the implementation of these advanced DD systems in the broader context of existing Gal4-UAS resources.

Table 28. Comparative overview of gene expression systems in *Drosophila* research. Comparison of various gene expression systems, outlining their advantages and disadvantages. Cost estimations are based on prices from Sigma-Aldrich as of December 2023.

SYSTEM	ADVANTAGES	DISADVANTAGES	£/100mg
GAL4-UAS SYSTEM	Well-established, versatile system with a vast array of available driver lines. Enables targeted gene expression in specific tissues or at specific developmental stages	Lack of temporal control.	0
GAL80^{TS} SYSTEM	Compatible with all Gal4 lines, providing extensive flexibility in experimental design. Allows precise temporal control of gene expression.	Temperature may have unintended effects on the phenotype being studied. Requires the generation of transgenic lines for each new driver examined.	0
TET-OFF AND TET-ON SYSTEMS	Allows for reversible and tightly controlled gene expression. Gene expression is turned on or off in the presence or absence of tetracycline, providing temporal control.	Tetracycline can interfere with mitochondrial function. There may be a delay in gene suppression after tetracycline is added due to existing proteins.	0.2
Q SYSTEM	Provides a robust alternative to the Gal4-UAS system with less background activity. Can be combined with Gal4-UAS for more complex genetic manipulations	Potential leakiness in gene expression even in the absence of the inducer.	9.24
GENESWITCH SYSTEM	Provides temporal control of gene expression, enabling precise timing in gene regulation	Limited availability of lines The use of hormones to control gene expression may affect other physiological processes.	129
AID SYSTEM	Provides temporal control of gene expression and allows for partial degradation of the target protein. Compatible with all Gal4 lines, enhancing experimental flexibility.	Partial degradation of the target protein may limit the extent to which gene expression can be controlled.	0.1
GAL3 - DD	Offers temporal control of gene expression. Compatible with all Gal4 lines, providing flexibility in experimen^{ts}.	Requires a constitutively active Gal3 protein for compatibility with Gal4 lines, potentially limiting flexibility and ease of use.	0.91

1.3. Gal3c-DD

We propose the Gal3c-DD system to overcome the limitations of the Gal4-DD and Gal80-DD systems.

The Gal3c-DD system is an innovative genetic tool proposed to work within the existing Gal4-UAS framework used widely in *Drosophila* research. Rather than modifying Gal4, potentially disrupting its interaction with the existing UAS lines, the Gal3c-DD system focuses on the Gal3 protein.

In *Saccharomyces cerevisiae*, Gal3 detects galactose and activates the GAL genes responsible for galactose metabolism by enhancing the function of the transcriptional activator Gal4. In the absence of galactose, Gal80 binds to Gal4, and this complex prevents Gal4 from binding to the UAS sequence and activating the transcription of the GAL genes. When galactose is present, it changes the conformation of Gal3 and activates it, which then recruits Gal80 from the nuclei to the cytoplasm, which frees Gal4. Gal4 can bind to the UAS sequence to initiate transcription (**Figure 32**) (Pannala et al., 2010).

In *Drosophila*, the natural galactose sensing and gene activation pathway via Gal3 is absent. For this DD system, a constitutively active Gal3 variant (Gal3c) independent of galactose is required.

This constitutively active Gal3 variant has already been identified. In 1997, Blank et al. (1997) identified five distinct Gal3 mutant alleles with altered Gal80 binding properties, enabling them to activate Gal4 independently of galactose. Key mutations include substituting phenylalanine at position 237 with tyrosine (F237Y), aspartic acid at position 368 with valine (D368V), and serine at position 509 with proline (S509P) or leucine (S509L) (**Figure 31**). These mutations led to variations in gene expression levels and enhanced Gal3's ability to bind to Gal80, ultimately amplifying Gal4 activation.

In our proposed Gal3c-DD system, a constitutively active Gal3 protein would need to be fused to one destabilising domain derived from the ecDHFR enzyme of *E. coli*. This fusion would make the Gal3 protein unstable, leading to its degradation in the absence of the stabilising ligand, TMP (**Figure 32**).

When added, TMP binds to the destabilising domains, stabilising the Gal3 protein, preventing its degradation and allowing it to function. This activation of Gal3 could

then drive the expression of genes downstream of the UAS sequences when paired with Gal4 lines (**Figure 32**).

The Gal3c-DD system would be beneficial because it maintains compatibility with the Gal4-UAS lines and provides an ON alternative; TMP is added to active gene expression and is a cost-effective way to regulate gene expression (**Table 26**).

By applying TMP to the fly food for 24 hours, researchers can precisely control when and where the Gal3 protein is active, offering a dynamic tool for studying gene function and regulation in *Drosophila*.

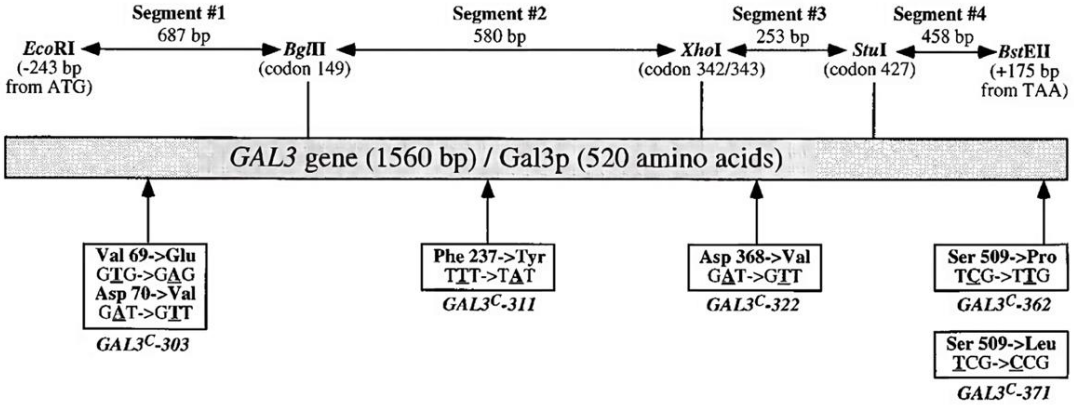

Figure 31. Schematic representation of the Gal3 gene and mutations for constitutive activity. Gal3 gene along with its nucleotide length and locations of key restriction enzyme sites used in molecular cloning. Specific mutations introduced into the Gal3 gene are highlighted, showing changes in amino acid sequences at positions 69, 237, 368, and 509. Each mutation is labelled with its respective Gal3 variant nomenclature (e.g., Gal3C.303, Gal3C.311). These engineered alterations are aimed at creating a constitutively active protein variant. Figure adapted from (Blank et al., 1997).

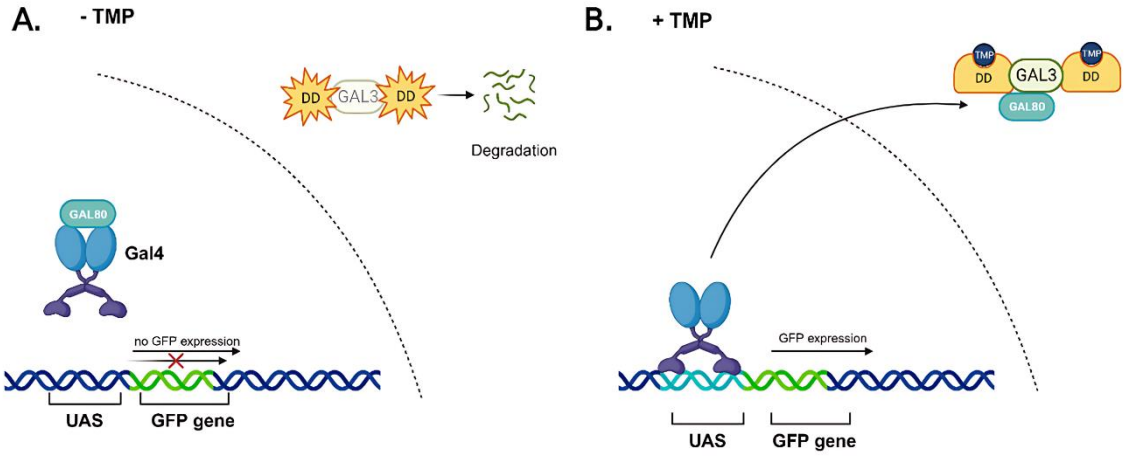

Figure 32. Conditional gene expression regulation via the Gal3c-DD System. **A**. **In the absence of TMP,** DDs target the Gal3 protein for degradation, preventing Gal4 from initiating GFP gene expression due to inhibition by Gal80. **B. When TMP is present,** TMP binds to the DDs, stabilising the Gal3 protein, which in turn releases Gal4 from Gal80 inhibition, activating GFP gene expression through the UAS. *Illustration created with BioRender.com.*

1.4. Aim

The primary objective of this thesis chapter is to evaluate the safety and efficiency of trimethoprim (TMP) in *the midgut of Drosophila melanogaster*. We intend to establish TMP's potential as a stabilising ligand for the proposed system targeting the constitutively active Gal3 protein.

2 Methods

2.1. Fly stocks, food preparation, and drug supplementation

w^{1118} flies (BDSC #5905) were used in the developmental survival and fertility experiments. Flies were kept at 25°C on standard *Drosophila* food supplemented (just before being aliquoted into vials/bottles/plates) with TMP (Sigma T7883).

For the preparation of the TMP stock solution, 2.903 g of TMP was dissolved in 30 ml ethanol to yield a 0.3 M stock solution. For the drug supplementation, TMP was first dissolved in ethanol. However, TMP did not dissolve completely in ethanol and formed a whitish suspension. To remedy this, we kept stirring the TMP-ethanol suspension until the food was dispensed. At this juncture, the TMP dissolved more efficiently into the larger volume of food medium. Control media were also prepared, with the addition of an equivalent volume of ethanol, to ensure a basis for comparison. Following this, adult *Drosophila* were reared on this TMP-supplemented food for the entire duration of their life or survival study. Three different concentrations of TMP were used for the experiments: 0.1 mM, 1 mM, and 10 mM.

2.2. Lifespan assay and statistical analysis

All cohorts were age-synchronised (purped) as in (Clancy & Kennington, 2001; Linford et al., 2013). Upon eclosion, adults were transferred to fresh media and allowed to mate for 48 hours, followed by deposition within the MultiFlipper housing rack. The MultiFlipper is a specialised system devised as an efficient alternative to the traditional manual transfer process of *Drosophila*. This innovation combines 3D-printed physical componen^{ts} with user-friendly software, which is compatible across various operating systems and is designed to operate as a standalone application. I^{ts} ergonomic design was verified for ease of use, with participan^{ts} in the trial able to operate the MultiFlipper correctly after only brief instructions (Trinca, 2022).

Adult flies were raised on a defined medium with 0–10 mM TMP from eclosion to death. Each experimental group contained 10 *Drosophila* of either sex, which were transferred to fresh media using the MultiFlipper 2-3 times weekly. During each transfer deaths/carried over/censored were recorded using experiment-specific data acquisition sheets compliant with the Lifespan Analyser's input requirements. These data sheets were digitised using a Python (v3.6) script, executed within the PyCharm IDE and Jupyter notebook (Trinca, 2022).

Lifespan survival datasets were visualised with Kaplan-Meier (KM) plots. All datasets underwent log-rank testing and Cox Proportional hazard (CoxPH) modelling using the R package Survminer.

When multiple variables were under study, as well as potential interactions, only CoxPH modelling was performed. CoxPH modelling relies on the assumption that hazard risk is proportional, i.e. independent of time; Schoenfeld residuals test was used to check this assumption (Bradburn et al., 2003). CoxPH models were visualised with forest plots using the R Survminer package. For each independent variable, the significance (p-value) and hazard ratio (HR) were reported. HR can be described as a comparison of the probabilities of events (deaths) between experimental groups (Clark et al., 2003). For example, an HR of 0.75 would mean a 25% lower risk of death.

2.3. Female fertility assay

Flies were collected within 24 hours of eclosion and allowed to age for 3-5 days with yeast paste. An equal combination of males and females (20 in total) was then placed on TMP-dosed or control media for 5 days, during which they mated.

Virgin female offspring from both TMP and control groups were collected, aged for a further 3-5 days, and then mated with naive males on TMP-free media for 48 hours. Post-mating, these females were relocated to cages equipped with a juice-agar plate. Plates containing yeast paste, specifically formulated for embryo collection, were attached to the bottom of the plastic laying pots. Over the next 24 hours, they laid eggs on these plates. The plates were replaced daily for 6 days, and the number of eggs laid and those hatching into larvae were counted for each 24-hour interval.

Data were subjected to a normality check using the Shapiro-Wilks test, followed by statistical analysis with the Student's T-test. The dataset for eggs laid was non-normally distributed. Therefore, the non-parametric Kruskal-Wallis test was performed which does not assume normal distribution.

Egg hatching rate was normally distributed data, and an ANOVA test was used.

2.4. Dissection and immunofluerence imaging

UAS-GFP-DD/Su(H)-Gal4 female flies, aged to 5 days post-mating, were then maintained for an additional 48 hours on TMP-containing medium. Post ageing, these flies were anesthetised using CO2 and dissected under a Nikon SMZ-2B microscope. Following standard protocol, intestines were extracted and fixed in 4% PFA in PBS for 15 minutes. The PBS was then replaced with mounting media composed of 85% glycerol and 2.5% propyl gallate. The prepared samples were transferred onto glass slides and covered with siliconised coverslips.

Imaging of GFP expression was conducted using an Olympus BX50 inverted epifluorescence microscope equipped with GFP-specific filters (excitation at 488 nm). Optimal microscope settings for GFP fluorescence imaging, including exposure time, gain, and image resolution.

3 Results

3.1. TMP allows robust GFP expression in the midgut of UAS-GFP-DD transgenic flies after 48-hour treatment.

The ecDHFR-derived destabilising domain (DD) has proven to be a valuable tool in various biological studies, including those involving the model organism *Drosophila melanogaster* (Kogenaru & Isalan, 2018; Sethi & Wang, 2017).

Although the ecDHFR-DD has been effectively used in *Drosophila* research to regulate protein stability in neurons, its application within the midgut remains untested.

To address this gap, we aimed to investigate the efficacy of the ecDHFR-derived destabilising domain (DD) in controlling GFP expression levels, specifically in the enteroblasts of the midgut.

We used UAS-GFP-DD transgenic flies and the gut-specific Su(H)-Gal4 driver to drive GFP-DD expression in the EBs of adult flies. Following a 48-hour treatment with 1 mM TMP, we observed a significant increase in GFP fluorescence within the midgut, particularly within the nuclei of these cells (**Figure 33B**). This observation contrasts with the control group, which did not receive TMP treatment and exhibited non-detectable GFP expression (**Figure 33A**).

The presence of a strong GFP signal in **Figure 33B** is indicative of the successful induction of GFP expression via the ecDHFR-derived destabilising domain (DD) in the *Drosophila* adult midgut.

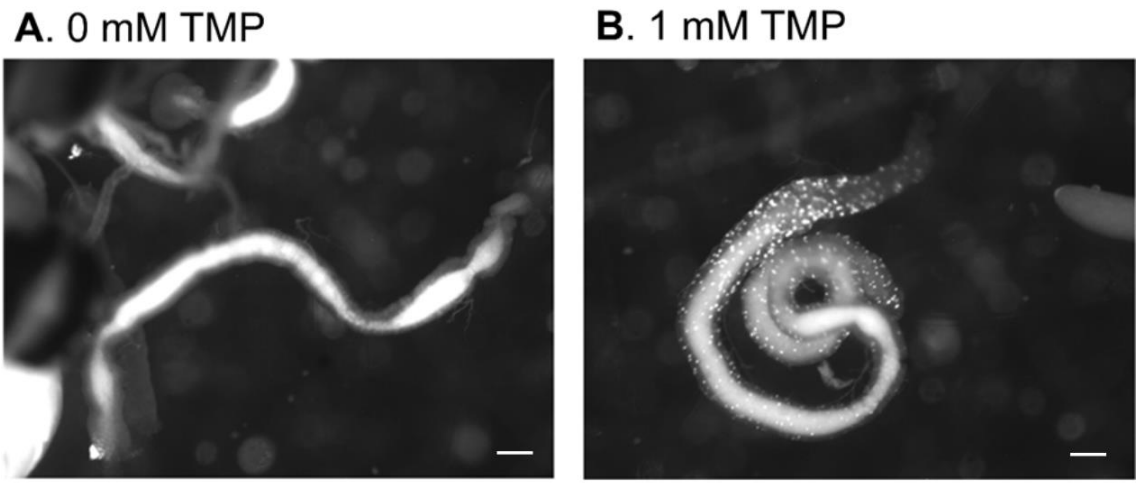

Figure 33. Enhanced GFP expression in the midgut of UAS-GFP-DD transgenic flies following 48-hour 1 mM TMP treatment. A. Control (0 mM TMP): midgut of a fly without TMP treatment. Baseline GFP expression levels are visible in the enteroblasts due to the specificity of the Su(H)-Gal4 driver. **B. Treatment (1 mM TMP):** midgut of a fly treated with 1 mM TMP for 48 hours. Enhanced GFP expression in the enteroblasts indicates the activation of the GFP-DD fusion protein by the Su(H)-Gal4 driver. Ingested food in the midgut lumen exhibited autofluorescence. Scale bar is 200 μm.

3.2. No significant effect of TMP on egg production in female flies

Our research aims to develop and employ the ecDHFR-derived DD system for studying midgut turnover, specifically in mated female *Drosophila*. Given the fertility issues with gene regulation systems like GeneSwitch, using RU486 (Tower et al., 2017), and the temperature-sensitive Gal80ts system (Maurya et al., 2021), we want to determine if the DD system, especially its TMP ligand, could affect female reproductive health.

To evaluate the potential impact of TMP on female fertility, we administered varying concentrations of TMP (0 to 10 mM) to adult, mated w^{1118} female flies over 48 hours.

Initial analysis of the total egg count revealed no statistically significant differences among the treatment groups (**Figure 34A**).

A more comprehensive analysis of egg production trends over 6 days revealed intriguing insights (**Figure 34B**). When flies were fed TMP concentrations of 0.1 mM and 10 mM, distinct trends in egg production were observed, deviating from the control group. Notably, egg production significantly differed at 10 mM TMP while remaining consistent at 0.1 mM TMP. However, there were no significant differences in egg production when the TMP concentration was 1 mM.

On the second day of the experiment (**Figure 34C**), results did not reveal any statistically significant variations (p-value = 0.1835), although noticeable differences were observed, particularly at 10 mM TMP. The egg production reduction for each treatment was 19.2 % for 0.1 mM TMP, 14.1 % for 1 mM TMP, and a substantial 50.4 % reduction for 10 mM TMP.

Similar to day 2, there were no statistically significant variations when comparing egg production on day 3 (p-value = 0.4803) (**Figure 34D**). Still, there were differences in average egg production among the treatment groups on day 3. The reduction in egg production compared to the control group for each treatment was 33.9 % for 0.1 mM TMP, 35.3 % for 1 mM TMP, and 41.4 % for 10 mM TMP.

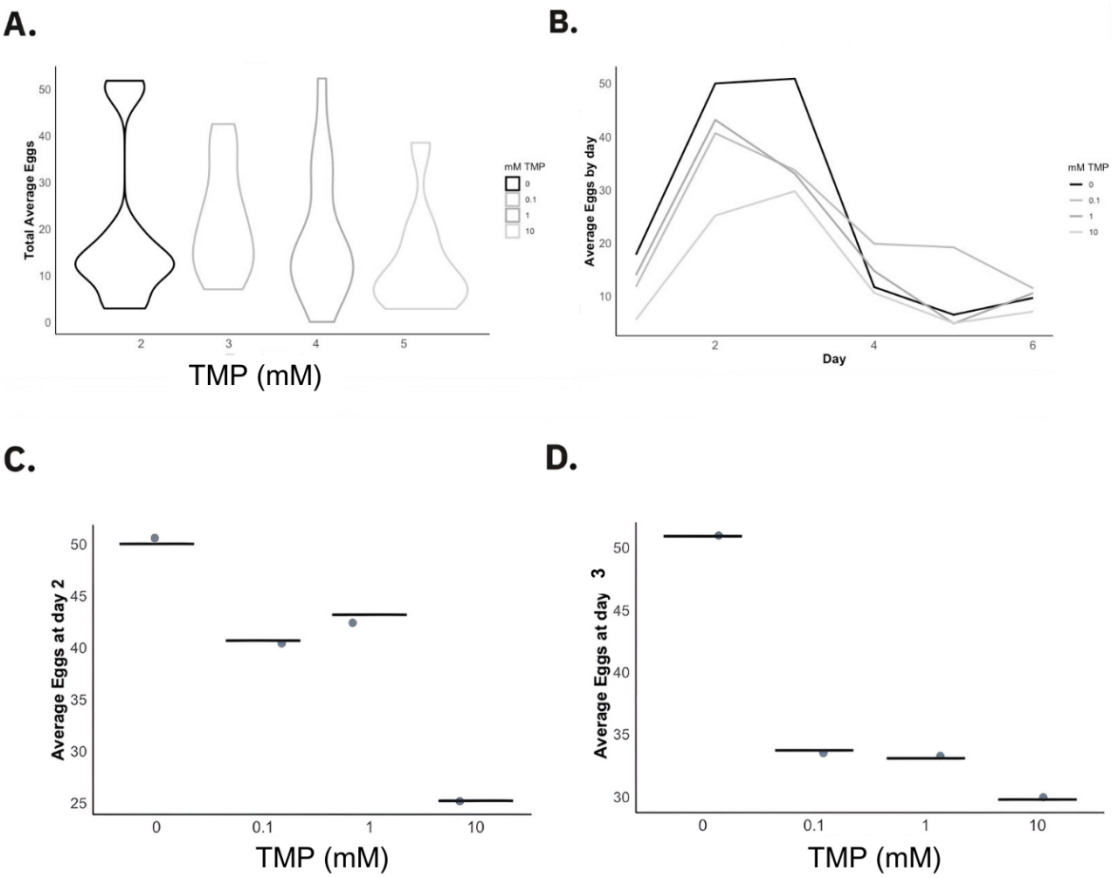

Figure 34. Fertility analysis of TMP-treated adult female *Drosophila*. A. Average egg production comparison: Violin plot showing overall egg production across different TMP treatment[ts] (0, 0.1, 1, and 10 mM), with no significant differences (p-value = 0.05771). **B. Egg production trend:** Line plot tracking the daily egg production per treatment over 6 days, revealing temporal fertility patterns. **C. Egg production on Day 2:** Jitter plot detailing average egg production on the second day for each TMP treatment, with no significant differences found (p-value = 0.1835). **D. Egg production on Day 3:** Jitter plot for average egg production on the third day, showing no significant differences across treatment groups (p-value = 0.4803). Statistical analysis was conducted using Kruskal-Wallis tests.

3.3. Reduced hatching rate of eggs laid by TMP-fed female flies

To evaluate fertility, the egg-laying capacity must be compared with the survival rate of the eggs in the larvae (hatching rate).

Hatching rate was determined to be significantly different (p-value = 0.0326) between the different concentrations of TMP and the control cohort at the peak of female fertility, days 2 and 3, after 48h of feeding.

On day 2, the results showed a significant impairment in the hatching rate at 0.1 mM TMP (p-value = 0.0285) and 1 mM TMP (p-value = 0.0131). Specifically, on day 2, the average hatching rate at 0.1 mM TMP was 37 %, and at 1 mM TMP, it was 30 %. In comparison, the control group at 0 mM had an average hatching rate of 54 % (**Figure 35A**).

Despite the lower number of eggs collected, no significant difference in hatching rates is seen at the highest concentration of 10 mM compared to the control group (p-value = 0.5978). At 10 mM TMP, the hatching rate was 51 %, while the control group had an average hatching rate of 54 % (**Figure 35A**).

On day 3, we observed no statistically significant differences in the hatching rate. The average hatching rate for the control group (0 mM) on day 3 was 58 %. When compared to this control group, the treatment with 0.1 mM TMP exhibited a hatching rate of 60 %. The 1 mM TMP treatment displayed a hatching rate of 64 %. In comparison, the treatment with 10 mM TMP had a lower hatching rate of 42 %, suggesting a decrease in hatching when compared to the control, although not statistically significant (**Figure 35B**).

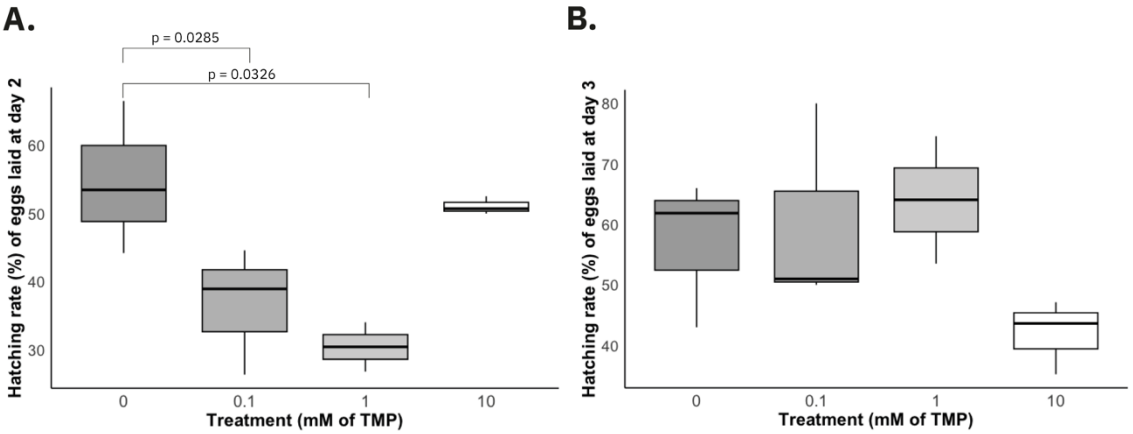

Figure 35. Hatching rate analysis of TMP-fed female flies on eggs laid on days 2 and 3. A. Day 2 hatching rates: Boxplot illustrating the significant differences in egg hatching rates on day 2 after 48 hours of TMP treatment (0, 0.1, 1, and 10 mM). There is a notable decrease in hatching rates at 0.1 mM ($p = 0.0285$) and 1 mM ($p = 0.0131$) TMP concentrations compared to the control (0 mM). **B. Day 3 hatching rates:** Boxplot showing the hatching rates on day 3. No significant differences were detected among any of the treatment groups. Statistical analysis was conducted using an ANOVA test.

3.4. TMP feeding causes minimal impact on *Drosophila* survival

Survival analysis, a crucial component of our study, investigated the broader biological implications of TMP exposure in *Drosophila*. Previous research has indicated indirect impacts on survival with other gene expression systems, notably GeneSwitch, which employs RU486.

The impact of auxins, crucial for the AID system, on *Drosophila* survival remains debated. Research from the lab has shown that different auxins have varied effects on *Drosophila* lifespan. While IAA had no significant impact on lifespan at high doses (10 mM), continuous NAA exposure substantially reduced longevity, increasing the risk of early death by 1.8 times compared to controls (Trinca, 2022).

The effect of various dosages of TMP (ranging from 0 mM to 10 mM) on the lifespan of adult w^{1118} *Drosophila* for both sexes was examined (**Figure 36A-B**). A Cox proportional hazards (CoxPH) model was constructed to evaluate TMP's effect on survival in flies, incorporating 'Treatment,' 'Sex,' and their interaction as explanatory variables. Since the interaction between sex and treatment was not statistically significant (p-value = 0.5), it was excluded from the final model for cleaner results.

As seen in **Figure 36C**, in the CoxPH model, the variable 'Treatment,' indicating flies fed with TMP at concentrations of 0 mM, 0.1 mM, 1 mM, and 10 mM, emerged as a significant determinant of survival. The hazard ratio (HR) for 'Treatment' was 0.97 (95% CI: 0.95, 0.99), with a p-value of 0.013, suggesting a slight but significant effect on survival (**Figure 36C**).

We observed a trend where males had a higher HR of 1.17 (95 % CI: 1.00, 1.37) compared to females, although this difference was not statistically significant (p = 0.052) (**Figure 36C**).

The test for the proportional hazards assumption confirmed the model's robustness, indicating that neither the treatment (p-value = 0.194), sex (p-value = 0.051), nor their interaction (p-value = 0.051) violated the proportional hazards assumption, implying consistent hazard ratios over time.

Further analysis by sex (**Figure 37A-B**) revealed that TMP treatment did not significantly affect survival in male flies (p-value = 0.2) (**Figure 37A, C**). The HR for the various TMP concentrations in males was 0.98 (95% CI: 0.95, 1.01), indicating no substantial difference in the hazard of death between treated and control

groups. Conversely, TMP treatment had a statistically significant effect on female flies' survival (p-value = 0.022). The HR for females was 0.97 (95% CI: 0.94, 1.00), suggesting that TMP exposure reduced the hazard of death by 3% compared to controls, though this effect was minimal (**Figure 37B, D**).

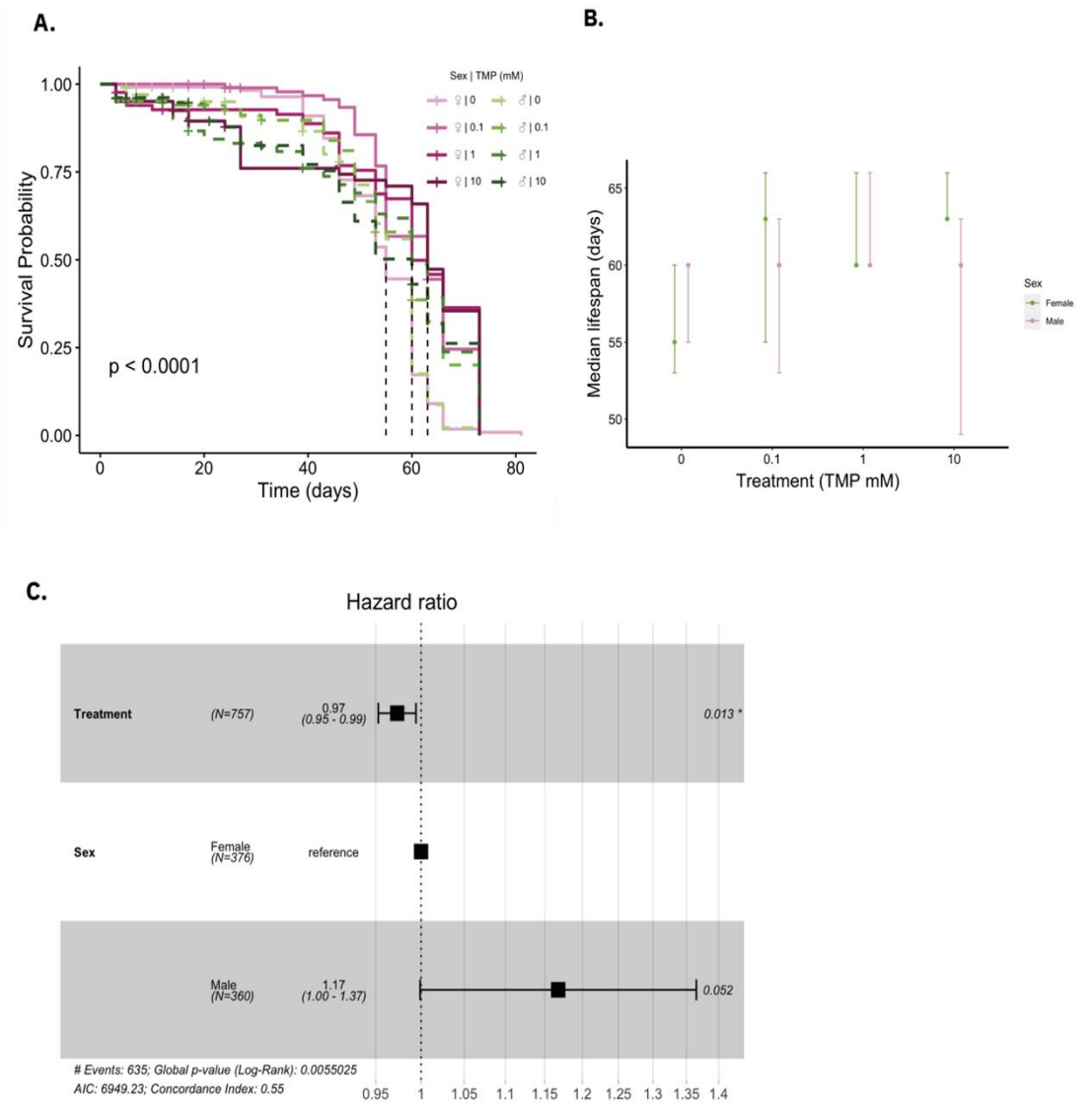

Figure 36. Impact of trimethoprim (TMP) on *Drosophila melanogaster* survival. A. Survival probability over time: Kaplan-Meier survival curves for combined sexes, with each line representing a different TMP concentration (0, 0.1, 1, and 10 mM). **B. Median lifespan:** Bar graph showing duration from each technical replicate (vial) is presented for various TMP dosages, separately for females and males. Error bars represent the 95% Confidence Interval (CI). The dataset comprises N = 800 individuals, with 100 flies in each arm**. C. Risk analysis by treatment and sex:** Cox Proportional Hazards model showing hazard ratios for TMP treatmen[ts], with sex as a covariate.

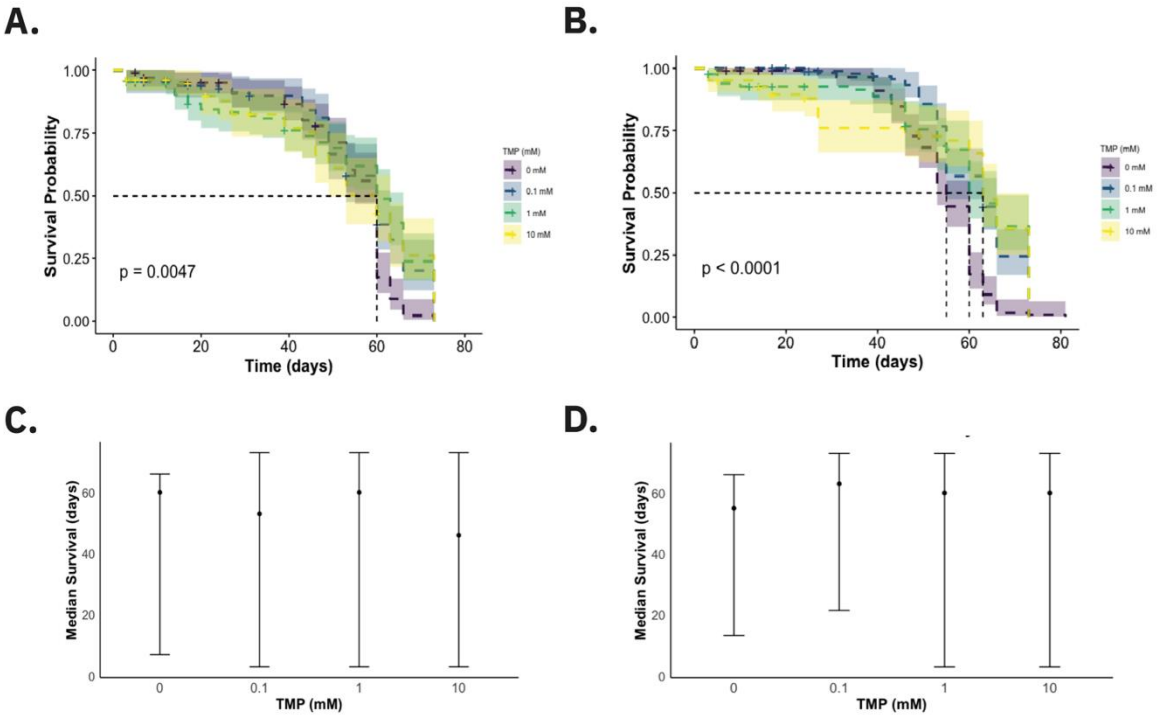

Figure 37. Survival analysis of *w*^{1118} *Drosophila* by sex in response to TMP feeding. A. Male survival probability: Kaplan-Meier survival curve for male flies exposed to varying TMP concentrations (0, 0.1, 1, and 10 mM), with the shaded area representing the 95% Confidence Interval (CI) and dashed lines indicating median survival times. **B. Female survival probability:** Kaplan-Meier survival curve for female flies exposed to the same TMP concentrations, with shaded areas and dashed lines as in A**. C. Male median survival:** Scatter plot showing the median survival days for males at each TMP concentration, error bars representing 95% CI**. D. Female median survival:** Scatter plot showing the median survival days for females at each TMP concentration, error bars representing 95% CI. Statistical significance determined by log-rank test.

4 Discussion

4.1. Effectiveness of the DD system in the *Drosophila* midgut

Destabilising domains (DDs) and trimethoprim (TMP) are recognised as valuable tools for regulating protein abundance and controlling gene expression.

In *Drosophila*, DDs technology has demonstrated the ability to regulate gene expression levels with a low background and a wide dynamic range, allowing for reversible modulation without detectable side effects (Sethi & Wang, 2017)

These domains can be fused to target proteins, making them unstable and targeting them for degradation unless a particular ligand stabilises them (Huang et al., 2018). TMP, a commonly used antibiotic, can act as a stabilising ligand for DDs (Peng et al., 2019). When TMP is present, it binds to the DD-fused protein and stops it from degradation.

Although DDs have shown promise in regulating protein abundance across diverse organisms, the *Drosophila* midgut has been relatively underexplored in this context.

Our investigation aimed to assess the efficacy of the ecDHFR-derived DD in regulating the level of GFP expression within the midgut of adult *Drosophila*.

Strong GFP expression was observed throughout the endoblast of *Drosophila* melanogaster flies' midgut when subjected to a 48-hour treatment with a 1 mM concentration of TMP (**Figure 34**). These findings indicate that the DD is a valuable tool for precise control of GFP expression in the *Drosophila* midgut.

However, to encourage its broad adoption, we aimed to assess its impact on *Drosophila* survival and fertility for safety considerations.

To determine its biological effects, we exposed adult flies to TMP concentrations from 0 to 10 mM.

Our findings revealed no significant differences in egg production or female fertility, consistent with the findings of Sethi & Wang (2017) (**Figure 35**).

However, we did observe notable differences in egg-hatching rates among various TMP concentrations and a control group on days 2 and 3 after 48 hours of TMP exposure. On day 2, hatching rates were significantly lower at 0.1 mM TMP and 1 mM TMP compared to the control group. Interestingly, there was no significant difference in hatching rates at 10 mM TMP. On day 3, there were no statistically

significant variations in hatching rates, but 10 mM TMP exhibited a lower hatching rate compared to the control (**Figure 36**).

While consistent egg production suggested that TMP did not negatively impact female fertility, the decrease in hatching rates on day 2 could potentially limit the availability of flies for future generations or experiments. This decrease might also pose challenges for interpreting experimental results, particularly in mating behaviour and reproductive fitness studies.

Nevertheless, our assessment of hatching rates was limited to days 2 and 3, the peak of the egg production (**Figure 36**). Hatching rates in *Drosophila* can vary due to various factors and might peak later than in the control group, similar to overall egg production (**Figure 35**).

Previous research has reported emergence rates ranging from 70% to 90% for *Drosophila melanogaster* (Church & Robertson, 1966; Reaume & Sokolowski, 2006). In this scenario, the hatching rate for the remainder of the 6 days could increase to compensate for the overall hatching rates, which did not reach those values in the control group. This may suggest that the overall hatching rate may not have exhibited a significant difference.

We further demonstrated that TMP has a minimal effect on survival in *Drosophila* melanogaster, with an HR close to 1, indicating little difference in survival odds between treated and control groups for both females and males.

TMP had no statistically significant effect on male flies, whereas in female flies, it resulted in a 3% lower hazard of experiencing the event compared to the control group. However, this effect is considered minimal as the HR is very close to 1, suggesting no substantial impact on survival. This aligns with literature indicating that antibiotics could enhance female reproductive potential. For instance, findings demonstrate that mifepristone can extend the lifespan of mated female *Drosophila* without evident antibacterial activity (Landis et al., 2015). Supporting this, research shows that lifespan can be increased through microbial removal via antibiotics without harmful consequences (Lee et al., 2019).

Although minimal, the observation of an effect on survival in mated female flies after TMP feeding stands in contrast to the findings reported by Sethi & Wang (2017), necessitating a careful evaluation of the statistical methodologies applied in our and their survival study.

We employed a Cox proportional hazards model, whereas, in the study conducted by Sethi & Wang, the authors Utilised the log-rank statistic, which is associated with certain limitations. It does not work within Bayesian statistical methods, which are essential for incorporating prior knowledge into analysis. Additionally, the log-rank test is limited to fixed categories and cannot properly analyse variables that change in value, like the TMP exposure in our study (Gu et al., 2023).

Methodological differences could account for the discrepancy in findings, as the CoxPH seems more appropriate for our kind of analysis and more sensitive to very small differences between groups.

4.2. Possible limitations of TMP using

While TMP has been a valuable tool in controlling protein stability, several limitations and challenges must be considered.

As previously stated, feeding antibiotics has been shown to significantly increase the lifespan of mated female flies, which can affect the consistency and reproducibility of experimental outcomes. Antibiotics also reduce both commensal and pathogenic bacterial populations in the flies and their food (Lee et al., 2019).

However, some bacterial strains may offer resistance, mitigating the expected widespread changes to the Drosophila gut microbiota from antibiotic use. For instance, *Acetobacter* and *Komagataeibacter* are resistant to TMP (Cepec & Trček, 2022). Additionally, *Lactobacillus* spp. might show decreased susceptibility to TMP due to a variant of the enzyme dihydrofolate reductase (Danielsen & Wind, 2003).

Thus, using TMP in *Drosophila* feed may not lead to the drastic microbial changes typically seen with antibiotics. This would be particularly beneficial when using TMP as a ligand for gene expression control in *Drosophila*, suggesting its application may have a minimal disruptive impact on microbiota-dependent physiological processes.

4.3. Future directions:

4.3.1. TMP activation and degradation kinetics

Future directions include the exploration of activation and degradation kinetics of TMP within the *Drosophila* gut.

Activation kinetics will involve investigating the speed at which the DD fusion protein becomes stabilised upon the introduction of TMP. This aspect of our research aims to uncover the dynamics of TMP binding to the DD-fused protein and the subsequent modulation of gene expression levels.

Conversely, degradation kinetics experiments will be conducted to elucidate the rate at which the DD fusion protein is naturally degraded in the absence of the stabilising ligand TMP. Establishing the baseline expression level of GFP in the absence of TMP is essential for distinguishing between genuine gene expression and background expression caused by factors such as leaky expression or incomplete degradation of the DD fusion protein.

4.3.2. Gal3c-DD proposal

Considering the promising potential of TMP as a ligand in the Gal3c-DD system, we propose further development of the Gal3c-DD system with several critical steps ahead.

Building on prior research that identified mutations in Gal3 proteins affecting Gal80p binding and thereby altering transcription levels in yeast (Blank et al., 1997), we aim to adapt these findings to the *Drosophila* model.

In our lab, we have tried to replicate yeast-specific mutations in *Drosophila*'s Gal3, ranging from complex quadruple mutations to simpler single ones. So far, we have not seen the expected results, but these attempts are the next step towards fine-tuning our method to accurately control gene expression in the *Drosophila* midgut.

CHAPTER 6: CONCLUSIONS

1 *Drosophila* ISCs exhibit pulsed turnover following heat shock, supporting the quiescence-division switch model

The traditional neutral competition model is founded on the assumption of a constant rate of cell division for intestinal stem cells. However, recent evidence indicates a more intricate framework in which regions with both slow and fast turnover can coexist. This challenges the assumption underlying the neutral competition mathematical model, which posits a uniform rate of turnover shared among all ISCs.

We introduce a novel model, the quiescence-division switch model, as an alternative for the replacement of intestinal tissue in the adult *Drosophila* midgut. This model, unlike the traditional neutral competition model, suggests that the division rate remains constant within the stem cell compartment but can vary between compartments.

This model suggests that in homeostasis, intestinal stem cells can be either in quiescence ($\lambda \approx 0$) or actively dividing ($\lambda > 0$). This concept is not accounted for in the neutral competition model, which assumes a constant turnover rate. However, it is addressed by the quiescence-division switch model, which explains the coexistence of regions with slow and fast turnover in the same intestinal tissue.

Our model raises the question of what causes the switch from quiescence to division. Lineage-tracing experiments conducted at different induction temperatures, showing different turnover rates (de Navascués et al., 2012; Jiang et al., 2009) suggest that temperature could be a possible trigger. The 37°C heat shock used in de Navascués et al. (2012) experiment, showing a faster turnover rate, could indicate that this higher temperature could be activating a switch in ISCs from quiescence to division.

Our immunofluorescence experiments provide evidence for the quiescence-division switch model, showing that heat stress triggers a faster turnover rate. Following a heat shock at 37ºC, our research demonstrates that intestinal stem cells increase their mitotic activity while maintaining the same cell density. The distinct pattern of cell division activity, characterised by a wave-like increase and subsequent return to baseline, aligns with the model's proposal of two distinct homeostatic states and transitions between them following stress. We have termed this pattern "pulsed-

turnover." Similar mitotic waves have been observed in other systems, such as the coordinated waves of cell division during *Drosophila* embryonic development driven by Cdk1 activity (Deneke et al., 2016; Hayden et al., 2022). These waves play a crucial role in proper development and tissue organisation. Mitotic waves are also documented in other species, such as during *Xenopus* embryo cleavage (Chang & Ferrell, 2013).

Despite the findings that support the quiescence-division switch model, our current approach has some limitations. Although we observed increased levels of mitotic markers such as cyclin A and phosphohistone H3 (PH3), indicating cell division, we did not observe the expected rise in other markers such as polo-like kinase 1 (PLK1), a marker of mitosis, and proliferating cell nuclear antigen (PCNA), which is associated with DNA replication during the S-phase. One possible explanation could be the presence of redundant cell cycle regulatory mechanisms, which is a well-documented phenomenon in eukaryotes (Basu et al., 2022; Gérard et al., 2012).

Furthermore, we did not observe an increase in caspase 3. Despite keeping cell density unchanged, we would have anticipated an increase in apoptosis coupled with the observed increase in stem cell proliferation.

Future studies could address these limitations and explore the possibility of redundancy by incorporating additional analyses. One possible approach could be to employ TUNEL assays, which detect DNA fragmentation, a hallmark of various cell death pathways not necessarily captured by caspase-3 expression alone. Additionally, visualising FUCCI cell cycle reporters would be valuable (Zielke et al., 2014; Zielke & Edgar, 2015). These fluorescent reporters visualise different cell cycle phases in living tissues, potentially clarifying discrepancies between markers like cyclin A and the absence of a corresponding increase in PLK1 or PCNA. Finally, combining live imaging with EdU incorporation could provide real-time cell division monitoring and identification of newly formed cells, offering valuable insights into ISC reactivation dynamics (Daul et al., 2010; Martin et al., 2018).

2 WGCNA reveals distinct responses in enterocytes and possible progenitor cells following heat shock in the *Drosophila* midgut

We conducted RNA-seq analyses to elucidate the transcriptional changes underlying the observed protein expression patterns. Our initial differential gene expression analysis did not yield significant results. However, when applying less stringent criteria, we identified a dozen differentially expressed genes under certain conditions. Although initially surprising, this finding may support the quiescence-division switch model rather than indicating a strong regenerative response. The heat shock response appears to involve subtle changes in gene expression, aligning with the model's premise of a homeostatic switch between quiescence and division, which may not be captured by standard differential expression analysis, which detects more pronounced changes, for example, those seen in regenerative response.

We employed Weighted Gene Co-expression Network Analysis (WGCNA) to gain deeper insights into the data. WGCNA constructs co-expression networks based on correlations between genes and identifies modules of highly correlated genes. This analytical approach revealed three distinct modules (blue, black and brown) following heat shock, which were mapped to two cell populations according to the *Drosophila* midgut single-cell RNA-seq dataset: enterocytes and an unannotated Cluster 39.

Modules blue and black encompass genes primarily expressed in enterocytes, the differentiated intestinal cells responsible for nutrient absorption. This module displayed genes' downregulation in metabolism and developmental processes (e.g., *syb*, *nd-acp*, *metallothionein A*). This coordinated downregulation suggests a well-documented strategy of conserving energy during stress, a response observed across diverse organisms (Cristodero et al., 2021; Khoutorsky et al., 2016; Riahi et al., 2019).

The brown module also provided insights into the response of another cell population, which likely represents progenitor cells within the intestinal epithelium and maps to the unannotated Cluster 39. This module exhibited a marked upregulation of genes involved in cell cycle regulation, particularly in mitosis. This increase in genes involved in mitosis (*klp67A*, *klp61F*, *polα2*, *pbl*, *cdks*, *cyclins*) supports the notion that these cells could be an uncharacterised population of

progenitor cells that actively divide in response to heat shock, potentially contributing to the observed pulsed turnover.

We also observed the upregulation of genes related to stress response (*hsp26*, *hsp27*, *mu2*) and DNA repair (*cort*, *rrp1*). Additionally, the observed upregulation of genes traditionally associated with reproductive processes (*nanos*, *png*, *otu*, *ovo*, *bam*, *spn-E*, *qua*) is intriguing, although many of these genes are also involved in cell regulation. This shift in cellular priorities towards cell cycle progression under heat shock might be a homeostatic response to ensure cell division and tissue integrity, aligning with the "pulsed turnover" dynamic.

The results from WGCNA could provide valuable insights into a limitation of our current model, namely the lack of attention to the quiescence aspect of the quiescence-division switch. This gap exists due to the absence of established markers for quiescent stem cells or their reactivation in the Drosophila midgut. However, Cluster 39 within the module exhibits characteristics that may be linked to the reactivation of ISC states.

In this context, the upregulation of the *Setd8* gene in the cluster is particularly noteworthy. This gene is responsible for encoding a histone methyltransferase and is being considered as a potential marker for the reactivation of neural stem cells (Huang, Gujar, et al., 2021). Although its role in the *Drosophila* midgut is not yet known, its increased activity in the potential progenitor cell cluster suggests that it may play a part in their reactivation during heat shock. Exploring the functional importance of *Setd8* could yield a valuable marker for the reactivation of ISC in the *Drosophila* midgut, filling a crucial gap in our current knowledge.

Nevertheless, the entire module holds promise for future studies. We propose focusing on exploring gene expression changes associated with this module by conducting an RNA-seq analysis on cells isolated via Fluorescence-Activated Cell Sorting (FACS) based on markers identified in Cluster 39. This targeted approach could provide more informative insights than a bulk RNA-seq experiment (Davie et al., 2018).

3 Threshold concentration of Da:Sc bHLH factors dimerisation trigger enteroendocrine differentiation of ISCs

It is important to understand how specialised cells differentiate, beyond how stem cells proliferate, in order to maintain homeostasis. Therefore, we have also studied the role of bHLH transcription factors in controlling this differentiation. These factors are crucial for maintaining the balance between stem cell self-renewal and differentiation, which is essential for normal tissue function.

Given their well-established importance, we have focused on examining the role of bHLH Daughterless (Da) and Scute (Sc) in directing ISC differentiation towards the enteroendocrine lineage by forming heterodimers.

Previous studies (Puig Barbe, 2018; Puig-Barbe et al., 2023) have shown that Da: Sc heterodimers play a critical role in initiating pre-entroendocrine (pre-EE) cell formation and maintaining intestinal stem cells in an undifferentiated state. On the other hand, Da: Da homodimers are responsible for inhibiting EE cell formation. The research aims to understand how the balance between Da: Da and Da: Sc dimers is modulated within cells, leading to a shift from maintaining ISC renewal to promoting differentiation. Two scenarios are proposed: the "Sc Threshold Scenario," based on Da: Sc dimer concentration triggering EE differentiation, and the "Da Titration Scenario," focusing on the ratio of Da: Sc to Da: Da dimers in promoting EE cell differentiation.

Our findings support the Sc Threshold scenario, suggesting a critical balance for differentiation initiation. We observed that a minimum concentration of Da:Sc heterodimers is necessary for ISCs to commit to the pre-EE cell fate. We particularly observed a significant increase in pre-EE cells following Scute expression, regardless of Da copy number. This suggests a critical threshold for the Da:Sc complex to initiate differentiation, acting as a gatekeeper for this transition.

The importance of bHLH factors extends far beyond the *Drosophila* midgut. The formation of bHLH dimers is a conserved mechanism observed in other *Drosophila* tissues and organisms, regulating cell fate determination and differentiation (Fan et al., 2019; X. Li et al., 2017; Mikheeva et al., 2024).

4 TMP is a safe and versatile ligand for use with destabilising domain gene expression systems in the *Drosophila* midgut

Throughout our experiments, heat shock has been consistently present. We used heat shock as a trigger for the quiescence-division switch in our investigation of the quiescence-division switch model. Similarly, we employed heat shock as a genetic tool for Scute gene expression in our study of the differentiation pathway into enteroendocrine cells. Although the HS-Gal4, UAS-Target gene system is a well-established method in *Drosophila*, it has limitations for further exploring the homeostatic model in the intestine. In our case, temperature itself is a confounding variable.

The limitations of heat shock, particularly its potential to introduce confounding variables due to temperature fluctuations, highlight the need for more precise and versatile gene expression control systems in *Drosophila* research. However, this need extends beyond overcoming the shortcomings of heat shock. *Drosophila* researchers are driven to explore new binary gene expression systems that enhance their ability to investigate gene regulation and function, pushing the boundaries of existing methods. Existing systems like GAL4-UAS, LexA/LexAop, and QF/QUAS have undoubtedly expanded the versatility of genetic analyses in *Drosophila*. However, a significant limitation remains – the need to generate multiple collections of transgenic fly strains for each system. This impedes their broader experimental application. While novel systems like LexA/LexAop offer promising advancements in areas like metabolism, development, and neurobiology, they may not be universally applicable.

In response to these limitations, we proposed the Gal3c-DD system. By fusing a Gal3 constitutively active variant with destabilising domains from the ecDHFR enzyme and stabilising it with trimethoprim (TMP), we would achieve controlled activation of genes downstream of UAS sequences. This system would be compatible with existing Gal4-UAS lines and could provide a dynamic tool for *Drosophila* gene regulation.

To advance the development of this system, which others have attempted using Gal4 and Gal80, we first tested the safety and efficacy of the exogenous molecular that would act as the driver of expression: the antibiotic trimethoprim.

Moving forward, the development of the Gal3c-DD system holds promise for enhancing our understanding of gene regulation in *Drosophila* midgut research. Initial tests confirming the safety and efficacy of the system pave the way for its further refinement. For instance, future investigations could delve into determining the optimal number of double degron units required for precise gene control. Additionally, there is a specific need for the development of the Gal3 constitutively active protein with the described mutations, which could further enhance the system's efficiency and versatility. Moreover, as TMP is an antibiotic, it prompts the necessity for experiments exploring the impact on the microbiota. If TMP, which is an antibiotic, leads to significant changes in the microbiota after 24 hours, it could pose a challenge for our system. This could potentially make TMP unsuitable as a ligand due to its impact on the microbiota, similar to how temperature can affect our system.

- Our research provides new insights into intestinal stem cell behaviour in the *Drosophila* midgut. We propose the quiescence-division switch model to refine the traditional neutral competition model. This model effectively explains the observed variations in turnover rates across ISC compartments while maintaining a constant rate within each. The key feature of this model is the homeostatic switch between quiescence and dividing states for individual stem cells, which may explain the "pulsed turnover" pattern seen after heat shock.
- Maintaining homeostasis requires not only regulating stem cell division but also ensuring proper differentiation. Our investigation into bHLH transcription factors, particularly Da and Sc, clarified their role in directing ISC differentiation towards the enteroendocrine lineage. We found that a threshold concentration of Da:Sc heterodimers is sufficient to trigger the differentiation pathway. This finding highlights the importance of specific transcriptional control mechanisms in maintaining the delicate balance within the ISC niche.
- Furthermore, to overcome limitations associated with current genetic tools like those that use an inductive heat shock, we explored TMP as a potential ligand for a new destabilisation domain system. This innovative system leverages existing Gal4 lines, offering the possibility of precise gene expression control. This approach holds promise for future studies investigating ISC behaviour and other processes in *Drosophila*.

5 REFERENCES

Afgan, E., Baker, D., Batut, B., van den Beek, M., Bouvier, D., Čech, M., Chilton, J., Clements, D., Coraor, N., Grüning, B. A., Guerler, A., Hillman-Jackson, J., Hiltemann, S., Jalili, V., Rasche, H., Soranzo, N., Goecks, J., Taylor, J., Nekrutenko, A., & Blankenberg, D. (2018). The Galaxy platform for accessible, reproducible and collaborative biomedical analyses: 2018 update. *Nucleic Acids Research*, *46*, W537-W544. https://doi.org/10.1093/nar/gky379

Aguirre, A., Rubio, M. E., & Gallo, V. (2010). Notch and EGFR pathway interaction regulates neural stem cell number and self-renewal. *Nature*, *467*(7313). https://doi.org/10.1038/nature09347

Aittokallio, T., & Schwikowski, B. (2006). Graph-based methods for analysing networks in cell biology. *Briefings in Bioinformatics*, *7*(3), 243-255. https://doi.org/10.1093/bib/bbl022

Allaire, J. M., Crowley, S. M., Law, H. T., Chang, S.-Y., Ko, H.-J., & Vallance, B. A. (2018). The Intestinal Epithelium: Central Coordinator of Mucosal Immunity. *Trends in Immunology*, *39*(9), 677-696. https://doi.org/10.1016/j.it.2018.04.002

Allen, J. D., Xie, Y., Chen, M., Girard, L., & Xiao, G. (2012). Comparing Statistical Methods for Constructing Large Scale Gene Networks. *PLOS ONE*, *7*(1). https://doi.org/10.1371/journal.pone.0029348

Althoff, F., Viktorinová, I., Kastl, J., & Lehner, C. F. (2009). *Drosophila* Cyclin J is a mitotically stable Cdk1 partner without essential functions. *Developmental Biology*, *333*(2), 263-272. https://doi.org/10.1016/j.ydbio.2009.06.042

Amcheslavsky, A., Jiang, J., & Ip, Y. T. (2009). Tissue damage-induced intestinal stem cell division in *Drosophila*. *Cell Stem Cell*, *4*(1), 49-61. https://doi.org/10.1016/j.stem.2008.10.016

Antonello, Z. A. (2017). *Mechanisms of epithelial homeostasis in adult Drosophila midgut*. [Doctoral dissertation, Universidad Miguel Hernandez] http://dspace.umh.es/handle/11000/3786

Antonello, Z., Reiff, T., Ballesta-Illan, E., & Domínguez, M. (2015). Robust intestinal homeostasis relies on cellular plasticity in enteroblasts mediated by miR-8-Escargot switch. *The EMBO Journal, 34(15), 2025-2041*. https://doi.org/10.15252/embj.201591517

Aquino Perez, C., Palek, M., Stolarova, L., von Morgen, P., & Macurek, L. (2020). Phosphorylation of PLK3 Is Controlled by Protein Phosphatase 6. *Cells*, *9*(6). https://doi.org/10.3390/cells9061506

Ariyapala, I. S., Holsopple, J. M., Popodi, E. M., Hartwick, D. G., Kahsai, L., Cook, K. R., & Sokol, N. S. (2020). Identification of Split-GAL4 Drivers and Enhancers That Allow Regional Cell Type Manipulations of the *Drosophila* melanogaster Intestine. *Genetics*, *216*(4), 891-903. https://doi.org/10.1534/genetics.120.303625

Asaoka, M., Hanyu-Nakamura, K., Nakamura, A., & Kobayashi, S. (2019). Maternal Nanos inhibits Importin-α2/Pendulin-dependent nuclear import to prevent somatic

gene expression in the *Drosophila* germline. *PLoS Genetics*, *15*(5). https://doi.org/10.1371/journal.pgen.1008090

Avila, D. B., Melendez-Alvarez, J. R., & Tian, X.-J. (2021). Control of tissue homeostasis, tumorigenesis, and degeneration by coupled bidirectional bistable switches. *PLOS Computational Biology*, *17*(11). https://doi.org/10.1371/journal.pcbi.1009606

Banaszynski, L. A., Chen, L.-C., Maynard-Smith, L. A., Ooi, A. G. L., & Wandless, T. J. (2006). A rapid, reversible, and tunable method to regulate protein function in living cells using synthetic small molecules. *Cell*, *126*(5), 995-1004. https://doi.org/10.1016/j.cell.2006.07.025

Bandura, J. L., Jiang, H., Nickerson, D. W., & Edgar, B. A. (2013). The molecular chaperone Hsp90 is required for cell cycle exit in *Drosophila* melanogaster. *PLoS Genetics*, *9*(9). https://doi.org/10.1371/journal.pgen.1003835

Bardin, A. J., Perdigoto, C. N., Southall, T. D., Brand, A. H., & Schweisguth, F. (2010). Transcriptional control of stem cell maintenance in the *Drosophila* intestine. *Development*, *137*(5), 705-714. https://doi.org/10.1242/dev.039404

Barker, N. (2014). Adult intestinal stem cells: Critical drivers of epithelial homeostasis and regeneration. *Nature Reviews Molecular Cell Biology*, *15*(1), 19-33. https://doi.org/10.1038/nrm3721

Barker, N., Bartfeld, S., & Clevers, H. (2010). Tissue-Resident Adult Stem Cell Populations of Rapidly Self-Renewing Organs. *Cell Stem Cell*, *7*(6), 656-670. https://doi.org/10.1016/j.stem.2010.11.016

Barwell, T., Geld, S., & Seroude, L. (2017). Comparison of GAL80ts and Tet-off GAL80 transgenes. *microPublication Biology*, *2023*. https://doi.org/10.17912/micropub.biology.000770

Basu, S., Greenwood, J., Jones, A. W., & Nurse, P. (2022). Core control principles of the eukaryotic cell cycle. *Nature*, *607*(7918). https://doi.org/10.1038/s41586-022-04798-8

Bayer, F. E., Zimmermann, M., Preiss, A., & Nagel, A. C. (2018). Overexpression of the *Drosophila* ATR homologous checkpoint kinase Mei-41 induces a G2/M checkpoint in *Drosophila* imaginal tissue. *Hereditas*, *155*(1), 27. https://doi.org/10.1186/s41065-018-0066-4

Bello, B., Resendez-Perez, D., & Gehring, W. J. (1998). Spatial and temporal targeting of gene expression in *Drosophila* by means of a tetracycline-dependent transactivator system. *Development*, *125*(12), 2193-2202. https://doi.org/10.1242/dev.125.12.2193

Bence, M., Jankovics, F., Lukácsovich, T., & Erdélyi, M. (2017). Combining the auxin-inducible degradation system with CRISPR/Cas9-based genome editing for the conditional depletion of endogenous *Drosophila* melanogaster proteins. *The FEBS Journal*, *284*(7), 1056-1069. https://doi.org/10.1111/febs.14042

Bertoli, C., Skotheim, J. M., & de Bruin, R. A. M. (2013). Control of cell cycle transcription during G1 and S phases. *Nature Reviews Molecular Cell Biology*, *14*(8). https://doi.org/10.1038/nrm3629

Bertrand, N., Castro, D. S., & Guillemot, F. (2002). Proneural genes and the specification of neural cell types. *Nature Reviews. Neuroscience*, *3*(7), 517-530. https://doi.org/10.1038/nrn874

Beumer, J., & Clevers, H. (2016). Regulation and plasticity of intestinal stem cells during homeostasis and regeneration. *Development*, *143*(20), 3639-3649. https://doi.org/10.1242/dev.133132

Bieschke, E. T., Wheeler, J. C., & Tower, J. (1998). Doxycycline-induced transgene expression during *Drosophila* development and aging. *Molecular & General Genetics: MGG*, *258*(6), 571-579. https://doi.org/10.1007/s004380050770

Biteau, B., Hochmuth, C. E., & Jasper, H. (2011). Maintaining tissue homeostasis: Dynamic control of somatic stem cell activity. *Cell stem cell*, *9*(5), 402-411. https://doi.org/10.1016/j.stem.2011.10.004

Biteau, B., & Jasper, H. (2011). EGF signaling regulates the proliferation of intestinal stem cells in *Drosophila*. *Development*, *138*(6), 1045-1055. https://doi.org/10.1242/dev.056671

Biteau, B., & Jasper, H. (2014). Slit/Robo Signaling Regulates Cell Fate Decisions in the Intestinal Stem Cell Lineage of *Drosophila*. *Cell Reports*, *7*(6). https://doi.org/10.1016/j.celrep.2014.05.024

Blank, T. E., Woods, M. P., Lebo, C. M., Xin, P., & Hopper, J. E. (1997). Novel Gal3 proteins showing altered Gal80p binding cause constitutive transcription of Gal4p-activated genes in Saccharomyces cerevisiae. *Molecular and Cellular Biology*, *17*(5). https://doi.org/10.1128/MCB.17.5.2566

Blank, U., Karlsson, G., & Karlsson, S. (2008). Signaling pathways governing stem-cell fate. *Blood*, *111*(2), 492-503. https://doi.org/10.1182/blood-2007-07-075168

Blanpain, C., & Fuchs, E. (2009). Epidermal homeostasis: A balancing act of stem cells in the skin. *Nature Reviews Molecular Cell Biology*, *10*(3). https://doi.org/10.1038/nrm2636

Bloomington Drosophila Stock Center. (n.d). Bloomington *Drosophila* Stock Center. Retrieved 7 de octubre de 2023, de https://bdsc.indiana.edu/

Bohin, N., Keeley, T. M., Carulli, A. J., Walker, E. M., Carlson, E. A., Gao, J., Aifantis, I., Siebel, C. W., Rajala, M. W., Myers, M. G., Jones, J. C., Brindley, C. D., Dempsey, P. J., & Samuelson, L. C. (2020). Rapid Crypt Cell Remodeling Regenerates the Intestinal Stem Cell Niche after Notch Inhibition. *Stem Cell Reports*, *15*(1), 156-170. https://doi.org/10.1016/j.stemcr.2020.05.010

Bolger, A. M., Lohse, M., & Usadel, B. (2014). Trimmomatic: A flexible trimmer for Illumina sequence data. *Bioinformatics*, *30*(15), 2114-2120. https://doi.org/10.1093/bioinformatics/btu170

Bond, D., & Foley, E. (2012). Autocrine Platelet-derived Growth Factor-Vascular Endothelial Growth Factor Receptor-related (Pvr) Pathway Activity Controls Intestinal Stem Cell Proliferation in the Adult *Drosophila* Midgut. *The Journal of Biological Chemistry*, *287*(33), 27359-27370. https://doi.org/10.1074/jbc.M112.378018

Bonfini, A., Liu, X., & Buchon, N. (2016). From pathogens to microbiota: How *Drosophila* intestinal stem cells react to gut microbes. *Developmental & Comparative Immunology*, *64*, 22-38. https://doi.org/10.1016/j.dci.2016.02.008

Brand, A. H., & Perrimon, N. (1993). Targeted gene expression as a means of altering cell fates and generating dominant phenotypes. *Development*, *118*(2), 401-415. https://doi.org/10.1242/dev.118.2.401

Buchon, N., Broderick, N. A., Kuraishi, T., & Lemaitre, B. (2010). *Drosophila*EGFR pathway coordinates stem cell proliferation and gut remodeling following infection. *BMC Biology*, *8*(1). https://doi.org/10.1186/1741-7007-8-152

Buchon, N., Broderick, N. A., Poidevin, M., Pradervand, S., & Lemaitre, B. (2009). *Drosophila* intestinal response to bacterial infection: Activation of host defense and stem cell proliferation. *Cell Host & Microbe*, *5*(2), 200-211. https://doi.org/10.1016/j.chom.2009.01.003

Buchon, N., Osman, D., David, F. P. A., Fang, H. Y., Boquete, J.-P., Deplancke, B., & Lemaitre, B. (2013). Morphological and molecular characterization of adult midgut compartmentalization in *Drosophila*. *Cell Reports*, *3*(5), 1725-1738. https://doi.org/10.1016/j.celrep.2013.04.001

Calderon-Villalobos, L. I., Tan, X., Zheng, N., & Estelle, M. (2010). Auxin Perception—Structural Insights. *Cold Spring Harbor Perspectives in Biology*, *2*(7). https://doi.org/10.1101/cshperspect.a005546

Calvi, B. R. (2013). Making big cells: One size does not fit all. *Proceedings of the National Academy of Sciences*, *110*(24), 9621-9622. https://doi.org/10.1073/pnas.1306908110

Carpenter, A. E., Jones, T. R., Lamprecht, M. R., Clarke, C., Kang, I. H., Friman, O., Guertin, D. A., Chang, J. H., Lindquist, R. A., Moffat, J., Golland, P., & Sabatini, D. M. (2006). CellProfiler: Image analysis software for identifying and quantifying cell phenotypes. *Genome Biology*, *7*(10). https://doi.org/10.1186/gb-2006-7-10-r100

Caygill, E. E., & Brand, A. H. (2016). The GAL4 System: A Versatile System for the Manipulation and Analysis of Gene Expression. In C. Dahmann (Ed.), *Drosophila: Methods and Protocols* (pp. 33-52). Springer. https://doi.org/10.1007/978-1-4939-6371-3_2

Cepec, E., & Trček, J. (2022). Antimicrobial Resistance of Acetobacter and Komagataeibacter Species Originating from Vinegars. *International Journal of*

Environmental Research and Public Health, *19*(1). https://doi.org/10.3390/ijerph19010463

Chang, J. T.-Y., & Ferrell, J. E. (2013). Mitotic trigger waves and the spatial coordination of the Xenopus cell cycle. *Nature*, *500*(7464). https://doi.org/10.1038/nature12321

Chang, W., Wang, H., Kim, W., Liu, Y., Deng, H., Li, H., Jiang, Z., Niu, Z., Sheng, W., Nápoles, O. C., Sun, Y., Xu, J., Sepulveda, A. R., Hayakawa, Y., Bass, A. J., & Wang, Y. (2020). Hormonal Suppression of Stem Cells Inhibits Symmetric Cell Division and Gastric Tumorigenesis. *Cell Stem Cell*, *26*(5). https://doi.org/10.1016/j.stem.2020.01.020

Chatterjee, M., & Ip, Y. T. (2009). Pathogenic stimulation of intestinal stem cell response in *Drosophila*. *Journal of Cellular Physiology*, *220*(3). https://doi.org/10.1002/jcp.21808

Chatzispyrou, I. A., Held, N. M., Mouchiroud, L., Auwerx, J., & Houtkooper, R. H. (2015). Tetracycline antibiotics impair mitochondrial function and its experimental use confounds research. *Cancer research*, *75*(21). https://doi.org/10.1158/0008-5472.CAN-15-1626

Chen, C., Fingerhut, J. M., & Yamashita, Y. M. (2016). The ins(ide) and outs(ide) of asymmetric stem cell division. *Current Opinion in Cell Biology*, *43*, 1-6. https://doi.org/10.1016/j.ceb.2016.06.001

Chen, H.-J., Li, Q., Nirala, N. K., & Ip, Y. T. (2020). The Snakeskin-Mesh Complex of Smooth Septate Junction Restricts Yorkie to Regulate Intestinal Homeostasis in *Drosophila*. *Stem Cell Reports*, *14*(5), 828-844. https://doi.org/10.1016/j.stemcr.2020.03.021

Chen, T., Zhang, J., Wang, Y., & Zhou, H. (2022). Identification of Survival-Related Genes in Acute Myeloid Leukemia (AML) Based on Cytogenetically Normal AML Samples Using Weighted Gene Coexpression Network Analysis. *Disease Markers*, *2022*. https://doi.org/10.1155/2022/5423694

Chen, W., Werdann, M., & Zhang, Y. (2018). The auxin-inducible degradation system enables conditional PERIOD protein depletion in the nervous system of *Drosophila* melanogaster. *The FEBS Journal*, *285*(23), 4378-4393. https://doi.org/10.1111/febs.14677

Chen, Y.-C., Guo, Y.-F., He, H., Lin, X., Wang, X.-F., Zhou, R., Li, W.-T., Pan, D.-Y., Shen, J., & Deng, H.-W. (2016). Integrative Analysis of Genomics and Transcriptome Data to Identify Potential Functional Genes of BMDs in Females. *Journal of Bone and Mineral Research*, *31*(5), 1041-1049. https://doi.org/10.1002/jbmr.2781

Cheung, T. H., & Rando, T. A. (2013). Molecular regulation of stem cell quiescence. *Nature reviews. Molecular cell biology*, *14*(6). https://doi.org/10.1038/nrm3591

Chhabra, S. N., & Booth, B. W. (2021). Asymmetric cell division of mammary stem cells. *Cell Division*, *16*(1). https://doi.org/10.1186/s13008-021-00073-w

Chia, W., Somers, W. G., & Wang, H. (2008). *Drosophila* neuroblast asymmetric divisions: Cell cycle regulators, asymmetric protein localization, and tumorigenesis. *The Journal of Cell Biology*, *180*(2), 267-272. https://doi.org/10.1083/jcb.200708159

Cho, U., Zimmerman, S. M., Chen, L., Owen, E., Kim, J. V., Kim, S. K., & Wandless, T. J. (2013). Rapid and tunable control of protein stability in Caenorhabditis elegans using a small molecule. *PloS One*, *8*(8). https://doi.org/10.1371/journal.pone.0072393

Choi, N. H., Lucchetta, E., & Ohlstein, B. (2011). Nonautonomous regulation of *Drosophila* midgut stem cell proliferation by the insulin-signaling pathway. *Proceedings of the National Academy of Sciences*, *108*(46), 18702-18707. https://doi.org/10.1073/pnas.1109348108

Christofi, T., & Apidianakis, Y. (2013). *Drosophila* and the hallmarks of cancer. *Advances in Biochemical Engineering/Biotechnology*, *135*, 79-110. https://doi.org/10.1007/10_2013_190

Church, R. B., & Robertson, F. W. (1966). A biochemical study of the growth of *Drosophila* melanogaster. *Journal of Experimental Zoology*, *162*(3), 337-351. https://doi.org/10.1002/jez.1401620309

Clancy, D., & Kennington, W. (2001). A simple method to achieve consistent larval density in bottle cultures. *Drosophila Information Service*, *84*, 168-169.

Clapp, M., Aurora, N., Herrera, L., Bhatia, M., Wilen, E., & Wakefield, S. (2017). Gut microbiota's effect on mental health: The gut-brain axis. *Clinics and Practice*, *7*(4). https://doi.org/10.4081/cp.2017.987

Clark, T. G., Bradburn, M. J., Love, S. B., & Altman, D. G. (2003). Survival analysis part I: Basic concepts and first analyses. *British Journal of Cancer*, *89*(2), 232-238. https://doi.org/10.1038/sj.bjc.6601118

Conduit, P. T., Wainman, A., Novak, Z. A., Weil, T. T., & Raff, J. W. (2015). Re-examining the role of *Drosophila* Sas-4 in centrosome assembly using two-colour-3D-SIM FRAP. *eLife*, *4*. https://doi.org/10.7554/eLife.08483

Cordero, J. B., Stefanatos, R. K., Scopelliti, A., Vidal, M., & Sansom, O. J. (2012). Inducible progenitor-derived Wingless regulates adult midgut regeneration in *Drosophila*. *The EMBO Journal*, *31*(19), 3901-3917. https://doi.org/10.1038/emboj.2012.248

Costa, C. A. M., Wang, X.-F., Ellsworth, C., & Deng, W.-M. (2022). Polyploidy in development and tumor models in *Drosophila*. *Seminars in cancer biology*, *81*, 106-118. https://doi.org/10.1016/j.semcancer.2021.09.011

Cristodero, M., Brogli, R., Joss, O., Schimanski, B., Schneider, A., & Polacek, N. (2021). tRNA 3′ shortening by LCCR4 as a response to stress in *Trypanosoma brucei*. *Nucleic Acids Research*, *49*(3). https://doi.org/10.1093/nar/gkaa1261

Cui, M., Han, S., Wang, D., Haider, M. S., Guo, J., Zhao, Q., Du, P., Sun, Z., Qi, F., Zheng, Z., Huang, B., Dong, W., Li, P., & Zhang, X. (2022). Gene Co-expression Network Analysis of the Comparative Transcriptome Identifies Hub Genes Associated With Resistance to Aspergillus flavus L. in Cultivated Peanut (Arachis hypogaea L.). *Frontiers in Plant Science*, *13*. https://www.frontiersin.org/articles/10.3389/fpls.2022.899177

Cuperus, J. T., Lo, R. S., Shumaker, L., Proctor, J., & Fields, S. (2015). A tetO Toolkit To Alter Expression of Genes in *Saccharomyces cerevisiae*. *ACS Synthetic Biology*, *4*(7). https://doi.org/10.1021/sb500363y

Dang, R., Qu, B., Guo, K., Zhou, S., Sun, H., Wang, W., Han, J., Feng, K., Lin, J., & Hu, Y. (2022). Weighted Co-Expression Network Analysis Identifies RNF181 as a Causal Gene of Coronary Artery Disease. *Frontiers in Genetics*, *12*. https://doi.org/10.3389/fgene.2021.818813

Danielsen, M., & Wind, A. (2003). Susceptibility of Lactobacillus spp. To antimicrobial agents. *International Journal of Food Microbiology*, *82*(1), 1-11. https://doi.org/10.1016/s0168-1605(02)00254-4

Das, D., Fletcher, R. B., & Ngai, J. (2020). Cellular mechanisms of epithelial stem cell self-renewal and differentiation during homeostasis and repair. *WIREs Developmental Biology*, *9*(1). https://doi.org/10.1002/wdev.361

Daul, A. L., Komori, H., & Lee, C.-Y. (2010). EdU (5-ethynyl-2'-deoxyuridine) labeling of *Drosophila* mitotic neuroblasts. *Cold Spring Harbor Protocols*, *2010*(7). https://doi.org/10.1101/pdb.prot5461

Davie, K., Janssens, J., Koldere, D., Waegeneer, M. D., Pech, U., Kreft, Ł., Aibar, S., Makhzami, S., Christiaens, V., González-Blas, C. B., Poovathingal, S., Hulselmans, G., Spanier, K. I., Moerman, T., Vanspauwen, B., Geurs, S., Voet, T., Lammertyn, J., Thienpont, B., … Aerts, S. (2018). A Single-Cell Transcriptome Atlas of the Aging *Drosophila* Brain. *Cell*, *174*(4), 982-998.e20. https://doi.org/10.1016/j.cell.2018.05.057

De Filippis, L., & Binda, E. (2012). Concise Review: Self-Renewal in the Central Nervous System: Neural Stem Cells from Embryo to Adult. *Stem Cells Translational Medicine*, *1*(4), 298-308. https://doi.org/10.5966/sctm.2011-0045

de la Fuente, A. (2010). From «differential expression» to 'differential networking'—Identification of dysfunctional regulatory networks in diseases. *Trends in Genetics: TIG*, *26*(7), 326-333. https://doi.org/10.1016/j.tig.2010.05.001

De Logu, F., Nassini, R., Materazzi, S., Carvalho Gonçalves, M., Nosi, D., Rossi Degl'Innocenti, D., Marone, I. M., Ferreira, J., Li Puma, S., Benemei, S., Trevisan, G., Souza Monteiro de Araújo, D., Patacchini, R., Bunnett, N. W., & Geppetti, P. (2017). Schwann cell TRPA1 mediates neuroinflammation that sustains macrophage-dependent neuropathic pain in mice. *Nature Communications*, *8*(1). https://doi.org/10.1038/s41467-017-01739-2

de Martin, X., Sodaei, R., & Santpere, G. (2021). Mechanisms of Binding Specificity among bHLH Transcription Factors. *International Journal of Molecular Sciences*, *22*(17). https://doi.org/10.3390/ijms22179150

De Mey, J. R., & Freund, J.-N. (2013). Understanding epithelial homeostasis in the intestine. *Tissue Barriers*, *1*(2). https://doi.org/10.4161/tisb.24965

de Navascués, J., Perdigoto, C. N., Bian, Y., Schneider, M. H., Bardin, A. J., Martínez-Arias, A., & Simons, B. D. (2012). *Drosophila* midgut homeostasis involves neutral competition between symmetrically dividing intestinal stem cells. *The EMBO Journal*, *31*(11), 2473-2485. https://doi.org/10.1038/emboj.2012.106

Del Poggetto, E., Ho, I.-L., Balestrieri, C., Yen, E.-Y., Zhang, S., Citron, F., Shah, R., Corti, D., Diaferia, G. R., Li, C.-Y., Loponte, S., Carbone, F., Hayakawa, Y., Valenti, G., Jiang, S., Sapio, L., Jiang, H., Dey, P., Gao, S., … Viale, A. (2021). Epithelial memory of inflammation limits tissue damage while promoting pancreatic tumorigenesis. *Science*, *373*(6561). https://doi.org/10.1126/science.abj0486

Demirci, S., Leonard, A., & Tisdale, J. F. (2020). Hematopoietic stem cells from pluripotent stem cells: Clinical potential, challenges, and future perspectives. *Stem Cells Translational Medicine*, *9*(12), 1549-1557. https://doi.org/10.1002/sctm.20-0247

Deneke, V. E., Melbinger, A., Vergassola, M., & Di Talia, S. (2016). Waves of Cdk1 Activity in S Phase Synchronize the Cell Cycle in *Drosophila* Embryos. *Developmental Cell*, *38*(4), 399-412. https://doi.org/10.1016/j.devcel.2016.07.023

Deng, H., Gerencser, A. A., & Jasper, H. (2015). Signal integration by Ca(2+) regulates intestinal stem-cell activity. *Nature*, *528*(7581). https://doi.org/10.1038/nature16170

Derks, W., Murganti, F., & Bergmann, O. (2020). Cardiomyocyte renewal in the failing heart: Lessons from the neonate? *Biophysical Reviews*, *12*(4), 785-787. https://doi.org/10.1007/s12551-020-00739-9

Dong, S., & Wu, H. (2018). Regenerating β cells of the pancreas – potential developments in diabetes treatment. *Expert opinion on biological therapy*, *18*(2), 175-185. https://doi.org/10.1080/14712598.2018.1402885

Donnelly, H., Salmeron-Sanchez, M., & Dalby, M. J. (2018). Designing stem cell niches for differentiation and self-renewal. *Journal of the Royal Society, Interface*, *15*(145). https://doi.org/10.1098/rsif.2018.0388

Doupé, D. P., Marshall, O. J., Dayton, H., Brand, A. H., & Perrimon, N. (2018). *Drosophila* intestinal stem and progenitor cells are major sources and regulators of homeostatic niche signals. *Proceedings of the National Academy of Sciences of the United States of America*, *115*(48), 12218-12223. https://doi.org/10.1073/pnas.1719169115

Dronamraju, R., & Mason, J. M. (2009). Recognition of Double Strand Breaks by a Mutator Protein (MU2) in *Drosophila* melanogaster. *PLoS Genetics*, *5*(5). https://doi.org/10.1371/journal.pgen.1000473

Drummond-Barbosa, D. (2008). Stem Cells, Their Niches and the Systemic Environment: An Aging Network. *Genetics*, *180*(4), 1787-1797. https://doi.org/10.1534/genetics.108.098244

Duffy, J. B. (2002). GAL4 system in *Drosophila*: A fly geneticist's Swiss army knife. *Genesis (New York, N.Y.: 2000)*, *34*(1-2), 1-15. https://doi.org/10.1002/gene.10150

Dumont, N. A., Bentzinger, C. F., Sincennes, M.-C., & Rudnicki, M. A. (2015). Satellite Cells and Skeletal Muscle Regeneration. *Comprehensive Physiology*, *5*(3), 1027-1059. https://doi.org/10.1002/cphy.c140068

Dutta, D. (2015). Regional Cell Specific RNA Expression Profiling of FACS Isolated *Drosophila* Intestinal Cell Populations. *Current Protocols in Stem Cell Biology*, *34*. https://doi.org/10.1002/9780470151808.sc02f02s34

Dwivedi, S., D'Souza, L. C., Shetty, N. G., Raghu, S. V., & Sharma, A. (2022). Hsp27, a potential EcR target, protects nonylphenol-induced cellular and organismal toxicity in *Drosophila* melanogaster. *Environmental Pollution*, *293*. https://doi.org/10.1016/j.envpol.2021.118484

Dzierzak, E., & Bigas, A. (2018). Blood Development: Hematopoietic Stem Cell Dependence and Independence. *Cell Stem Cell*, *22*(5), 639-651. https://doi.org/10.1016/j.stem.2018.04.015

Eaves, C. J. (2015). Hematopoietic stem cells: Concepts, definitions, and the new reality. *Blood*, *125*(17), 2605-2613. https://doi.org/10.1182/blood-2014-12-570200

Egeler, E. L., Urner, L. M., Rakhit, R., Liu, C. W., & Wandless, T. J. (2011). Ligand-switchable Substrates for a Ubiquitin-Proteasome System *. *Journal of Biological Chemistry*, *286*(36), 31328-31336. https://doi.org/10.1074/jbc.M111.264101

Elliott, D. A., & Brand, A. H. (2008). The GAL4 system: A versatile system for the expression of genes. *Methods in Molecular Biology (Clifton, N.J.)*, *420*, 79-95. https://doi.org/10.1007/978-1-59745-583-1_5

Enserink, J. M., & Kolodner, R. D. (2010). An overview of Cdk1-controlled targets and processes. *Cell Division*, *5*(1). https://doi.org/10.1186/1747-1028-5-11

Eschenhagen, T., Bolli, R., Braun, T., Field, L. J., Fleischmann, B. K., Frisén, J., Giacca, M., Hare, J. M., Houser, S., Lee, R. T., Marbán, E., Martin, J. F., Molkentin, J. D., Murry, C. E., Riley, P. R., Ruiz-Lozano, P., Sadek, H. A., Sussman, M. A., & Hill, J. A. (2017). Cardiomyocyte Regeneration: A Consensus Statement. *Circulation*, *136*(7), 680-686. https://doi.org/10.1161/CIRCULATIONAHA.117.029343

Fan, X., Waardenberg, A. J., Demuth, M., Osteil, P., Sun, J., Loebel, D. A. F., Graham, M. E., Tam, P., & Fossat, N. (2019). *TWIST1 homodimers and heterodimers orchestrate lineage-specific differentiation*. https://doi.org/10.1101/672824

Fendrik, A. J., Romanelli, L., & Rotondo, E. (2019). Stochastic cell renewal process and lengthening of cell cycle. *Physical Biology*, *17*(1). https://doi.org/10.1088/1478-3975/ab576c

Fink, M., & Wrana, J. L. (2023). Regulation of homeostasis and regeneration in the adult intestinal epithelium by the TGF-β superfamily. *Developmental Dynamics*, *252*(4), 445-462. https://doi.org/10.1002/dvdy.500

Flegel, K., Grushko, O., Bolin, K., Griggs, E., & Buttitta, L. (2016). Roles for the Histone Modifying and Exchange Complex NuA4 in Cell Cycle Progression in *Drosophila* melanogaster. *Genetics*, *203*(3). https://doi.org/10.1534/genetics.116.188581

Ford, E., Pearlman, J., Ruan, T., Manion, J., Waller, M., Neely, G. G., & Caron, L. (2020). Human Pluripotent Stem Cells-Based Therapies for Neurodegenerative Diseases: Current Status and Challenges. *Cells*, *9*(11). https://doi.org/10.3390/cells9112517

Fox, D. T., & Duronio, R. J. (2013). Endoreplication and polyploidy: Insights into development and disease. *Development (Cambridge, England)*, *140*(1), 3-12. https://doi.org/10.1242/dev.080531

Fu, J., Hagan, I. M., & Glover, D. M. (2015). The Centrosome and Its Duplication Cycle. *Cold Spring Harbor Perspectives in Biology*, *7*(2). https://doi.org/10.1101/cshperspect.a015800

Fuchs, E. (2016). Chapter Nineteen - Epithelial Skin Biology: Three Decades of Developmental Biology, a Hundred Questions Answered and a Thousand New Ones to Address. In P. M. Wassarman (Ed.), *Current Topics in Developmental Biology* (Vol. 116, pp. 357-374). Academic Press. https://doi.org/10.1016/bs.ctdb.2015.11.033

Fuchs, E., & Blau, H. M. (2020). Tissue Stem Cells: Architects of Their Niches. *Cell Stem Cell*, *27*(4), 532-556. https://doi.org/10.1016/j.stem.2020.09.011

Fuchs, E., & Chen, T. (2013). A matter of life and death: Self-renewal in stem cells. *EMBO Reports*, *14*(1), 39-48. https://doi.org/10.1038/embor.2012.197

Gao, X.-M., Zhou, X.-H., Jia, M.-W., Wang, X.-Z., & Liu, D. (2023). Identification of key genes in sepsis by WGCNA. *Preventive Medicine*, *172*. https://doi.org/10.1016/j.ypmed.2023.107540

Gattazzo, F., Urciuolo, A., & Bonaldo, P. (2014). Extracellular matrix: A dynamic microenvironment for stem cell niche. *Biochimica et Biophysica Acta (BBA) - General Subjects*, *1840*(8), 2506-2519. https://doi.org/10.1016/j.bbagen.2014.01.010

Gavet, O., & Pines, J. (2010). Progressive activation of CyclinB1-Cdk1 coordinates entry to mitosis. *Developmental cell*, *18*(4), 533-543. https://doi.org/10.1016/j.devcel.2010.02.013

Ge, S. X., Jung, D., & Yao, R. (2020). ShinyGO: A graphical gene-set enrichment tool for animals and plants. *Bioinformatics*, *36*(8), 2628-2629. https://doi.org/10.1093/bioinformatics/btz931

Gehart, H., & Clevers, H. (2019). Tales from the crypt: New insights into intestinal stem cells. *Nature Reviews. Gastroenterology & Hepatology*, *16*(1), 19-34. https://doi.org/10.1038/s41575-018-0081-y

Gérard, C., Gonze, D., & Goldbeter, A. (2012). Effect of positive feedback loops on the robustness of oscillations in the network of cyclin-dependent kinases driving the mammalian cell cycle. *The FEBS Journal*, *279*(18). https://doi.org/10.1111/j.1742-4658.2012.08585.x

Ghenoiu, C., Wheelock, M. S., & Funabiki, H. (2013). Autoinhibition and Polo-Dependent Multisite Phosphorylation Restrict Activity of the Histone H3 Kinase Haspin to Mitosis. *Molecular Cell*, *52*(5), 734-745. https://doi.org/10.1016/j.molcel.2013.10.002

Gómez-López, S., Lerner, R. G., & Petritsch, C. (2014). Asymmetric cell division of stem and progenitor cells during homeostasis and cancer. *Cellular and Molecular Life Sciences*, *71*(4), 575-597. https://doi.org/10.1007/s00018-013-1386-1

Gong, J., Nirala, N. K., Chen, J., Wang, F., Gu, P., Wen, Q., Ip, Y. T., & Xiang, Y. (2023). TrpA1 is a shear stress mechanosensing channel regulating intestinal stem cell proliferation in *Drosophila*. *Science Advances*, *9*(21). https://doi.org/10.1126/sciadv.adc9660

Graf, T., & Enver, T. (2009). Forcing cells to change lineages. *Nature*, *462*(7273), 587-594. https://doi.org/10.1038/nature08533

Gu, J., Zhang, Y., & Yin, G. (2023). Bayesian Log-Rank Test. *The American Statistician*, *77*(3), 292-300. https://doi.org/10.1080/00031305.2022.2161637

Guisoni, N., Martinez-Corral, R., Garcia-Ojalvo, J., & de Navascués, J. (2017). Diversity of fate outcomes in cell pairs under lateral inhibition. *Development*, *144*(7), 1177-1186. https://doi.org/10.1242/dev.137950

Guo, Z., Driver, I., & Ohlstein, B. (2013). Injury-induced BMP signaling negatively regulates *Drosophila* midgut homeostasis. *Journal of Cell Biology*, *201*(6). https://doi.org/10.1083/jcb.201302049

Guo, Z., Lucchetta, E., Rafel, N., & Ohlstein, B. (2016a). Maintenance of the adult *Drosophila* intestine: All roads lead to homeostasis. *Current Opinion in Genetics & Development*, *40*, 81-86. https://doi.org/10.1016/j.gde.2016.06.009

Guo, Z., Lucchetta, E., Rafel, N., & Ohlstein, B. (2016b). Maintenance of the adult *Drosophila* intestine: All roads lead to homeostasis. *Current Opinion in Genetics & Development*, *40*, 81-86. https://doi.org/10.1016/j.gde.2016.06.009

Hasankhani, A., Bahrami, A., Sheybani, N., Fatehi, F., Abadeh, R., Ghaem Maghami Farahani, H., Bahreini Behzadi, M. R., Javanmard, G., Isapour, S., Khadem, H., & Barkema, H. W. (2021). Integrated Network Analysis to Identify Key Modules and Potential Hub Genes Involved in Bovine Respiratory Disease: A Systems Biology Approach. *Frontiers in Genetics*, *12*. https://www.frontiersin.org/articles/10.3389/fgene.2021.753839

Hastie, T., & Tibshirani, R. (1986). Generalized Additive Models. *Statistical Science*, *1*(3), 297-310. https://doi.org/10.1214/ss/1177013604

Havens, C. G., & Walter, J. C. (2011). Mechanism of CRL4Cdt2, a PCNA-dependent E3 ubiquitin ligase. *Genes & Development*, *25*(15), 1568-1582. https://doi.org/10.1101/gad.2068611

Hayden, L., Hur, W., Vergassola, M., & Di Talia, S. (2022). Manipulating the nature of embryonic mitotic waves. *Current Biology*, *32*(22), 4989-4996.e3. https://doi.org/10.1016/j.cub.2022.10.014

He, L., Si, G., Huang, J., Samuel, A. D. T., & Perrimon, N. (2018). Mechanical regulation of stem cell differentiation through stretch-activated Piezo channel. *Nature*, *555*(7694), 103-106. https://doi.org/10.1038/nature25744

He, Y. R., He, S., Kandel, M. E., Lee, Y. J., Hu, C., Sobh, N., Anastasio, M. A., & Popescu, G. (2022). Cell Cycle Stage Classification Using Phase Imaging with Computational Specificity. *ACS Photonics*, *9*(4), 1264-1273. https://doi.org/10.1021/acsphotonics.1c01779

Hégarat, N., Crncec, A., Suarez Peredo Rodriguez, M. F., Echegaray Iturra, F., Gu, Y., Busby, O., Lang, P. F., Barr, A. R., Bakal, C., Kanemaki, M. T., Lamond, A. I., Novak, B., Ly, T., & Hochegger, H. (2020). Cyclin A triggers Mitosis either via the Greatwall kinase pathway or Cyclin B. *The EMBO Journal*, *39*(11). https://doi.org/10.15252/embj.2020104419

Herrera, S. C., & Bach, E. A. (2019). JAK/STAT signaling in stem cells and regeneration: From *Drosophila* to vertebrates. *Development*, *146*(2). https://doi.org/10.1242/dev.167643

Herrero, D., Albericio, G., Higuera, M., Herranz-López, M., García-Brenes, M. A., Cordero, A., Roche, E., Sepúlveda, P., Mora, C., & Bernad, A. (2022). The Vascular Niche for Adult Cardiac Progenitor Cells. *Antioxidants*, *11*(5). https://doi.org/10.3390/antiox11050882

Hochmuth, C. E., Biteau, B., Bohmann, D., & Jasper, H. (2011). Redox Regulation by Keap1 and Nrf2 Controls Intestinal Stem Cell Proliferation in *Drosophila*. *Cell Stem Cell*, *8*(2), 188-199. https://doi.org/10.1016/j.stem.2010.12.006

Homem, C. C. F., & Knoblich, J. A. (2012). *Drosophila* neuroblasts: A model for stem cell biology. *Development*, *139*(23), 4297-4310. https://doi.org/10.1242/dev.080515

Houtz, P., Bonfini, A., Liu, X., Revah, J., Guillou, A., Poidevin, M., Hens, K., Huang, H.-Y., Deplancke, B., Tsai, Y.-C., & Buchon, N. (2017). Hippo, TGF-β, and Src-MAPK pathways regulate transcription of the upd3 cytokine in *Drosophila* enterocytes upon bacterial infection. *PLOS Genetics*, *13*(11). https://doi.org/10.1371/journal.pgen.1007091

Hsu, Y.-C., Li, L., & Fuchs, E. (2014). Emerging interactions between skin stem cells and their niches. *Nature Medicine*, *20*(8). https://doi.org/10.1038/nm.3643

Hu, D. J.-K., & Jasper, H. (2019). Control of Intestinal Cell Fate by Dynamic Mitotic Spindle Repositioning Influences Epithelial Homeostasis and Longevity. *Cell Reports*, *28*(11), 2807-2823.e5. https://doi.org/10.1016/j.celrep.2019.08.014

Huang, J., Gujar, M. R., Deng, Q., Y Chia, S., Li, S., Tan, P., Sung, W.-K., & Wang, H. (2021). Histone lysine methyltransferase Pr-set7/SETD8 promotes neural stem cell reactivation. *EMBO Reports*, *22*(4). https://doi.org/10.15252/embr.202050994

Huang, J., Liu, L., Qin, L., Huang, H., & Li, X. (2021). Weighted Gene Coexpression Network Analysis Uncovers Critical Genes and Pathways for Multiple Brain Regions in Parkinson's Disease. *BioMed Research International*, *2021*. https://doi.org/10.1155/2021/6616434

Imayoshi, I., Ishidate, F., & Kageyama, R. (2015). Real-time imaging of bHLH transcription factors reveals their dynamic control in the multipotency and fate choice of neural stem cells. *Frontiers in Cellular Neuroscience*, *9*. https://doi.org/10.3389/fncel.2015.00288

Inaba, M., & Yamashita, Y. M. (2012). Asymmetric Stem Cell Division: Precision for Robustness. *Cell Stem Cell*, *11*(4), 461-469. https://doi.org/10.1016/j.stem.2012.09.003

Ito, F., & Awasaki, T. (2022). Comparative analysis of temperature preference behavior and effects of temperature on daily behavior in 11 *Drosophila* species. *Scientific Reports*, *12*(1). https://doi.org/10.1038/s41598-022-16897-7

Ito, K., & Suda, T. (2014). Metabolic requirements for the maintenance of self-renewing stem cells. *Nature reviews. Molecular cell biology*, *15*(4), 243-256. https://doi.org/10.1038/nrm3772

Iwamoto, M., Björklund, T., Lundberg, C., Kirik, D., & Wandless, T. J. (2010). A general chemical method to regulate protein stability in the mammalian central nervous system. *Chemistry & Biology*, *17*(9). https://doi.org/10.1016/j.chembiol.2010.07.009

Jiang, H., & Edgar, B. A. (2011a). Intestinal stem cells in the adult *Drosophila* midgut. *Experimental cell research*, *317*(19), 2780-2788. https://doi.org/10.1016/j.yexcr.2011.07.020

Jiang, H., & Edgar, B. A. (2011b). Intestinal stem cells in the adult *Drosophila* midgut. *Experimental cell research*, *317*(19), 2780-2788. https://doi.org/10.1016/j.yexcr.2011.07.020

Jiang, H., & Edgar, B. A. (2012). Intestinal stem cell function in *Drosophila* and Mice. *Current opinion in genetics & development*, *22*(4), 354-360. https://doi.org/10.1016/j.gde.2012.04.002

Jiang, H., Grenley, M., Bravo, M. J., Blumhagen, R. Z., & Edgar, B. A. (2011). EGFR/Ras/MAPK Signaling Mediates Adult Midgut Epithelial Homeostasis and Regeneration in *Drosophila*. *Cell Stem Cell*, *8*(1). https://doi.org/10.1016/j.stem.2010.11.026

Jiang, H., Patel, P. H., Kohlmaier, A., Grenley, M. O., McEwen, D. G., & Edgar, B. A. (2009a). Cytokine/Jak/Stat signaling mediates regeneration and homeostasis in the *Drosophila* midgut. *Cell*, *137*(7), 1343-1355. https://doi.org/10.1016/j.cell.2009.05.014

Jiang, H., Patel, P. H., Kohlmaier, A., Grenley, M. O., McEwen, D. G., & Edgar, B. A. (2009b). Cytokine/Jak/Stat signaling mediates regeneration and homeostasis in the *Drosophila* midgut. *Cell*, *137*(7). https://doi.org/10.1016/j.cell.2009.05.014

Jiang, H., Tian, A., & Jen, J. (2016). Intestinal stem cell response to injury: Lessons from *Drosophila*. *Cellular and Molecular Life Sciences*, *73*(17). https://doi.org/10.1007/s00018-016-2235-9

Jin, Y., Ha, N., Forés, M., Xiang, J., Gläßer, C., Maldera, J., Jiménez, G., & Edgar, B. A. (2015). EGFR/Ras Signaling Controls *Drosophila* Intestinal Stem Cell Proliferation via Capicua-Regulated Genes. *PLOS Genetics*, *11*(12). https://doi.org/10.1371/journal.pgen.1005634

Jin, Y., Patel, P. H., Kohlmaier, A., Pavlovic, B., Zhang, C., & Edgar, B. A. (2017). Intestinal Stem Cell Pool Regulation in *Drosophila*. *Stem Cell Reports*, *8*(6), 1479-1487. https://doi.org/10.1016/j.stemcr.2017.04.002

Jing, J., Wu, Z., Wang, J., Luo, G., Lin, H., Fan, Y., & Zhou, C. (2023). Hedgehog signaling in tissue homeostasis, cancers, and targeted therapies. *Signal Transduction and Targeted Therapy*, *8*(1), 1-33. https://doi.org/10.1038/s41392-023-01559-5

Joly, A., & Rousset, R. (2020). Tissue Adaptation to Environmental Cues by Symmetric and Asymmetric Division Modes of Intestinal Stem Cells. *International Journal of Molecular Sciences*, *21*(17). https://doi.org/10.3390/ijms21176362

Jones, S. (2004). An overview of the basic helix-loop-helix proteins. *Genome Biology*, *5*(6). https://doi.org/10.1186/gb-2004-5-6-226

Jurkowski, M. P., Bettio, L., K. Woo, E., Patten, A., Yau, S.-Y., & Gil-Mohapel, J. (2020). Beyond the Hippocampus and the SVZ: Adult Neurogenesis Throughout the Brain. *Frontiers in Cellular Neuroscience*, *14*. https://www.frontiersin.org/articles/10.3389/fncel.2020.576444

Kalderon, D. (2022). Investigating Adult Stem Cells through Lineage Analyses. *Stem cell reviews and reports*, *18*(1), 2-22. https://doi.org/10.1007/s12015-021-10282-z

Kempermann, G. (2015). Activity Dependency and Aging in the Regulation of Adult Neurogenesis. *Cold Spring Harbor Perspectives in Biology*, *7*(11). https://doi.org/10.1101/cshperspect.a018929

Kernan, J., Bonacci, T., & Emanuele, M. J. (2018). Who guards the guardian? Mechanisms that restrain APC/C during the cell cycle. *Biochimica et Biophysica Acta (BBA) - Molecular Cell Research*, *1865*(12), 1924-1933. https://doi.org/10.1016/j.bbamcr.2018.09.011

Khlusov, I., Litvinova, L., Yurova, K., & Khlusova, M. (2022). Precise tissue bioengineering and niches of mesenchymal stem cells: Their size and hierarchy matter. *BIOCELL*, *46*(6), 1365-1373. https://doi.org/10.32604/biocell.2022.018917

Khoutorsky, A., Sorge, R. E., Prager-Khoutorsky, M., Pawlowski, S., Longo, G., Jafarnejad, S. M., Tahmasebi, S., Martin, L. J., Pitcher, M., Gkogkas, C. G., Sharif-Naeini, R., Ribeiro-da-Silva, A., Bourque, C. W., Cerveró, F., Mogil, J. S., & Sonenberg, N. (2016). eIF2α phosphorylation controls thermal nociception. *Proceedings of the National Academy of Sciences*, *113*(42). https://doi.org/10.1073/pnas.1614047113

Kim, D., Langmead, B., & Salzberg, S. L. (2015). HISAT: A fast spliced aligner with low memory requirements. *Nature Methods*, *12*(4), 357-360. https://doi.org/10.1038/nmeth.3317

Kim, M., Delos Santos, K., & Moon, N.-S. (2021). Proper CycE-Cdk2 activity in endocycling tissues requires regulation of the cyclin-dependent kinase inhibitor Dacapo by dE2F1b in *Drosophila*. *Genetics*, *217*(1), 1-15. https://doi.org/10.1093/genetics/iyaa029

Klimczak, A., & Kozlowska, U. (2015). Mesenchymal Stromal Cells and Tissue-Specific Progenitor Cells: Their Role in Tissue Homeostasis. *Stem Cells International*, *2016*. https://doi.org/10.1155/2016/4285215

Knoblich, J. A. (2008). Mechanisms of Asymmetric Stem Cell Division. *Cell*, *132*(4), 583-597. https://doi.org/10.1016/j.cell.2008.02.007

Kogenaru, M., & Isalan, M. (2018). Drug-Inducible Control of Lethality Genes: A Low Background Destabilizing Domain Architecture Applied to the Gal4-UAS System in *Drosophila*. *ACS Synthetic Biology*, *7*(6), 1496-1506. https://doi.org/10.1021/acssynbio.7b00302

Komarova, N. L. (2013). Principles of regulation of self-renewing cell lineages. *PloS One*, *8*(9). https://doi.org/10.1371/journal.pone.0072847

Kosan, C., & Godmann, M. (2016). Genetic and Epigenetic Mechanisms That Maintain Hematopoietic Stem Cell Function. *Stem Cells International*, *2016*. https://doi.org/10.1155/2016/5178965

Kotas, M. E., & Medzhitov, R. (2015). Homeostasis, Inflammation, and Disease Susceptibility. *Cell*, *160*(5), 816-827. https://doi.org/10.1016/j.cell.2015.02.010

Koval, L., Proshkina, E., Shaposhnikov, M., & Moskalev, A. (2020). The role of DNA repair genes in radiation-induced adaptive response in *Drosophila* melanogaster is differential and conditional. *Biogerontology*, *21*(1), 45-56. https://doi.org/10.1007/s10522-019-09842-1

Kowalski, T. W., Gomes, J. do A., Feira, M. F., Dupont, Á. de V., Recamonde-Mendoza, M., & Vianna, F. S. L. (2020). Anticonvulsants and Chromatin-Genes Expression: A Systems Biology Investigation. *Frontiers in Neuroscience*, *14*. https://doi.org/10.3389/fnins.2020.591196

Kubrak, O., Koyama, T., Ahrentløv, N., Jensen, L., Malita, A., Naseem, M. T., Lassen, M., Nagy, S., Texada, M. J., Halberg, K. V., & Rewitz, K. (2022). The gut hormone Allatostatin C/Somatostatin regulates food intake and metabolic homeostasis under nutrient stress. *Nature Communications*, *13*. https://doi.org/10.1038/s41467-022-28268-x

Kux, K., & Pitsouli, C. (2014). Tissue communication in regenerative inflammatory signaling: Lessons from the fly gut. *Frontiers in Cellular and Infection Microbiology*, *4*. https://www.frontiersin.org/article/10.3389/fcimb.2014.00049

Lambrus, B. G., Moyer, T. C., & Holland, A. J. (2018). Chapter 5—Applying the auxin-inducible degradation system for rapid protein depletion in mammalian cells. In H. Maiato & M. Schuh (Eds.), *Methods in Cell Biology* (Vol. 144, pp. 107-135). Academic Press. https://doi.org/10.1016/bs.mcb.2018.03.004

Landis, G. N., Salomon, M. P., Keroles, D., Brookes, N., Sekimura, T., & Tower, J. (2015). The progesterone antagonist mifepristone/RU486 blocks the negative effect on life span caused by mating in female *Drosophila*. *Aging*, *7*(1), 53-69.

Langfelder, P., & Horvath, S. (2008). WGCNA: An R package for weighted correlation network analysis. *BMC Bioinformatics*, *9*. https://doi.org/10.1186/1471-2105-9-559

LaRocque, J. R., Jaklevic, B., Su, T. T., & Sekelsky, J. (2007). *Drosophila* ATR in double-strand break repair. *Genetics*, *175*(3), 1023-1033. https://doi.org/10.1534/genetics.106.067330

Lee, H. O., Davidson, J. M., & Duronio, R. J. (2009). Endoreplication: Polyploidy with purpose. *Genes & Development*, *23*(21), 2461-2477. https://doi.org/10.1101/gad.1829209

Lee, H.-J., Chung, Y., Chung, K. Y., Kim, Y.-K., Lee, J. H., Koh, Y. J., & Lee, S. H. (2022). Use of a graph neural network to the weighted gene co-expression network analysis of Korean native cattle. *Scientific Reports*, *12*. https://doi.org/10.1038/s41598-022-13796-9

Lee, H.-Y., Lee, S.-H., Lee, J.-H., Lee, W.-J., & Min, K.-J. (2019). The role of commensal microbes in the lifespan of *Drosophila melanogaster*. *Aging*, *11*(13), 4611-4640. https://doi.org/10.18632/aging.102073

Lee, J. Y., & Hong, S.-H. (2019). Hematopoietic Stem Cells and Their Roles in Tissue Regeneration. *International Journal of Stem Cells*, *13*(1), 1-12. https://doi.org/10.15283/ijsc19127

Lele, U. N., Baig, U. I., & Watve, M. G. (2011). Phenotypic Plasticity and Effects of Selection on Cell Division Symmetry in Escherichia coli. *PLOS ONE*, *6*(1). https://doi.org/10.1371/journal.pone.0014516

Leri, A., Rota, M., Pasqualini, F. S., Goichberg, P., & Anversa, P. (2015). Origin of Cardiomyocytes in the Adult Heart. *Circulation research*, *116*(1), 150-166. https://doi.org/10.1161/CIRCRESAHA.116.303595

Levine, M., & Davidson, E. H. (2005). Gene regulatory networks for development. *Proceedings of the National Academy of Sciences*, *102*(14), 4936-4942. https://doi.org/10.1073/pnas.0408031102

Li, H., Janssens, J., De Waegeneer, M., Kolluru, S. S., Davie, K., Gardeux, V., Saelens, W., David, F., Brbić, M., Spanier, K., Leskovec, J., McLaughlin, C. N., Xie, Q., Jones, R. C., Brueckner, K., Shim, J., Tattikota, S. G., Schnorrer, F., Rust, K., … Aerts, S. (2022). Fly Cell Atlas: A single-nucleus transcriptomic atlas of the adult fruit fly. *Science*, *375*(6584). https://doi.org/10.1126/science.abk2432

Li, J., Zhou, D., Qiu, W., Shi, Y., Yang, J.-J., Chen, S., Wang, Q., & Pan, H. (2018). Application of Weighted Gene Co-expression Network Analysis for Data from Paired Design. *Scientific Reports*, *8*(1). https://doi.org/10.1038/s41598-017-18705-z

Li, K., & Gong, Z. (2016). Feeling Hot and Cold: Thermal Sensation in *Drosophila*. *Neuroscience Bulletin*, *33*(3), 317-322. https://doi.org/10.1007/s12264-016-0087-9

Li, Q., & Stavropoulos, N. (2016). Evaluation of Ligand-Inducible Expression Systems for Conditional Neuronal Manipulations of Sleep in *Drosophila*. *G3: Genes|Genomes|Genetics*, *6*(10), Article 10. https://doi.org/10.1534/g3.116.034132

Li, S., Wang, H., & Groth, C. (2014). *Drosophila* neuroblasts as a new model for the study of stem cell self-renewal and tumour formation. *Bioscience Reports*, *34*(4). https://doi.org/10.1042/BSR20140008

Li, W., Huang, X., Yu, W., Xu, Y., Huang, R., Park, J., Moshaverinia, A., Arora, P., & Chen, C. (2022). Activation of Functional Somatic Stem Cells Promotes Endogenous Tissue Regeneration. *Journal of Dental Research*, *101*(7). https://doi.org/10.1177/00220345211070222

Li, X., Chen, R., & Zhu, S. (2017). bHLH-O proteins balance the self-renewal and differentiation of *Drosophila* neural stem cells by regulating Earmuff expression. *Developmental Biology*, *431*(2). https://doi.org/10.1016/j.ydbio.2017.09.011

Liang, W., Sun, F., Zhao, Y., Shan, L., & Lou, H. (2020). Identification of Susceptibility Modules and Genes for Cardiovascular Disease in Diabetic Patients Using WGCNA Analysis. *Journal of Diabetes Research*, *2020*. https://doi.org/10.1155/2020/4178639

Liao, Y., Smyth, G. K., & Shi, W. (2014). featureCounts: An efficient general purpose program for assigning sequence reads to genomic features. *Bioinformatics*, *30*(7), 923-930. https://doi.org/10.1093/bioinformatics/btt656

Lin, G., Zhang, X., Ren, J., Pang, Z., Wang, C., Xu, N., & Xi, R. (2013). Integrin signaling is required for maintenance and proliferation of intestinal stem cells in *Drosophila*. *Developmental Biology*, *377*(1), 177-187. https://doi.org/10.1016/j.ydbio.2013.01.032

Lin, W., Wang, Y., Chen, Y., Wang, Q., Gu, Z., & Zhu, Y. (2021). Role of Calcium Signaling Pathway-Related Gene Regulatory Networks in Ischemic Stroke Based on Multiple WGCNA and Single-Cell Analysis. *Oxidative Medicine and Cellular Longevity*, *2021*. https://doi.org/10.1155/2021/8060477

Linford, N. J., Bilgir, C., Ro, J., & Pletcher, S. D. (2013). Measurement of lifespan in *Drosophila* melanogaster. *Journal of Visualized Experiments: JoVE*, *71*. https://doi.org/10.3791/50068

Liu, J., Jing, L., & Tu, X. (2016). Weighted gene co-expression network analysis identifies specific modules and hub genes related to coronary artery disease. *BMC Cardiovascular Disorders*, *16*. https://doi.org/10.1186/s12872-016-0217-3

Liu, L., Michowski, W., Inuzuka, H., Shimizu, K., Nihira, N. T., Chick, J. M., Li, N., Geng, Y., Meng, A. Y., Ordureau, A., Kołodziejczyk, A., Ligon, K. L., Bronson, R. T., Polyak, K., Harper, J. W., Gygi, S. P., Wei, W., & Sicinski, P. (2017). G1 cyclins link proliferation, pluripotency and differentiation of embryonic stem cells. *Nature Cell Biology*, *19*(3), 177-188. https://doi.org/10.1038/ncb3474

Liu, L., Michowski, W., Kolodziejczyk, A., & Sicinski, P. (2019). The cell cycle in stem cell proliferation, pluripotency and differentiation. *Nature cell biology*, *21*(9), 1060-1067. https://doi.org/10.1038/s41556-019-0384-4

Liu, Q., & Jin, L. H. (2017). Tissue-resident stem cell activity: A view from the adult *Drosophila* gastrointestinal tract. *Cell Communication and Signaling*, *15*(1). https://doi.org/10.1186/s12964-017-0184-z

Liu, Z., Sun, Q., & Wang, X. (2016). PLK1, A Potential Target for Cancer Therapy. *Translational Oncology*, *10*(1), 22-32. https://doi.org/10.1016/j.tranon.2016.10.003

Lopez-Garcia, C., Klein, A. M., Simons, B. D., & Winton, D. J. (2010). Intestinal Stem Cell Replacement Follows a Pattern of Neutral Drift. *Science*, *330*(6005), 822-825. https://doi.org/10.1126/science.1196236

López-Lázaro, M. (2018). The stem cell division theory of cancer. *Critical Reviews in Oncology/Hematology*, *123*, 95-113. https://doi.org/10.1016/j.critrevonc.2018.01.010

Loreti, M., & Sacco, A. (2022). The jam session between muscle stem cells and the extracellular matrix in the tissue microenvironment. *Npj Regenerative Medicine*, *7*(1). https://doi.org/10.1038/s41536-022-00204-z

Losick, V. P., Morris, L. X., Fox, D. T., & Spradling, A. (2011). *Drosophila* stem cell niches: A decade of discovery suggests a unified view of stem cell regulation. *Developmental Cell*, *21*(1), 159-171. https://doi.org/10.1016/j.devcel.2011.06.018

Loudhaief, R. (2016). *Enteroendocrine Cells, A Potential Way to Control Intestinal Stem Cell Proliferation*. https://clinmedjournals.org/articles/ijscrt/international-journal-of-stem-cell-research-and-therapy-ijscrt-3-037.php?jid=ijscrt

Love, M. I., Huber, W., & Anders, S. (2014). Moderated estimation of fold change and dispersion for RNA-seq data with DESeq2. *Genome Biology*, *15*(12). https://doi.org/10.1186/s13059-014-0550-8

Loyer, N., & Januschke, J. (2020). Where does asymmetry come from? Illustrating principles of polarity and asymmetry establishment in *Drosophila* neuroblasts. *Current Opinion in Cell Biology*, *62*, 70-77. https://doi.org/10.1016/j.ceb.2019.07.018

Lu, C. P., Polak, L., Rocha, A. S., Pasolli, H. A., Chen, S.-C., Sharma, N., Blanpain, C., & Fuchs, E. (2012). Identification of Stem Cell Populations in Sweat Glands and Ducts Reveals Roles in Homeostasis and Wound Repair. *Cell*, *150*(1), 136-150. https://doi.org/10.1016/j.cell.2012.04.045

Lu, J.-M., Chen, Y.-C., Ao, Z.-X., Shen, J., Zeng, C.-P., Lin, X., Peng, L.-P., Zhou, R., Wang, X.-F., Peng, C., Xiao, H.-M., Zhang, K., & Deng, H.-W. (2019). System network analysis of genomics and transcriptomics data identified type 1 diabetes-associated pathway and genes. *Genes & Immunity*, *20*(6). https://doi.org/10.1038/s41435-018-0045-9

Lucchetta, E. M., & Ohlstein, B. (2012). The *Drosophila* midgut: A model for stem cell driven tissue regeneration. *WIREs Developmental Biology*, *1*(5), 781-788. https://doi.org/10.1002/wdev.51

Ma, C., & Li, H. (2021). Hub Gene and Its Key Effects on Diffuse Large B-Cell Lymphoma by Weighted Gene Coexpression Network Analysis. *BioMed Research International*, *2021*. https://doi.org/10.1155/2021/8127145

Maloy, K. J., & Powrie, F. (2011). Intestinal homeostasis and its breakdown in inflammatory bowel disease. *Nature*, *474*(7351), 298-306. https://doi.org/10.1038/nature10208

Mannino, G., Russo, C., Maugeri, G., Musumeci, G., Vicario, N., Tibullo, D., Giuffrida, R., Parenti, R., & Lo Furno, D. (2022). Adult stem cell niches for tissue homeostasis. *Journal of Cellular Physiology*, *237*(1), 239-257. https://doi.org/10.1002/jcp.30562

Marianes, A., & Spradling, A. C. (2013). Physiological and stem cell compartmentalization within the *Drosophila* midgut. *eLife*, *2*. https://doi.org/10.7554/eLife.00886

Martin, J. L., Sanders, E. N., Moreno-Roman, P., Jaramillo Koyama, L. A., Balachandra, S., Du, X., & O'Brien, L. E. (2018). Long-term live imaging of the *Drosophila* adult midgut reveals real-time dynamics of division, differentiation and loss. *eLife*, *7*. https://doi.org/10.7554/eLife.36248

Marygold, S. J., Attrill, H., Speretta, E., Warner, K., Magrane, M., Berloco, M., Cotterill, S., McVey, M., Rong, Y., & Yamaguchi, M. (2020). The DNA polymerases of *Drosophila* melanogaster. *Fly*, *14*(1-4), 49-61. https://doi.org/10.1080/19336934.2019.1710076

Massari, M. E., & Murre, C. (2000). Helix-Loop-Helix Proteins: Regulators of Transcription in Eucaryotic Organisms. *Molecular and Cellular Biology*, *20*(2), 429-440. https://doi.org/10.1128/MCB.20.2.429-440.2000

Mathur, D., Bost, A., Driver, I., & Ohlstein, B. (2010). A Transient Niche Regulates the Specification of *Drosophila* Intestinal Stem Cells. *Science*, *327*(5962), 210-213. https://doi.org/10.1126/science.1181958

Matova, N., Mahajan-Miklos, S., Mooseker, M. S., & Cooley, L. (1999). *Drosophila* Quail, a villin-related protein, bundles actin filaments in apoptotic nurse cells. *Development*, *126*(24), 5645-5657. https://doi.org/10.1242/dev.126.24.5645

Matson, J. P., Dumitru, R., Coryell, P., Baxley, R. M., Chen, W., Twaroski, K., Webber, B. R., Tolar, J., Bielinsky, A.-K., Purvis, J. E., & Cook, J. G. (2017). Rapid DNA replication origin licensing protects stem cell pluripotency. *eLife*, *6*. https://doi.org/10.7554/eLife.30473

Matthews, D. A., Bolin, J. T., Burridge, J. M., Filman, D. J., Volz, K. W., & Kraut, J. (1985). Dihydrofolate reductase. The stereochemistry of inhibitor selectivity. *The Journal of Biological Chemistry*, *260*(1), 392-399.

Maynard-Smith, L. A. (2007). A Directed Approach for Engineering Conditional Protein Stability Using Biologically Silent Small Molecules*. 282(34).

McCarthy, N., Kraiczy, J., & Shivdasani, R. A. (2020). Cellular and molecular architecture of the intestinal stem cell niche. *Nature Cell Biology*, *22*(9), Article 9. https://doi.org/10.1038/s41556-020-0567-z

McGuire, S. E., Mao, Z., & Davis, R. L. (2004). Spatiotemporal gene expression targeting with the TARGET and gene-switch systems in *Drosophila*. *Science's STKE: Signal Transduction Knowledge Environment*, *2004*(220), pl6. https://doi.org/10.1126/stke.2202004pl6

McGuire, S. E., Roman, G., & Davis, R. L. (2004). Gene expression systems in *Drosophila*: A synthesis of time and space. *Trends in Genetics: TIG*, *20*(8), 384-391. https://doi.org/10.1016/j.tig.2004.06.012

Meissner, G. W., Nern, A., Dorman, Z., DePasquale, G. M., Forster, K., Gibney, T., Hausenfluck, J. H., He, Y., Iyer, N. A., Jeter, J., Johnson, L., Johnston, R. M., Lee,

K., Melton, B., Yarbrough, B., Zugates, C. T., Clements, J., Goina, C., Otsuna, H., … FlyLight Project Team. (2023). A searchable image resource of *Drosophila* GAL4 driver expression patterns with single neuron resolution. *eLife*, *12*. https://doi.org/10.7554/eLife.80660

Meng, Z., Moroishi, T., & Guan, K.-L. (2016). Mechanisms of Hippo pathway regulation. *Genes & Development*, *30*(1), 1-17. https://doi.org/10.1101/gad.274027.115

Micchelli, C. A., & Perrimon, N. (2006). Evidence that stem cells reside in the adult *Drosophila* midgut epithelium. *Nature*, *439*(7075), 475-479. https://doi.org/10.1038/nature04371

Michael, A. K., Stoos, L., Crosby, P., Eggers, N., Nie, X. Y., Makasheva, K., Minnich, M., Healy, K. L., Weiss, J., Kempf, G., Cavadini, S., Kater, L., Seebacher, J., Vecchia, L., Chakraborty, D., Isbel, L., Grand, R. S., Andersch, F., Fribourgh, J. L., … Thomä, N. H. (2023). Cooperation between bHLH transcription factors and histones for DNA access. *Nature*, *619*(7969), 385-393. https://doi.org/10.1038/s41586-023-06282-3

Michalopoulos, G. K. (2017). Hepatostat: Liver regeneration and normal liver tissue maintenance. *Hepatology*, *65*(4), 1384-1392. https://doi.org/10.1002/hep.28988

Miguel-Aliaga, I., Jasper, H., & Lemaitre, B. (2018). Anatomy and Physiology of the Digestive Tract of *Drosophila* melanogaster. *Genetics*, *210*(2), 357-396. https://doi.org/10.1534/genetics.118.300224

Mikheeva, S. A., Funk, C. C., Horner, P. J., Rostomily, R. C., & Mikheev, A. M. (2024). Novel TCF4:TCF12 heterodimer inhibits glioblastoma growth. *Molecular Oncology*, *18*(3), 517-527. https://doi.org/10.1002/1878-0261.13496

Montagnani, S., Rueger, M. A., Hosoda, T., & Nurzynska, D. (2016). Adult Stem Cells in Tissue Maintenance and Regeneration. *Stem Cells International*, *2016*. https://doi.org/10.1155/2016/7362879

Montagne, C., & Gonzalez-Gaitan, M. (2014). Sara endosomes and the asymmetric division of intestinal stem cells. *Development (Cambridge, England)*, *141*(10), 2014-2023. https://doi.org/10.1242/dev.104240Moris, N., Pina, C., & Arias, A. M. (2016). Transition states and cell fate decisions in epigenetic landscapes. *Nature Reviews. Genetics*, *17*(11), 693-703. https://doi.org/10.1038/nrg.2016.98

Morrisey, E. (2018). Modelling of clone size data from «*Drosophila* midgut homeostasis involves neutral competition between symmetrically dividing intestinal stem cells» [Personal communication].

Morrison, S. J., & Kimble, J. (2006). Asymmetric and symmetric stem-cell divisions in development and cancer. *Nature*, *441*(7097), 1068-1074. https://doi.org/10.1038/nature04956

Morrow, A., Underwood, J., Seldin, L., Hinnant, T., & Lechler, T. (2019). Regulated spindle orientation buffers tissue growth in the epidermis. *eLife*, *8*. https://doi.org/10.7554/eLife.48482

Morrow, G., & Tanguay, R. M. (2003). Heat shock proteins and aging in *Drosophila* melanogaster. *Seminars in Cell & Developmental Biology*, *14*(5), 291-299. https://doi.org/10.1016/j.semcdb.2003.09.023

Morrow, G., & Tanguay, R. M. (2015). *Drosophila* Small Heat Shock Proteins: An Update on Their Features and Functions. In R. M. Tanguay & L. E. Hightower (Eds.), *The Big Book on Small Heat Shock Proteins* (pp. 579-606). Springer International Publishing. https://doi.org/10.1007/978-3-319-16077-1_25

Moullan, N., Mouchiroud, L., Wang, X., Ryu, D., Williams, E. G., Mottis, A., Jovaisaite, V., Frochaux, M. V., Quiros, P. M., Deplancke, B., Houtkooper, R. H., & Auwerx, J. (2015). Tetracyclines Disturb Mitochondrial Function across Eukaryotic Models: A Call for Caution in Biomedical Research. *Cell Reports*, *10*(10). https://doi.org/10.1016/j.celrep.2015.02.034

Murke, F., Castro, S. V. C., Giebel, B., & Görgens, A. (2015). Concise Review: Asymmetric Cell Divisions in Stem Cell Biology. *Symmetry*, *7*(4). https://doi.org/10.3390/sym7042025

Murre, C. (2005). Helix-loop-helix proteins and lymphocyte development. *Nature Immunology*, *6*(11), 1079-1086. https://doi.org/10.1038/ni1260

Murre, C. (2019). Helix–loop–helix proteins and the advent of cellular diversity: 30 years of discovery. *Genes & Development*, *33*(1-2), 6-25. https://doi.org/10.1101/gad.320663.118

Murre, C., Bain, G., van Dijk, M. A., Engel, I., Furnari, B. A., Massari, M. E., Matthews, J. R., Quong, M. W., Rivera, R. R., & Stuiver, M. H. (1994). Structure and function of helix-loop-helix proteins. *Biochimica Et Biophysica Acta*, *1218*(2), 129-135. https://doi.org/10.1016/0167-4781(94)90001-9

Nadal-Ginard, B., Ellison, G. M., & Torella, D. (2014). The cardiac stem cell compartment is indispensable for myocardial cell homeostasis, repair and regeneration in the adult. *Stem Cell Research*, *13*(3), 615-630. https://doi.org/10.1016/j.scr.2014.04.008

Nakamura, T., Saito, H., & Takekawa, M. (2013). SAPK pathways and p53 cooperatively regulate PLK4 activity and centrosome integrity under stress. *Nature Communications*, *4*, 1775. https://doi.org/10.1038/ncomms2752

Nakamuta, A., Yoshido, K., & Naoki, H. (2022). Stem cell homeostasis regulated by hierarchy and neutral competition. *Communications Biology*, *5*(1). https://doi.org/10.1038/s42003-022-04218-7

Neophytou, C., & Pitsouli, C. (2022). Biotin controls intestinal stem cell mitosis and host-microbiome interactions. *Cell Reports*, *38*(10). https://doi.org/10.1016/j.celrep.2022.110505

Neumüller, R. A., & Knoblich, J. A. (2009). Dividing cellular asymmetry: Asymmetric cell division and its implications for stem cells and cancer. *Genes & Development*, *23*(23), 2675-2699. https://doi.org/10.1101/gad.1850809

Nicholson, L., Singh, G. K., Osterwalder, T., Roman, G. W., Davis, R. L., & Keshishian, H. (2008). Spatial and temporal control of gene expression in *Drosophila* using the inducible GeneSwitch GAL4 system. I. Screen for larval nervous system drivers. *Genetics*, *178*(1), 215-234. https://doi.org/10.1534/genetics.107.081968

Nishimura, K., Fukagawa, T., Takisawa, H., Kakimoto, T., & Kanemaki, M. (2009). An auxin-based degron system for the rapid depletion of proteins in nonplant cells. *Nature Methods*, *6*(12), 917-922. https://doi.org/10.1038/nmeth.1401

Novak, Z. A., Wainman, A., Gartenmann, L., & Raff, J. W. (2016). Cdk1 Phosphorylates *Drosophila* Sas-4 to Recruit Polo to Daughter Centrioles and Convert Them to Centrosomes. *Developmental Cell*, *37*(6), 545-557. https://doi.org/10.1016/j.devcel.2016.05.022

O'Brien, L. E. (2022). Tissue Homeostasis and Non-Homeostasis: From Cell Life Cycles to Organ States. *Annual Review of Cell and Developmental Biology*, *38*(1), 395-418. https://doi.org/10.1146/annurev-cellbio-120420-114855

Ohlstein, B., & Spradling, A. (2006). The adult *Drosophila* posterior midgut is maintained by pluripotent stem cells. *Nature*, *439*(7075), 470-474. https://doi.org/10.1038/nature04333

Okumura, R., & Takeda, K. (2017). Roles of intestinal epithelial cells in the maintenance of gut homeostasis. *Experimental & Molecular Medicine*, *49*(5). https://doi.org/10.1038/emm.2017.20

Osman, D., Buchon, N., Chakrabarti, S., Huang, Y.-T., Su, W.-C., Poidevin, M., Tsai, Y.-C., & Lemaitre, B. (2012). Autocrine and paracrine unpaired signaling regulate intestinal stem cell maintenance and division. *Journal of Cell Science*, *125*(24), 5944-5949. https://doi.org/10.1242/jcs.113100

Otsuki, L., & Brand, A. H. (2018). Cell cycle heterogeneity directs the timing of neural stem cell activation from quiescence. *Science*, *360*(6384), 99-102. https://doi.org/10.1126/science.aan8795

Øvrebø, J. I., & Edgar, B. A. (2018). Polyploidy in tissue homeostasis and regeneration. *Development*, *145*(14). https://doi.org/10.1242/dev.156034

Pan, D. (2010). The Hippo Signaling Pathway in Development and Cancer. *Developmental cell*, *19*(4), 491-505. https://doi.org/10.1016/j.devcel.2010.09.011

Panayidou, S., & Apidianakis, Y. (2013). Regenerative Inflammation: Lessons from *Drosophila* Intestinal Epithelium in Health and Disease. *Pathogens*, *2*(2). https://doi.org/10.3390/pathogens2020209

Pannala, V. R., Bhat, P. J., Bhartiya, S., & Venkatesh, K. V. (2010). Systems biology of GAL regulon in Saccharomyces cerevisiae. *WIREs Systems Biology and Medicine*, *2*(1), 98-106. https://doi.org/10.1002/wsbm.38

Pannérec, A., Marazzi, G., & Sassoon, D. (2012). Stem cells in the hood: The skeletal muscle niche. *Trends in Molecular Medicine*, *18*(10), 599-606. https://doi.org/10.1016/j.molmed.2012.07.004

Park, J.-S., Na, H.-J., Pyo, J.-H., Kim, Y.-S., & Yoo, M.-A. (2015). Requirement of ATR for maintenance of intestinal stem cells in aging *Drosophila*. *Aging*, *7*. https://doi.org/10.18632/aging.100743

Pascut, D., Pratama, M. Y., Gilardi, F., Giuffrè, M., Crocè, L. S., & Tiribelli, C. (2020). Weighted miRNA co-expression networks analysis identifies circulating miRNA predicting overall survival in hepatocellular carcinoma patients. *Scientific Reports*, *10*(1). https://doi.org/10.1038/s41598-020-75945-2

Patel, P. H., Dutta, D., & Edgar, B. A. (2015). Niche Appropriation by *Drosophila* Intestinal Stem Cell Tumors. *Nature cell biology*, *17*(9), 1182-1192. https://doi.org/10.1038/ncb3214

Patterson, R. A., Juarez, M. T., Hermann, A., Sasik, R., Hardiman, G., & McGinnis, W. (2013). Serine Proteolytic Pathway Activation Reveals an Expanded Ensemble of Wound Response Genes in *Drosophila*. *PLOS ONE*, *8*(4). https://doi.org/10.1371/journal.pone.0061773

Pellettieri, J., & Sánchez Alvarado, A. (2007). Cell turnover and adult tissue homeostasis: From humans to planarians. *Annual Review of Genetics*, *41*, 83-105. https://doi.org/10.1146/annurev.genet.41.110306.130244

Peng, Z., Rojas, A. P., Kropff, E., Bahnfleth, W., Buonanno, G., Dancer, S., Kurnitski, J., Li, Y., Loomans, M., Marr, L., Morawska, L., Nazaroff, W., Noakes, C., Querol, X., Sekhar, C., Tellier, R., Greenhalgh, T., Bourouiba, L., Boerstra, A., … Jimenez, J. (2022). Practical Indicators for Risk of Airborne Transmission in Shared Indoor Environments and Their Application to COVID-19 Outbreaks. *Environmental Science and Technology*, *56*(2), 1125-1137. https://doi.org/10.1021/acs.est.1c06531

Peterson, L. W., & Artis, D. (2014). Intestinal epithelial cells: Regulators of barrier function and immune homeostasis. *Nature Reviews. Immunology*, *14*(3). https://doi.org/10.1038/nri3608

Petsakou, A., & Perrimon, N. (2023). Bioelectric regulation of intestinal stem cells. *Trends in cell biology*, *33*(7), 555-567. https://doi.org/10.1016/j.tcb.2022.10.003

Picerno, A., Stasi, A., Franzin, R., Curci, C., di Bari, I., Gesualdo, L., & Sallustio, F. (2021). Why stem/progenitor cells lose their regenerative potential. *World Journal of Stem Cells*, *13*(11), 1714-1732. https://doi.org/10.4252/wjsc.v13.i11.1714

Pichavant, C., & Pavlath, G. K. (2014). Incidence and severity of myofiber branching with regeneration and aging. *Skeletal Muscle*, *4*(1). https://doi.org/10.1186/2044-5040-4-9

Pillitteri, L. J., Guo, X., & Dong, J. (2016). Asymmetric cell division in plants: Mechanisms of symmetry breaking and cell fate determination. *Cellular and Molecular Life Sciences*, *73*(22), 4213-4229. https://doi.org/10.1007/s00018-016-2290-2

Pintard, L., & Archambault, V. (2018). A unified view of spatio-temporal control of mitotic entry: Polo kinase as the key. *Open Biology*, *8*(8). https://doi.org/10.1098/rsob.180114

Poon, R. Y. C. (2016). Cell Cycle Control: A System of Interlinking Oscillators. In A. S. Coutts & L. Weston (Eds.), *Cell Cycle Oscillators: Methods and Protocols* (pp. 3-19). Springer. https://doi.org/10.1007/978-1-4939-2957-3_1

Potter, C. J., & Luo, L. (2011). Using the Q system in *Drosophila* melanogaster. *Nature Protocols*, *6*(8). https://doi.org/10.1038/nprot.2011.347

Potter, C. J., Tasic, B., Russler, E. V., Liang, L., & Luo, L. (2010). The Q system: A repressible binary system for transgene expression, lineage tracing, and mosaic analysis. *Cell*, *141*(3), 536-548. https://doi.org/10.1016/j.cell.2010.02.025

Prigent, C., & Dimitrov, S. (2003). Phosphorylation of serine 10 in histone H3, what for? *Journal of Cell Science*, *116*(18), 3677-3685. https://doi.org/10.1242/jcs.00735

Puig Barbe, A. (2018). A network of bHLH factors controls self-renewal and bipotential differentiation in the *Drosophila* intestine [Phd, Cardiff University]. https://orca.cardiff.ac.uk/id/eprint/119786/

Puig, Ó., Marr, M. T., Ruhf, M.-L., & Tjian, R. (2003). Control of cell number by*Drosophila*FOXO: Downstream and feedback regulation of the insulin receptor pathway. *Genes &Amp; Development*, *17*(16). https://doi.org/10.1101/gad.1098703

Puig-Barbe, A., Dettmann, S., Nirello, V. D., Azami, S., Edgar, B. A., Varga-Weisz, P., Korzelius, J., & Navascués, J. de. (2023). *Homo- and heterodimerization of bHLH transcription factors balance stemness with bipotential differentiation in the Drosophila gut*. bioRxiv. https://doi.org/10.1101/685347

Qian, Y., Li, T., Zhou, S., Chen, X., & Yang, Y. (2023). A Single-Component Optogenetic Gal4-UAS System Allows Stringent Control of Gene Expression in Zebrafish and *Drosophila*. *ACS Synthetic Biology*, *12*(3), 664-671. https://doi.org/10.1021/acssynbio.2c00410

Quintino, L., Namislo, A., Davidsson, M., Breger, L. S., Kavanagh, P., Avallone, M., Elgstrand-Wettergren, E., Isaksson, C., & Lundberg, C. (2018). Destabilizing Domains Enable Long-Term and Inert Regulation of GDNF Expression in the Brain. *Molecular Therapy - Methods & Clinical Development*, *11*, 29-39. https://doi.org/10.1016/j.omtm.2018.08.008

Radford, S. J., Go, A. M. M., & McKim, K. S. (2017). Cooperation Between Kinesin Motors Promotes Spindle Symmetry and Chromosome Organization in Oocytes. *Genetics*, *205*(2), 517-527. https://doi.org/10.1534/genetics.116.194647

Radtke, F., & Clevers, H. (2005). Self-renewal and cancer of the gut: Two sides of a coin. *Science*, *307*(5717), 1904-1909. https://doi.org/10.1126/science.1104815

Rakhit, R., Edwards, S. R., Iwamoto, M., & Wandless, T. J. (2011). Evaluation of FKBP and DHFR based destabilizing domains in Saccharomyces cerevisiae. *Bioorganic &Amp; Medicinal Chemistry Letters*, *21*(17). https://doi.org/10.1016/j.bmcl.2011.06.006

Ramadan, R., van Driel, M. S., Vermeulen, L., & van Neerven, S. M. (2022). Intestinal stem cell dynamics in homeostasis and cancer. *Trends in Cancer*, *8*(5), 416-425. https://doi.org/10.1016/j.trecan.2022.01.011

Reaume, C. J., & Sokolowski, M. B. (2006). The nature of *Drosophila* melanogaster. *Current Biology: CB*, *16*(16), R623-628. https://doi.org/10.1016/j.cub.2006.07.042

Reilein, A., Melamed, D., Tavaré, S., & Kalderon, D. (2018). Division-independent differentiation mandates proliferative competition among stem cells. *Proceedings of the National Academy of Sciences of the United States of America*, *115*(14), E3182-E3191. https://doi.org/10.1073/pnas.1718646115

Reilein, A. R. (2017). Multiple stem cells, population asymmetry and position-dependent heterogeneity emerge as common features of a niche for *Drosophila* Follicle Stem Cells and mammalian Intestinal Stem Cells. The Node. https://thenode.biologists.com/multiple-stem-cells-population-asymmetry-position-dependent-heterogeneity-emerge-common-features-niche-*Drosophila*-follicle-stem-cells-mammalian-intestinal-stem-cells/research/

Ren, F., Wang, B., Tao, Y., Yun, E. Y., Ip, Y. T., & Jen, J. (2010). Hippo signaling regulates *Drosophila* intestine stem cell proliferation through multiple pathways. *Proceedings of the National Academy of Sciences*, *107*(49). https://doi.org/10.1073/pnas.1012759107

Rhind, N., & Russell, P. (2012). Signaling Pathways that Regulate Cell Division. *Cold Spring Harbor Perspectives in Biology*, *4*(10). https://doi.org/10.1101/cshperspect.a005942

Riabinina, O., & Potter, C. J. (2016). The Q-System: A Versatile Expression System for *Drosophila*. *Methods in Molecular Biology*, *1478*, 53-78. https://doi.org/10.1007/978-1-4939-6371-3_3

Riahi, H., Brekelmans, C., Foriel, S., Merkling, S. H., Lyons, T. A., Itskov, P. M., Kleefstra, T., Ribeiro, C., Rij, R. P. van, Kramer, J. M., & Schenck, A. (2019). The histone methyltransferase G9a regulates tolerance to oxidative stress–induced energy consumption. *PLOS Biology*, *17*(3). https://doi.org/10.1371/journal.pbio.2006146

Roman, G., Endo, K., Zong, L., & Davis, R. L. (2001). P{Switch}, a system for spatial and temporal control of gene expression in *Drosophila* melanogaster. *Proceedings of the National Academy of Sciences*, *98*(22), 12602-12607. https://doi.org/10.1073/pnas.221303998

Roxström-Lindquist, K., Terenius, O., & Faye, I. (2004). Parasite-specific immune response in adult *Drosophila* melanogaster: A genomic study. *EMBO Reports*, *5*(2), 207-212. https://doi.org/10.1038/sj.embor.7400073

Saelens, W., Cannoodt, R., & Saeys, Y. (2018). A comprehensive evaluation of module detection methods for gene expression data. *Nature Communications*, *9*(1). https://doi.org/10.1038/s41467-018-03424-4

Sagaradze, G., Basalova, N., Kirpatovsky, V., Ohobotov, D., Nimiritsky, P., Grigorieva, O., Popov, V., Kamalov, A., Tkachuk, V., & Efimenko, A. (2019). A magic kick for regeneration: Role of mesenchymal stromal cell secretome in spermatogonial stem cell niche recovery. *Stem Cell Research & Therapy*, *10*(1). https://doi.org/10.1186/s13287-019-1479-3

Sánchez-Baizán, N., Ribas, L., & Piferrer, F. (2022). Improved biomarker discovery through a plot twist in transcriptomic data analysis. *BMC Biology*, *20*(1). https://doi.org/10.1186/s12915-022-01398-w

Savoian, M. S., & Glover, D. M. (2010). *Drosophila* Klp67A binds prophase kinetochores to subsequently regulate congression and spindle length. *Journal of Cell Science*, *123*(5), 767-776. https://doi.org/10.1242/jcs.055905

Sawai, C. M., Babovic, S., Upadhaya, S., Knapp, D. J. H. F., Lavin, Y., Lau, C. M., Goloborodko, A., Feng, J., Fujisaki, J., Ding, L., Mirny, L. A., Merad, M., Eaves, C. J., & Reizis, B. (2016). Hematopoietic Stem Cells Are the Major Source of Multilineage Hematopoiesis in Adult Animals. *Immunity*, *45*(3), 597-609. https://doi.org/10.1016/j.immuni.2016.08.007

Sawicka, A., & Seiser, C. (2012). Histone H3 phosphorylation – A versatile chromatin modification for different occasions. *Biochimie*, *94*(11), 2193-2201. https://doi.org/10.1016/j.biochi.2012.04.018

Schneider, C. A., Rasband, W. S., & Eliceiri, K. W. (2012). NIH Image to ImageJ: 25 years of image analysis. *Nature Methods*, *9*(7), Article 7. https://doi.org/10.1038/nmeth.2089

Schweitzer, B. I., Dicker, A. P., & Bertino, J. R. (1990). Dihydrofolate reductase as a therapeutic target. *The FASEB Journal*, *4*(8), 2441-2452. https://doi.org/10.1096/fasebj.4.8.2185970

Scialo, F., Sriram, A., Stefanatos, R., & Sanz, A. (2016). Practical Recommendations for the Use of the GeneSwitch Gal4 System to Knock-Down Genes in *Drosophila* melanogaster. *PLoS ONE*, *11*(8). https://doi.org/10.1371/journal.pone.0161817

Sei, Y., Feng, J., Chow, C. C., & Wank, S. A. (2019). Asymmetric cell division-dominant neutral drift model for normal intestinal stem cell homeostasis. *American Journal of Physiology - Gastrointestinal and Liver Physiology*, *316*(1), G64-G74. https://doi.org/10.1152/ajpgi.00242.2018

Sekelsky, J. (2017). DNA Repair in *Drosophila*: Mutagens, Models, and Missing Genes. *Genetics*, *205*(2). https://doi.org/10.1534/genetics.116.186759

Senturk, S., Shirole, N. H., Nowak, D. G., Corbo, V., Pal, D., Vaughan, A., Tuveson, D. A., Trotman, L. C., Kinney, J. B., & Sordella, R. (2017). Rapid and tunable method to temporally control gene editing based on conditional Cas9 stabilization. *Nature Communications*, *8*(1),. https://doi.org/10.1038/ncomms14370

Sethi, S., & Wang, J. W. (2017). A versatile genetic tool for post-translational control of gene expression in *Drosophila* melanogaster. *eLife*, *6*. https://doi.org/10.7554/eLife.30327

Shahriyari, L., & Komarova, N. L. (2013). Symmetric vs. Asymmetric Stem Cell Divisions: An Adaptation against Cancer? *PLoS ONE*, *8*(10). https://doi.org/10.1371/journal.pone.0076195

Sharp, D. J., & Rath, U. (2009). Mitosis: KLP61F Goes Wee! *Current Biology*, *19*(19), R899-R901. https://doi.org/10.1016/j.cub.2009.09.003

Sher, N., Von Stetina, J. R., Bell, G. W., Matsuura, S., Ravid, K., & Orr-Weaver, T. L. (2013). Fundamental differences in endoreplication in mammals and *Drosophila* revealed by analysis of endocycling and endomitotic cells. *Proceedings of the National Academy of Sciences of the United States of America*, *110*(23), 9368-9373. https://doi.org/10.1073/pnas.1304889110

Shetty, A., Reim, N. I., & Winston, F. (2019). Auxin-inducible degron system for depletion of proteins in S. cerevisiae. *Current protocols in molecular biology*, *128*(1). https://doi.org/10.1002/cpmb.104

Shi, L., Kong, R., Li, Z., Zhao, H., Ma, R., Bai, G., Li, J., & Li, Z. (2021). Identification of a new allele of O-fucosyltransferase 1 involved in *Drosophila* intestinal stem cell regulation. *Biology Open*, *10*(11). https://doi.org/10.1242/bio.058910

Shi, Z., Li, X., Zhang, L., Luo, Y., Shrestha, B., & Hu, X. (2021). Potential Novel Modules and Hub Genes as Prognostic Candidates of Thyroid Cancer by Weighted Gene Co-Expression Network Analysis. *International Journal of General Medicine*, *14*, 9433-9444. https://doi.org/10.2147/IJGM.S329128

Shin, M., Ferguson, M., Willms, R. J., Jones, L. O., Petkau, K., & Foley, E. (2022). Immune regulation of intestinal-stem-cell function in *Drosophila*. *Stem Cell Reports*, *17*(4), 741-755. https://doi.org/10.1016/j.stemcr.2022.02.009

Singh, S. R. (2012). Stem cell niche in tissue homeostasis, aging and cancer. *Current Medicinal Chemistry*, *19*(35), 5965-5974. https://doi.org/10.2174/092986712804485917

Sivakumar, S., & Gorbsky, G. J. (2015). Spatiotemporal regulation of the anaphase-promoting complex in mitosis. *Nature Reviews Molecular Cell Biology*, *16*(2). https://doi.org/10.1038/nrm3934

Snippert, H. J., Flier, L. G. van der, Sato, T., Es, J. H. van, Born, M. van den, Kroon-Veenboer, C., Barker, N., Klein, A. M., Rheenen, J. van, Simons, B. D., & Clevers, H. (2010). Intestinal Crypt Homeostasis Results from Neutral Competition between Symmetrically Dividing Lgr5 Stem Cells. *Cell*, *143*(1), 134-144. https://doi.org/10.1016/j.cell.2010.09.016

Srinivasan, T., Than, E. B., Bu, P., Tung, K.-L., Chen, K.-Y., Augenlicht, L., Lipkin, S. M., & Shen, X. (2016). Notch signalling regulates asymmetric division and inter-conversion between lgr5 and bmi1 expressing intestinal stem cells. *Scientific Reports*, *6*(1). https://doi.org/10.1038/srep26069

Staley, B. K., & Irvine, K. D. (2010). Warts and Yorkie Mediate Intestinal Regeneration by Influencing Stem Cell Proliferation. *Current Biology*, *20*(17), 1580-1587. https://doi.org/10.1016/j.cub.2010.07.041

Stebbins, M. J., Urlinger, S., Byrne, G., Bello, B., Hillen, W., & Yin, J. C. P. (2001). Tetracycline-inducible systems for *Drosophila*. *Proceedings of the National Academy of Sciences of the United States of America*, *98*(19), 10775-10780. https://doi.org/10.1073/pnas.121186498

Stine, R. R., & Matunis, E. L. (2013). Stem cell competition: Finding balance in the niche. *Trends in Cell Biology*, *23*(8), 357-364. https://doi.org/10.1016/j.tcb.2013.03.001

Strilbytska, O. M., Semaniuk, U. V., Storey, K. B., Yurkevych, I. S., & Lushchak, O. (2020). Insulin Signaling in Intestinal Stem and Progenitor Cells as an Important Determinant of Physiological and Metabolic Traits in *Drosophila*. *Cells*, *9*(4). https://doi.org/10.3390/cells9040803

Strzalka, W., & Ziemienowicz, A. (2011). Proliferating cell nuclear antigen (PCNA): A key factor in DNA replication and cell cycle regulation. *Annals of Botany*, *107*(7), 1127-1140. https://doi.org/10.1093/aob/mcq243

Sunchu, B., & Cabernard, C. (2020). Principles and mechanisms of asymmetric cell division. *Development*, *147*(13). https://doi.org/10.1242/dev.167650

Swanhart, L. M., Sanders, A. N., & Duronio, R. J. (2007). Normal regulation of Rbf1/E2f1 target genes in *Drosophila* type 1 protein phosphatase mutants. *Developmental Dynamics*, *236*(9), 2567-2577. https://doi.org/10.1002/dvdy.21265

Swanson, C. I., Meserve, J. H., McCarter, P. C., Thieme, A., Mathew, T., Elston, T. C., & Duronio, R. J. (2015). Expression of an S phase-stabilized version of the CDK inhibitor Dacapo can alter endoreplication. *Development*, *142*(24), 4288-4298. https://doi.org/10.1242/dev.115006

Takashima, S., Aghajanian, P., Younossi-Hartenstein, A., & Hartenstein, V. (2016). *Origin and dynamic lineage characteristics of the developing Drosophila midgut stem cells*. https://www.sciencedirect.com/science/article/pii/S0012160616303748

Tanaka, S., Miyazawa-Onami, M., Iida, T., & Araki, H. (2015). iAID: An improved auxin-inducible degron system for the construction of a «tight» conditional mutant in the budding yeast Saccharomyces cerevisiae. *Yeast*, *32*(8), 567-581. https://doi.org/10.1002/yea.3080

Tang, R., & Liu, H. (2019). Identification of Temporal Characteristic Networks of Peripheral Blood Changes in Alzheimer's Disease Based on Weighted Gene Co-expression Network Analysis. *Frontiers in Aging Neuroscience*, *11*. https://doi.org/10.3389/fnagi.2019.00083

Thorel, F., Népote, V., Avril, I., Kohno, K., Desgraz, R., Chera, S., & Herrera, P. L. (2010). Conversion of adult pancreatic α-cells to β-cells after extreme β-cell loss. *Nature*, *464*(7292). https://doi.org/10.1038/nature08894

Tian, A., Benchabane, H., & Ahmed, Y. (2018). Wingless/Wnt Signaling in Intestinal Development, Homeostasis, Regeneration and Tumorigenesis: A *Drosophila* Perspective. *Journal of Developmental Biology*, *6*(2). https://doi.org/10.3390/jdb6020008

Tian, A., Benchabane, H., Wang, Z., & Ahmed, Y. (2016). Regulation of Stem Cell Proliferation and Cell Fate Specification by Wingless/Wnt Signaling Gradients Enriched at Adult Intestinal Compartment Boundaries. *PLOS Genetics*, *12*(2). https://doi.org/10.1371/journal.pgen.1005822

Tian, A., & Jen, J. (2014). Intestinal epithelium-derived BMP controls stem cell self-renewal in *Drosophila* adult midgut. *eLife*, *3*. https://doi.org/10.7554/elife.01857

Tian, A., & Jen, J. (2017). Dual role of BMP signaling in the regulation of *Drosophila* intestinal stem cell self-renewal. *Fly*, *11*(4). https://doi.org/10.1080/19336934.2017.1384104

Tian, A., Shi, Q., Jiang, A., Li, S., Wang, B., & Jiang, J. (2015). Injury-stimulated Hedgehog signaling promotes regenerative proliferation of *Drosophila* intestinal stem cells. *The Journal of Cell Biology*, *208*(6), 807-819. https://doi.org/10.1083/jcb.201409025

Trinca, T. (2022). *Developing a Drosophila model of radiation induced toxicity to identify risk loci* [Phd, Cardiff University]. https://orca.cardiff.ac.uk/id/eprint/154017/

Trost, M., Blattner, A. C., & Lehner, C. F. (2016). Regulated protein depletion by the auxin-inducible degradation system in *Drosophila* melanogaster. *Fly*, *10*(1). https://doi.org/10.1080/19336934.2016.1168552

Uy Gonzales, K. A., & Fuchs, E. (2017). Skin and Its Regenerative Powers: An Alliance between Stem Cells and Their Niche. *Developmental cell*, *43*(4), 387-401. https://doi.org/10.1016/j.devcel.2017.10.001

van Berlo, J. H., & Molkentin, J. D. (2014). An emerging consensus on cardiac regeneration. *Nature Medicine*, *20*(12). https://doi.org/10.1038/nm.3764

Vancamelbeke, M., & Vermeire, S. (2017). The intestinal barrier: A fundamental role in health and disease. *Expert review of gastroenterology & hepatology*, *11*(9), 821-834. https://doi.org/10.1080/17474124.2017.1343143

Vardy, L., & Orr-Weaver, T. L. (2007). The *Drosophila* PNG Kinase Complex Regulates the Translation of Cyclin B. *Developmental Cell*, *12*(1), 157-166. https://doi.org/10.1016/j.devcel.2006.10.017

Veenstra, J. A., Agricola, H.-J., & Sellami, A. (2008). Regulatory peptides in fruit fly midgut. *Cell and Tissue Research*, *334*(3), 499-516. https://doi.org/10.1007/s00441-008-0708-3

Velichko, A. K., Petrova, N. V., Kantidze, O. L., & Razin, S. V. (2012). Dual effect of heat shock on DNA replication and genome integrity. *Molecular Biology of the Cell*, *23*(17), 3450-3460. https://doi.org/10.1091/mbc.e11-12-1009

Venkei, Z. G., & Yamashita, Y. M. (2018). Emerging mechanisms of asymmetric stem cell division. *The Journal of Cell Biology*, *217*(11), 3785-3795. https://doi.org/10.1083/jcb.201807037

Venken, K. J. T., Simpson, J. H., & Bellen, H. J. (2011). Genetic Manipulation of Genes and Cells in the Nervous System of the Fruit Fly. *Neuron*, *72*(2). https://doi.org/10.1016/j.neuron.2011.09.021

Vermeulen, L., & Snippert, H. J. (2014). Stem cell dynamics in homeostasis and cancer of the intestine. *Nature Reviews. Cancer*, *14*(7), 468-480. https://doi.org/10.1038/nrc3744

Vertii, A., Kaufman, P. D., Hehnly, H., & Doxsey, S. (2018). New dimensions of asymmetric division in vertebrates. *Cytoskeleton*, *75*(3), 87-102. https://doi.org/10.1002/cm.21434

Viana, F. (2016). TRPA1 channels: Molecular sentinels of cellular stress and tissue damage. *The Journal of Physiology*, *594*(15), 4151-4169. https://doi.org/10.1113/JP270935

Vigneron, S., Sundermann, L., Labbé, J.-C., Pintard, L., Radulescu, O., Castro, A., & Lorca, T. (2018). Cyclin A-cdk1-Dependent Phosphorylation of Bora Is the Triggering Factor Promoting Mitotic Entry. *Developmental Cell*, *45*(5), 637-650.e7. https://doi.org/10.1016/j.devcel.2018.05.005

Wang, C. C. N., Li, C. Y., Cai, J.-H., Sheu, P. C.-Y., Tsai, J. J. P., Wu, M.-Y., Li, C.-J., & Hou, M.-F. (2019). Identification of Prognostic Candidate Genes in Breast Cancer by Integrated Bioinformatic Analysis. *Journal of Clinical Medicine*, *8*(8). https://doi.org/10.3390/jcm8081160

Wang, J., Li, C., & Wang, E. (2010). Potential and flux landscapes quantify the stability and robustness of budding yeast cell cycle network. *Proceedings of the National Academy of Sciences*, *107*(18), 8195-8200. https://doi.org/10.1073/pnas.0910331107

Wang, J., Zhu, Y., Zhang, C., Duan, R., Kong, F., Zheng, X., & Hua, Y. (2022). A conserved role of bam in maintaining metabolic homeostasis via regulating intestinal microbiota in *Drosophila*. *PeerJ*, *10*. https://doi.org/10.7717/peerj.14145

Wang, L., Dai, W., & Lu, L. (2011). Hyperosmotic Stress-Induced Corneal Epithelial Cell Death through Activation of Polo-like Kinase 3 and c-Jun. *Investigative Ophthalmology & Visual Science*, *52*(6), 3200-3206. https://doi.org/10.1167/iovs.10-6485

Wang, L., Dai, W., & Lu, L. (2014). Osmotic Stress-induced Phosphorylation of H2AX by Polo-like Kinase 3 Affects Cell Cycle Progression in Human Corneal Epithelial Cells *. *Journal of Biological Chemistry*, *289*(43), 29827-29835. https://doi.org/10.1074/jbc.M114.597161

Wang, W., Jiang, W., Hou, L., Duan, H., Wu, Y., Xu, C., Tan, Q., Li, S., & Zhang, D. (2017). Weighted gene co-expression network analysis of expression data of monozygotic twins identifies specific modules and hub genes related to BMI. *BMC Genomics*, *18*. https://doi.org/10.1186/s12864-017-4257-6

Weterings, S. D. C., van Oostrom, M. J., & Sonnen, K. F. (2021). Building bridges between fields: Bringing together development and homeostasis. *Development (Cambridge, England)*, *148*(14). https://doi.org/10.1242/dev.193268

White-Cooper, H. (2012). Tissue, cell type and stage-specific ectopic gene expression and RNAi induction in the *Drosophila* testis. *Spermatogenesis*, *2*(1), 11-22. https://doi.org/10.4161/spmg.19088

Wickham, H. (2011). Ggplot2. *WIREs Computational Statistics*, *3*(2), 180-185. https://doi.org/10.1002/wics.147

Wilmington, S. R., & Matouschek, A. (2016). An Inducible System for Rapid Degradation of Specific Cellular Proteins Using Proteasome Adaptors. *PLOS ONE*, *11*(4). https://doi.org/10.1371/journal.pone.0152679

Wilson, A., Laurenti, E., Oser, G., van der Wath, R. C., Blanco-Bose, W., Jaworski, M., Offner, S., Dunant, C. F., Eshkind, L., Bockamp, E., Lió, P., Macdonald, H. R., & Trumpp, A. (2008). Hematopoietic stem cells reversibly switch from dormancy to self-renewal during homeostasis and repair. *Cell*, *135*(6), 1118-1129. https://doi.org/10.1016/j.cell.2008.10.048

Wilson, S. R., Gerhold, K. A., Bifolck-Fisher, A., Liu, Q., Patel, K. N., Dong, X., & Bautista, D. M. (2011). TRPA1 is required for histamine-independent, Mas-related G protein–coupled receptor–mediated itch. *Nature Neuroscience*, *14*(5). https://doi.org/10.1038/nn.2789

Winer, D. A., Luck, H., Tsai, S., & Winer, S. (2016). The Intestinal Immune System in Obesity and Insulin Resistance. *Cell Metabolism*, *23*(3), 413-426. https://doi.org/10.1016/j.cmet.2016.01.003

Wright, V. M., Vogt, K. L., Smythe, E., & Zeidler, M. P. (2011). Differential activities of the *Drosophila* JAK/STAT pathway ligands Upd, Upd2 and Upd3. *Cellular Signalling*, *23*(5), 920-927. https://doi.org/10.1016/j.cellsig.2011.01.020

Wu, Z., Hai, E., Di, Z., Ma, R., Shang, F., Wang, Y., Wang, M., Liang, L., Rong, Y., Pan, J., Wu, W., Su, R., Wang, Z., Wang, R., Zhang, Y., & Li, J. (2020). Using WGCNA (weighted gene co-expression network analysis) to identify the hub genes of skin hair follicle development in fetus stage of Inner Mongolia cashmere goat. *PLoS ONE*, *15*(12). https://doi.org/10.1371/journal.pone.0243507

Xiang, J., Bandura, J., Zhang, P., Jin, Y., Reuter, H., & Edgar, B. A. (2017). EGFR-dependent TOR-independent endocycles support *Drosophila* gut epithelial regeneration. *Nature Communications*, *8*. https://doi.org/10.1038/ncomms15125

Xu, C., Luo, J., He, L., Montell, C., & Perrimon, N. (2017). Oxidative stress induces stem cell proliferation via TRPA1/RyR-mediated Ca2+ signaling in the *Drosophila* midgut. *eLife*, *6*. https://doi.org/10.7554/eLife.22441

Xu, D., Dai, W., & Li, C. (2017). Polo-like kinase 3, hypoxic responses, and tumorigenesis. *Cell Cycle*, *16*(21), 2032-2036. https://doi.org/10.1080/15384101.2017.1373224

Xu, N., Wang, S. Q., Tan, D., Gao, Y., Lin, G., & Xi, R. (2011). EGFR, Wingless and JAK/STAT signaling cooperatively maintain *Drosophila* intestinal stem cells. *Developmental Biology*, *354*(1), 31-43. https://doi.org/10.1016/j.ydbio.2011.03.018

Xu, P., Yang, J., Liu, J., Yang, X., Liao, J., Yuan, F., Xu, Y., Liu, B., & Chen, Q. (2018). Identification of glioblastoma gene prognosis modules based on weighted gene co-expression network analysis. *BMC Medical Genomics*, *11*(1), 96. https://doi.org/10.1186/s12920-018-0407-1

Yamada, R., Deshpande, S. A., Keebaugh, E. S., Ehrlich, M. R., Soto Obando, A., & Ja, W. W. (2017). Mifepristone Reduces Food Palatability and Affects *Drosophila* Feeding and Lifespan. *The Journals of Gerontology. Series A, Biological Sciences and Medical Sciences*, *72*(2), 173-180. https://doi.org/10.1093/gerona/glw072

Yamaguchi, M., & Yoshida, H. (2018). *Drosophila* as a Model Organism. In M. Yamaguchi (Ed.), *Drosophila Models for Human Diseases* (pp. 1-10). Springer. https://doi.org/10.1007/978-981-13-0529-0_1

Yang, M., He, H., Peng, T., Lu, Y., & Yu, J. (2022). Identification of 9 Gene Signatures by WGCNA to Predict Prognosis for Colon Adenocarcinoma. *Computational Intelligence and Neuroscience*, *2022*. https://doi.org/10.1155/2022/8598046

Yang, R., Liu, F., Wang, J., Chen, X., Xie, J., & Xiong, K. (2019). Epidermal stem cells in wound healing and their clinical applications. *Stem Cell Research & Therapy*, *10*(1). https://doi.org/10.1186/s13287-019-1312-z

Yin, H., Price, F., & Rudnicki, M. A. (2013). Satellite Cells and the Muscle Stem Cell Niche. *Physiological Reviews*, *93*(1), 23-67. https://doi.org/10.1152/physrev.00043.2011

Yu, H., Du, X., Zhao, Q., Yin, C., & Song, W. (2022). Weighted gene Co-expression network analysis (WGCNA) reveals a set of hub genes related to chlorophyll metabolism process in chlorella (Chlorella vulgaris) response androstenedione. *Environmental Pollution*, *306*. https://doi.org/10.1016/j.envpol.2022.119360

Zakrzewski, W., Dobrzyński, M., Szymonowicz, M., & Rybak, Z. (2019). Stem cells: Past, present, and future. *Stem Cell Research & Therapy*, *10*(1). https://doi.org/10.1186/s13287-019-1165-5

Zamproni, L. N., Mundim, M. T. V. V., & Porcionatto, M. A. (2021). Neurorepair and Regeneration of the Brain: A Decade of Bioscaffolds and Engineered Microtissue. *Frontiers in Cell and Developmental Biology*, *9*. https://doi.org/10.3389/fcell.2021.649891

Zappia, M. P., Damschroder, D., Westacott, A., Wessells, R. J., & Frolov, M. V. (2023). *The RU486-dependent activation of the GeneSwitch system in adult muscles leads to severe adverse effects in Drosophila*. bioRxiv. https://doi.org/10.1101/2023.09.07.556712

Zeng, X., & Hou, S. X. (2015). Enteroendocrine cells are generated from stem cells through a distinct progenitor in the adult *Drosophila* posterior midgut. *Development*, *142*(4), 644-653. https://doi.org/10.1242/dev.113357

Zhang, H., Wang, C., Zhang, K., Kamau, P. M., Luo, A., Tian, L., & Lai, R. (2022). The role of TRPA1 channels in thermosensation. *Cell Insight*, *1*(6). https://doi.org/10.1016/j.cellin.2022.100059

Zhang, J., Huang, C., Liu, Z., Ren, S., Shen, Z., Han, K., Xin, W., He, G., & Liu, J. (2022). Screening of Potential Biomarkers in the Peripheral Serum for Steroid-Induced Osteonecrosis of the Femoral Head Based on WGCNA and Machine Learning Algorithms. *Disease Markers*, *2022*. https://doi.org/10.1155/2022/2639470

Zhang, J., Wan, L., Dai, X., Sun, Y., & Wei, W. (2014). Functional characterization of Anaphase Promoting Complex/Cyclosome (APC/C) E3 ubiquitin ligases in tumorigenesis. *Biochimica et Biophysica Acta (BBA) - Reviews on Cancer*, *1845*(2), 277-293. https://doi.org/10.1016/j.bbcan.2014.02.001

Zhang, W., Lou, Y.-R., Zhou, J., & He, Z. (2022). Editorial: Stem Cells in Tissue Homeostasis and Disease. *Frontiers in Cell and Developmental Biology*, *10*. https://www.frontiersin.org/article/10.3389/fcell.2022.876060

Zhang, Y., Lahmann, I., Baum, K., Shimojo, H., Mourikis, P., Wolf, J., Kageyama, R., & Birchmeier, C. (2021). Oscillations of Delta-like1 regulate the balance between differentiation and maintenance of muscle stem cells. *Nature Communications*, *12*(1). https://doi.org/10.1038/s41467-021-21631-4

Zhao, B., Tumaneng, K., & Guan, K.-L. (2011). The Hippo pathway in organ size control, tissue regeneration and stem cell self-renewal. *Nature cell biology*, *13*(8), 877-883. https://doi.org/10.1038/ncb2303

Zhao, X., & Moore, D. (2018). Neural stem cells: Developmental mechanisms and disease modeling. *Cell and tissue research*, *371*(1), 1-6. https://doi.org/10.1007/s00441-017-2738-1

Zheng, Y., & Pan, D. (2019). The Hippo Signaling Pathway in Development and Disease. *Developmental Cell*, *50*(3), 264-282. https://doi.org/10.1016/j.devcel.2019.06.003

Zhou, D., Tian, F., Tian, X., Sun, L., Huang, X., Zhao, F., Zhou, N., Chen, Z., Zhang, Q., Yang, M., Yang, Y., Guo, X., Li, Z., Liu, J., Wang, J., Wang, J., Wang, B., Zhang, G., Sun, B., … Li, X. (2020). Diagnostic evaluation of a deep learning model for optical diagnosis of colorectal cancer. *Nature Communications*, *11*(1). https://doi.org/10.1038/s41467-020-16777-6

Zhou, F., Rasmussen, A., Lee, S., & Agaisse, H. (2013). The UPD3 cytokine couples environmental challenge and intestinal stem cell division through modulation of JAK/STAT signaling in the stem cell microenvironment. *Developmental Biology*, *373*(2), 383-393. https://doi.org/10.1016/j.ydbio.2012.10.023

Zhou, J., & Boutros, M. (2023). Intestinal stem cells and their niches in homeostasis and disease. *Cells & Development*, *175*. https://doi.org/10.1016/j.cdev.2023.203862

Zhou, Q., Zhou, L.-Q., Li, S.-H., Yuan, Y.-W., Liu, L., Wang, J.-L., Wu, D.-Z., Wu, Y., & Xin, L. (2020). Identification of subtype-specific genes signature by WGCNA for prognostic prediction in diffuse type gastric cancer. *Aging (Albany NY)*, *12*(17), 17418-17435. https://doi.org/10.18632/aging.103743

Zhou, X., Ding, G., Li, J., Xiang, X., Rushworth, E., & Song, W. (2020). Physiological and Pathological Regulation of Peripheral Metabolism by Gut-Peptide Hormones in *Drosophila*. *Frontiers in Physiology*, *11*. https://doi.org/10.3389/fphys.2020.577717

Zielke, N., & Edgar, B. A. (2015). FUCCI sensors: Powerful new tools for analysis of cell proliferation. *Wiley Interdisciplinary Reviews. Developmental Biology*, *4*(5), 469-487. https://doi.org/10.1002/wdev.189

Zielke, N., Kim, K. J., Tran, V., Shibutani, S. T., Bravo, M.-J., Nagarajan, S., van Straaten, M., Woods, B., von Dassow, G., Rottig, C., Lehner, C. F., Grewal, S. S., Duronio, R. J., & Edgar, B. A. (2011). Control of *Drosophila* endocycles by E2F and CRL4CDT2. *Nature*, *480*(7375). https://doi.org/10.1038/nature10579

Zielke, N., Korzelius, J., van Straaten, M., Bender, K., Schuhknecht, G. F. P., Dutta, D., Xiang, J., & Edgar, B. A. (2014). Fly-FUCCI: A Versatile Tool for Studying Cell Proliferation in Complex Tissues. *Cell Reports*, *7*(2), 588-598. https://doi.org/10.1016/j.celrep.2014.03.020

SUPPLEMENTARY INFORMATION

1 WGCNA SCRIPT IN R studio

Set up directory structure:

We initialized the working environment by establishing directories for data, plots, and results. Locations for data and metadata files were also specified. Furthermore, we confirmed the installation of all necessary R packages.

```
# Set your desired working directory
# Replace "your/desired/directory/path" with the actual path to your desired directory
setwd("/Users/cristinafernandezgarcia/Desktop/RNASEQ copia")

# Check the current working directory to verify if it has been set correctly
getwd()


#Directory structure

if (!dir.exists("data")) {
  dir.create("data")
}

plots_dir <- "plots"

if (!dir.exists(plots_dir)) {
  dir.create(plots_dir)
}

results_dir <- "results"

if (!dir.exists(results_dir)) {
  dir.create(results_dir)

# Define file paths for data and metadata

data_dir <- file.path("data", "SRP140558")
data_file <- file.path(data_dir, "SRP140558.tsv")
metadata_file <- file.path(data_dir, "metadata_SRP140558.tsv")

# Check if the specified files exist
file.exists(data_file)
file.exists(metadata_file)
```

Installation of required packages

All requisite R packages were installed to ensure the availability of tools necessary for the analysis.

```
if (!("DESeq2" %in% installed.packages())) {
  # Install this package if it isn't installed yet
  BiocManager::install("DESeq2", update = FALSE)
}

if (!("impute" %in% installed.packages())) {
  # Install this package if it isn't installed yet
  BiocManager::install("impute")
}

BiocManager::install("preprocessCore")
if (!("WGCNA" %in% installed.packages())) {
  # Install this package if it isn't installed yet
  install.packages("WGCNA")
}

if (!("ggforce" %in% installed.packages())) {
  # Install this package if it isn't installed yet
```

```
  install.packages("ggforce")
}

if (!("ComplexHeatmap" %in% installed.packages())) {
  # Install this package if it isn't installed yet
  install.packages("ComplexHeatmap")

#Attach some of the packages we need for this analysis.

# Attach the DESeq2 library
library(DESeq2)

# We will need this so we can use the pipe: %>%
library(magrittr)

# We'll need this for finding gene modules
library(WGCNA)

# We'll be making some plots
library(ggplot2)


#Import and set up data
The data from refine.bio includes metadata and gene expression data. Both are loaded into the R environment.


# Read in metadata TSV file
metadata <- readr::read_tsv(metadata_file)

# Read in data TSV file and set gene IDs as row names
df <- readr::read_tsv(data_file) %>%
  tibble::column_to_rownames("Gene")


#Ensure Consistency in order
#Before proceeding, we need to make sure the gene expression data and metadata are in the same order.


# Order data by metadata's accession code
df <- df %>%
  dplyr::select(metadata$refinebio_accession_code)

# Transform data to matrix and add pseudo-zero
df <- as.matrix(df) + 1

# Verify order
all.equal(colnames(df), metadata$refinebio_accession_code)
```

Data preprocessing for analysis:

Gene expression data was preprocessed for DESeq2 analysis. Metadata was organized by time points and treatments, data was formatted for normalization, and a variance stabilising transformation was applied—paving the way for WGCNA.

```
# Convert values to integers and filter out genes with low counts
df <- round(df) %>%
  as.data.frame() %>%
  dplyr::filter(rowSums(.) >= 50)

#Set Up Experimental Group Variable

# Classify samples based on time points
metadata <- metadata %>%
  dplyr::mutate(
    time_point = dplyr::case_when(
      stringr::str_detect(refinebio_time, "1") ~ "Day 1",
      stringr::str_detect(refinebio_time, "3") ~ "Day 3",
      stringr::str_detect(refinebio_time, "5") ~ "Day 5",
      stringr::str_detect(refinebio_time, "7") ~ "Day 7"
    ),
    time_point = as.factor(time_point)
  )

# Classify samples based on treatment
metadata <- metadata %>%
  dplyr::mutate(
    treatment = dplyr::case_when(
      stringr::str_detect(refinebio_treatment, "1") ~ "heatshock",
      stringr::str_detect(refinebio_treatment, "0") ~ "control"
    ),
    treatment = as.factor(treatment)
  )

#Verify Factor Levels

levels(metadata$time_point)
levels(metadata$treatment)

#Create a DESeqDataset

dds <- DESeqDataSetFromMatrix(
  countData = df,
  colData = metadata,
  design = ~1
)
```

```
  geom_hline(yintercept = 0.80, col = "red") +
  ylim(c(min(sft_df$model_fit), 1.05)) +
  xlab("Soft Threshold (power)") +
  ylab("Scale Free Topology Model Fit, signed R^2") +
  ggtitle("Scale independence") +
  theme_classic()


#Checking mean connectivity

# Defining the powers variable for labeling points on the scatter plots
powers <- sft$fitIndices[, 1]

par(mfrow = c(1,2));
cex1 = 0.9;

plot(sft$fitIndices[, 1],
     -sign(sft$fitIndices[, 3]) * sft$fitIndices[, 2],
     xlab = "Soft Threshold (power)",
     ylab = "Scale Free Topology Model Fit, signed R^2",
     main = paste("Scale independence")
)
text(sft$fitIndices[, 1],
     -sign(sft$fitIndices[, 3]) * sft$fitIndices[, 2],
     labels = powers, cex = cex1, col = "red"
)
abline(h = 0.80, col = "red")
plot(sft$fitIndices[, 1],
     sft$fitIndices[, 5],
     xlab = "Soft Threshold (power)",
     ylab = "Mean Connectivity",
     type = "n",
     main = paste("Mean connectivity")
)
text(sft$fitIndices[, 1],
     sft$fitIndices[, 5],
     labels = powers,
     cex = cex1, col = "red")
```

WGCNA

Module identification

The blockwiseModules function was utilised to detect co-expression modules within the gene expression data.

```
bwnet <- blockwiseModules(normalized_counts,
  maxBlockSize = 5000,
  TOMType = "signed",
  power = 14,
  numericLabels = FALSE,
  randomSeed = 1234
)
```

Hierarchical Clustering

Hierarchical clustering was performed, and a dendrogram based on TOM dissimilarity was created to hierarchically represent gene co-expression patterns.

```
 # Convert the adjacency matrix (ADJ1) to a dissimilarity matrix.
dissADJ=1-ADJ1

# Calculate the topological overlap matrix (TOM) distance for the adjacency matrix.
dissTOM=TOMdist(ADJ1)

# Clear unused memory to optimize performance.
collectGarbage()


par(mar = c(0.5, 0.5, 0.5, 0.5))

geneTree = hclust(as.dist(dissTOM), method="average")
sizeGrWindow(9,9)
plot(geneTree, xlab="", sub="",main="Gene clustering on TOM-based dissimilarity",
     labels= FALSE)

dynamicColors = labels2colors(dynamicMods)
table(dynamicColors)
colorh1= dynamicColors

# Plot the dendrogram and colors underneath
sizeGrWindow(6,6)
plotDendroAndColors(geneTree, dynamicColors, "Dynamic Tree Cut",
                    dendroLabels = FALSE, hang = 0.03,
                    addGuide = TRUE, guideHang = 0.05,
                    main = "Gene dendrogram and module colors")
```

Explore WGCNA results

The dataset from WGCNA analysis, particularly the MEs slot containing eigengene module data, was examined. This encapsulates the summarized expression profiles of genes within each module.

```
datME<- blockwiseModules(normalized_counts,
                                maxBlockSize = 5000,
                                TOMType = "signed",
                                power = 14,
                                numericLabels = FALSE,
                                randomSeed = 1234)

module_eigengenes <- datME$MEs
all.equal(metadata$refinebio_accession_code, rownames(module_eigengenes))

# Create the design matrix from the `time_point` and "treatment" variable
des_mat <- model.matrix(~ time_point + treatment, data=metadata)


#Running Linear Models on Each Module

# lmFit() needs a transposed version of the matrix
fit <- limma::lmFit(t(module_eigengenes), design = des_mat)

# Apply empirical Bayes to smooth standard errors
fit <- limma::eBayes(fit)

#Multiple Testing Correction

stats_df <- limma::topTable(fit, number = ncol(module_eigengenes)) %>%
  tibble::rownames_to_column("module")
```

Clustering of ME

Eigengenes from different modules were clustered based on similarity, aiding in the identification of module groups with analogous expression patterns across various conditions.

```
MEList = moduleEigengenes(normalized_counts, colors = dynamicColors)
MEs = MEList$eigengenes
# Calculate dissimilarity of module eigengenes
MEDiss = 1-cor(MEs);
# Cluster module eigengenes
METree = hclust(as.dist(MEDiss), method = "average");
# Plot the result
sizeGrWindow(7, 6)
plot(METree, main = "Clustering of module eigengenes",
     xlab = "", sub = "")
```

Diagnostics - Heat map

Heat maps were generated for the visual inspection of gene expression patterns within specified modules to validate WGCNA

```
sizeGrWindow(8,7);
which.module="brown"
ME=module_eigengenes[,paste("ME",which.module, sep="")]
par(mfrow=c(2,1), mar=c(0.3, 5.5, 3, 2))

# Subset rows based on the condition in colorh1
subset_data <- normalized_counts[colorh1 == which.module, ]

# Use subset_data in the plotMat function
plotMat(scale(subset_data),
        nrgcols=30, rlabels=F, rcols=which.module,
        main=which.module, cex.main=2)

plotMat(scale(normalized_counts[,colorh1==which.module ]),
        nrgcols=30,rlabels=F,rcols=which.module,
        main=which.module, cex.main=2)
par(mar=c(5, 4.2, 0, 0.7))
barplot(ME, col=which.module, main="", cex.main=2,
        ylab="eigengene expression",xlab="array sample")

datMe=module_eigengenes(normalized_counts, colorh1)$eigengenes
```

ME and metadata

Relationships between module eigengenes and metadata labels were explored to ensure sample consistency.

```
# Compare the row names of module eigengenes to the sample accession codes in the metadata to ensure order
all.equal(metadata$refinebio_accession_code, rownames(module_eigengenes))

# Merge module eigengenes with relevant metadata
module_df <- module_eigengenes %>%
  tibble::rownames_to_column("accession_code") %>%
  dplyr::inner_join(metadata %>%
    dplyr::select(refinebio_accession_code, time_point, treatment),
  by = c("accession_code" = "refinebio_accession_code")
  )
```

Genes in each module

The $colors slot was analysed to determine the genes constituting each module.

```
gene_module_key <- tibble::enframe(bwnet$colors, name = "gene", value = "module") %>%
  dplyr::mutate(module = paste0("ME", module))


library(dplyr)
library(tidyr)

blue_genes <- gene_module_key %>%
  filter(module == "MEblue") %>%
  pull(gene) %>%
  unlist()  # Convert the list to a vector

blue_module_expression <- normalized_counts[,blue_genes ]


print(blue_module_expression)


# Convert expression matrix to a long format dataframe
library(dplyr)
expr_long <- as.data.frame(blue_module_expression) %>%
  tibble::rownames_to_column("gene") %>%
  tidyr::pivot_longer(cols = -gene, names_to = "refinebio_accession_code", values_to = "expression")


# Merge with metadata
expr_with_metadata <- left_join(expr_long, metadata, by = "refinebio_accession_code")

# Group by gene, refinebio_time, and refinebio_treatment to compute the mean expression
averaged_expression <- expr_with_metadata %>%
  group_by(gene, refinebio_time, refinebio_treatment) %>%
  summarize(mean_expression = mean(expression, na.rm = TRUE))

# Convert back to a wide format
blue_averaged_expression_wide <- averaged_expression %>%
  pivot_wider(names_from = c("refinebio_time", "refinebio_treatment"), values_from = "mean_expression")

library(writexl)
write_xlsx(blue_averaged_expression_wide, path = "/Users/cristinafernandezgarcia/Desktop/RNASEQ copia/averaged_expression.xlsx")
```

Gene network analysis

Multidimensional Scaling (MDS) was conducted on the dissTOM data to identify outliers and refine the gene network analysis.

```
cmd1=cmdscale(as.dist(dissTOM),2)
# Setting thresholds based on provided ranges
threshold1_lower <- -0.45
threshold1_upper <- 0.35
threshold2_lower <- -0.26
threshold2_upper <- 0.37

# Identify points outside these ranges
outliers <- which(cmd1[,1] < threshold1_lower | cmd1[,1]
76y> threshold1_upper | cmd1[,2] < threshold2_lower | cmd1[,2] > threshold2_upper)

normalized_counts <- normalized_counts[-outliers, ]
metadata <- metadata[-outliers, ]


sizeGrWindow(7, 6)
par(mfrow=c(1,1))
plot(cmd1, col=as.character(colorh1), main="MDS plot",
xlab="Scaling Dimension 1", ylab="Scaling Dimension 2")

moduleLabels = datME$colors
moduleColors = labels2colors(datME$colors)


# Define numbers of genes and samples
nGenes = ncol(normalized_counts);
nSamples = nrow(normalized_counts);
# Recalculate MEs with color labels
MEs0 = moduleEigengenes(normalized_counts, colors = dynamicColors)
MEs = MEList$eigengenes
moduleTraitCor = cor(MEs, metadata, use = "p");
moduleTraitPvalue = corPvalueStudent(moduleTraitCor, nSamples);
```

Gene relationship to trait and important modules:

Associations between individual genes and traits were evaluated, and a quantitative measure of module membership was defined to assess gene similarity within the network.

```
module = "green"
column = match(module, modNames);
moduleGenes = moduleColors==module;
sizeGrWindow(7, 7);
par(mfrow = c(1,1));
verboseScatterplot(abs(geneModuleMembership[moduleGenes, column]),

abs(geneTraitSignificance[moduleGenes, 1]),
xlab = paste("Module Membership in", module, "module"),
ylab = "Gene significance for treatment",
main = paste("Module membership vs. gene significance\n"),
cex.main = 1.2, cex.lab = 1.2, cex.axis = 1.2, col = module)


# Calculate the gene significance for the 'treatment' (heat-shock) using correlation.
GS1=as.numeric(cor(treatment, normalized_counts, use="p"))

# Calculate the absolute gene significance for further analysis.
GeneSignificance=abs(GS1)

# Calculate the module significance by taking the average gene significance for each module.
ModuleSignificance = tapply(GeneSignificance, colorh1, mean, na.rm=T)

# Create a plot to visualize the module significance using the 'plotModuleSignificance' function.
sizeGrWindow(10,12)
par(mfrow = c(1,1))
plotModuleSignificance(GeneSignificance, colorh1)
```

Summary output of network analysis results

The summary integrates statistical outcomes with gene annotations, and the combined data is made ready for export, allowing for further examination in spreadsheet applications or other analytical tools.

```
# Create the starting data frame
gene= t(head(normalized_counts,1))
geneInfo0 = data.frame(gene = gene,
moduleColor = moduleColors,
geneTraitSignificance,
GSPvalue)
# Order modules by their significance for weight
modOrder = order(-abs(cor(MEs, treatment, use = "p")));
# Add module membership information in the chosen order
for (mod in 1:ncol(geneModuleMembership))
{
oldNames = names(geneInfo0)
geneInfo0 = data.frame(geneInfo0, geneModuleMembership[, modOrder[mod]],
MMPvalue[, modOrder[mod]]);
names(geneInfo0) = c(oldNames, paste("MM.", modNames[modOrder[mod]], sep=""),
paste("p.MM.", modNames[modOrder[mod]], sep=""))
}
# Order the genes in the geneInfo variable first by module color, then by geneTraitSignificance
geneOrder = order(geneInfo0$moduleColor, -abs(geneInfo0$GS.weight));
geneInfo = geneInfo0[geneOrder, ]

write.csv(geneInfo, file = "geneInfo.csv")
```

2 DA VS SC SCRIPT IN PYTHON

Initial set up:

We established the structure for our dataset by defining the cell types and criteria using the CellCounter plugin in FIJI/ImageJ, **as described in Chapter 4**. This involves mapping CellCounter numbers to specific cell types with criteria justifying their classification.

```
# the equivalence between CellCounter cell type numbers and your
specific cell types
type_eq = {'1':'EB/EC',
           '2':'EC Pros+',
           '3':'EE',
           '4':'preEE',
           '5':'ISC',
           '6':'Weak Pros+'}

# name columns for the Pandas DF
columns = ['imgfile',     # so we can always associate data to a
microscopy image, e.g. to ID special cases
           'marker type', # CellCounter cell type number
           'type_name',   # Our cell type name
           'X_coord',     # X, Y coordinates so we can then calculate
density, etc.
           'Y_coord']
```

Function to parse XML:

We created a function to read and process XML files, which contain our cell data. This function extracts the necessary information and organizes it into a pandas DataFrame.

```
import os

# directory location of the xml file (in JdN or CFG's computer)
xmlfolder =
'/Users/c1800648/Documents/GitHub/Sc_vs_Da_cell_counts/files_counts'
#xmlfolder = '/Users/JQ/Documents/_CODE
REPOS/GitHub/Sc_vs_Da_cell_counts/files_counts'

# get the list of files
# then 'trim' the list to only XML files with list comprehension and
some string condition
xmllist = os.listdir(xmlfolder)
xmllist = [x for x in xmllist if x.endswith('.xml')]
```

```
def cellcounter_xml2pandas(xmlpath,
                           columns,
                           type_eq):
    import pandas as pd
    import xml.etree.ElementTree as etree
    # open XML file
    tree = etree.parse(xmlpath)
    root = tree.getroot()

    # get the name of the corresponding image file
    imgfile =
root.find("Image_Properties").find("Image_Filename").text

    # read the data
    # (this could be looped over several XML files)
    MarkerDF = pd.DataFrame(columns=columns)
    for node in root.find('Marker_Data')[1:]:
        marker_type = node.findtext('Type')
        for el in node[1:]:
            X = el.findtext('MarkerX')
            Y = el.findtext('MarkerY')
            data = [[imgfile, marker_type, type_eq[marker_type], X,
Y]]
            MarkerDF = pd.concat([MarkerDF,

pd.DataFrame(columns=columns,data=data)]).reset_index(drop = True)
    return MarkerDF
```

Testing the function:

To ensure our function worked as intended, we tested it by parsing the first XML file in our list and examining the first few entries of the resulting DataFrame.

```
# not test
xmlpath = os.path.join(xmlfolder, xmllist[0])
DF = cellcounter_xml2pandas(xmlpath,
                            columns,
                            type_eq)
DF.head(5)
```

```
                                                imgfile marker_type
type_name  \
0  Counter Window - MAX_20180618_hsw[+]-sc42_DaX1...           1
EB/EC
1  Counter Window - MAX_20180618_hsw[+]-sc42_DaX1...           1
EB/EC
2  Counter Window - MAX_20180618_hsw[+]-sc42_DaX1...           1
EB/EC
3  Counter Window - MAX_20180618_hsw[+]-sc42_DaX1...           1
EB/EC
4  Counter Window - MAX_20180618_hsw[+]-sc42_DaX1...           1
EB/EC

  X_coord Y_coord
0     177     113
1     149      96
2     119      91
3     133      91
4     144      83
```

Looping over XML files:

With our function verified, we proceed to loop over all XML files in the designated folder, accumulating their data into a single DataFrame.

```
import pandas as pd
cell_data = pd.DataFrame(columns = columns)
for xmlfile in xmllist:
    xmlpath = os.path.join(xmlfolder, xmlfile)
    #cellcounter_xml2pandas(xmlpath, columns, type_eq).iloc(1)
    cell_data = pd.concat([cell_data,
                           cellcounter_xml2pandas(xmlpath, columns,
type_eq)]
                          ).reset_index(drop = True)

len(cell_data)
```

```
48550
```

Extracting genotype/treatment information:

The next step was to discern genotype and treatment conditions from the image file names. We started by isolating unique file names from our large dataset, then applied predefined criteria to decode the relevant information.

```
da_conversion = {1: ['VallecasXda[10', 'da[10]het','DaX1'],
                 2: ['Vallecas_',"Dax2",'DaX2'], # also may need to be
defined by the absence of the other substrings
                 4: ['DaX4', 'Dax4']}
sc_transgene = {True: ['hs-sc42','hsw']}
hs_length = { 0: ["hs0'", 'NI'], # also may need to be defined by the
absence of the other substrings
             15: ["15","15'"],
             30: ["30'", '30min37C', "30m37C", "30"],
             60: ["60m37C", "60min37C"],}
```

```
import numpy as np
#This is an array that has been converted into a list []
np.unique(cell_data.imgfile).tolist
```

```
<function ndarray.tolist>
```

```
sc_transgene
```

```
{True: ['hs-sc42', 'hsw']}
```

```
# import numpy as np

# mylist=[]
# for filename in [x for x in np.unique(cell_data.imgfile)]:
#     print(da_conversion)


da_conversion[2]
```

```
['Vallecas_', 'Dax2', 'DaX2']
```

```
geno_treat = []
for img_file_name in np.unique(cell_data.imgfile)[:141]:
    genotreat item = {'da':None, 'sc':None, 'hs':None}
    # first look at what's going on with da copy number
    for copy_no in da_conversion.keys():
        for substring in da conversion[copy_no]:
            if substring in img file name:
                genotreat_item['da'] = copy_no
    # second look at what's going on with the presence of the hs-Gal4,
UAS-sc42 transgenes
    for substring in sc_transgene[True]:
        if substring in img_file_name:
            genotreat_item['sc'] = True
        else:
            genotreat_item['sc'] = False

    # third look at how long is the heat treatment
    for mins in hs_length.keys():
        for substring in hs length[mins]:
            if substring in img_file_name:
                genotreat_item['hs'] = mins
    if genotreat item['hs'] is None:
        genotreat_item['hs'] = 0


    geno_treat.append(genotreat_item)
```

Merging data and final steps:

Having identified the genotype and treatment information, we combined it with the cell data. The merged data was then saved as a CSV file for further analysis in R environment.

```
cell_data_vf = pd.concat([cell_data,geno_treat_df], axis=1)
```

```
cell data vf.to csv('C:/Users/c1800648/Documents/GitHub/
export_dataframe.csv', index = False, header=True)
```